METAL ION PROMOTED HYDROLYSIS OF THE ORGANOPHOSPHORUS PESTICIDE, DIAZINON.

By

Martin Wyer

A thesis submitted to the Department of Chemistry in conformity with the requirements for the degree of a Masters of Science

Queen's University

Kingston, Ontario, Canada

January, 2008

Abstract

The chemical fate of organophosphorus pesticides is influenced by several factors, one being the chemistry of their aquatic environment. Dissolved metal ions have been shown in several instances to promote the hydrolysis of organophosphorus pesticides, with various reasons forwarded as to the intimate mechanism of metal ion promoted hydrolysis. Several postulates have suggested metal ion co-ordination of Lewis sites to be an important factor in promoting the reaction. In view of this, the study herein reports on the promoted hydrolysis of diazinon at various pH's in the presence of several metal ions including Hg^{2+}, Cu^{2+}, Cd^{2+} and Ag^{+}.

The observed ^{1}H and ^{31}P NMR data indicated complexation of Cu^{2+} and Ag^{+} with diazinon through the formation of a six-membered ring (chelate), via co-ordination at both nitrogen and sulfur Lewis base sites. In contrast, NMR results with Hg^{2+} indicated Hg^{2+} ion promoted hydrolysis of diazinon through co-ordination at sulfur alone, possibly through stronger binding to the altered transition state than the reactant state. Another possibility would entail lowering of the pKa of H_2O on metal complexation, thus facilitating nucleophilic attack.

Electrospray ionization mass spectrometry (ESI-MS) substantiated the proposed metal ion complexation. In the case of Cu^{2+} and Ag^{+}, complexation between diazinon and metal ions was observed at given m/z ratios, while subsequent MS/MS analysis of the complexed ions revealed co-ordination at both S and N sites by Cu^{2+} and Ag^{+}. No complexation between diazinon and Hg^{2+} was observed in ESI-MS; however Hg^{2+} was

shown to complex the hydrolytic product O,O diethyl phosphorothioic acid, presumably through sulfur.

Hydrolysis of diazinon was studied at several pH's at 22^{o}C in the presence of Hg^{2+}, Cu^{2+}, Cd^{2+} and Ag^{+}, by following spectrophotometrically the appearance of 2-isopropyl-6-methylpyrimidin-4-ol. Kinetic data showed Hg^{2+}, Cu^{2+} and Ag^{+} to be extremely effective in neutral-to-mildly acidic conditions, with a reduced effect in the presence of Cd^{2+}. Smaller rate enhancements were also observed at slightly lower pH of 4.0. Possible factors include; 1) Competing acid hydrolysis involving protonation at one heterocyclic N of diazinon (N-3). 2) The dominant nature of the $HgCl_2$ species at pH 4.0. 3) Metal speciation.

STATEMENT OF ORIGINALITY

Although the hydrolysis of organophosphorus pesticides has been studied extensively by other co-workers, the thesis, to the best of the author's knowledge comprises the following original work.

1) This is the first work to investigate the catalytic effect of a range of dissolved metal ions on the hydrolysis of diazinon.
2) The study is to first to show that dissolved metal ions (Hg^{2+}, Ag^{+} and Cd^{2+}) have a catalytic effect on the hydrolysis of diazinon in the pH range 7.0-4.0. Cu^{2+} ($CuCl_2$) had previously been shown to promote the hydrolysis of diazinon at pH 5.0-6.0. The present study used $Cu(NO_3)_2$.
3) This is the first study to give direct spectroscopic evidence, both ^{1}H and ^{31}P, of metal ion interactions with the organophosphorus pesticide diazinon.
4) This is the first work to establish complexation between diazinon and Ag^{+} using ESI-MS, and also to report complexation between Cu^{2+} and the hydrolytic compound PA.

ACKNOWLEDGEMENTS

I am sincerely grateful for the help of my supervisors, Professors E. Buncel and G.W. vanLoon on the experimental portion of this work and the writing of this document. Their guidance and knowledge has been invaluable and I greatly appreciate the support I received along the way.

I would also like to extend thanks to Professor J.M. Dust (visiting Professor from Sir Wilfred Grenfell College, Memorial University of Newfoundland) and Professor I.-H. Um (visiting Professor from Ewha Womans University, South Korea) for their suggestive inputs and guidance during their visits to the Buncel-vanLoon laboratory.

I would additionally like to acknowledge the other staff members of the Department of Chemistry Dr. F. Sauriol and Jie Sui for their valuable assistance with my research. A special thanks to Mr. R. Roberts and Mr. E. Maracle in the electronics shop for keeping the computers and the spectrophotometers working. I would also like to thank the graduate secretary, Ms. A. Keyes, for helping with all the paper work required to obtain a Masters of Science.

My appreciation goes out to my present and past colleagues, Vesna Vukomanovic, Dildar Ali, Dr. Zhiyuan Tian, Dr. In Sun Koo and Dr. Dalia Abdallah. A special thank you to Sue Min for her dedication and contributions to the experimental work.

Thank you to my friends Jamie, Mark and Johan for always providing me with great company and stories to tell.

For their constant love and support I would like to thank my parents, without whose support and unflinching encouragement I would definitely have not finished.

Also I would like to thank Mick, Edel, Sarah and Linda and my nephew and niece, Ben and Sophia.

Finally my appreciation goes out to Vera Li for her constant encouragement and support and for whom I dedicate this thesis.

TABLE OF CONTENTS

LIST OF TABLES

List of Figures (selected)

CHAPTER 1 Introduction

1.1 General

Organophosphorus pesticides have shown an enormous increase in usage over the past several decades since the decline in the use of organochlorine pesticides in the 1960's and 1970's. They tend to be less persistent in the environment than their organochlorine counterparts, and as such, were considered to possess fewer long term implications to the environment and non-target organisms including humans. However, in recent times several governmental agencies including the US EPA have started to reconsider the widespread use of organophosphorus pesticides due to the concern about their effects on the central nervous system of humans and children in particular[1].

Pesticides are designed to be toxic to their target organisms by a number of mechanisms including, 1) hormonal system interference, and 2) enzyme disruption. These mechanisms may in addition affect humans and cause other adverse health effects such as development and reproductive failure, and or cause endocrine disruption. This has led to a vast interest in the regulation, monitoring and study of pesticides at both governmental and academic level. Extensive research has been carried out into the environmental fate of organophosphorus pesticides including oxidative, photochemical and hydrolysis processes. Whilst the decomposition processes for many organophosphorus pesticides are well understood, the effect of dissolved matter on such processes is a less studied and understood concept. The basis of the current study is to broaden the understanding of how dissolved matter, specifically metal ions, affects the rate of hydrolysis of OP pesticides.

1.2 Pesticides groups

Early generation pesticides such as arsenic, hydrogen cyanide and pyrethrum were utilised by farmers in managing pest control[2] but were abandoned as a consequence of their high toxicity and replaced largely with a range of synthetic organic compounds. One of the first synthetic organic pesticides to be utilized in pest control was dichlorodiphenyltrichloroethane, more commonly known as DDT (Figure 1.1).

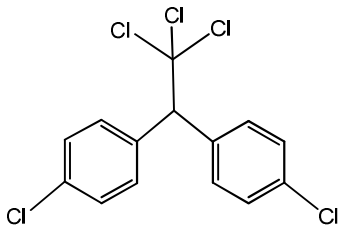

Figure 1.1 DDT

Interestingly DDT was first synthesised in 1879 by Othmer Zeidler, however its effectiveness as an insecticide was not discovered until 1948 by Paul Müller who obtained a Noble Prize for his discovery. The subsequent development of synthetic pesticides led to many different forms, however it can be broken down by looking at the three major families of pesticides in usage:

a) Carbamates:

These compounds act in a very similar fashion to organophosphorus pesticides. The general formula for Carbamates is $R^1NH\text{-}C(O)\text{-}OR^2$ with some common examples shown in Figure 1.2.

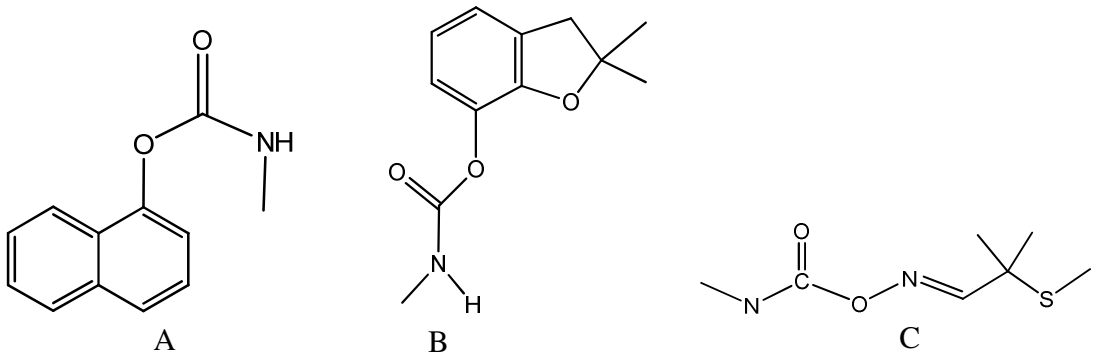

Figure 1.2 Some Carbamate pesticide structures, (a) Carbofuran, (b) Carbonyl and (c) Aldicarb.

(b) Chlorinated hydrocarbons or organochlorines:

These pesticides break down chemically very slowly and can remain in the environment for long periods of time. Dieldrin, chlordane, aldrin and heptachlor are pesticides of this type. They have been widely replaced by the use of the less persistent organophosphates.

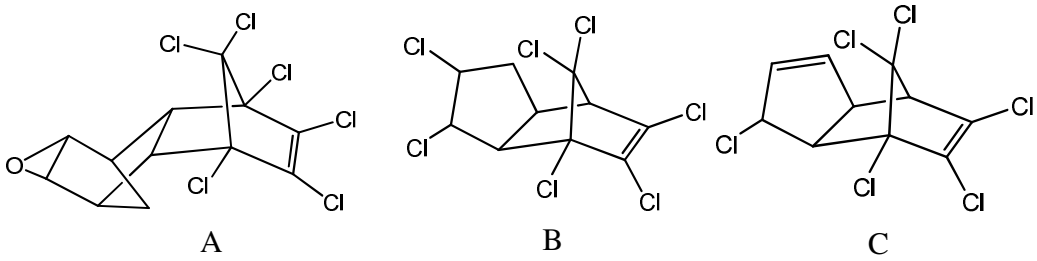

Figure 1.3 Some common organochlorine pesticides, (a) Dieldrin, (b) Chlordane, (c) Heptachlor.

(b) Organic phosphates or organophosphates:

These pesticides are toxic to humans but do not remain in the environment for long periods of time especially in comparison to organochlorine pesticides. Schrader and co-workers prepared the first organophosphorus pesticide O,O-diethyl-O-(4-nitrophenyl) thiophosphate, more commonly known as parathion[3, 4]. In the 1970's and 1980's the use of organophosphorus pesticides accelerated to the point that over 200 OP pesticides were

marketed worldwide[4]. An array of organophosphorus compounds is shown in Figure 1.4, paying particular attention to those previously studied with regards to degradation processes including Diazinon. It is interesting to note the similarity in the structures but also the distinct differences such as the availability and location of Lewis base sites.

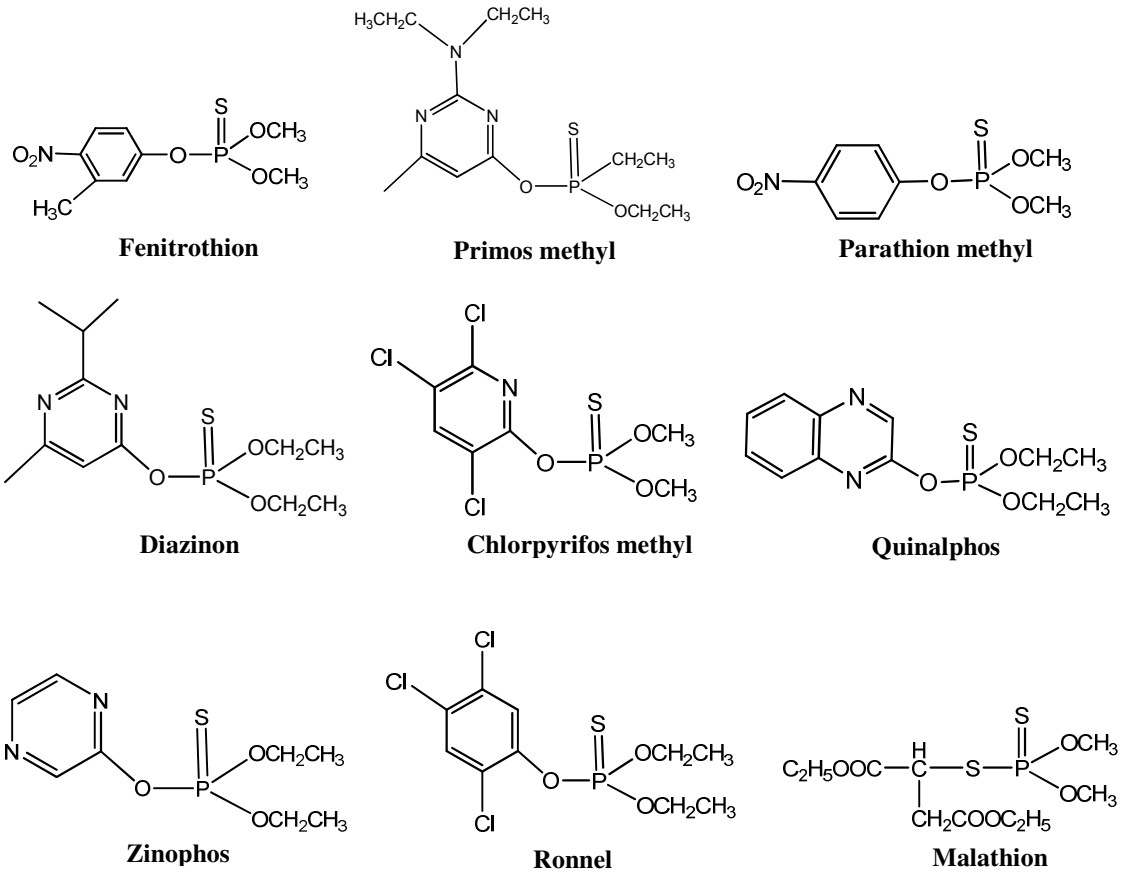

Figure 1.4 Some common organophosphorus pesticides

Owing both to their extensive use in agriculture and their suspected effects on human health, extensive studies into understanding the stability and transformations of OP pesticides have been undertaken. Several of the decomposition pathways are outlined in the following passages, especially in respect to diazinon, the OP pesticide of interest in the present study.

1.3 Decomposition of OP pesticides

The persistence of pesticides can generally be termed as its lasting power in the environment. Their persistence in the environment is controlled by a number of different factors, specifically the different routes by which a pesticide can degrade. Microbial degradation, photo-chemical degradation and hydrolysis are the principal routes of decomposition for most OP pesticides.

1.3.1 Photochemical degradation

Light can cause the photo-degradation of organophosphorus pesticides either by direct or indirect photolysis. In direct photolysis, photons from sunlight cause the decomposition of the pesticide by breaking covalent bonds directly. In indirect photolysis, light reacts with other compounds present in the atmosphere such as O_3, and NO_2. The result is the formation of compounds with unpaired electrons, or radicals, which tend to be very unstable and react quickly with other compounds in the environment such as volatile pesticides. Hydroxy radicals are the primary radicals in the atmosphere. The photodegradation of OP pesticides has been extensively studied, with rapid rates of degradation usually reported.

Dong et al[5]. Investigated the photochemical degradation of several OP pesticides including diazinon in UV-TiO_2, UV-H_2O_2 and UV-TiO_2-H_2O_2 systems. The authors found that the decomposition of diazinon was accelerated in the presence of TiO_2. Several other authors have investigated the photochemical degradation of diazinon in the presence of TiO_2, the TiO_2 induced photochemical degradation found to be much faster than direct photolysis[6, 7]. In some cases the photocatlaysis was found to be effective in as

little as 20 ppm of TiO_2. Dong et al.[8] also investigated the decomposition of several OP pesticides using UV radiation in combination with H_2O_2. The presence of iron species in the system was shown to significantly accelerate the rate of decomposition, with degradation shown to be first order with rate constants ranging from 0.0004 to 0.026 min^{-1}. The aforementioned studies suggest that heterogeneous photodegradation of OP pesticides may be an important decomposition pathway. The presence of semiconductor waste such as iron oxides and oxidants such as hydrogen peroxide in natural waters may aid such decomposition.

1.3.2 Microbial decomposition

Microbial degradation is the breakdown of OP pesticides by fungi, bacteria or other microorganisms using pesticides as a food source. In many cases microbial degradation is considered to be an efficient and cost effective method for decontamination of toxic organophosphorus compounds from the environment. Microorganisms can metabolize many pesticides, in fact possessing the unique capacity to completely mineralize many aliphatic, aromatic and heterocyclic compounds.

Microbial degradation may be broken into two major types; 1) Catabolism; where the organic chemical or a portion thereof is completely degraded, with the energy or nutrients gained contributing to cell growth of the microorganism. 2) Co-metabolism; this involves the partial degradation of the organic chemical and is of no benefit to the organism itself. Pesticide decomposition by microorganisms has been outlined in several reviews.

1.3.3 Hydrolysis

Although the decomposition pathways discussed above may play an important role in OP pesticide decomposition, in many instances hydrolysis is found to be the favored route of degradation[9]. Hydrolysis may take place by either homogeneous or heterogeneous processes. Homogenous catalysis is where the catalyst is in the same phase as the substrate, e.g. nucleophiles such as OH^-, H_2O or dissolved metal ions interact with the pesticide. Homogenous catalysis is of significant interest to the present study, where the hydrolysis of the organophosphorus pesticide diazinon will be studied in the presence of dissolved metals ions. Contrary to this is heterogeneous catalysis where solid materials are seen to accelerate the rate of hydrolysis.

Abiotic hydrolysis of diazinon has previously been studied in the Buncel-vanLoon laboratory and by various other researchers. These studies included investigation of abiotic hydrolysis under controlled conditions with NaOH, HCl and humic acid solutions by Doreen Churchill. The decomposition was observed spectrophotometrically by following the appearance of O,O diethyl phosphorothioic acid (PA) and 2-isopropyl-6-methylpyrimidin-4-ol (PY)[10].

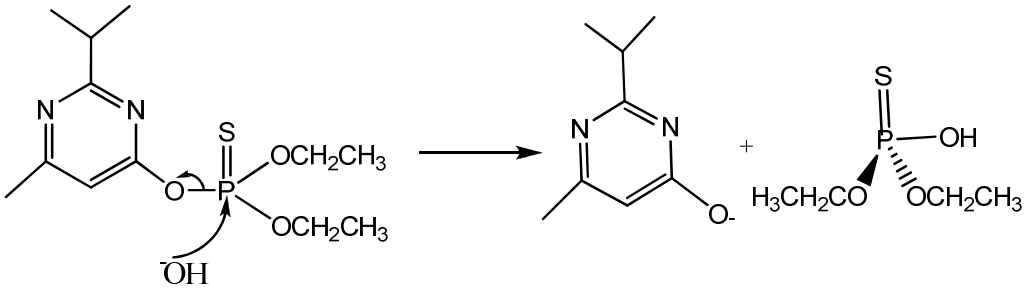

Figure 1.5 Diazinon base hydrolysis

The research indicated a linear relationship between ^{-}OH concentration and rate, showing specific base catalysis by ^{-}OH. The acid catalysis study however, suggested a more complicated system where the rate initially increased with acid concentration (2.6×10^{-3} M to 0.175 M), then decreased in rate (0.175 M to 6.13 M), and finally increased again with increasing acid concentration (6.13 M to 8.75 M). This effect was ascribed to the various protonation sites on diazinon and a decrease in the activity of water at elevated acid concentrations.

This concept was explored further in a recently published paper by the same author investigating diazinon hydrolysis in moderately concentrated sulfuric acid solutions[11]. Under the stated conditions the authors concluded that acid catalysis was by a less common A-S_E2 mechanism involving proton transfer to P=S from a hydronium ion, with concomitant proton transfer from water and attack at the P centre. This work also involved the broader study of the hydrolysis of diazinon in the presence of cyclodextrins (CD's) at pH 12. The study determined the binding constants (K_b) between diazinon and several CD's and the rate constants k_c for the hydrolysis of diazinon from such complexes. The author concluded that in general the CDs with low K_b values catalyzed the reaction whereas CDs with high K_b values tended to inhibit the hydrolysis.

Several other authors have studied the abiotic hydrolysis of diazinon. Noblet et al[12]. studied the rate of hydrolysis of diazinon and several other pesticides in three natural waters and concluded that the uncatalysed abiotic hydrolysis was slow for the OP pesticides studied including diazinon, Methylparathion, Chlorpyrifos. The half lives determined were 17 days, 10 days and 11 days respectively. The author also noted a

significant decrease (32%) in the rates of hydrolysis of Chlorpyrifos in the presence of high concentrations of dissolved organic matter (DOM) and concluded that a better understanding of the relative influence of DOM was required. This is a principal aim of the present study.

Michel[13] and co-workers investigated the fate of diazinon during the composting of leaves and grass, as diazinon was the most widely used lawn care pesticide. The author found from a water extract of the finished compost that the majority of the diazinon was hydrolysed to 2 -isopropyl-6-methylpyrimidin-4-ol (PY) with a very small amount mineralized to CO_2. Formation of the product PY suggested S_N2 (P) attack as the favored route for hydrolysis of diazinon.

1.4 Mechanisms of hydrolytic degradation of OP compounds

The general reaction of an OP pesticide with a nucleophile is shown in Scheme 1.1.

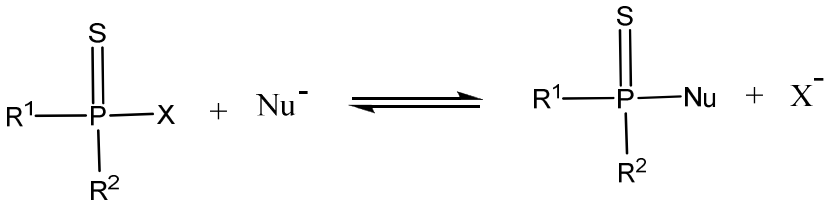

Scheme 1.1 General form of degradation of phosphorus triesters.
X = leaving group

R^1, R^2 = alkly, O-alkyl, aryl, O-aryl, OH, H.

The nucleophile defined as an electron pair donor attacks an electrophilic centre displacing the leaving group (X) with the resultant formation of the substituted product. In hydrolysis the nucleophile maybe OH^- or H_2O.

The mechanism of degradation of phosphorus triesters such as diazinon has been studied by different researchers in the past[14, 15, 16]. The mechanism of degradation can generally be broken down into three different mechanistic types; (1) S_N2 (P) at the phosphorus centre, (2) S_N2 (C) at an aliphatic carbon or (3) S_NAr. These mechanisms are typically nucleophilic substitution reactions where a substrate R-X bearing a leaving group X reacts with a nucleophile. The general form of the reaction is given in Scheme 1.1.

1.4.1 Mechanism at the phosphorus centre, S_N2 (P)

This mechanism involves nucleophilic attack at the electrophilic phosphorus centre. It is considered a concerted mechanism in which bond formation with the electrophilic phosphorus centre and nucleophile, and bond breakage between the same phosphorus centre and leaving group occur concertedly as depicted in Scheme 1.2.

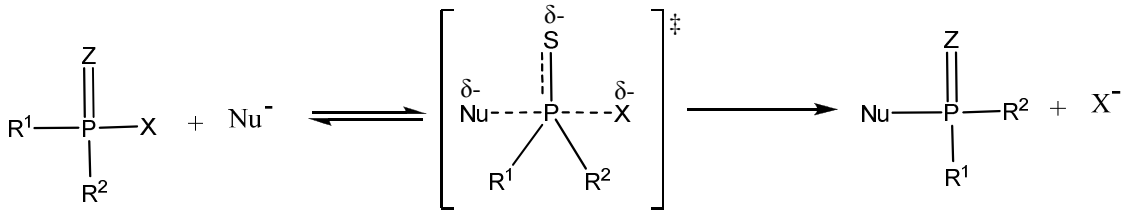

Scheme 1.2 Nucleophilic attack at the phosphorus electrophilic centre by S_N2 (P).

The mechanism envisages the formation of a trigonal bypyramidal transition state in which both the nucleophile and leaving group have a partial negative charge.

1.4.2 Mechanism at the carbon center, S_N2 (C)

Although attack at the phosphorus centre is more common, reaction can also take place at the aliphatic carbon of the O-alkyl groups attached to the phosphorus via a S_N2 (C) mechanism. This is depicted in Scheme 1.3.

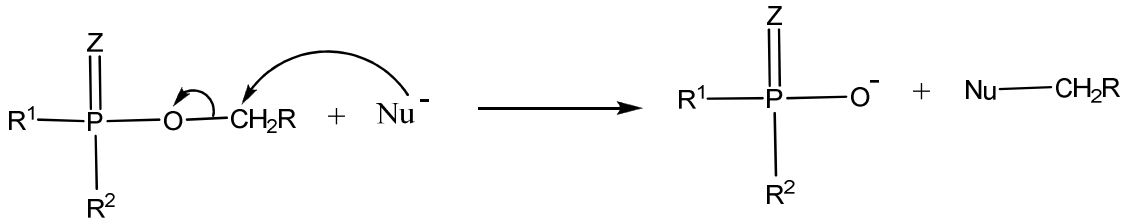

Scheme 1.3 Nucleophilic attack at the carbon electrophilic centre by S_N2 (C).

This process will only be expected to occur in either neutral or acidic conditions as ^{-}OH ion favors attack at the phosphorus electrophilic centre[17], or with nucleophiles such as I^{-}.

1.4.3 Mechanism at aromatic centre, S_NAr

A third possibility is nucleophilic attack at the aromatic ring of O-aryl groups. This pathway is generally only favored or considered possible with two or more strongly electron withdrawing substituents present on the ring such as NO_2.

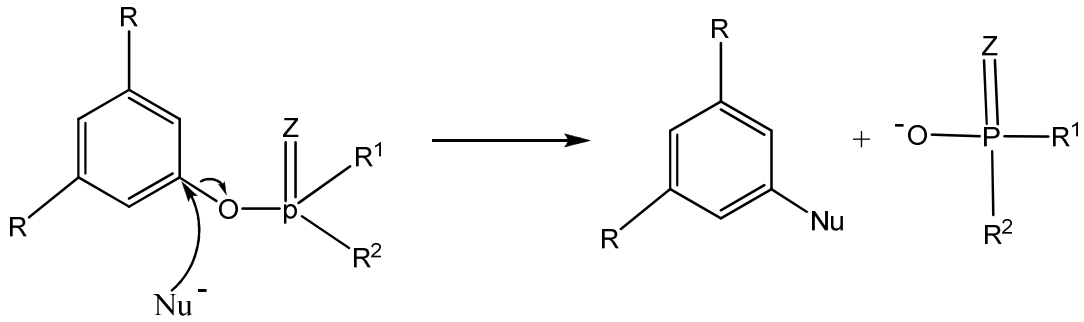

Scheme 1.4 Nucleophilic attack at the aromatic electrophilic centre (S_NAr).

1.5 Homogenous catalysis

As described earlier a homogenous catalyst is a substance that accelerates the rate of hydrolysis whilst being in the same phase as the substrate. Prime examples of homogenous catalysts are dissolved matter such as metal ions which through interaction(s) with the pesticide may accelerate the rate of hydrolysis. The aim of the present study is to explore such homogenous catalysis by studying the various

interactions between several different metal cations and the pesticide diazinon using common spectroscopic techniques. The observed interactions between metal and pesticide will then be used to explain any catalytic effect or lack off observed spectrophotometrically in the rate of hydrolysis.

1.5.1 Reasons for catalytic enhancement

Dissolved metals ions are known to play a wide and varied role in enhancing the rate of many significant hydrolysis reactions. In most cases the catalytic enhancement is attributed to metal co-ordination with the substrate. Several different mechanisms of catalysis by metal ions are outlined below;

1) The metal ion acts as an electrophile and co-ordinates the Z atom (either O or S). This has the effect of enhancing the electrophilicity of the phosphorus electrophilic centre making it more prone to attack by ^{-}OH or H_2O.

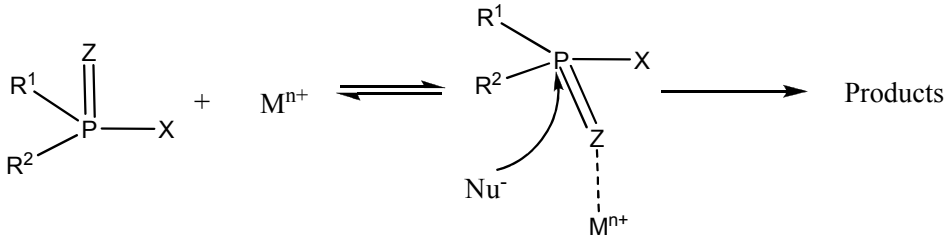

Scheme 1.5 Metal binding to Z, with resultant increase in the electrophilicity of phosphorus.

2) Metal ion co-ordinates the leaving group, with consequent facilitation of its departure by weakening the O-P bound.

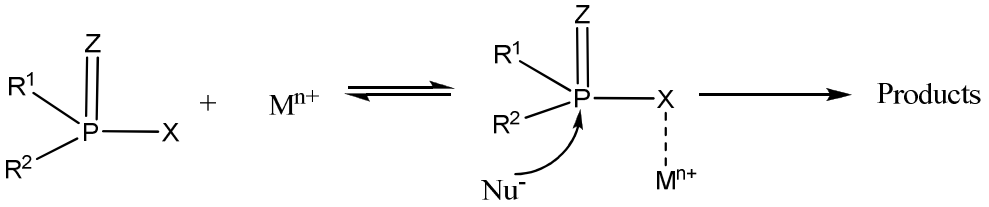

Scheme 1.6 Metal binding to X, with resultant facilitation of leaving group.

3) If two ligands are present in the OP pesticide the second ligand may act as an auxiliary ligand and enable either (a) the interplay of mechanism 1 and 2, or (b) facilitate the formation of a chelate.

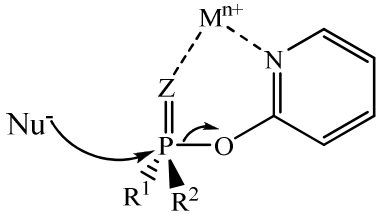

Scheme 1.7 Metal chelation

4) A fourth possible mechanism involves metal co-ordination of the nucleophile itself. Such a metal-hydroxide species can subsequently bind the pesticide, with resultant intramolecular $^{-}$OH attack on the pesticide. This mechanism is more likely to be prevalent in neutral or acidic conditions where the $^{-}$OH ion concentration is reduced

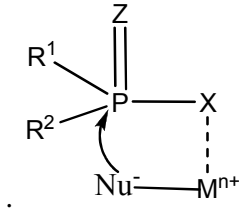

Scheme 1.8 Intramolecular nucleophilic attack

A number of studies have shown that dissolved metal ions can play an important role in catalysis of organophosphorus pesticides. These studies have attributed the metal catalysis to interactions between the substrate and metal cation. Several of these studies are outlined in the Discussion section in tandem with the results obtained for diazinon in the presence of metal cations. In most cases the catalytic enhancement was attributed to bonding between the metal cation and specific Lewis sites on the organophosphorus pesticides. diazinon itself has three Lewis sites with potential to bind metal ions, such as nitrogen, sulfur and oxygen. In order to learn more about the potential co-ordination of metal cations to diazinon and their resultant catalytic effects, four heavy metal ions were selected i.e. Hg^{2+}, Ag^{+}, Cu^{2+} and Cd^{2+}. These metals are known to have strong affinity for nitrogen and sulfur Lewis sites. To facilitate understanding of how the metal cations accelerate the rate of hydrolysis through co-ordination, ESI-MS and NMR techniques were used to aid in pin-pointing metal co-ordination to the substrate. NMR enables mapping of the different electronic effects metal co-ordination has on phosphorus and proton nuclei.

1.6 Methodology

1.6.1 Nuclear Magnetic Resonance

Although Electrospray Mass Spectrometry is an extremely effective technique in detecting interactions between the metal ions and pesticide, it is carried out in the gas phase and may not reproduce what is occurring in the solution phase. Consequently Nuclear Magnetic Resonance (NMR) studies will be performed to substantiate the results obtained utilising ESI-MS, whilst also giving a broader understanding of the metal ion-

pesticide interactions. These spectroscopic experiments including ^{31}P and ^{1}H can probe specific binding interactions between the metal cation and diazinon.

Solution NMR is one of the principal techniques in organic chemistry used to obtain structural information about a molecule and its interactions with other elements in solution. The principle is that nuclei in the NMR resonate at a slightly different frequency depending on the electron density around the nuclei, i.e. based on the other surrounding elements. The different nuclei have the effect of either shielding or de-shielding a particular nucleus to an external magnetic field.

As a result information about the chemical environment of nuclei such as phosphorus and proton can be derived from its resonant frequency. NMR can therefore be used to help elucidate where co-ordination between the metal and diazinon is occurring by observing changes in the chemical shift of both proton and phosphorus nuclei. This can be achieved by conducting ^{1}H and ^{31}P experiments with and without the presence of metal ions. The principal that a change in chemical environment of a nucleus will result in a change in its resonance frequency can then be utilised to infer where interactions between the metal ions and substrate is occurring.

^{31}P chemical shifts of organophosphorus pesticides have been well characterised. Miyata et al. subjected 23 such pesticides to Fourier-transform ^{31}P NMR and obtained a broad ppm range for the insecticides depending on structure; phosphates fall between 4 to -2 ppm, phosphorothiolates between 29-31ppm, phosphorothionates between 60-67 ppm and phosphorodithioates between 89-100ppm[18]. Ross et al. examined the ^{31}P chemical shifts of a more extensive range of organophosphorus insecticides detailing the chemical

shifts observed according to different classes of pesticides[19]. Five such classes are depicted in Table 1.1. The large variation in chemical shift depending on structure (from 120 ppm down to -30 ppm) is a very useful characterisation tool, which may be used to assess phosphorus containing hydrolysis products. The general structure for each pesticide is illustrated Scheme 1.9.

Table 1.1 List of ^{31}P chemical shifts for a range of organophosphorus pesticides

Compound	*Solvent*	*Chemical shift*	*Compound*	*Solvent*	*Chemical shift*
Phosphates			***Phosphorothioates***		
Azodrin	Acetone	118.1	Abate	Acetone	46.6
Bidrin	Neat	117.6	Coumaphos	Neat	50.3
Bomyl	Chloroform	118.9	Dasanit	Choroform	50.0
Ciodrin	Acetone	118.4	***Diazinon***	Neat	52.0
Compound 4072	Neat	117.3	Dursban	Acetone	52.2
DDVP	Neat	116.1	Fenthion	Neat	45.9
Diazoxon	Neat	120.5	Methyl parathion	Acetone	47.2
Paraoxon	Benzene	119.7	Nemacide (V'C-13)	Neat	49.7
Phosphamidon	Chloroform	117.4	Parathion	Benzene	46.0
Phosdrin	Acetone	118.4	Romnel	Acetone	46.6
Ronnoxon	Acetone	117.7	Zinophos	Neat	51.2
Phosphorodithiates			**Phosphorotrithioites**		
Betasan	Chloroform	21.3	Merphos	Neat	-4.9
Dimethoate	Acetone	15.3			
Disyston	Neat	18.2	**Phosphites**		
Ethion	Neat	20.0	2,4-DEP	Acetone	-27.1
Guthion	Acetone	18.2			
Imidan	Acetone	18.6			
Malathion	Neat	17.5			
Methyl Trithion	Acetone	15.9			

Phosphates **(115-121 ppm)** | Phosphorothioates **(45-55 ppm)** | Phosphorodithiates **(15-22 ppm)** | Phosphorotrithioites **(-4.9 ppm)**

Scheme 1.9 List of ^{31}P chemical shifts for a range of organophosphorus pesticides

^{1}H NMR studies of organophosphorus pesticides are also prevalent in the literature detailing trends in proton chemical shifts in relation to structure properties, effect of solvent on chemical shift values and coupling constants[20,21]. The splitting of the phosphorus signal by coupling with neighboring hydrogens is also widely researched.

Although ^{31}P and ^{1}H NMR have been extensively used in characterisation of organophosphorus pesticides, its use in probing metal ion binding on pesticides is limited. Several studies have been performed in the Buncel-vanLoon laboratory including Hamed Esbata[22] who investigated the homogenous catalysis of the oganophosphorothioate pesticide Quinalphos (Figure 2) using metals such as Hg^{2+}, Cu^{2+} and Ag^{+1}. Both ^{1}H and ^{31}P experiments were performed to depict whether complexation between the metal ion and pesticide was occurring and to probe exactly where this binding was occurring. Esbata found that binding with Hg^{2+} was predominately through the sulphur ligand, Cu^{2+} through the nitrogen ligand, and the softer Ag^{+} ion through both nitrogen and sulphur. Weak interactions were also observed between Cu^{2+} and the sulphur ligand and Hg^{2+} and the nitrogen ligands.

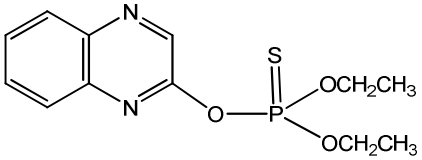

Figure 1.6 Quinalphos

Pehkonen et al. studied the role of Hg^{2+} in the hydrolysis of Demeton (Figure 3) using both ^{1}H and ^{31}P to locate where the interaction between the metal ion and pesticide was occurring. This study used two different mercury salts to investigate binding, the relatively non-ionized $HgCl_2$ and the more dissociated $Hg(NO_3)_2$. The authors used

chemical shift changes in both ^{1}H and ^{31}P NMR to pinpoint the source of binding if any and also to show the appearance of hydrolysis peaks. Interestingly the authors showed binding resulting from the $Hg(NO_3)_2$ salt, but suggested the formation of a stable complex through the two sulphur atoms in the ester side chain, with no resultant hydrolysis. Conversely, no binding was shown using $Hg(Cl)_2$ salt, however rapid hydrolysis occurred with a half life of only hours. The results of this study suggest that speciation of the metal ion is an extremely important factor in the binding and hydrolysis capability of mercury ions.

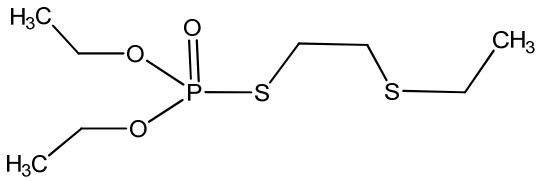

Figure 1.7 Demeton

1.6.2 Electrospray Mass Spectrometry

Electrospray mass spectrometry of diazinon and its hydrolysis products in the presence of metal cations is an extremely effective technique in pin-pointing the interactions between substrate(s) and metal. In mass spectrometry, analyte molecules are first ionised, then separated based on mass/charge ratio and detected. The ionisation process is extremely important in MS with several different types of ionisation processes available including Chemical ionisation (CI), Electron impact (EI) and Electrospray ionisation (ESI).

Electron impact ionisation (EI) is the most common ionisation source used in MS work, however due to its harsh nature it was not considered in the present study. In EI, electrically neutral molecules are converted to molecular ions (M^{n+}) by means of high energy electrons. In EI, ionisation is almost immediately followed by fragmentation of

the M^{n+} ion, resulting in a complicated fragmentation pattern emanating from the parent ion.

Contrasting this is the softer ionisation process associated with ESI-MS, which is ideally suited to the present work, where identifying complexation between the OP pesticide and metal is the objective. In the ES ionisation source little additional energy is imparted to the desolvated ions, with limited fragmentation. This is ideal for observing complexation between the metal cation and substrate. Further structural information can be obtained by coupling ESI with MS/MS. This allows specific m/z ions to be isolated and further fragmented in a secondary collision induced cell. This can aid in giving definitive information about the location of binding.

Several authors have used ESI-MS to investigate fragmentations and reactions of diazinon. Barr et al.[23] studied the fragmentations of diazinon using Electrospray ionisation ion trap mass spectrometry, proposing several novel fragmentations and rearrangements. One such peak observed at m/z 169 was attributed to a fragment emanating from a thiono-thiolo rearrangement of diazinon as depicted in Figure 1.8. Several other fragments were identified including the sequential loss of ethene from the ethoxy groups and protonated pyrimidinol. The author concluded that the use of ESI ion trapp mass spectrometry can reveal detailed structural information of the fragmentations and reactions of organophosphate esters.

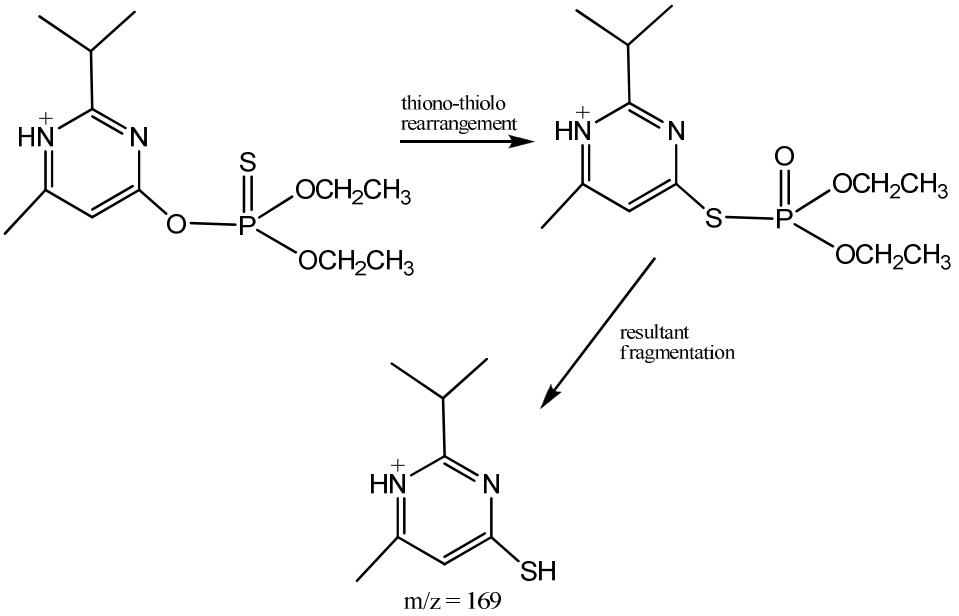

Figure 1.8 Novel thiono-thiolo rearrangement of diazinon in the gas phase proposed by Barr et al.[23].

Several studies in the Buncel-vanLoon Laboratory have used ESI-MS to investigate metal co-ordination with OP pesticides. As mentioned previously Esbata et al.[22] studied metal complexation with Quinalphos, using both NMR and ESI-MS to pin-point the location of binding. The ESI-MS gave evidence of metal binding with the substrate and subsequent CID experiments provided definite structural information with regard to location of co-ordination. Keller et al[24] also investigated the potential complexation between diazinon and Ag^{+}, Cu^{2+} and Hg^{2+} by ESI-MS; with several interactions proposed between the substrate and metal cations. These studies will be explored in more detail in the Discussion section in terms of the results obtained in the present dissertation.

1.6.3 UV spectroscopy

Hydrolysis of diazinon will be followed by observing the appearance of product peaks with ultraviolet absorption both in the absence and presence of various metal ions. As mentioned previously the abiotic hydrolysis of diazinon has previously been studied in the Buncel-vanLoon laboratory and by various other researchers. In some cases the decomposition was followed spectrophotometrically by following the appearance of O,O diethyl phosphorothioic acid (PA) and 2-isopropyl-6-methylpyrimidin-4-ol (PY)[10] in both acid and basic conditions. Mortland et al. also investigated the hydrolysis of diazinon in the presence of several salts including $CuCl_2$, $ZnSO_4$, $NiSO_4$ and $CaCl_2$. The hydrolysis was followed spectrophotometrically by observing the disappearance of substrate with time.

1.7 Purpose of the present study

In the Buncel-vanLoon laboratory several organophosphorus pesticides have been studied in an aim to broaden the understanding of the behavior of OP pesticides, with several of these studies concerning diazinon. The studies included investigating the abiotic hydrolysis of diazinon under controlled conditions in NaOH, HCl and humic acid[10]. Hydrolysis was also investigated in moderately concentrated sulfuric acid solutions and in the presence of several cyclodextrins[12].

This dissertation aims to add to the knowledge acquired from previous studies by examining the decomposition behavior of diazinon, specifically in regard to the presence of dissolved metal ions. This will be done in several ways;

1) Analysing the interactions between diazinon and its hydrolysis products with metal ions using ^{1}H and ^{31}P NMR

2) Corroborating NMR data by further probing the interactions of substrates and metal ions using ESI-MS.

3) Examining the base and acid hydrolysis of diazinon spectrophotometrically in the presence of metal ions including Ag^{+}, Hg^{2+}, Cu^{2+} and Cd^{2+}.

CHAPTER 2 Experimental section

2.1 Reagents

2.1.1 Water and deuterium oxide (D_2O)

Distilled de-ionised water (DDW) was used in the preparation of all co-solvent solutions employed in ESI-MS and kinetic studies. The water component of the co-solvent used in the NMR study utilised D_2O (Cambridge, 99.9%).

2.1.2 Methanol and methanol-D_4

Methanol (HPLC grade, Fischer chemicals) was used to prepare all solutions in the ESI-MS and kinetic studies. Methanol-CD_3OD (Cambridge Isotope Laboratories, Inc) was employed in the NMR studies.

2.1.3 Sodium Hydroxide (NaOH)

The kinetic hydrolysis in alkaline conditions involved the preparation of NaOH solutions (Sigma-Aldrich, 98%). The solutions were prepared by dissolving the appropriate amount of NaOH pellets in a chosen co-solvent of 70% methanol-30% water. The exact concentration of sodium hydroxide was determined by titration against the primary standard potassium hydrogen phthalate ($KHC_8H_4O_4$, KHP, B.D.H Laboratory Chemicals) using phenolphthalein as indicator.

2.1.4 2-Isopropyl-6-methylpyrimidinol-4-ol (pyrimidinol)

Pyrimidinol was purchased from Aldrich (99%). The purchased compound was found to contain a fine black impurity. Hot gravity filtration using acetone as solvent was used to remove the insoluble impurities from the crude product. White fine crystals were obtained on cooling and the purity of pyrimidinol was assessed using ^{1}H, ESI-MS (positive ion mode), IR and melting point analysis. The NMR spectra were obtained on a Bruker 400 MHz Advance spectrometer using $CDCl_3$ as solvent. All spectra were consistent with that of pyrimidinol and contained no impurity peaks. The lettering system for designating the pyrimidinol Spectra is shown below.

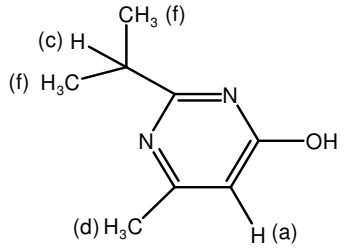

Pyrimidinol

NMR spectra were assigned as follows:

^{1}H: 6.075ppm (s, 1H, a), 2.805ppm (multiplet, S, $J_{Hc\text{-}Hf}$ 0.017 Hz, c), 2.107ppm (s, 3H, d), 1.164ppm (d, 6H, $J_{Hf\text{-}Hc}$ 0.017, f)

The ESI-MS (positive ion mode) peak at 153 m/z is consistent with the proposed compounds identity. The protonated form of pyrimidinol has a MW of 153 g/mol. The melting point determined on a Mel-temp melting point apparatus was found to be 172-174 °C.

2.1.5 Metal ions

All metal ion solutions for NMR, ESI-MS and kinetic studies were prepared in the chosen co-solvent of 70% methanol and 30% water.

2.1.5.1 Copper

Cupric nitrate solutions were prepared by dissolving a weighed quantity of $Cu(NO_3)_2$, (Aldrich) in 0.5ml of concentrated nitric acid (HNO_3, Fischer). The solution was then made up to the mark with a co-solvent of 70% methanol-30%water.

2.1.5.2 Mercury

Mercury chloride solutions were prepared by dissolving the required amount of $HgCl_2$ (Puratronic, 99.99%) in the chosen co-solvent. This was achieved by first dissolving the weighed amount in the water component (30%) and diluting to the mark with methanol (70%).

2.1.5.3 Silver nitrate

Silver nitrate ($AgNO_3$, Aldrich Chemical Comp., 99%) solutions were prepared by first dissolving the weighed amount of $AgNO_3$ in water and making up to the mark with methanol to give the chosen co-solvent ratio.

2.1.5.4 Cadmium nitrate

Cadmium nitrate ($Cd(NO_3)_2$, Fischer Scientific Comp.) solution was prepared as per silver nitrate.

2.2 Synthesis

2.2.1 Preparation of diazinon

Diazinon was synthesised using a method modified from Gysin and Margot via a two step process that initially involved formation of the potassium salt of pyrimidinol as depicted in Scheme 1. This was effected by reacting pyrimidinol (MW=152.20g/mol, 5.004g, Aldrich, 99%) with potassium hydroxide (MW=56.11, 1.899g, Aldrich, >90%) in hot absolute ethanol. The ethanol was then removed by rotary evaporation. Benzene (70ml) was added and water was azeotropically removed by distillation. The remaining benzene was removed by rotoevaporator.

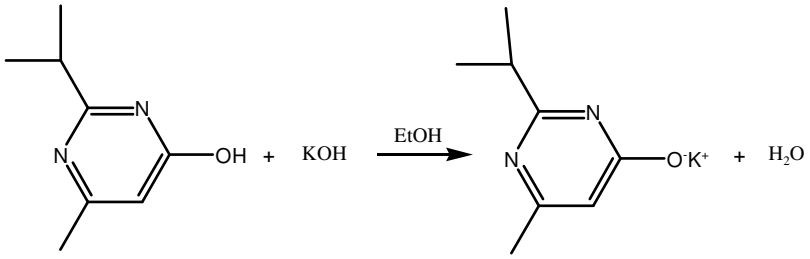

Scheme 2.2. 1 Synthesis of diazinon. Step 1.

The second step involved the reaction of the potassium salt with diethyl chlorothiophosphate to produce diazinon and insoluble potassium chloride as shown in Scheme 2.2.1.

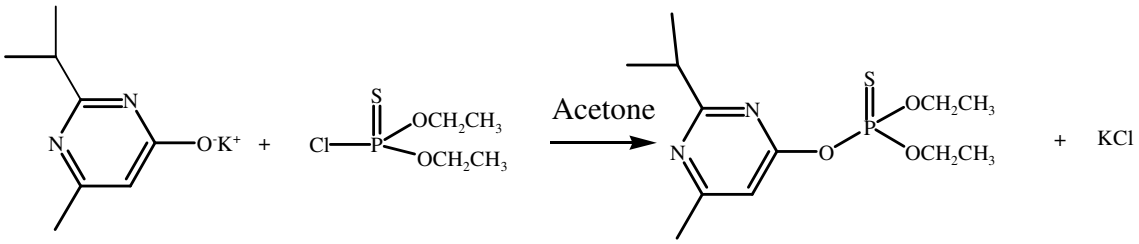

Scheme 2.2. 2 Synthesis of diazinon. Step 2.

O, O diethyl chlorothiophosphate (MW=188.61 g/mol, d=1.2g/mL, 6.20ml or 7.44g, Aldrich, 97%) was added to the potassium salt and heated at 35^0C for two days in acetone. The solution was then cooled and filtered through Celite to remove the insoluble potassium chloride. Acetone was removed by rotary evaporation to give an oil that contained both diazinon and starting material O, O diethyl chlorothiophosphate. The oil was purified by column chromatography using methylene chloride as eluent. The fraction containing diazinon was then rotoevaporated to remove methylene chloride and left over –night under high vacuum.

A white solid was obtained (unreacted pyrimidinol) in the diazinon fraction. The sample was placed in 40 ml of hexanes and extracted with 4 x 20 ml H_2O. The hexanes layer was dried with anhydrous $MgSO_4$, filtered to remove drying agent, rotoevaporated to remove hexanes and left overnight under high vacuum. diazinon was synthesised with a final yield of 46%.

2.2.2 Structural characterisation of diazinon

The purity of the diazinon was checked by ^{1}H, ^{31}P and ^{13}C (J-modulated), ESI-MS and IR. The NMR spectra were obtained on a Bruker 400 MHz Advance spectrometer using $CDCl_3$ as solvent. All spectra were consistent with that of diazinon and contained no impurity peaks. The lettering system for designating Spectra of diazinon is shown below and follows that employed for pyrimidinol. NMR spectra were assigned as follows:

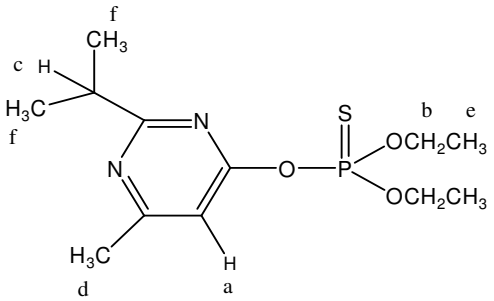

Diazinon

^{1}H: 6.656 ppm (s, 1H, a), 4.05 ppm (d of q, 4H, J_{HB-HE} 6.8 Hz and 7.2 Hz, b), 3.10 ppm (sept, 1H, J_{Hc-Hf} Hz, c), 2.480ppm (s, 3H, d), 1.387 ppm (t, 6H, J_{He-Hb} 6.8 Hz and 7.2 Hz, e), 1.31ppm (d, 6H, J_{Hf-Hc} 6.8 Hz, f).

^{13}C: 175 PPM (h), 169.87ppm (g), 164.491 (j), 106.90ppm (i), 65.33ppm (b), 37.43ppm (c), 24.20ppm (d), 21.54ppm (f), 15.91ppm (e)

^{31}P: 60.566ppm (s, P)

The ESI-MS (positive ion mode) spectrum shows a parent peak at 305 m/z. This is consistent with the protonated form of diazinon which has a MW=305 g/mol.

2.2.3 Preparation of O,O diethyl phosphorothioic acid (PA)

Preliminary PA synthesis was carried out by stepwise addition of diethyl chlorothiophosphate (MW=188.61 g/mol, d=1.2g/mL, 15.0ml, Aldrich, 97%) to a stirred solution of NaOH (7.50g, Aldrich, 98%) in absolute ethanol (150ml, Commercial Alcohols Inc.). The resulting solution was stirred for 3 hours. The solution was then cooled in an ice bath and the precipitated NaCl was removed by filtration. The filtrate was concentrated by rotary evaporation to produce a slurry. Distilled water (40ml) was added to the slurry and the resultant potassium salt solution was extracted with 3 x 40ml of chloroform. The solution was then acidified with HCL (6M, until pH indicator paper turned acidic) and extracted with 3 x 20ml of chloroform. The chloroform was taken off by rotoevaporator followed by drying under high-vacuum overnight. The procedure gave a % yield of O,O diethyl phosphorothioic acid of 12.3%.

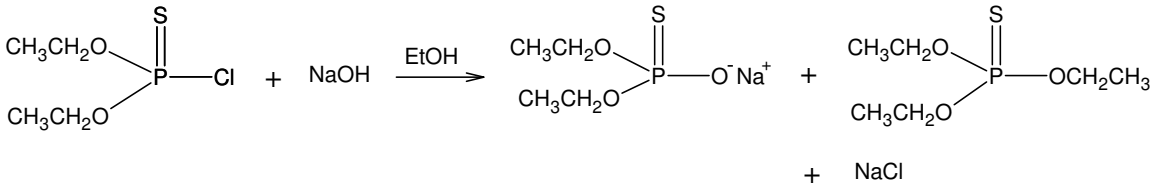

Scheme 2.2. 3 Preparation of O,O diethyl phosphorothioic acid.

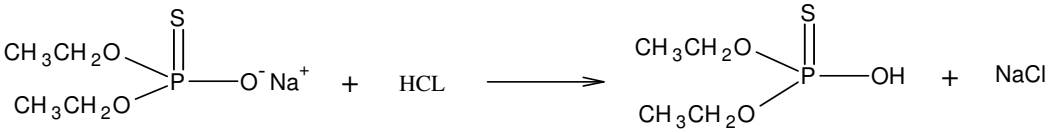

Scheme 2.2. 4 Preparation of O,O diethyl phosphorothioic acid. Step 2.

A competing reaction for the tri-ethoxide product was noted by this synthesis route as shown in Scheme 2.2.3 above; therefore modification was attempted by varying the solvent to either water or a 50% water/ethanol mix and the ratio of starting materials. The highest yield was obtained using water as solvent and a 1:1 ratio of O,O diethyl chlorothiophosphate and NaOH. This route involved the stepwise addition of O,O diethyl chlorothiophosphate (6.019g) to a stirred solution of NaOH (1.32g) in water. The solution was stirred for 3 hours. Next the solution was washed with toluene (2 x 30ml) and acidified with HCl (6M, 1ml). The water layer was then extracted with 4 x 30ml of chloroform. The chloroform was removed by rotoevaporator followed by drying under vacuum overnight. The modified procedure resulted in a percentage yield of O,O diethyl phosphorothioic acid of 28.5%.

2.2.4 Structural Characterisation of O,O diethyl phosphorothioic acid

O,O diethyl phosphorothioc acid (PA) was synthesised with a final yield of 28.5%. The purity of the product was ascertained by ^{1}H, ^{31}P and ^{13}C (J-modulated), ESI-MS and IR. The NMR spectra were obtained on a Bruker 400 MHz Advance spectrometer using $CDCl_3$ as solvent. All spectra were consistent with that of PA and contained no impurity peaks. The NMR spectra were assigned as follows:

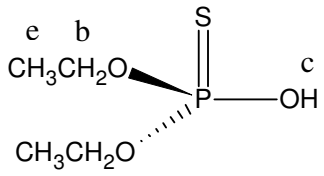

O,O diethyl phosphorothioic acid

^{1}H: 1.37ppm (t, J_{He-Hb} 6.9Hz, 6H, e), 4.18ppm (multiplet, J_{Hb-He} 6.9Hz, 4H, b), 5.78ppm (c).

^{13}C: 15.84 ppm (a), 64.392 ppm (b).

^{31}P: 59.28ppm (s, P)

The ESI-MS (negative ion mode) spectrum shows a parent peak at 169 m/z which is consistent with the proposed compounds identity. The ionised form of PA has a MW=169 g/mol.

2.3 Metal binding characterization by NMR

2.3.1 General overview

High resolution NMR can provide extremely useful information about the interaction of metal ions with the pesticide and its hydrolysis products by observing changes in the chemical environment of specific nuclei, for example proton and phosphorus nuclei. All spectra were taken on a Bruker Advance 300 spectrometer equipped with a ^{31}P probe. Phosphorus spectra were referenced to an external standard of 85% H_3PO_4. This was done by suspending a capillary tube containing phosphoric acid in the middle of the 5-mm NMR tube (H_3PO_4 has a chemical shift of 0.00 ppm in ^{31}P NMR). ^{1}H NMR spectra were referenced using an internal standard of residual solvent protons from methanol (3.34ppm).

2.3.2 Preparation of stock solutions for NMR study

Stock solutions of diazinon (1.0M), PA (1.0M) and PY (0.5M) were made up in deuturated methanol. The solubility of each metal was assessed in the co-solvent (70% CD_3OD-30% D_2O) and stock solutions of the following were prepared: $AgNO_3$ (0.5M, 0.2M, 0.02M), $Cu(NO_3)_2$ (0.5M), $Cd(NO_3)_2$ (0.5M) and $Hg(Cl)_2$ (0.01M, 0.1M). All NMR tubes were made up to 0.6 ml using the pertinent co-solvent giving a final solvent ratio in the NMR tubes for the diazinon and PA experiments of 70.5% CD_3OD -29.5% D_2O. In the metal binding studies with pyrimidinol, 20ul of 0.5M PY was used, the final solvent mix in the NMR tube is 71.0% CD_3OD -29.0% D_2O. ^{31}P and ^{1}H NMR spectra of diazinon and PA and ^{1}H NMR spectrum of PY were obtained in the co-solvent and used as standard reference values for proton and phosphorus chemical shifts for future

comparison on addition of metal ions. Varying volumes of the substrate and metal stock solutions were then used to prepare the individual NMR tubes to deduce the interactions between the different metals and substrates. Silver nitrate NMR solution preparation are outlined below with all other metal ion NMR solutions described in Appendix A2.

2.3.2.1 Silver nitrate NMR solutions

Table 2.3.1 ^{1}H and ^{31}P NMR chemical shift changes in the presence of Ag^{+}. Concentrations of O,O diethyl phosphorothioic acid, pyrimidinol and Ag^{+} in each NMR tube.

NMR tube Number	$[Ag^{+}] \times 10^{-2}$ Mol L^{-1}	$[PA] \times 10^{-2}$ Mol L^{-1}	Ratio Ag^{+}/PA	NMR tube Number	$[Ag^{+}] \times 10^{-2}$ Mol L^{-1}	$[Py] \times 10^{-2}$ Mol L^{-1}	Ratio Ag+/Py
1	0.33	1.67	0.2	1	0.167	1.67	0.1
2	0.67	1.67	0.4	2	0.833	1.67	0.5
3	1.33	1.67	0.8	3	1.67	1.67	1
4	1.67	1.67	1	4	4.17	1.67	2.5
5	4.17	1.67	2.5	5	8.33	1.67	5
6	8.33	1.67	5	6	16.7	1.67	10
7	16.7	1.67	10	7	41.7	1.67	25
8	41.7	1.67	25	-	-	-	-

[PA] = concentration of O, O diethyl phosphorothioic acid, Py = concentration of pyrimidinol.

Preliminary NMR experiments of diazinon in the presence of Ag^{2+} indicated hydrolysis had occurred by the appearance of additional peaks in the spectra. The aqueous hydrolysis of diazinon was therefore studied using ^{31}P and ^{1}H NMR over four ratios of $Ag(NO_3)$. The experiments were performed to determine the following; any phosphorus containing products of the reaction; to investigate silver binding to diazinon moiety itself and to show if changes in any nuclei in the products had occurred. The NMR tubes were

prepared by first adding the required quantity of metal solution to the co-solvent, followed by the required aliquot of diazinon. The first spectrum was recorded immediately following the addition of diazinon. Subsequent spectra were taken at specific predetermined time intervals (1 hour).

Table 2.3.2 ^{1}H and ^{31}P NMR study of the aqueous hydrolysis of diazinon in the presence of Ag^{+}. Concentrations of diazinon and Ag^{+} in each NMR tube.

NMR tube Number	$[Ag^{+}] \times 10^{-2}$ Mol L^{-1}	$[D] \times 10^{-2}$ Mol L^{-1}	Ratio Ag^{+}/D
1	0.67	1.67	0.4
2	1.67	1.67	1.0
3	16.7	1.67	10
4	41.7	1.67	25

The accelerated hydrolysis under the NMR conditions meant it was difficult to ascertain silver binding to diazinon at elevated ratios. Therefore to deduce these interactions a separate set of experiments were performed with just methanol as solvent to eliminate the effect of hydrolysis. The ratio range was reduced due to the limited solubility of Ag^{+} in methanol (0.2M).

Table 2.3.3 ^{31}P chemical shift of diazinon in the presence of Ag^{+} in CD_3OD. Concentrations of diazinon and Ag^{+}in each NMR tube.

NMR tube Number	$[Ag^{+}] \times 10^{-2}$ Mol L^{-1}	$[D] \times 10^{-2}$ Mol L^{-1}	Ratio Ag^{+}/D
1	0.33	1.67	0.2
2	0.83	1.67	0.5
3	1.67	1.67	1
4	3.33	1.67	2
5	6.67	1.67	4

2.3.2.2 Copper NMR solutions

The paramagnetic nature of Cu^{2+} makes the use of ^{1}H NMR in identifying changes in the chemical environment of nuclei difficult to assess. Paramagnetism itself causes line broadening and hyperfine shifts of proton signals in the vicinity of where the paramagnetic element is bound. ^{31}P was used in assessing Cu^{2+} binding to the PA moiety, whilst for pyrimidinol ^{1}H was used. Appendix A2 details the copper solutions prepared for NMR metal binding studies and hydrolysis experiments.

2.3.2.3 Cadmium NMR solutions

Analogous to Cu^{2+} and Ag^{+} the chemical shift of the nuclei of PA and PY were examined over a range of Cd^{2+}/substrate ratios as shown in Appendix A2. The hydrolysis of diazinon in the presence of Cd^{2+} was studied using ^{31}P and ^{1}H NMR at the highest ratio of Cd to diazinon (25 times) only. Lower ratios were not evaluated as no hydrolysis was observed at the uppermost concentration over four hours. Similarly the effect of Cd^{2+} binding to diazinon itself was assessed over a range of Cd^{2+}/D ratios in CD_3OD.

2.3.2.4 Mercury (Hg^{2+}) NMR solutions

Due to solubility limits of mercury in the chosen co-solvent the stock solutions of $Hg(Cl)_2$ prepared were 0.01M and 0.1M respectively. Varying volumes of stock metal solutions along with substrate were then added to make each NMR tube. A similar set of experiments were conducted in the presence of Hg^{2+} as per other metal cations.

2.4 Metal binding characterisation by Mass Spectrometry

2.4.1 General overview

The technique of Electrospray Mass Spectrometry was employed to investigate metal binding to the organophosphorus pesticide diazinon and it hydrolysis products. Electrospray ionisation is ideal for work where it is necessary to view the molecular ion or complex(s) formed between the metal ion and substrate due to its soft ionisation. All mass spectra were obtained using ESI-QqTOF technology on a QSTAR XL QqTOF mass spectrometer. Initial complexation and some fragmentation of the transition metals bound to the pesticide was undertaking in the ionisation source itself. This was effected by initially spraying the substrate molecules into the ionisation source at a flow rate of 6 μL/min. A second flow of metal solutions was then introduced into the ionisation source giving the best opportunity to view the complexed ion. Preliminary spectra were used to confirm metal binding to the pesticide by observing specific m/z ratios along with the isotopic patterns of the relevant metal.

Low energy CID MS/MS experiments were then performed on the complexed ion. The preliminary spectra confirm metal binding to the pesticide; however succeeding CID experiments gave definitive structural information of where exactly metal binding is occurring. Further evidence of metal binding to specific sites on the pesticide was attained by observing complexation between the metal ions and the hydrolysis products of PA and PY.

2.4.2 ESI-MS substrate solutions

Stock solutions of 1.028mM diazinon and 1.18mM O,O diethyl phosphorothioic acid were prepared in methanol (HPLC grade, Fischer). Subsequently 20µL of each was diluted to 2ml with methanol giving final concentrations of 10.28µM and 11.8µM respectively. A stock solution of 10mM pyrimidinol was prepared in methanol with resultant dilution to 10µM by taking 10µl of stock solution and diluting to 10ml. Typically Electrospray is carried out in acidic conditions to aid protonation for positive ion mode, therefore all substrate solutions were acidified to pH of 4 with 1.0 mol L^{-1} HCL and 1.0 mol L^{-1} NaOH.

2.4.3 ESI-MS metal solutions

A stock solution of 10 mM $AgNO_3$ was prepared in a co-solvent of 70%MeOH-30%H_2O. Concentrations of 1000 µM, 100 µM, and 10 µM in the co-solvent were prepared by successive 100 µL dilutions to 1ml. This solvent system was used as it corresponds to that used in the NMR study of metal binding. The different silver concentrations allow binding with diazinon to be observed over ratios of ≈ 1:1, 10:1 and 100:1. All other metals ion solutions were prepared as above.

2.5 Kinetic studies of the hydrolysis of diazinon in the absence and presence of metal ions.

2.5.1 General

Kinetics was followed by UV-VIS spectrophotometry using A Hewlett-Parkard- 8425A. Stock solutions (1.1×10^{-2}M) of diazinon, PA and PY were prepared in HPLC grade Methanol. Beer Lambert plots for diazinon and PY were carried out in neutral, acidic and basic conditions to calculate the molar absorbtivities for both substrate and products in the various media under investigation. This allowed the assessment of substrate and product spectral overlap with subsequent identification of suitable peaks to follow in the absorption spectrum during the hydrolysis. Ensuing from these observations a base and acid profile of the hydrolysis of diazinon in the absence of metal ions was performed over an appropriate range of OH^- and H^+ concentrations. This was done by following the appearance of product peaks which had good spectral separation from diazinon absorbances. All kinetics in the profile studies were carried out under pseudo first order conditions where the base or acid concentration was in large excess of substrate concentration. All kinetic experiments were performed at ambient temperature, 22.0 ± 0.5°C.

2.5.2 Kinetic methods in the absence of metal ions.

Initial repetitive scanning experiments of the hydrolysis of diazinon was carried out under basic and acidic conditions between 200-700nm to monitor for the appearance of products and the disappearance of diazinon. In the basic region the appearance of a peak at 266nm was used to kinetically monitor the hydrolysis of diazinon in basic media. This

peak is a result of an electronic transition from the aryl oxide form of PY arising in basic media, with a resultant bathochromic shift from that observed in neutral media (264nm). In the case of the acidic profile a second absorption belonging to PY at 230-232nm (dependant on acid concentration) was followed.

The hydrolysis reactions in NaOH and HCl were carried out in pseudo first order conditions and in triplicate. The pseudo first order rate constants were calculated for 3 half live ($3t_{1/2}$) with the A_∞ taken after 10 half lives. This was done by plotting $-\ln(A_\infty - A_t)$ against time with the slope equal to $k_{obs}(s^{-1})$. A_t is the absorbance at time t. A subsequent plot of k_{obs} versus [NaOH] or [HCl] yields the second order rate constant k_2 ($M^{-1}s^{-1}$). A typical UV quartz used in the base and acid profile studies is made by dispensing 15µL of diazinon (1.1×10^{-2}M) using a 25µL gas tight syringe, giving a final concentration of 8.25×10^{-5}M diazinon in 2ml . The requisite volume of co-solvent is then dispensed into the UV quartz cell to ensure a final volume of 2ml. The solvent system employed in the same as that utilised in the NMR and MS studies, 70%CH_3OH/30%H_2O. Finally the required volume of acid or base is added using gas tight syringes, followed by thorough mixing and UV analysis.

The kinetics methods used for the analysis of the hydrolysis of diazinon in the presence of metal ions subsequently found pH 10 to be the optimum base conditions for such runs. At higher pH's metal solubility problems arose for some metals due to speciation and the formation of insoluble metal hydroxides in basic media. It was therefore necessary to use the method of initial rates to re-examine the base profile and the effect of metal ions at pH 10, as pseudo first order conditions do not prevail in these circumstances (NaOH

concentration 0.0001M is not 28 times greater than diazinon=8.25 x 10^{-5}M). A comparison and validation of the data obtained under pseudo first order conditions and that acquired from the initial rate method was made.

2.5.3 Kinetic methods in the presence of metal ions

The solubility of the different metals in base was initially investigated over a range of pH to observe any effects on the spectrum i.e. any insolubility issues. The highest pH where solubility was not a factor for any metal was found to be pH 10. In-addition, prior to analysis of the hydrolysis of diazinon in the presence of metal ions, any changes in λmax of the product peaks in the presence of metals was investigated. This was done by running PY in equivalent concentrations of metal to be used in the hydrolysis experiments and recording any shifts in the position of the spectral peak due to metal binding. The observed λmax in the presence of metal was then followed kinetically during the hydrolysis. The method of initial rates was used to show the effect of metals on the rate of hydrolysis as pseudo first order conditions do not prevail at this pH. Stock metal solutions (1.1 x 10^{-2}M) were made up in co-solvent. A typical UV run consisted of dispensing 15µL of diazinon into a clean UV quartz cell. The requisite volume of co-solvent was then dispensed followed by 20 µL of 0.01M NaOH. Finally the necessary volume of metal was dispensed using gas tight syringes to give a final volume of 2 ml. Typical metal/substrate ratios used were 10:1 and 25:1 with all runs carried out in triplicate.

CHAPTER 3 Results section

3.1 Nuclear magnetic resonance study

The role metal ions play in the hydrolytic degradation of the organophosphorus pesticide diazinon was explored using Nuclear Magnetic Resonance. The chemical environment of specific nuclei of diazinon and its hydrolysis products, PA and PY, were observed both in the absence and presence of a range of metal ions, including silver, copper, mercury and cadmium. The experiments provide essential information about changes in the chemical environment of ^{1}H and ^{31}P nuclei in the presence of these metal ions.

The parameters used in the NMR experiments including sample preparation, ratio of metal to substrate and instrumentation are outlined in the Experimental Section. The chemical shift changes induced by the addition of metal ions are reported in parts per million (ppm) relative to standard values. These values are calculated by subtracting the ppm value obtained in the absence of metal ions from that obtained in the presence of metals. The chemical shift changes observed upon addition of metal ions may be attributed to a change in the electron screening of specific nuclei or more simply to a change in the chemical environment of the nuclei under observation. Structural relationships and interactions between the substrates and the metal ions can be proposed from such observations (*vide infra*).

3.1.1 Standard chemical shift data in the absence of metal ions

^{31}P and ^{1}H NMR spectra of diazinon, O,O diethyl phosphorothioic acid and ^{1}H NMR spectra of pyrimidinol were obtained in the pertinent co-solvent system and used as standard chemical shift values for future comparison with spectra recorded after addition of metal ions. The standard chemical shift data in ppm, in addition to the lettering system used for each substrate are shown in Tables 3.1.1-3.1.5. Note that the protons are labeled in PA based on the system used for diazinon.

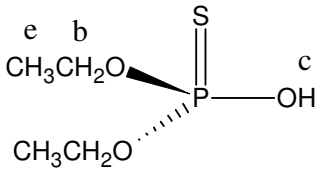

O,O diethyl phosphorothioic acid (PA)

Table 3.1.1 ^{31}P chemical shift for PA in the absence of metal ions (70%CD_3OD-30%D_2O v/v).

Phosphorus	Chemical shift (ppm)	Multiplicity
(δ) ^{31}P	60.165	Singlet

Table 3.1.2 ^{1}H Chemical shifts for PA in the absence of metal ions (70%CD_3OD-30%D_2O v/v).

Proton	Chemical shift (ppm)	Multiplicity
(δ) $^{1}H^{b}$	4.048	Multiplet
(δ) $^{1}H^{e}$	1.306	Triplet

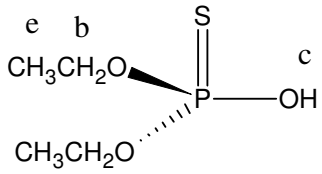

O,O diethyl phosphorothioic acid (PA)

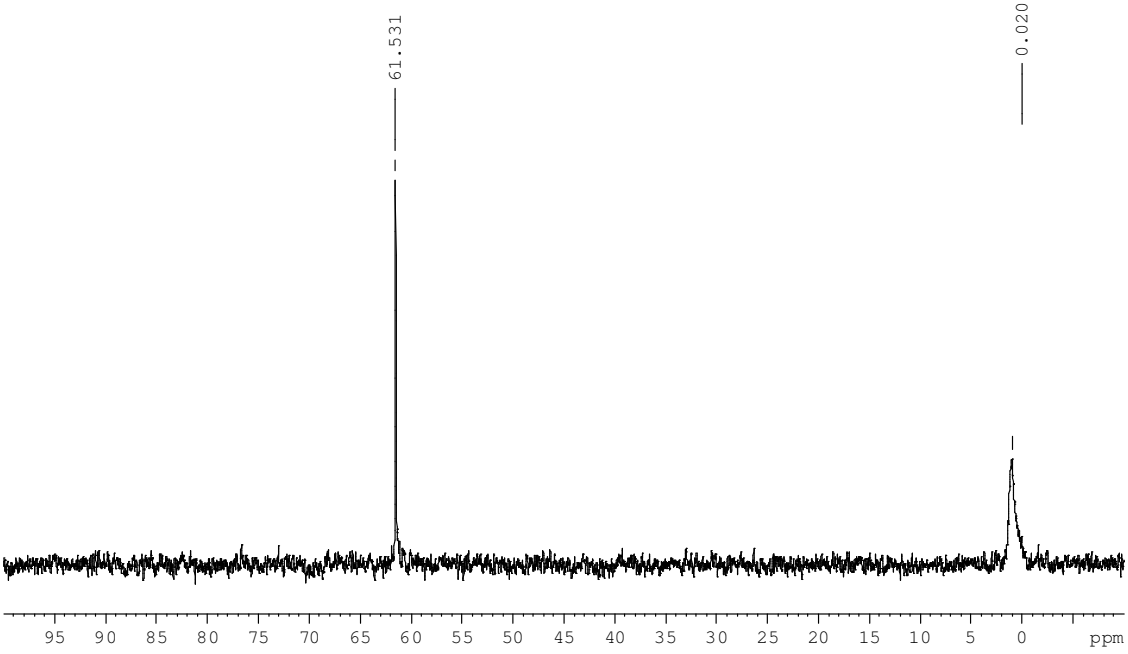

Figure 3.1.1 Standard ^{31}P spectrum of PA in the absence of metal ions (70%CD_3OD-30%D_2O v/v).

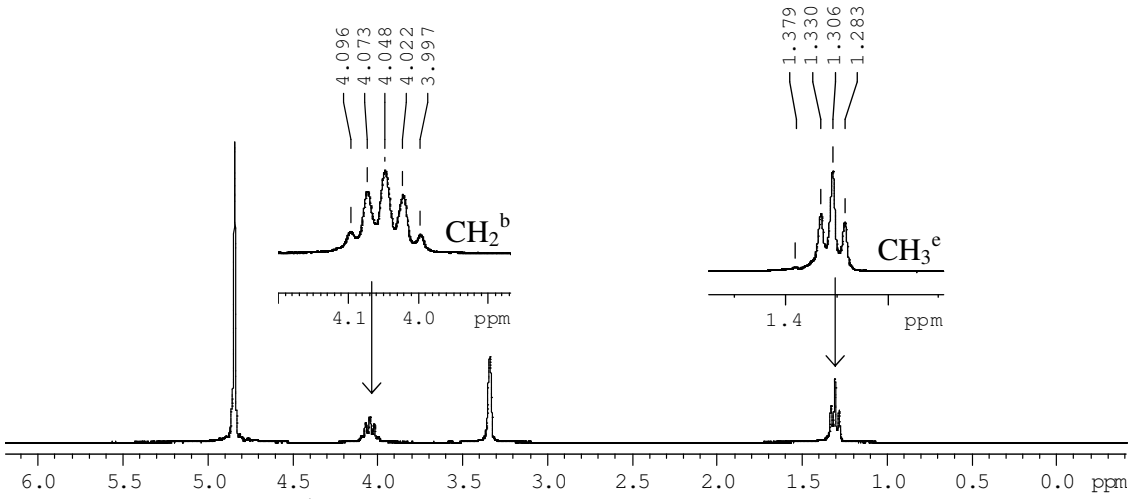

Figure 3.1.2 Standard ^{1}H spectrum of PA in the absence of metal ions (70%CD_3OD-30%D_2O v/v).

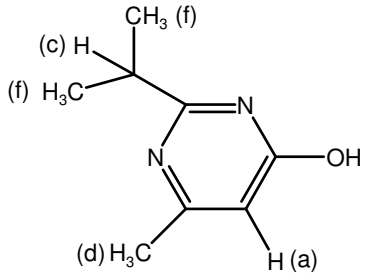

Pyrimidinol (PY)

Table 3.1.3 ^{1}H chemical shifts for PY in the absence of metal ions (70% CD_3OD-30% D_2O v/v).

Proton	Chemical shift (ppm)	Multiplicity
(δ) $^{1}H^{a}$	6.208	Singlet
(δ) $^{1}H^{c}$	2.936	Multiplet
(δ) CH_3^{d}	2.322	Singlet
(δ) CH_3^{f}	1.329	Doublet

Protons are labeled in the same way as in diazinon.

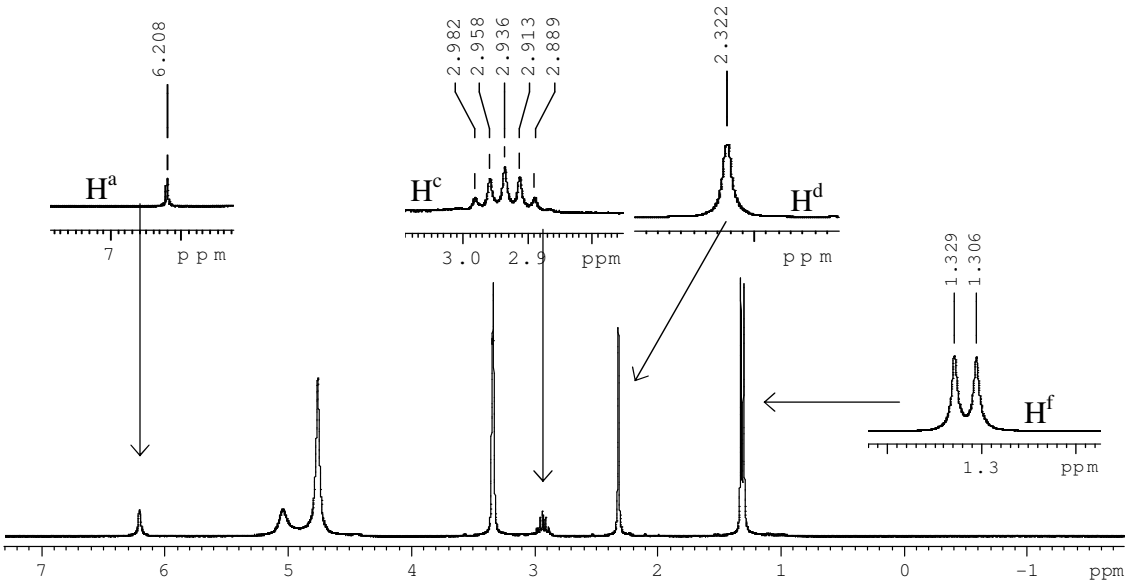

Figure 3.1.3 Standard ^{1}H spectrum of PY in the absence of metal ions (70% CD_3OD-30% D_2O v/v).

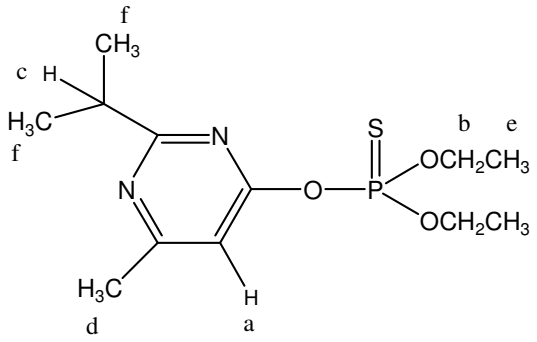

diazinon

Table 3.1.4 ^{31}P chemical shift for diazinon in the absence of metal ions (70% CD_3OD-30% D_2O v/v).

Phosphorus	Chemical shift (ppm)	Multiplicity
(δ) ^{31}P	61.531	Singlet

Table 3.1.5 ^{1}H chemical shift data for diazinon in the absence of metal ions (70% CD_3OD-30% D_2O v/v).

Proton	Chemical shift (ppm)	Multiplicity
(δ) $^{1}H^{a}$	6.891	Singlet
(δ) $^{1}H^{b}$	4.371	Mulitplet
(δ) CH_3^{c}	3.129	Multiplet
(δ) CH_3^{d}	2.538	Singlet
(δ) CH_3^{e}	1.399	Triplet
(δ) CH_3^{f}	1.327	Doublet

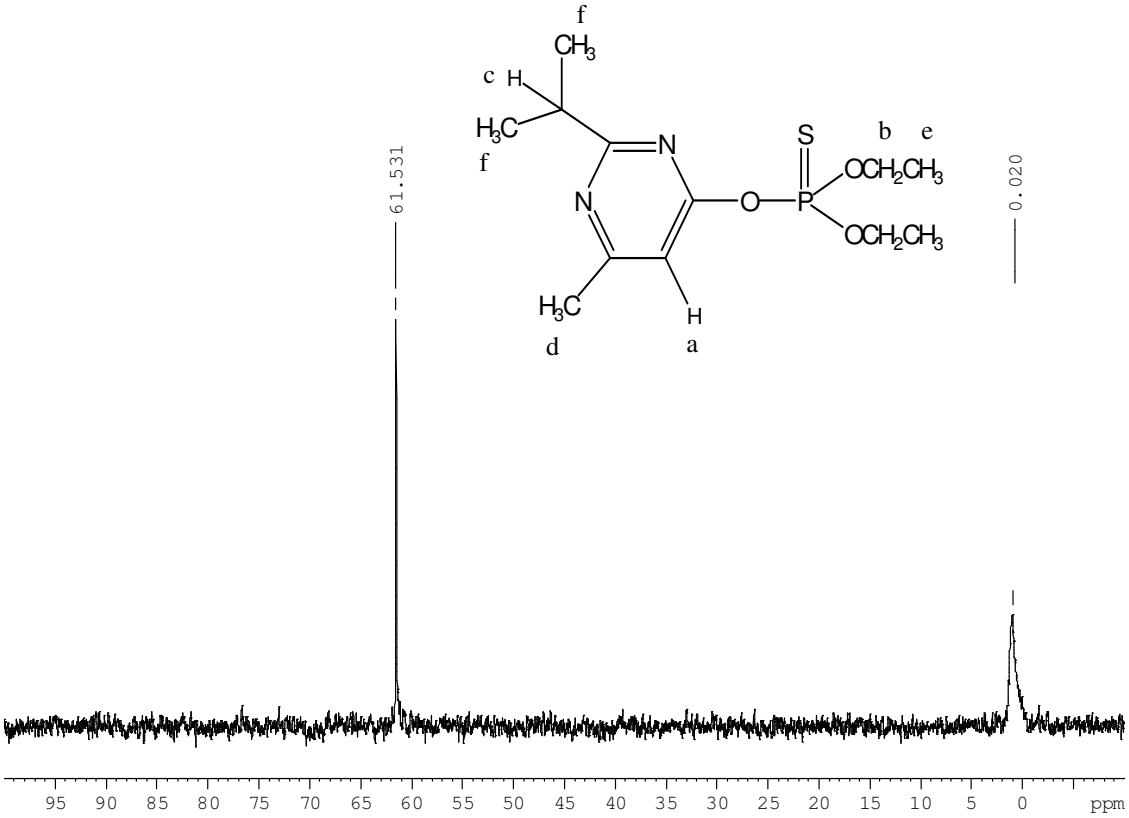

Figure 3.1.4 Standard ^{31}P spectrum of diazinon in the absence of metal ions (70%CD_3OD-30%D_2O v/v).

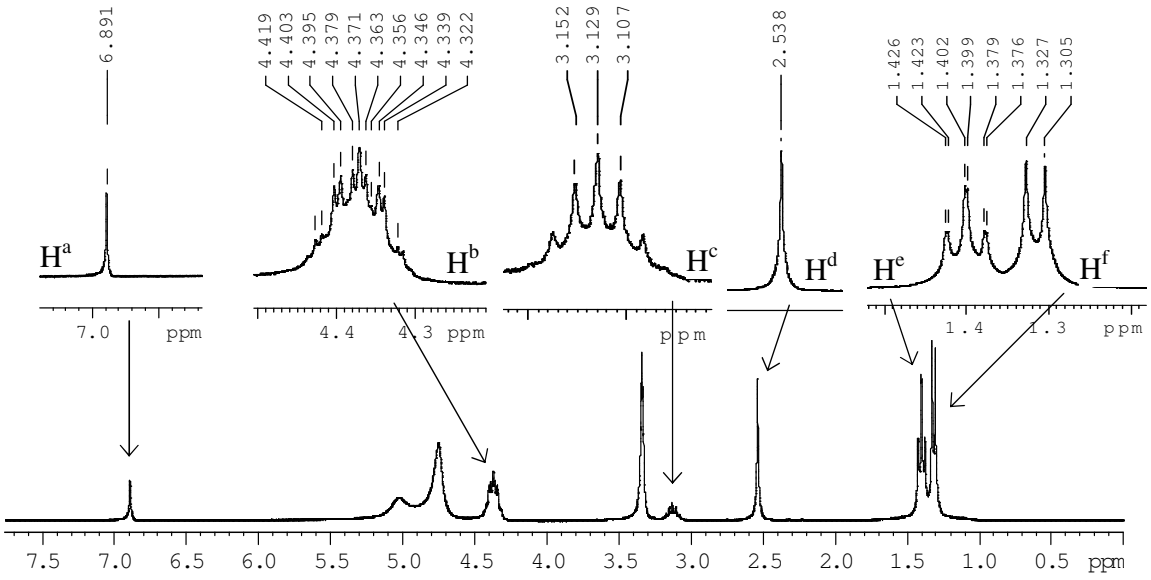

Figure 3.1.5 Standard ^{1}H spectrum of diazinon in the absence of metal ions (70%CD_3OD-30%D_2O v/v).

3.1.2 O,O diethyl phosphorothioic acid (PA) metal ion NMR binding study

NMR studies were performed on PA in presence of various concentrations of metal ions to help elucidate the interactions between these catalytic ions and the PA moiety. This will determine whether specific metal ions bind with the sulfur ligand causing a change in the electron density around the phosphorus nuclei. This decrease in the electron density around the phosphorus nuclei makes it more susceptible to nucleophilic attack, consequently accelerating the rate of hydrolysis. It must be noted here that this is just one possible mechanism of how the rate of hydrolysis may be accelerated, with additional possibilities being binding at nitrogen or interplay of binding at both sites (chelation).

3.1.2.1 Studies in the presence of silver nitrate (Ag^+)

Both ^{31}P and ^{1}H NMR of PA were taken in the presence of increasing Ag^+ concentrations, with the chemical shift data acquired indicating degrees of electron shielding in comparison to PA in the absence of Ag^+ ions. Appendix A3, Tables A3.1 and A3.2 lists the concentrations, chemical shifts observed and the change in chemical shift (ppm) induced due to Ag^+ binding with PA. Overlay of ^{31}P and ^{1}H spectra in the presence of Ag^+ are shown in Figures 3.1.6 and 3.1.7.

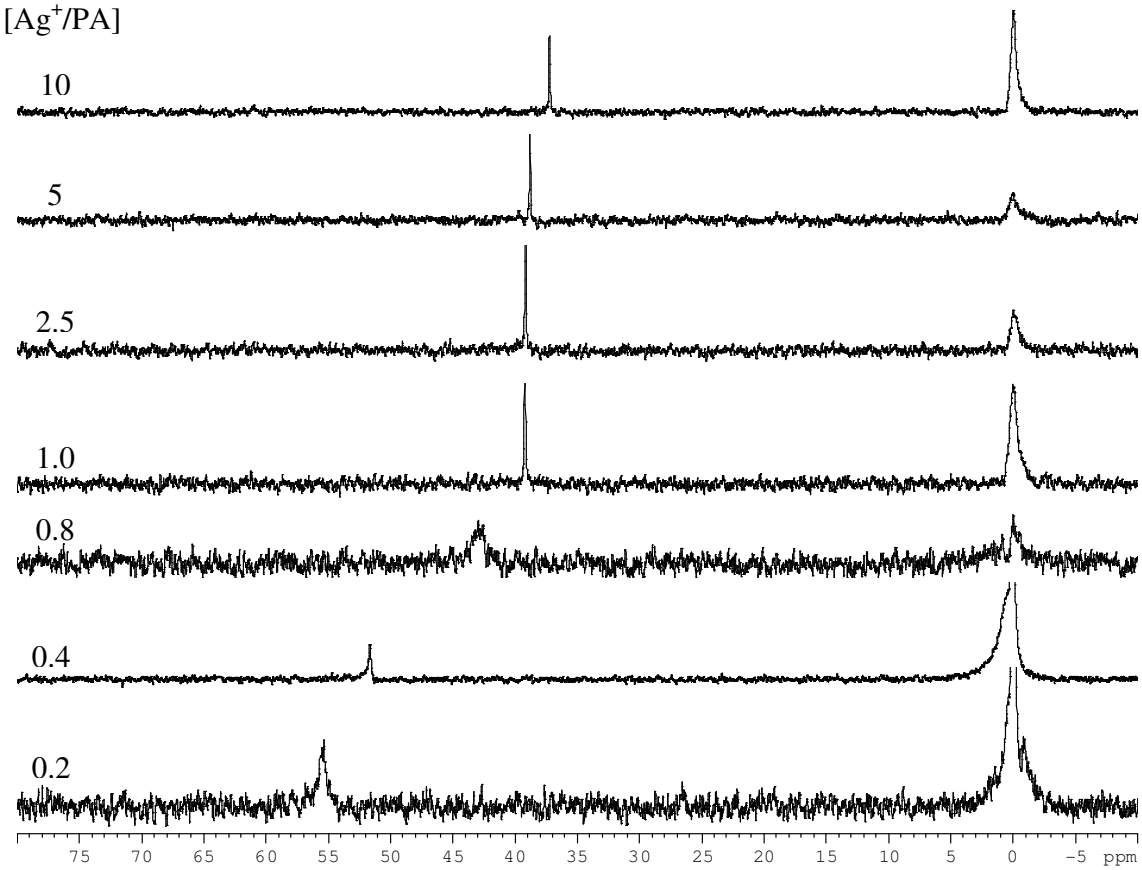

Figure 3.1.6 ^{31}P NMR spectra depicting the chemical shift change of PA phosphorus peak in the presence of increasing Ag^+ concentrations (70%CD_3OD-30%D_2O v/v).

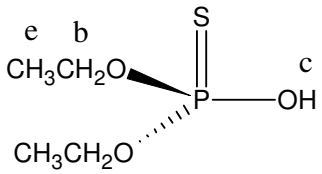

O,O diethyl phosphorothioic acid (PA)

The result with ratio 0.4 indicates a dynamic equilibrium between bound and unbound Ag^+ ions on the NMR time-scale. If strong binding between PA and the metal ion existed one would expect to see two peaks present in the phosphorus NMR, one for unbound PA at 60.165 ppm and a second peak shifted upfield due to metal coordination. However only one peak is observed.

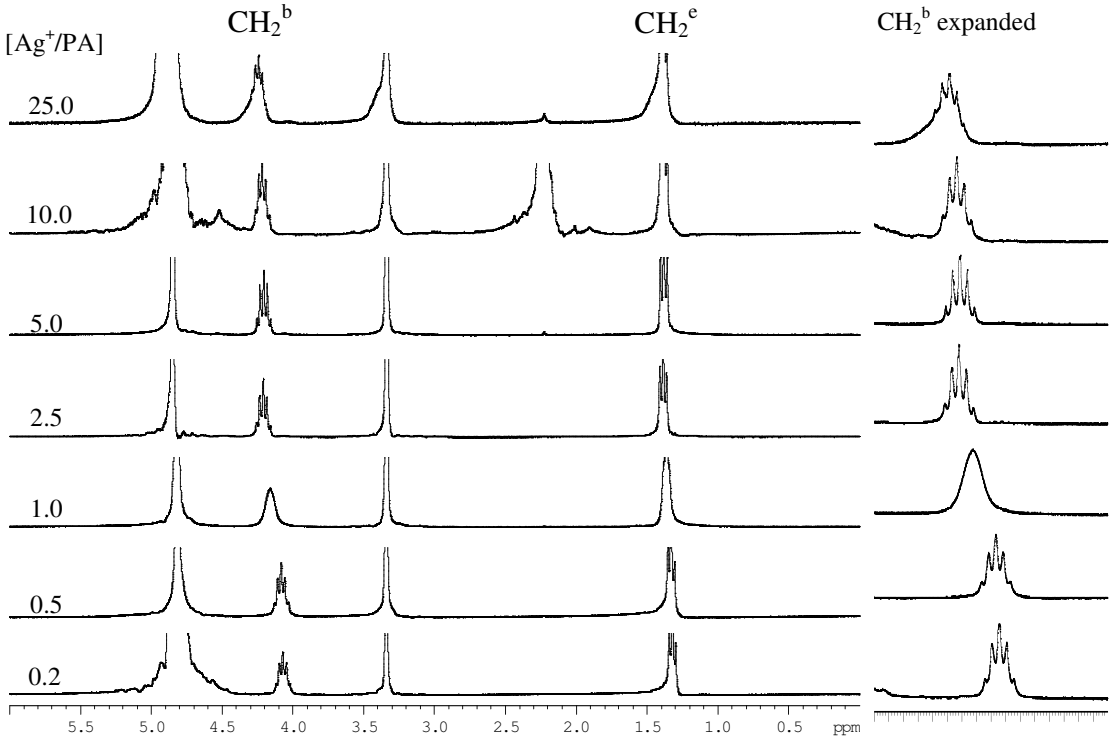

Figure 3.1.7 ^{1}H spectra depicting the chemical shift change of PA proton peaks with increasing Ag^{2+} concentrations (with expanded CH_2^b peaks).

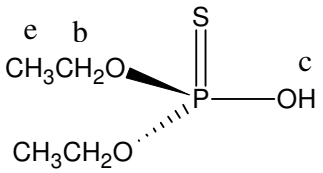

O,O diethyl phosphorothioic acid (PA)

The chemical shift changes induced by the binding of Ag^+ to the sulfur ligand are shown in Figures 3.1.8 and 3.1.9. The figures clearly show that as the concentration of Ag^+ is increased a concomitant up-field shift in the phosphorus nuclei is observed, indicating a change in its chemical environment. This up-field shift provides clear evidence to support Ag^+ binding to sulfur with the resultant effect on the electronic environment of the phosphorus nuclei as shown in Figure 3.1.6. "Soft" metal ions such as Ag^+ are known to have a strong affinity for ligands such as sulfur. This change in the chemical environment is also observed at the more distant CH_2 protons as shown in Figure 3.1.9.

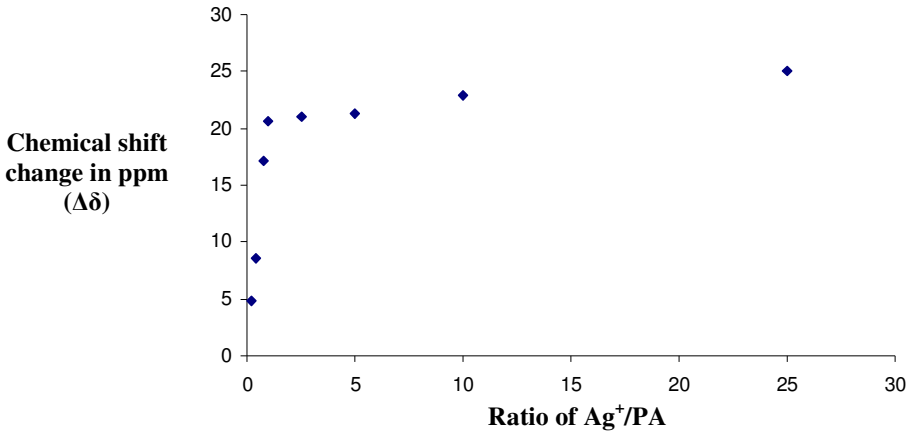

Figure 3.1.8 Effect on the chemical shift of the phosphorus nuclei of PA upon addition of increasing concentrations of Ag^+.

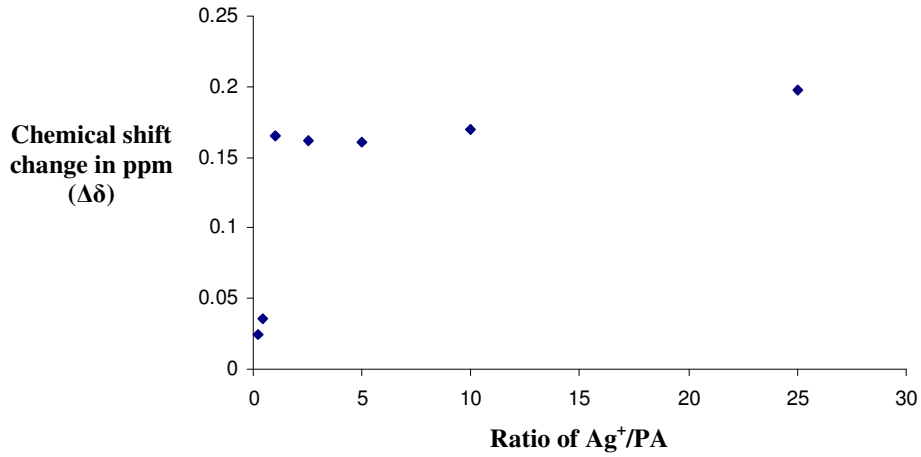

Figure 3.1.9 Effect on the chemical shift change of the CH_2^b protons of PA upon addition of increasing concentrations of Ag^+.

3.1.2.2 Mercuric chloride (Hg^{2+})

The characterisation of Hg^{2+} interaction with PA was effected by investigating the ^{1}H and ^{31}P chemical shifts of PA with increasing Hg^{2+} concentrations. Overlay of ^{1}H and ^{31}P spectra of PA in the presence of Hg^{2+} are shown in Figures 3.1.10 and 3.1.11 with numerical data shown in Appendix 3 (Tables A3.3 and A3.4). Analogous to Ag^{+} ions, the appearance of only one phosphorus peak at the lower ratios indicates a dynamic equilibrium between bound and unbound Hg^{2+} ions.

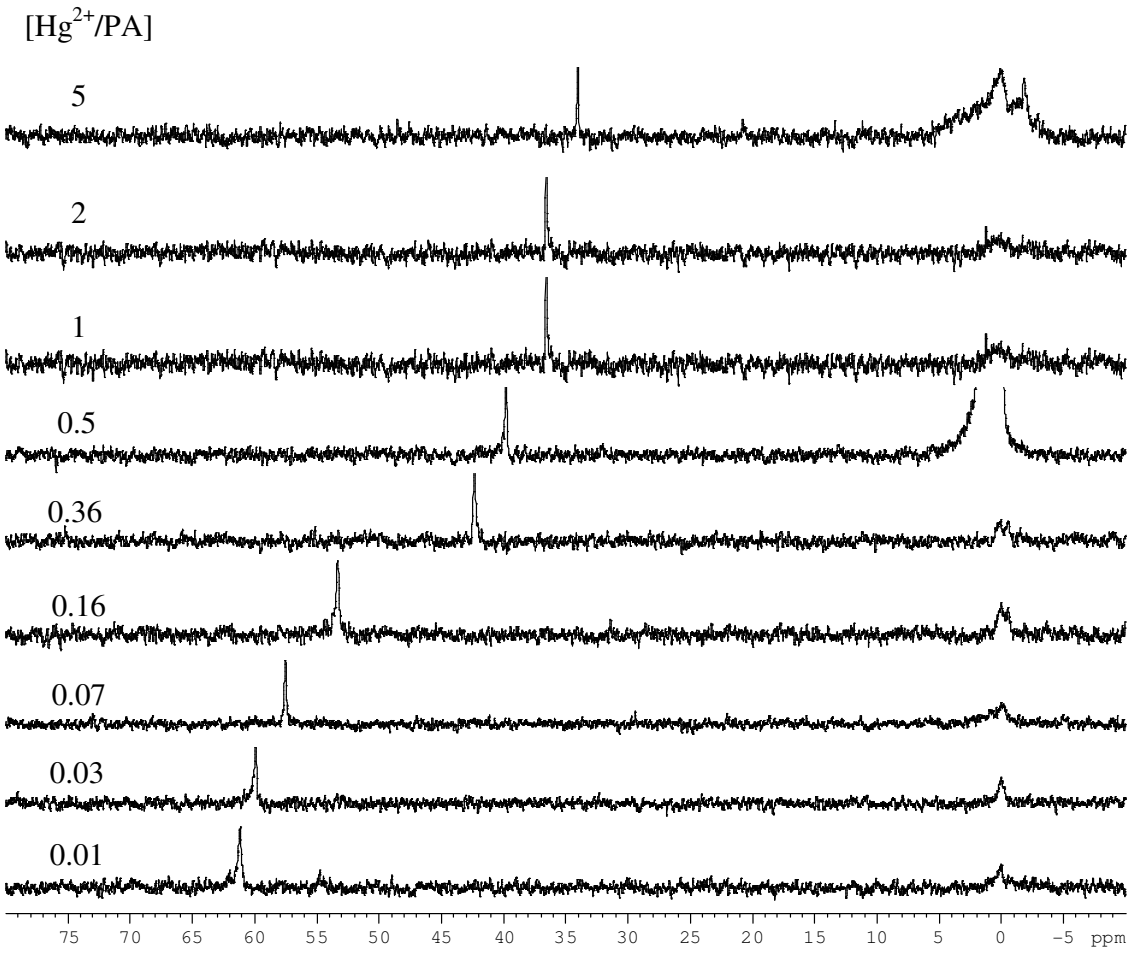

Figure 3.1.10 ^{31}P NMR spectra depicting the chemical shift change ($\Delta\delta$) of PA phosphorus peak in the presence of increasing Hg^{2+} concentrations (70% CD_3OD-30% D_2O v/v).

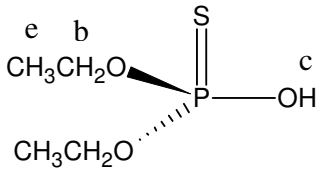

O,O diethyl phosphorothioic acid (PA)

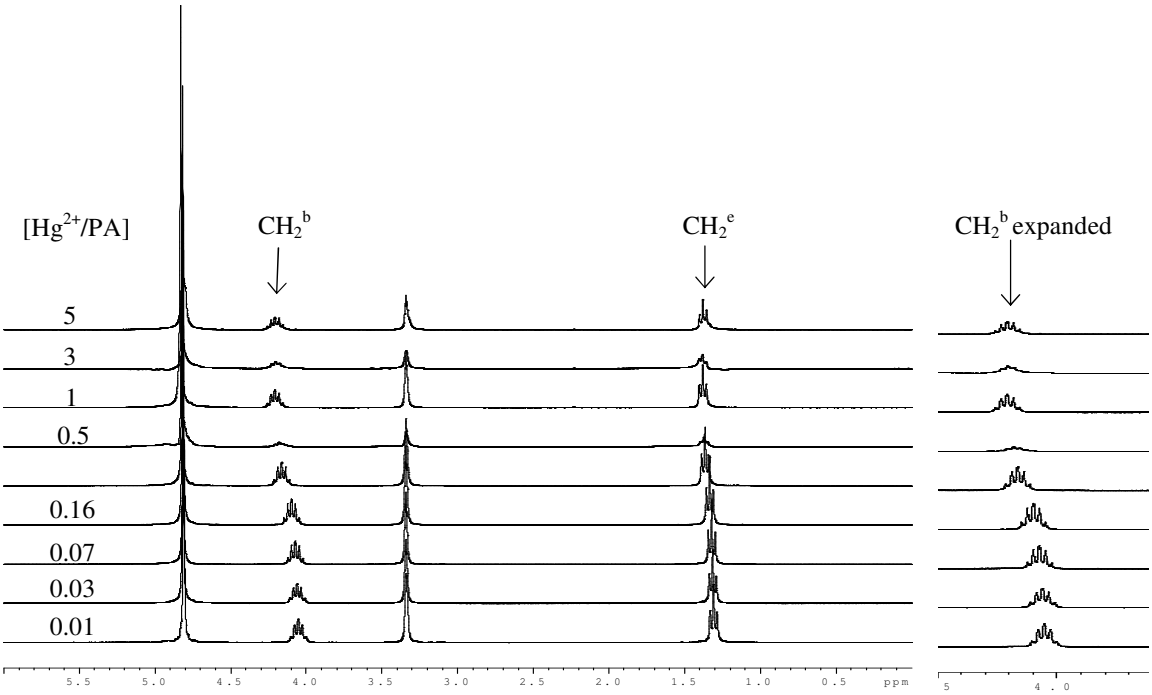

Figure 3.1.11 ^{1}H spectra depicting the chemical shift change of PA proton peaks with increasing Hg^{2+} concentrations (with expanded CH_2^{b} peaks).

The chemical shift changes observed for both the proton and phosphorus NMR signals of PA upon addition of Hg^{2+} ions gives direct spectroscopic evidence of Hg^{2+} interaction with the sulfur ligand. As with Ag^{+} there is a concurrent up-field shift of similar magnitude in the position of the PA phosphorus nuclei as the concentration of Hg^{2+} is increased. This is shown graphically in Figures 3.1.12 and 3.1.13.

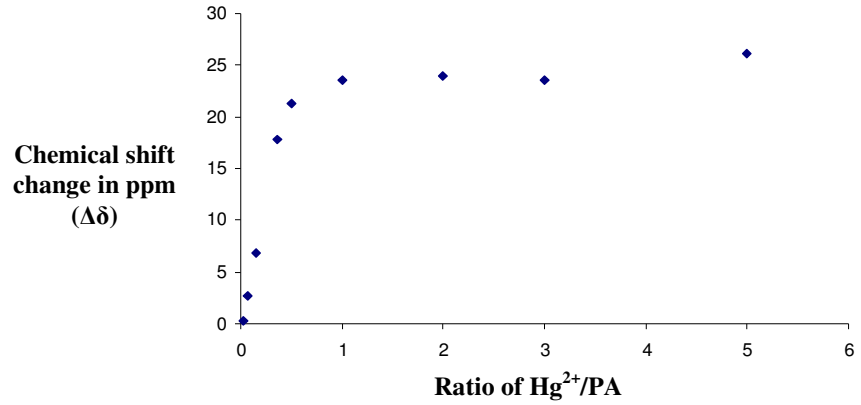

Figure 3.1.12 Effect of the chemical shift of the phosphorus nuclei upon addition of increasing concentrations of Hg^{2+}.

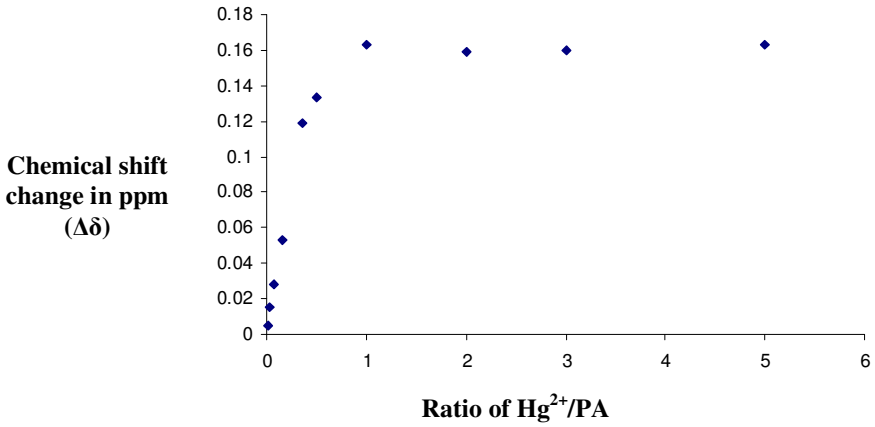

Figure 3.1.13 Effect on the chemical shift of the CH_2^b protons of PA upon addition of increasing concentrations of Hg^{2+}.

3.1.2.3 Cadmium nitrate (Cd^{2+})

The interaction of Cd^{2+} with PA was studied using ^{1}H and ^{31}P spectroscopy. The effect of Cd^{2+} binding on the chemical environment of the phosphorus and proton nuclei of PA is shown in Figures 3.1.14 and 3.1.15.

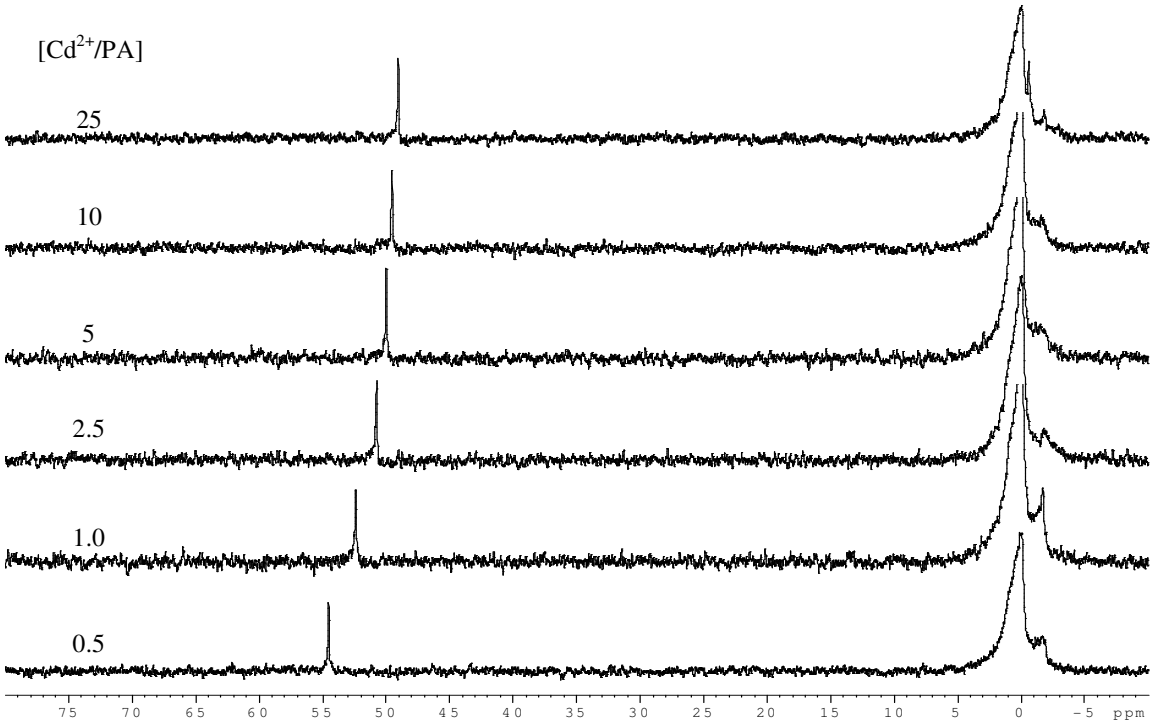

Figure 3.1.14 ^{31}P NMR spectra depicting the chemical shift change ($\Delta\delta$) of PA phosphorus peak in the presence of increasing Cd^{2+} concentrations (70% CD_3OD-30% D_2O v/v).

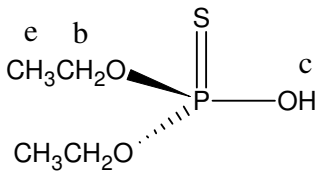

O,O diethyl phosphorothioic acid (PA)

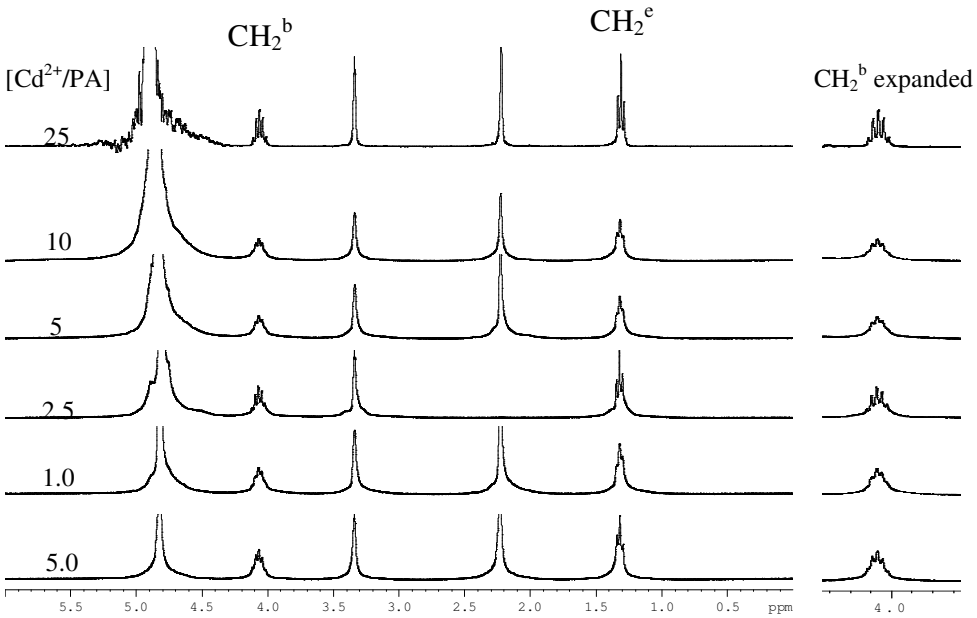

Figure 3.1.15 ^{1}H spectra depicting the chemical shift change of PA proton peaks with increasing Cd^{2+} concentrations (with expanded CH_2 protons).

The corollary of cadmium binding to the sulfur ligand on the chemical shift of phosphorus is shown in Figure 3.1.16. The Figure is different from those obtained for Ag^+ and Hg^{2+} (with $\Delta\delta$ of ca. 25 ppm) , as the maximum chemical shift change observed for a ratio of 25:1 Cd^{2+}/PA is 11 ppm. This dissimilarity of Cd^{2+} in respect of Hg^{2+} and Ag^+ is also apparent in the proton data where a diminished effect is observed on the chemical shift of the CH_2^b protons.

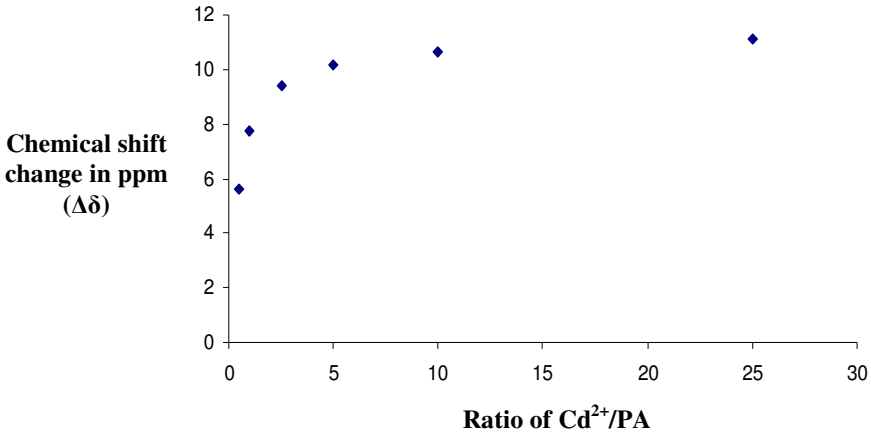

Figure 3.1.16 Effect on the chemical shift of the phosphorus nuclei of PA upon addition of increasing concentrations of Cd^{2+}.

3.1.2.4 Copper nitrate (Cu^{2+})

^{31}P NMR spectra were obtained of PA in the presence of increasing amount of Cu^{2+}. Figure 3.1.17 shows the overlap of spectra obtained.

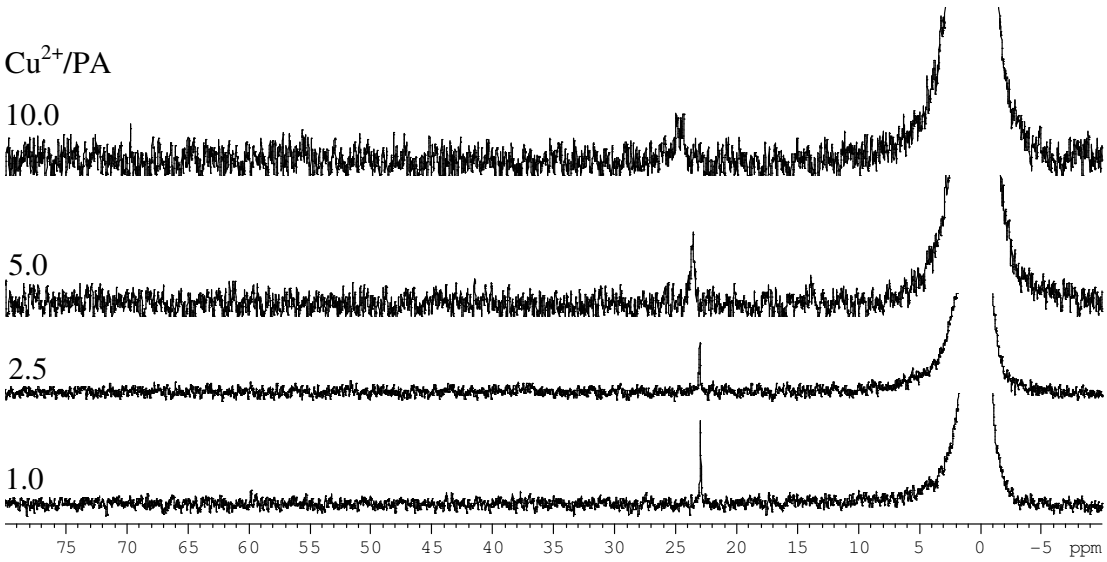

Figure 3.1.17 ^{31}P NMR spectra depicting the chemical shift change of PA phosphorus peak in the presence of increasing Cu^{2+} concentrations (70% CD_3OD-30% D_2O v/v).

In contrast to the previous metals studied, copper does not show a steady up-field shift in chemical shift of the phosphorus nuclei as the concentration of metal is increased. The addition of increasing amounts of copper results in the recurrent appearance of a peak at 23ppm. It is important to note here that during the experiments a colour change was observed with addition of copper solution to PA in the pertinent co-solvent. The colour change was from blue (copper nitrate) to different degrees of green dependent on the amount of copper added. The colour change may indicate a reduction of Cu^{2+} to Cu^{+}, due to the interaction of the metal cation with PA or with the solvent methanol in an oxidation-reduction process.

3.1.3 Pyrimidinol-metal ion NMR binding study

Spectroscopic experiments, specifically ^{1}H, were performed on PY in the presence of metal ions known to promote hydrolysis of organophosphorus pesticides. The NMR experiments will assist in probing any PY-metal interactions through the nitrogens of the ring. The numerical data including concentrations, ratio of metal to PY, observed chemical shifts and changes in chemical shifts induced due to metal binding are shown in Appendix 4 (Tables A4.1 – A4.6).

3.1.3.1 Silver nitrate (Ag^{2+})

^{1}H NMR spectra of PY in the presence of various concentrations of Ag^{+} were obtained and compared to the proton chemical shift values of PY acquired in solution free of metal ions (Table 3.1.3).

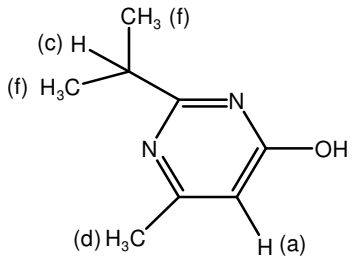

Pyrimidinol (PY)

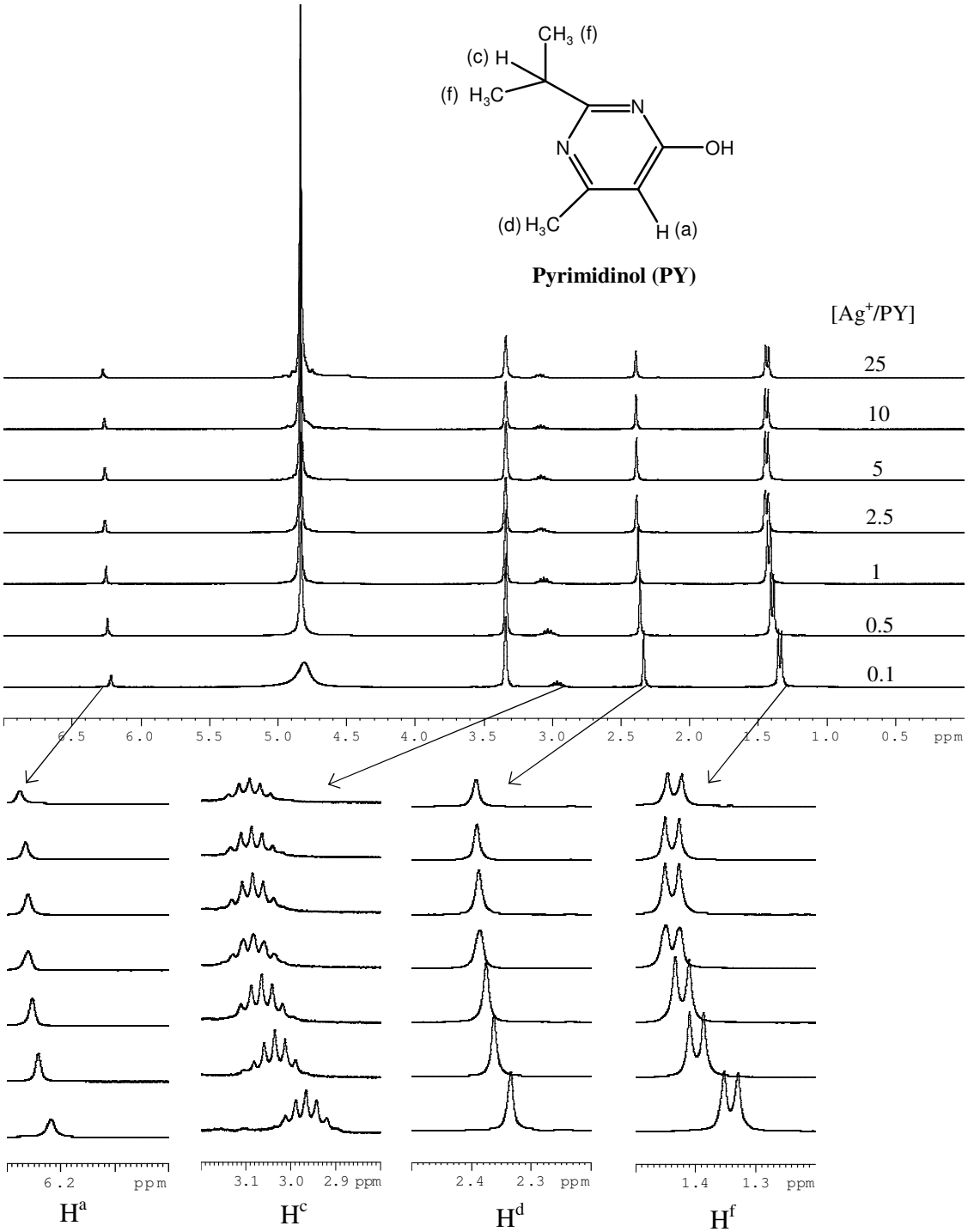

Figure 3.1.18 ^{1}H NMR spectra showing the proton chemical shifts of PY with increasing Ag^{+} concentration, in addition to expanded view of protons (70% CD_3OD-30% D_2O v/v).

The chemical shift induced by binding of Ag^+ to PY is shown below in Figure 3.1.19. The protons most affected are those of the isopropyl group, H^c and H^f, with H^c being the most exposed to the external magnetic field upon Ag^+ binding. This data strongly suggests coordination of Ag^+ to nitrogen, where one would expect the H^c protons to be most affected.

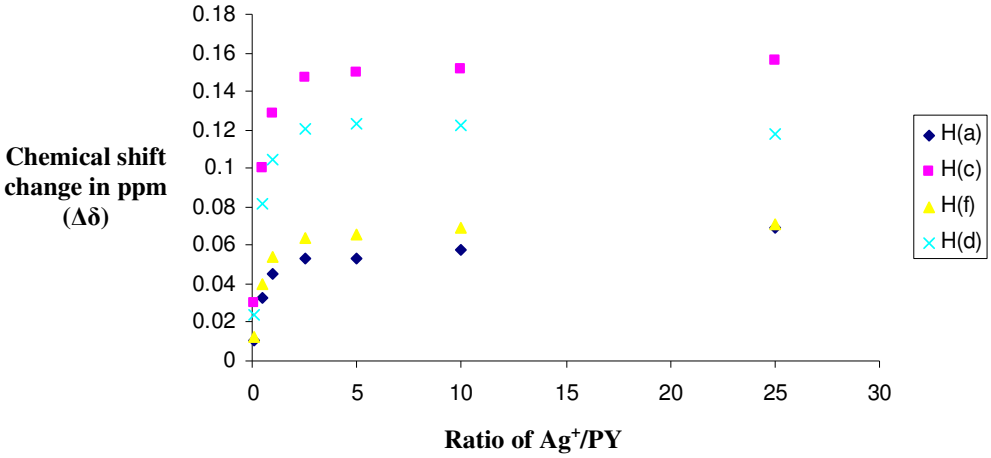

Figure 3.1.19 Effect of various concentrations of Ag^+ on the proton chemical shifts of PY (70% CD_3OD-30% D_2O v/v).

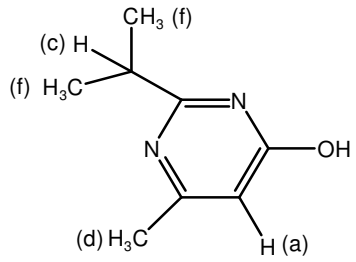

Pyrimidinol (PY)

3.1.3.2 Mercuric chloride (Hg^{2+})

The potential of Hg^{2+} to bind to the nitrogen's of PY was investigated using ^{1}H NMR. Appendix 4 lists the concentrations, chemical shifts observed and the change in ppm induced due to Hg^{+} ion binding. Overlay of ^{1}H spectra in the presence of Hg^{2+} is shown in Figure 3.1.21.

Figure 3.1.20 depicts the ^{1}H chemical shift changes induced in PY in presence of Hg^{2+}. No observable change in the chemical shift of the protons is evident up to a ratio of 1 Hg^{2+}/PY. However at ratios greater than 1 there is a slight change to downfield values in comparison to the standard values for all protons, with H^{c} and H^{f} showing the largest shifts. However the relatively small changes observed in comparison to Ag^{+} indicate Hg^{2+} affinity for the nitrogens of PY is weak.

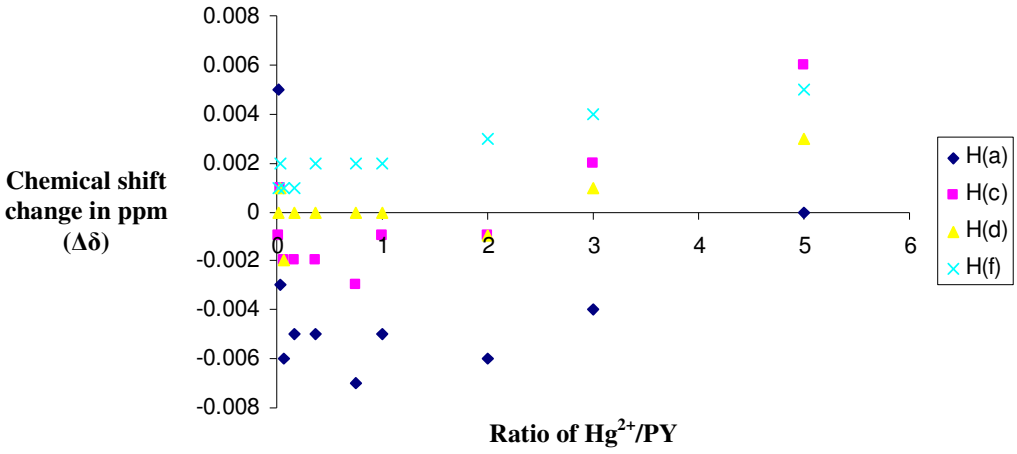

Figure 3.1.20 Effect of various concentrations of Hg^{2+} on the proton chemical shifts of PY (70%CD_3OD-30%D_2O v/v).

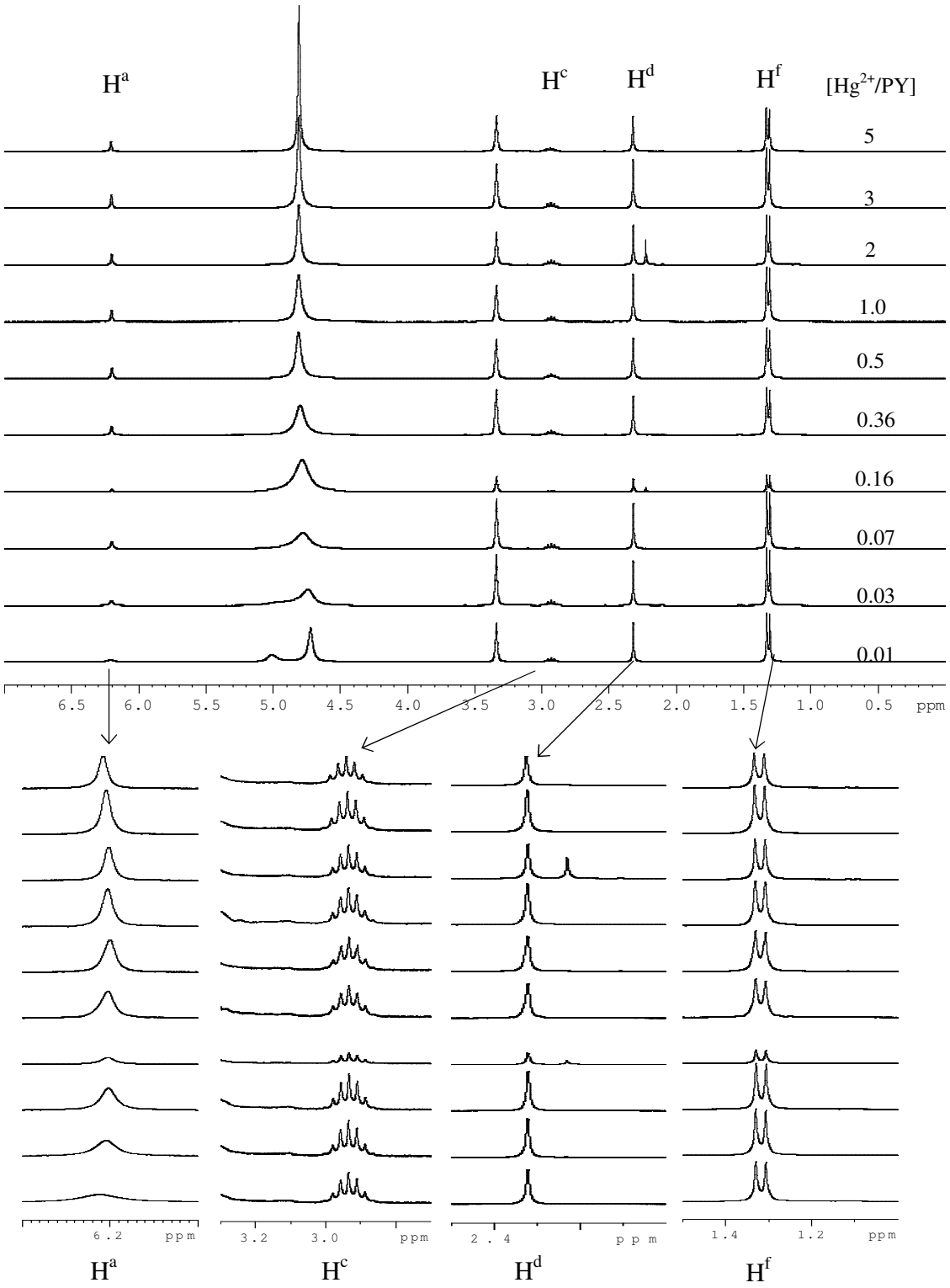

Figure 3.1.21 ^{1}H NMR spectra showing the proton chemical shifts of PY with increasing Hg^{2+} concentration. Additional expanded view of proton peaks.

3.1.3.3 Cadmium nitrate (Cd^{2+})

Cd^{2+} affinity for the nitrogen's of PY was similarly investigated as above by exploring changes observed in the chemical shielding of particular nuclei upon addition of cadmium. The effect cadmium has on the proton chemical shifts of PY is illustrated in Figure 3.1.22, with protons H_a and H_c most affected. The shifts were intermediate in magnitude between those observed in the presence of Ag^{+} and Hg^{2+}.

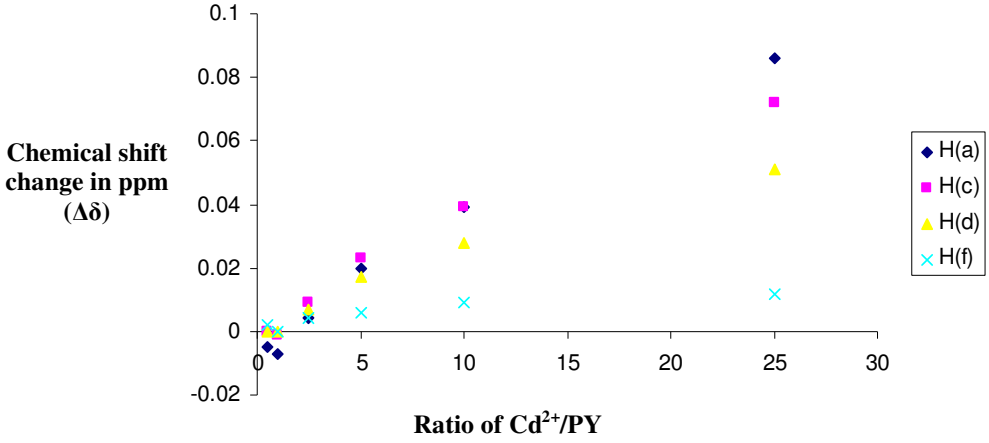

Figure 3.1.22 Effects of various concentrations of Cd^{2+} on the proton chemical shifts of PY (70%CD_3OD-30%D_2O v/v).

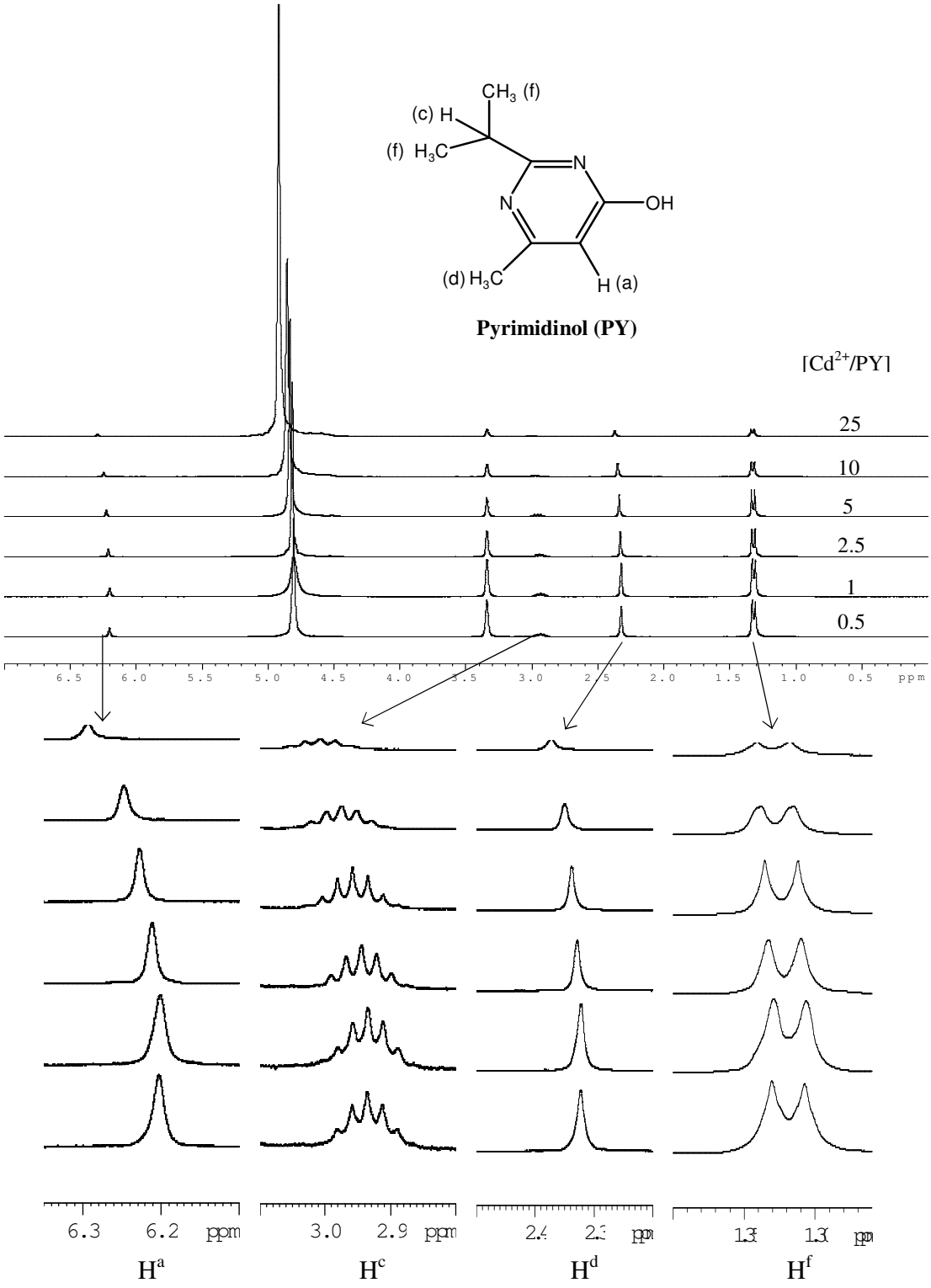

Figure 3.1.23 ^{1}H NMR spectra showing the proton chemical shifts of PY with increasing Cd^{2+} concentration. Additional expanded view of protons.

3.1.3.4 Copper nitrate (Cu^{2+})

^1H NMR spectra of PY in the presence of various concentrations of Cu^{2+} were obtained and compared to the proton chemical shift values of PY acquired in solution free of metal ions. Similarly to Ag^+ ions, the spectra show changes in the chemical shift of protons, particularly at H^c and H^f, with H^c being the most exposed to the external magnetic field upon Cu^{2+} binding. This data strongly suggests coordination of Cu^{2+} at N, where one would expect the H^c protons to be most affected. The paramagnetic nature of Cu^{2+} made it difficult to show binding effects at Higher ratios of Cu^{2+}/PY due to the broadening of spectral peaks.

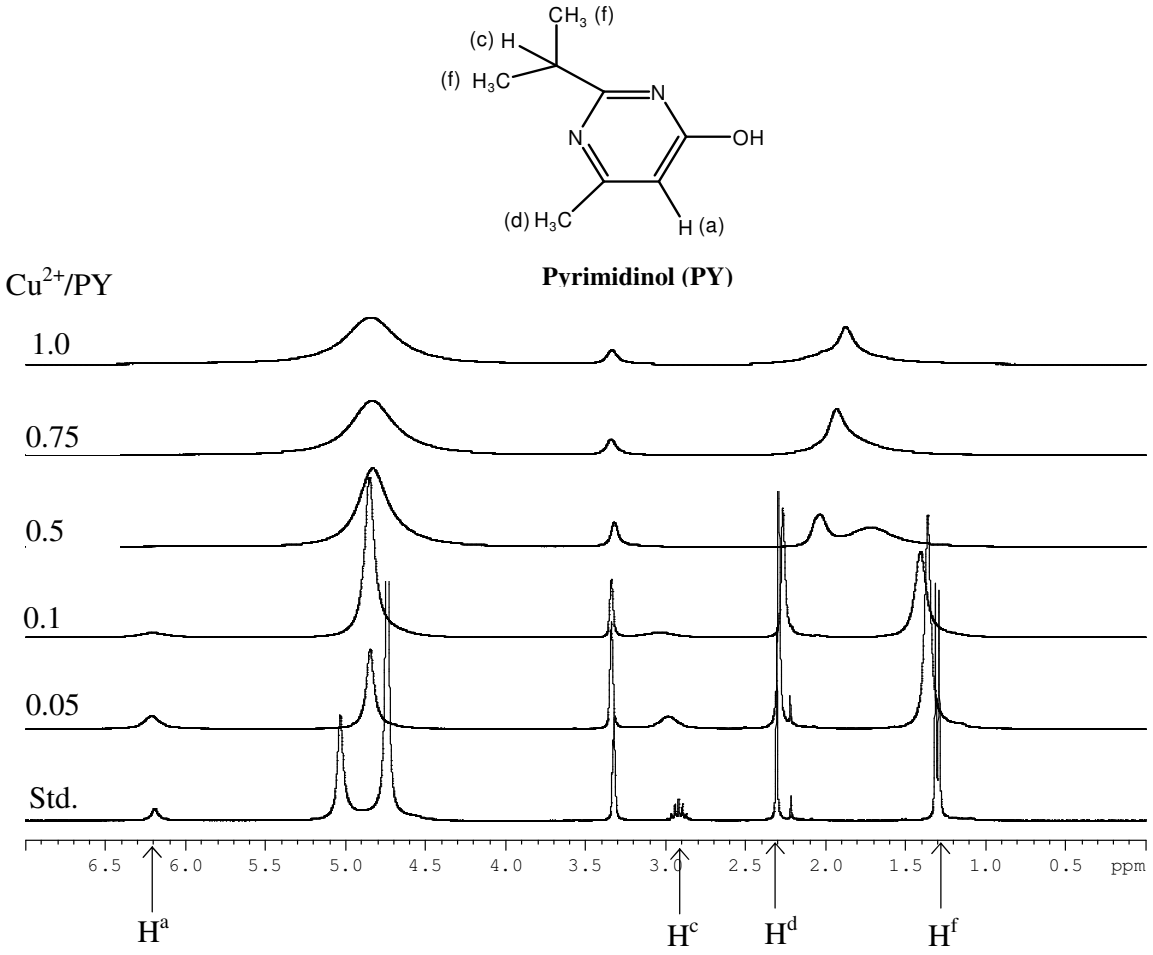

Pyrimidinol (PY)

Figure 3.1.24 ^1H NMR spectra showing the proton chemical shifts of PY with increasing Cu^{2+} concentration.

3.1.4 Hydrolysis and metal ion NMR binding study of diazinon.

Phosphorus and proton NMR have been shown to be extremely useful techniques for monitoring the hydrolysis of organophosphorus pesticides such as diazinon. Nucleophilic attack on the central phosphorus atom or alternatively attack at a carbon atom on the aliphatic chain are the expected modes of action for the hydrolysis of diazinon. A third possible pathway, nucleophilic attack at the aromatic ring (S_NAr), is not an expected mode of action for diazinon, as this generally requires at least two strongly electron-withdrawing groups to be positioned on the ring. The progress of such chemical transformations and their acceleration in the presence of metal ions is suitably followed by ^{31}P and ^{1}H NMR by analysing the chemical shifts of the observed product peaks. Comparison of these product peaks with the chemical shifts obtained in PY and PA studies and literature sources assist in elucidating the mechanism of nucleophilic attack ***(Product profile section).***

The second aspect of the experiments is to observe any changes in chemical shifts of diazinon and its hydrolysis products in the presence of metal ions. These changes or lack thereof may be used to draw conclusions about the extent and location of metal binding to the substrate and its hydrolysis products. Inferences about the metal's role in any observed acceleration of hydrolysis may be drawn from such changes in the electronic environment of specific nuclei ***(Chemical shift profile).***

The technique, whilst particularly useful for product identification and assessment of metal binding, may be simultaneously used to follow the kinetics of the reaction both in

the absence and presence of metal ions. The reaction system can be continuously monitored *in situ* for both the disappearance of diazinon and the appearance of product peaks. The pseudo first order rate constants k_{obs} are determined from the integral of the ^{31}P signal of diazinon and the observed product signal. A plot of natural log (peak area) vs time will yield k_{obs} via the equation below ***(Kinetic profile).***

$$\ln(\text{Integral diazinon}_{\text{initial}} - \text{Integral product}_{\text{time}}) = -k_{obs}t + \text{Constant}$$

3.1.4.1 Diazinon hydrolysis in the absence of metal ions

The hydrolysis of diazinon was studied in the absence of metal ions in unbuffered co-solvent by placing an aliquot of diazinon in the pertinent co-solvent in the NMR tube and monitoring the disappearance of its characteristic phosphorus signal by ^{31}P NMR at regular time intervals. Figure 3.1.25 shows the obtained spectra over a period of 16 days, demonstrating the relative resistance of diazinon to hydrolysis over the period examined under the stated experimental conditions. The product peak seen next to diazinon at 59-60 ppm is the characteristic chemical shift of PA in the absence of metal ions. This infers that S_N2 attack at P is the favored mode of hydrolysis for diazinon in the absence of metal ions. As observed in the previous PA metal binding NMR studies and product analysis in this section, significant shifts up-field are observed in the electronic environment of PA in the presence of metal ions.

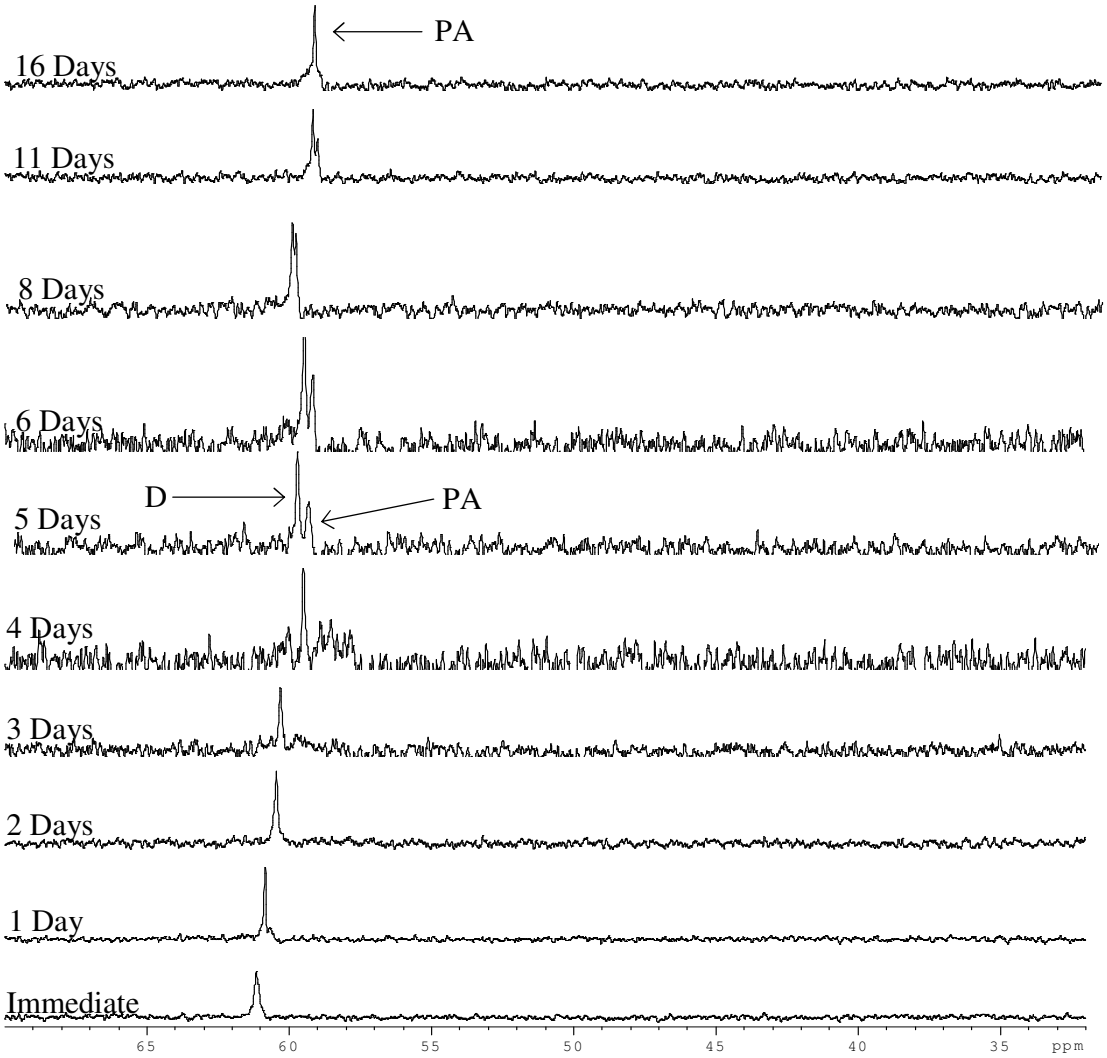

Figure 3.1.25 ^{31}P spectra of the hydrolysis of diazinon in the absence of metal ions (70%CD_3OD-30%D_2O v/v).

3.1.4.2 Diazinon hydrolysis in the presence of silver nitrate (Ag^+)

The kinetics and product profile of the hydrolysis of diazinon in the presence of Ag^+ was examined over four ratios of Ag^+/D including 0.4, 1, 10 and 25. Figures 3.1.26-3.1.31 show the obtained spectra in the presence of Ag^+. Spectra were recorded immediately after mixing and then at regular time intervals.

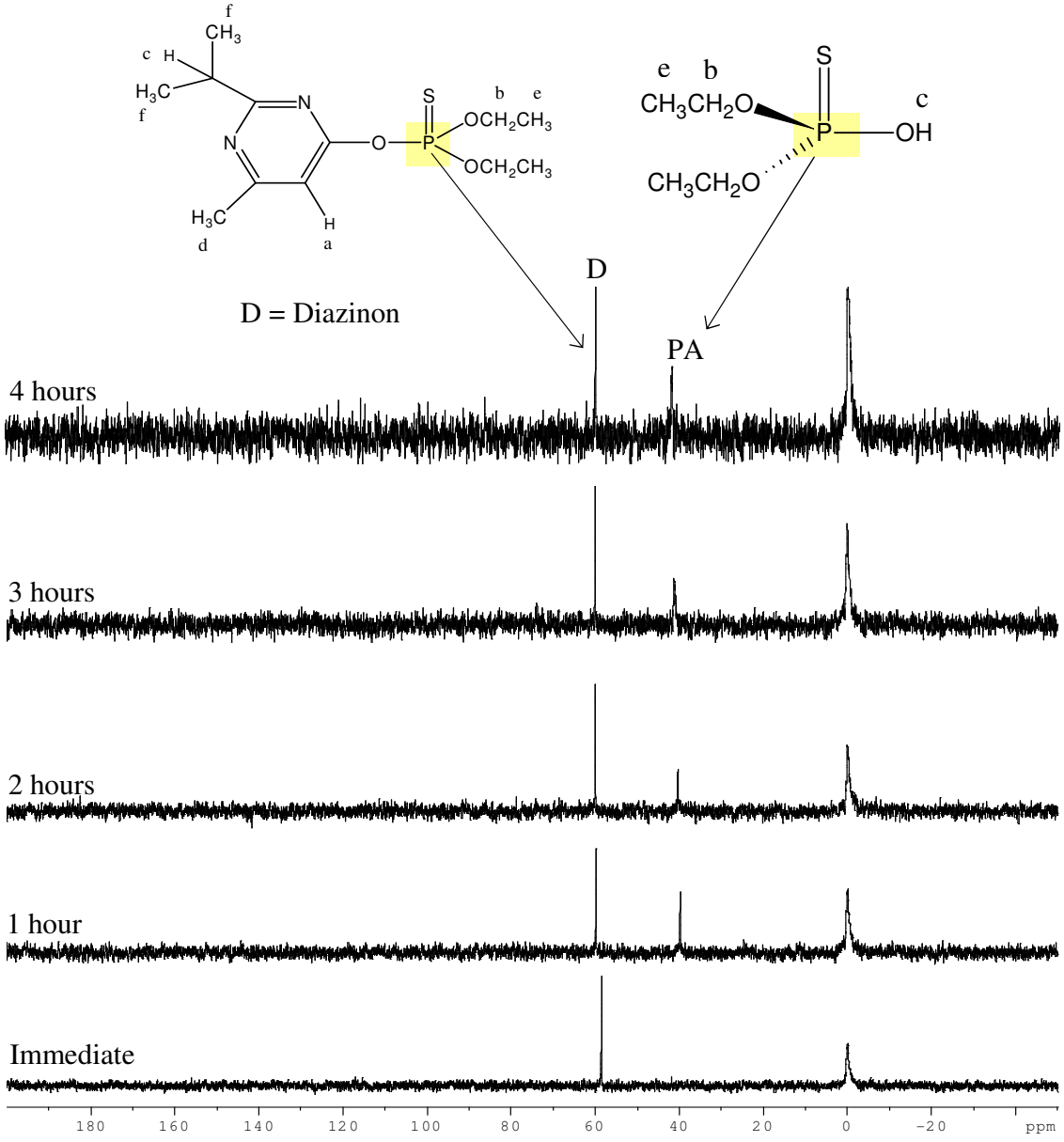

Figure 3.1.26 ^{31}P spectra of the hydrolysis of diazinon in the presence of Ag^+. Ratio of 0.4 Ag^+/D (70%CD_3OD-30%D_2O v/v).

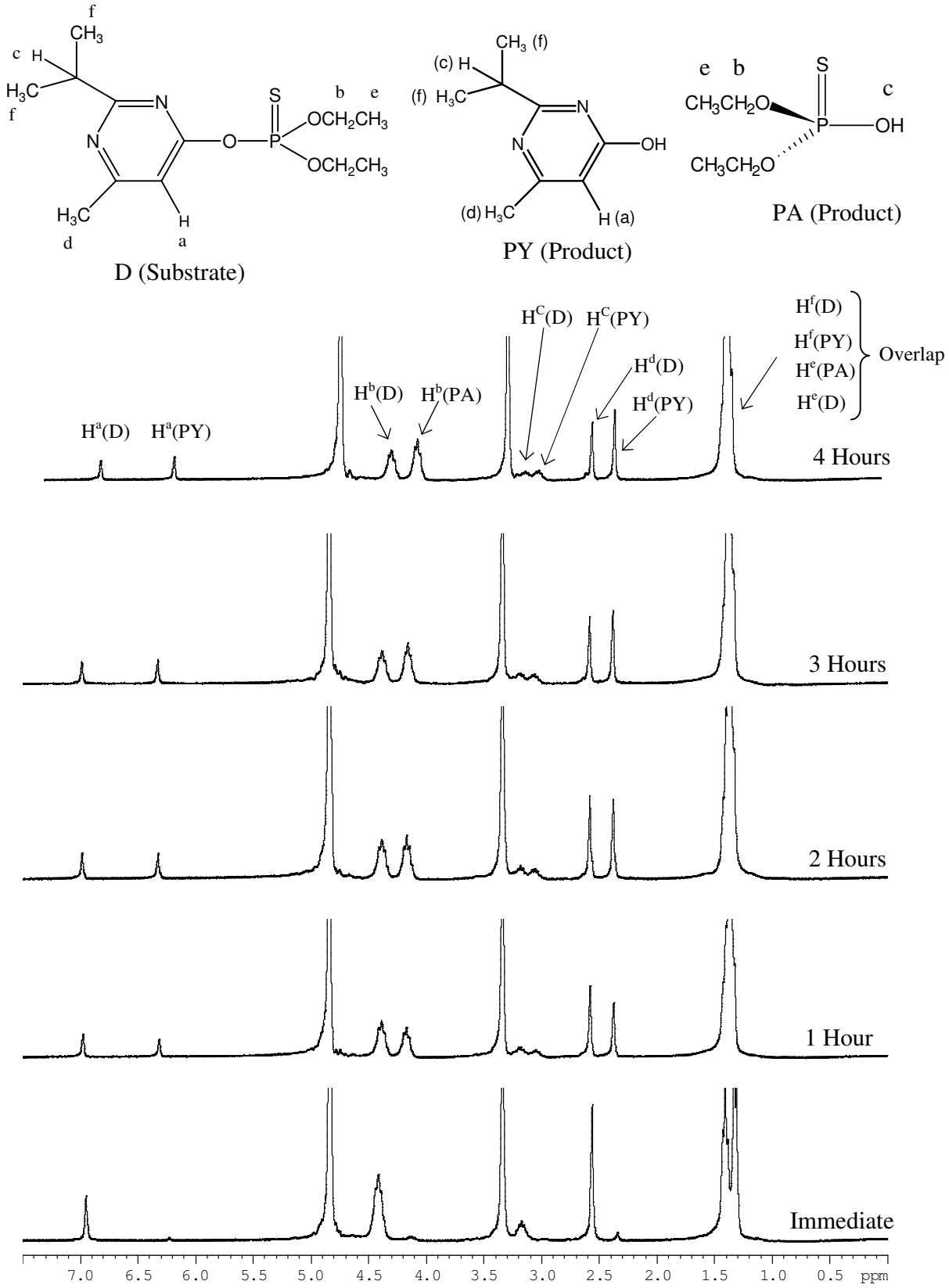

Figure 3.1.27 ^{1}H spectra of the hydrolysis of diazinon in the presence of Ag^+ (Ratio of 0.4 Ag^+/D). Depicts both the appearance of product peaks and disappearance of Diazinon.

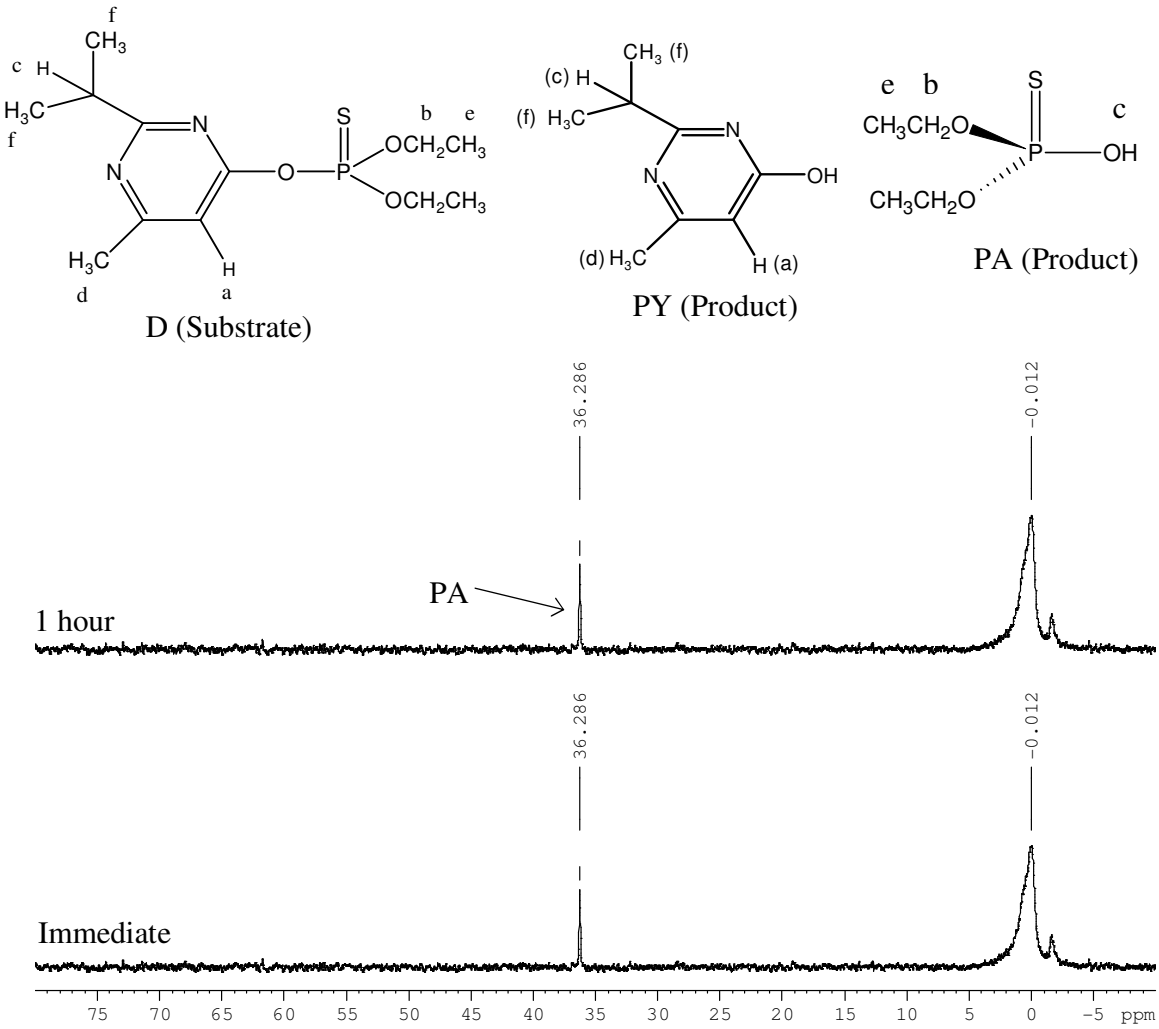

Figure 3.1.28 ^{31}P spectra of the hydrolysis of diazinon in the presence of Ag^+ (ratio of 1.0 Ag^+/D). Complete hydrolysis observed in first 10 minutes (70%CD_3OD-30%D_2O v/v)

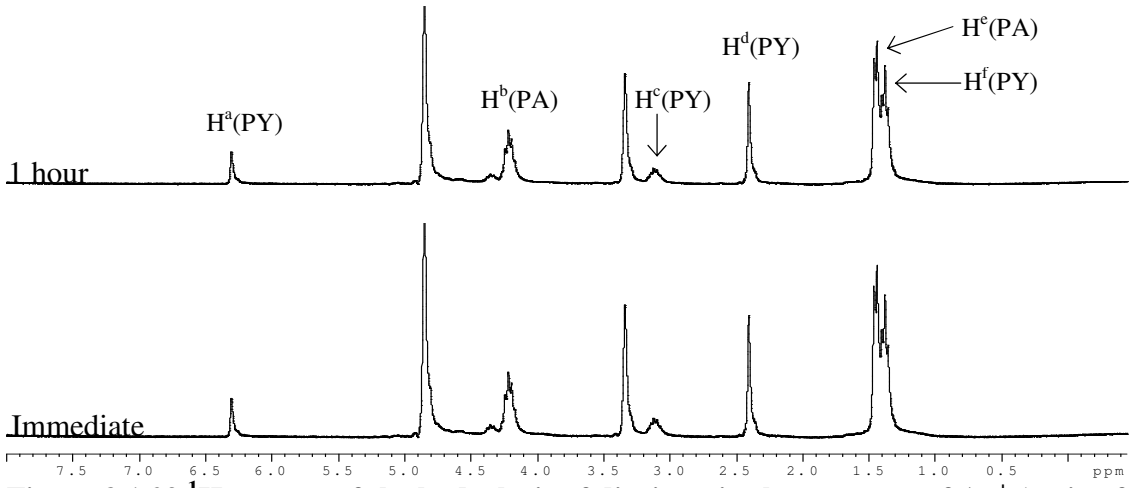

Figure 3.1.29 ^{1}H spectra of the hydrolysis of diazinon in the presence of Ag^+ (ratio of 1.0 Ag^+/D). Complete hydrolysis in first 10 minutes (70%CD_3OD-30%D_2O v/v).

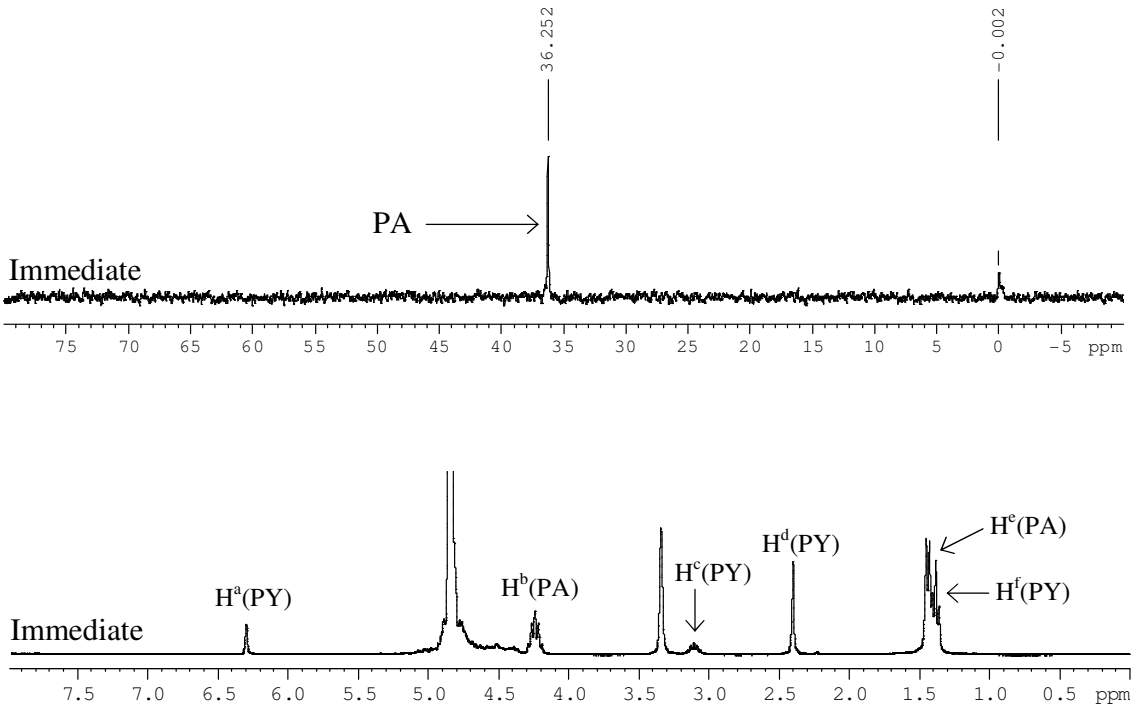

Figure 3.1.30 ^{1}H and ^{31}P spectra of the hydrolysis of diazinon in the presence of Ag^{+} (ratio of 10.0 Ag^{+}/D). Complete hydrolysis before immediate spectrum was taken (70% CD_3OD-30% D_2O v/v).

The spectra show unambiguously the facility of Ag^{+} to catalyze the rate of hydrolysis of diazinon when compared to hydrolysis in the absence of metal ions (Figure 3.1.25). The ^{1}H and ^{31}P spectra for ratios 1:1 and 10:1 represent complete hydrolysis within the time-frame required to obtain the initial spectrum, characteristically 10 minutes (dependent on shim time). Ratio 25:1 exhibits similar behavior and even ratio 0.4:1 of Ag^{+}/D depicts significant hydrolysis over 4 hours.

3.1.4.2.1 Product profile: The appearance of only one ^{31}P product signal for each ratio of Ag^{+}/D suggests that in the presence of Ag^{+}, diazinon undergoes hydrolysis by a single pathway. By comparing the observed ^{31}P chemical shift of the product signal to the ^{31}P signal acquired for authentic PA in equivalent concentrations of Ag^{+} (Appendix 3 Table A3.1), it is possible to evaluate whether the signal is consistent with PA. Table 3.1.6

shows the product chemical shift in comparison to the ^{31}P peaks attained in the PA study with the corresponding ratios of Ag^+/PA. This comparison enables identification of the phosphorus compound.

Table 3.1.6 ^{31}P chemical shift of observed product peak in comparison to authentic PA in the presence of matching concentrations of Ag^+. Standard PA = 60.165ppm.

Exp No.	Ratio of Ag^+/D	(δ) ^{31}P Product	Δδ from standard PA	Ratio of Ag^+/PA	(δ) ^{31}P PA	Δδ
1	0.4	39.843	20.322	0.4	51.658	8.507
2	1.0	39.578	20.587	1.0	39.569	20.596
3	10.0	36.286	23.879	10.0	37.239	22.836
4	25.0	36.252	23.913	25.0	35.124	25.041

The authentic PA phosphorus NMR signals in the presence of Ag^+ compare favorably with the observed chemical shifts of the product peaks except for Ag^+/D ratio 0.4 (compare columns 3 and 6 of Table 3.1.6). This is suggestive of attack (S_N2) at the phosphorus centre. Corroborative evidence of attack at P can be found in ^1H NMR spectra by comparison of ^1H product peaks with values obtained in the PY and PA NMR studies (Section 3.1.2 and 3.1.3) in the presence of equivalent concentrations Ag^+ ions. Comparison of proton signals was made for H_a, H_b(PA), H_c and H_d, however due to overlap of diazinon and product peaks it was not possible to evaluate H_f and H_e (1.3-1.51ppm).

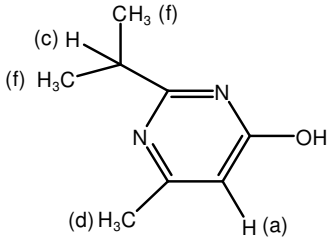

PY (Product)

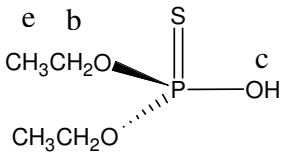

PA (Product)

Overlap with Diazinon peaks; H_f and H_e

No overlap; H_a, H_b, H_c and H_d

Compare columns 3 and 6.

Table 3.1.7 ^{1}H chemical shift of observed product peak in comparison to H^a of PY in the presence of matching concentrations of Ag^+. Standard H^a = 6.208ppm.

Exp No.	Ratio of Ag^+/D	δ of H^a product	Δδ from standard H^a (PY)	Ratio of Ag^+/PY	δ of H^a PY	Δδ
1	0.4	6.316	0.108	*0.5*	6.241	0.033
2	1.0	6.356	0.148	1.0	6.253	0.045
3	10.0	6.307	0.099	10.0	6.266	0.058
4	25.0	6.300	0.092	25.0	6.277	0.069

Table 3.1.8 ^{1}H chemical shift of observed product peak in comparison to H^c of PY in the presence of matching concentrations of Ag^+. Standard H^c = 2.936ppm.

Exp No.	Ratio of Ag^+/D	δ of H^c product	Δδ from Standard H^c (PY)	Ratio of Ag^+/PY	δ of H^c PY	Δδ
1	0.4	3.050	0.114	0.5	3.036	0.100
2	1.0	3.116	0.180	1.0	3.065	0.129
3	10.0	3.123	0.187	10.0	3.088	0.152
4	25.0	3.109	0.171	25.0	3.092	0.156

Table 3.1.9 ^{1}H chemical shift of observed product peak in comparison to H^d of PY in the presence of matching concentrations of Ag^+. Standard H^d = 2.322ppm.

Exp No.	Ratio of Ag^+/D	δ of H^d product	Δδ from Standard H^d(PY)	Ratio of Ag^+/PY	δ of H^d PY	Δδ
1	0.4	2.376	0.054	0.5	2.362	0.04
2	1.0	2.404	0.082	1.0	2.376	0.054
3	10.0	2.405	0.083	10.0	2.391	0.069
4	25.0	2.400	0.078	25.0	2.393	0.071

Table 3.1.10 ^{1}H chemical shift of observed product peak in comparison to H^b of PA in the presence of matching concentrations of Ag^+. Standard H^b = 4.048ppm.

Exp No.	Ratio of Ag^+/D	δ of H^b product	Δδ from Standard H^b(PA)	Ratio of Ag^+/PA	δ of H^b PA	Δδ
1	0.4	4.175	0.0127	0.5	4.085	0.037
2	1.0	4.189	0.141	1.0	4.213	0.165
3	10.0	4.218	0.170	10.0	4.218	0.170
4	25.0	4.241	0.193	25.0	4.245	0.197

The chemical shifts of the product proton peaks show good agreement with those of PY and PA in the presence of Ag^+ ions. In fact protons H^a, H^c and H^d are shifted more downfield than the equivalent protons in the PY NMR study in the presence of Ag^+. The PA products $^{1}H^b$ chemical shift shows good agreement with that of authentic PA in the presence of Ag^+ (Table 3.1.10, columns 3 and 6) The obtained chemical shifts for the product peaks from ^{1}H NMR data are in conformity with ^{31}P product peak analysis, therefore identifying attack at the phosphorus centre as the sole mechanism of hydrolysis in the presence of Ag^+.

***3.1.4.2.2 Chemical shift profile**:* As observed in Tables 3.1.6-3.1.10 the ^{1}H and ^{31}P chemical shifts of the products depict changes in position relative to the standard values specified for PA and PY in Table 3.1.1-3.1.3. There is a general downfield shift in the position of the ^{1}H chemical environments as the concentration of Ag^+ is increased, suggestive of metal binding in both PA and PY. The significant upfield shift in the phosphorus signal of the PA product undoubtedly points to Ag^+ binding at the sulfur ligand. It is important to point out that it is possible for both products to bind to Ag^+ post hydrolysis, therefore making it difficult to derive definitive information of metal binding to diazinon from the chemical shifts of the products.

Although metal binding in the products is indicative of the role Ag^+ plays in catalyzing the hydrolysis, a greater inference of the metal's role may be drawn from analysis of the chemical shifts of diazinon's nuclei in the presence of Ag^+ i.e. where complete hydrolysis has not occurred inside the time frame for the initial spectrum. diazinon itself shows a change in the chemical shifts of the phosphorus nuclei with addition of Ag^+ (column 4, Table 3.1.11), establishing an interaction between Ag^+ and diazinon.

Table 3.1.11 ^{31}P chemical shift data for Diazinon in the presence of Ag^+ ions.

Exp no.	Ratio of Ag^+/D	(δ) ^{31}P Diazinon	Δδ from standard Diazinon	(δ) ^{31}P Product
1	0.4	58.533	2.990	39.843
2	1.0	57.817	3.706	39.578
3	10.0	Complete hydrolysis	n/a	36.286
4	25.0	Complete hydrolysis	n/a	36.252

Interpretation of the ^{1}H NMR is an even better probe of the interactions of Ag^+ with diazinon as it encompasses analysis of the electronic environment of protons in the vicinity of both ligand sites, N and S. Comparison of proton signals was made for H_a, H_b(PA), H_c and H_d, however due to overlap of diazinon and product peaks it was not possible to evaluate H_f and H_e. The protons analyzed for chemical shift changes show appreciable shifts downfield from the standard diazinon proton shifts (Table 3.1.12-3.1.13, column 4), seen to increase with increasing Ag^+ concentration. Significantly, these downfield shifts are observed for both heterocyclic (near nitrogen) and aliphatic (near sulfur) protons. These changes in the chemical shift of both ^{1}H and ^{31}P nuclei close to both ligand sites certainly point to Ag^+ role in the acceleration of hydrolysis, which in

association with Electropsray mass spectrometry results will aid in pinpointing the location of metal binding.

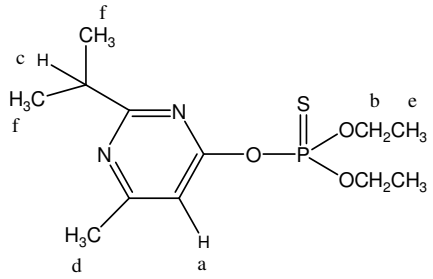

Table 3.1.12 ^{1}H chemical shift data for diazinon in the presence of Ag^{+} ions. Ratio Ag^{+}/D = 0.4.

^{1}H	(δ) of diazinon in the absence of Ag^{+}	(δ) of diazinon in the presence of Ag^{+} (ratio 0.4)	Δδ from standard diazinon
H^{a}	6.891	6.950	0.059
H^{b}	4.371	4.416	0.045
H^{c}	3.129	3.176	0.047
H^{d}	2.538	2.563	0.025

Table 3.1.13 ^{1}H chemical shift data for diazinon in the presence of Ag^{+} ions. Ratio Ag^{+}/D = 1.0.

^{1}H	(δ) of diazinon in the absence of Ag^{+} (ratio 1.0)	(δ) of diazinon in the presence of Ag^{+} (ratio 1.0)	Δδ from standard diazinon
H^{a}	6.891	7.048	0.157
H^{b}	4.371	4.455	0.084
H^{c}	3.129	3.242	0.113
H^{d}	2.538	2.612	0.074

3.1.4.2.3 Kinetic profile: The third aspect of the hydrolysis studies is the determination of the pseudo first order rate constants k_{obs}. This was estimated for ratio 0.4 Ag^+/D (Figure 3.1.27) from the integral of the ^{31}P signal of diazinon and the observed product signal. A plot of natural log (signal area of peak) vs time yields k_{obs} according to the equation below.

$$\ln(\text{Integral diazinon}_{\text{initial}} - \text{Integral product}_{\text{time}}) = -k_{obs}t + \text{Constant}$$

Table 3.1.14 NMR Kinetic data obtained for the hydrolysis of diazinon in the presence of Ag^+, ratio 0.4 Ag^+/D.

Time	Integral of diazinon ^{31}P signal	Integral of product(PA) ^{31}P signal	ln(Integral D_0 – Integral P_t)
Immediate	0.448	-	-
1hr	0.252	0.167	-1.270
2hr	0.239	0.208	-1.427
3hr	0.201	0.247	-1.604
4hr	0.188	0.260	-1.671

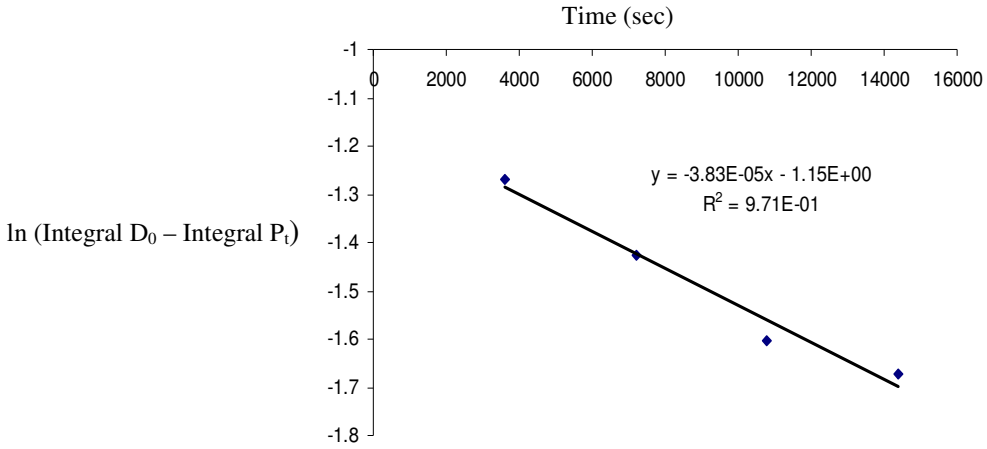

Figure 3.1.31 Plot of ln(Integral D_0 – Integral P_t) versus time for 0.4 ratio of Ag^+/diazinon.

3.1.4.3 Diazinon hydrolysis in the presence of mercuric chloride (Hg^{2+})

The product and kinetics profile of the hydrolysis of diazinon in the presence of Hg^{2+} ions was studied over 3 ratios of Hg^{2+}/D (0.5, 1.0 and 5). Overlay of ^{1}H and ^{31}P spectra are shown in Figures 3.1.32-3.1.34 for the 5 and 0.5 ratios.

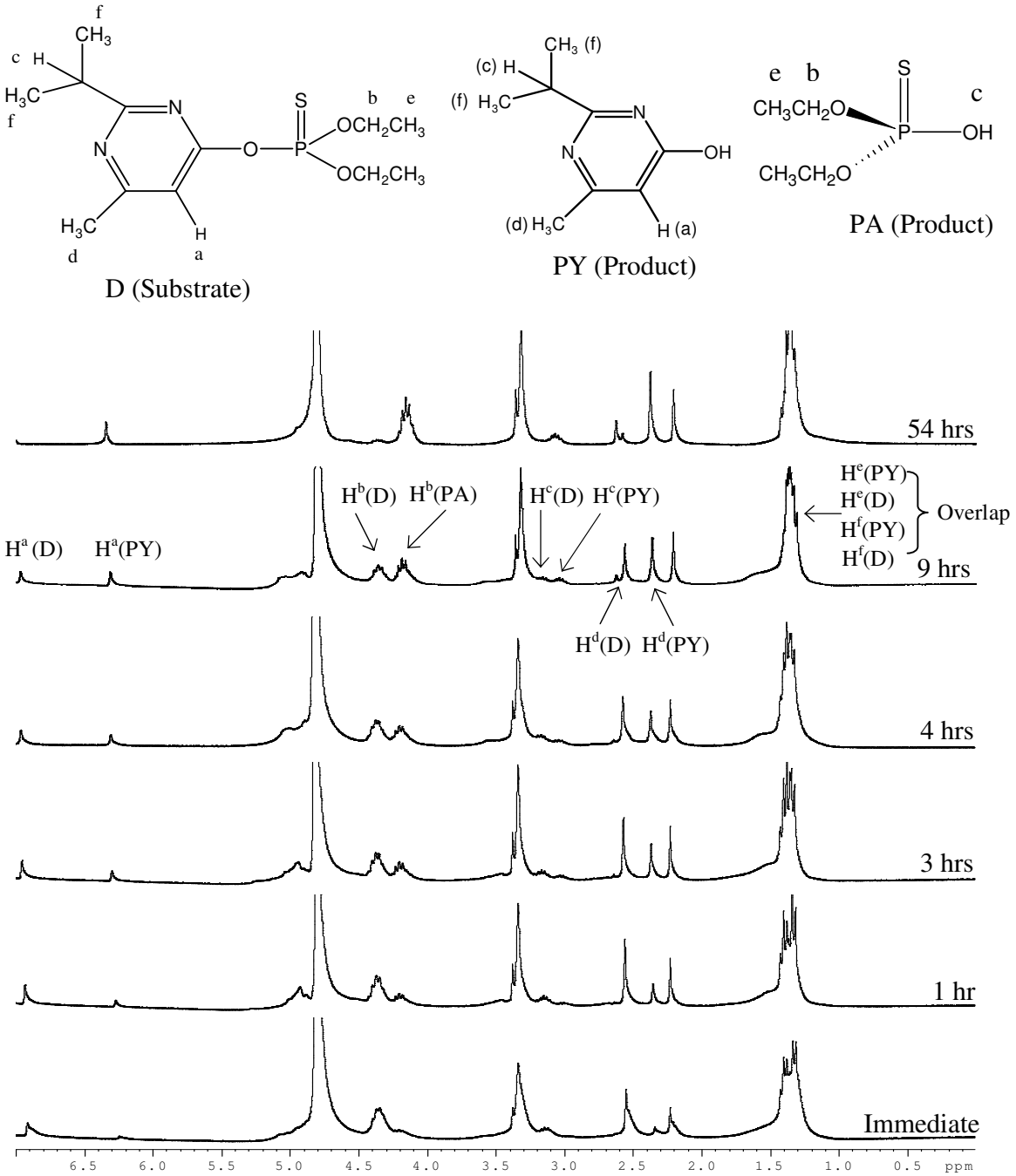

Figure 3.1.32 ^{1}H spectra of the hydrolysis of diazinon in the presence of Hg^{2+} (Ratio of 0.5 Hg^{2+}/D). Depicts both the appearance of product peaks and disappearance of diazinon.

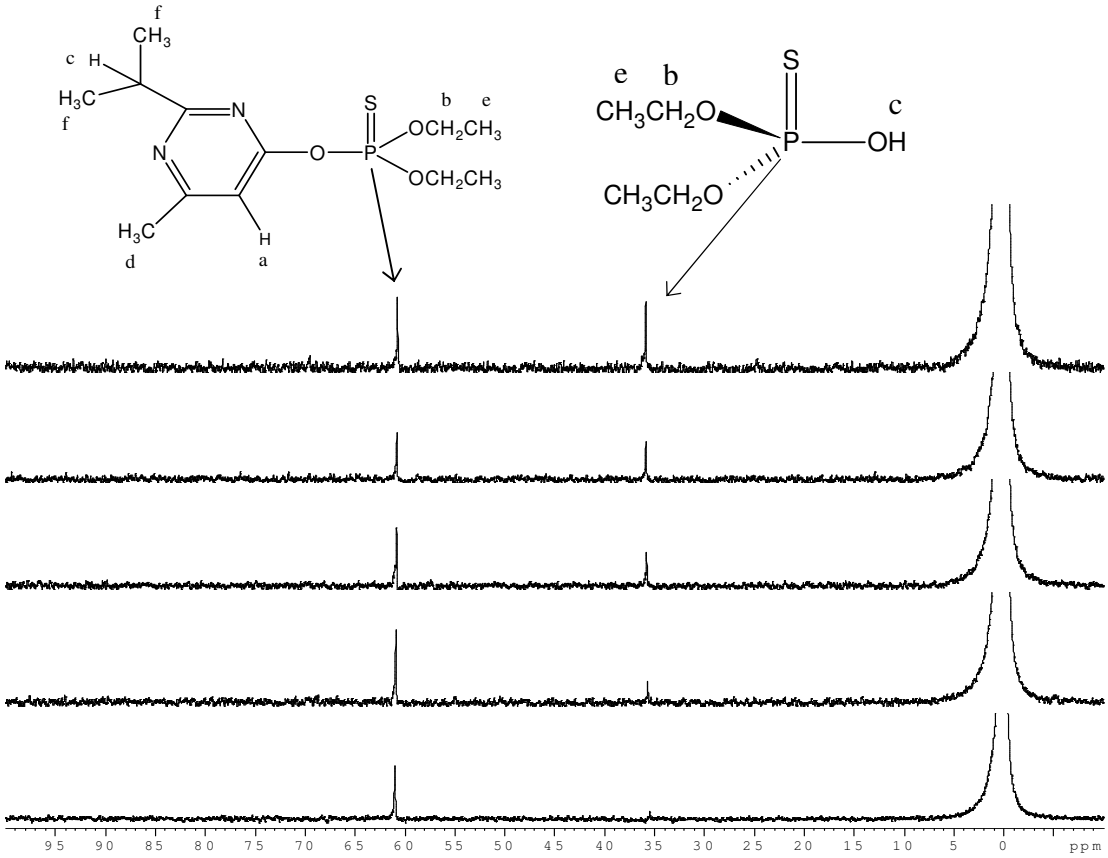

Figure 3.1.33 ^{31}P spectra of the hydrolysis of diazinon in the presence of Hg^{2+}. Ratio of 0.5 Hg^{2+}/D.

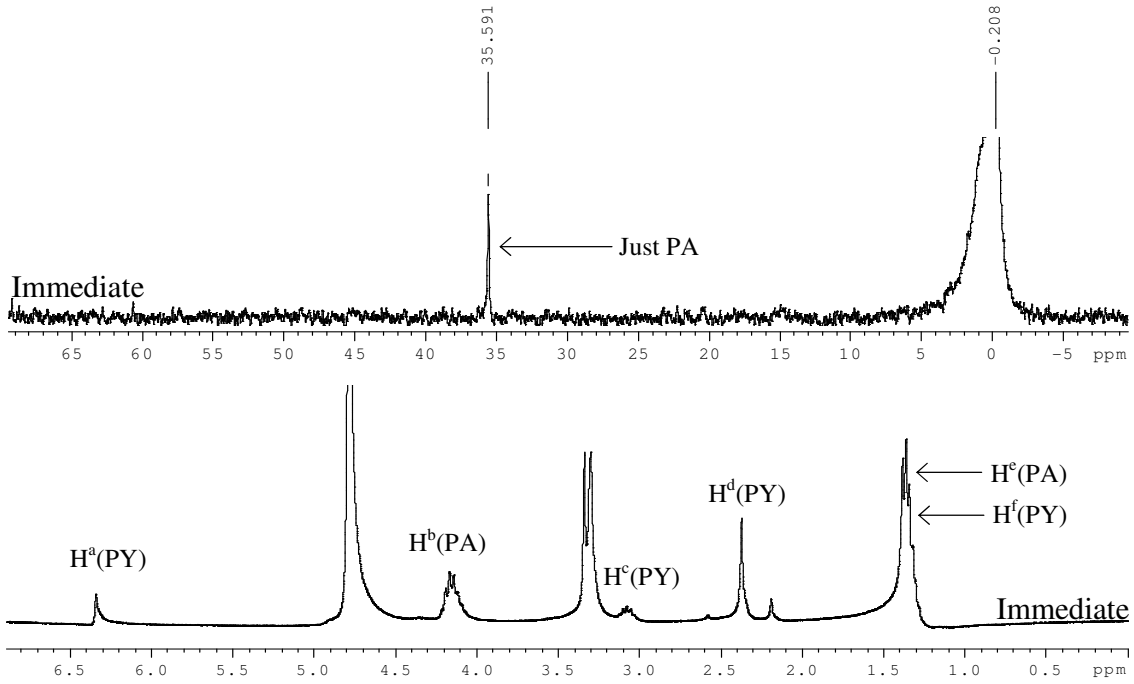

Figure 3.1.34 ^{31}P and ^{1}H NMR spectra of the hydrolysis of diazinon in the presence of Hg^{2+}. Ratio of 5.0 Hg^{2+}/D. Complete hydrolysis in first 10 minutes (70% CD_3OD-30% D_2O v/v).

Comparable to Ag^+, the presence of Hg^{2+} ions noticeably accelerates the rate of hydrolysis of diazinon. Complete hydrolysis within the first 10 minutes is observed for the ratio of 5:1 Hg^{2+}/D, with significant hydrolysis also observed with a ratio 0.5 Hg^{2+}/D.

3.1.4.3.1 Product profile: There is the appearance of only one phosphorus containing product peak, suggestive of a single mechanistic pathway of hydrolysis analogous to Ag^+ binding. The obtained ^{31}P chemical shift (ppm) of the product at each ratio shows good correlation with the recorded ppm shift of authentic PA with an equivalent ratio of Hg^{2+} (Table 3.1.15, compare columns 3 and 6).

Table 3.1.15 ^{31}P chemical shift of observed product peak in comparison to PA in the presence of matching concentrations of Hg^{2+}. Standard PA = 60.165ppm.

Exp No.	Ratio of Hg^{2+}/D	(δ) ^{31}P Product	Δδ from standard PA	Ratio of Hg^{2+}/PA	(δ) ^{31}P	Δδ
1	0.5	36.66	23.505	0.5	39.785	20.38
2	1.0	35.71	24.455	1.0	36.571	23.594
3	5.0	35.91	24.255	5.0	33.990	26.175

The ^{31}P evidence of attack at phosphorus is corroborated in the ^{1}H spectra. The ^{1}H chemical shifts in ppm of the product peaks are in the same ppm region as those obtained for authentic PA and PY (H_a, H_b(PA), H_c and H_d assessed) in equivalent concentrations of Hg^{2+} (Tables 3.1.16-3.1.19).

3.1.4.3.2 Chemical shift profile: A striking contrast to the authentic PY study in the presence of Hg^{2+} is the appreciable downfield shifts observed for the proton nuclei of PY product peaks (compare columns 4 and 7, Tables 3.1.16-3.1.18). Due to the established weak affinity of Hg^{2+} for nitrogen ligands (see Figure 3.1.20) it is hypothesized that the observed shifts are as a result of protonation of a nitrogen and not Hg^{2+} binding.

Comparable shifts are noted in diazinon with Hg^{2+} binding; suggestive of the role protonation may play in Hg^{2+} catalysis. Significant shifts are also recorded for the $CH_2{}^b$ protons of PA, attributed to Hg^{2+} interaction with the sulfur ligand of the PA product (column 4, Table 3.1.19). This shows Hg^{2+} bound to PA product post hydrolysis.

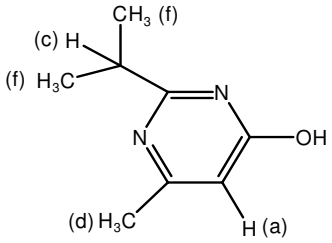

PY (Product)

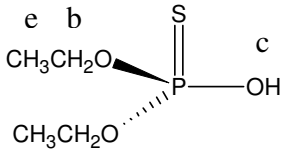

PA (Product)

Table 3.1.16 ^{1}H chemical shift of observed product peak in comparison to H^a(PY) in the presence of matching concentrations of Hg^{2+}. Standard H^a = 6.208ppm.

Exp No.	Ratio of Hg^{2+}/D	δ of H^a product	Δδ from standard H^a (PY)	Ratio of Hg^{2+}/PY	δ of H^a PY	Δδ
1	0.5	6.306	0.098	0.5	6.201	-0.007
2	1.0	6.314	0.106	1.0	6.203	-0.005
3	5.0	6.342	0.134	5.0	6.208	0.000

Table 3.1.17 ^{1}H chemical shift of observed product peak in comparison to H^c(PY) in the presence of matching concentrations of Hg^{2+}. Standard H^c = 2.936ppm.

Exp No.	Ratio of Hg^{2+}/D	δ of H^c product	Δδ from Standard H^c (PY)	Ratio of Hg^{2+}/PY	δ of H^c PY	Δδ
1	0.5	3.045	0.109	0.5	2.933	-0.003
2	1.0	3.062	0.126	1.0	2.935	-0.001
3	5.0	3.081	0.145	10.0	2.942	0.006

Table 3.1.18 ^{1}H chemical shift of observed product peak in comparison to H^{d}(PY) in the presence of matching concentrations of Hg^{2+}. Standard H^{d} = 2.322ppm.

Exp No.	Ratio of Hg^{2+}/D	δ of H^{d} product	Δδ from Standard H^{d}(PY)	Ratio of Hg^{2+}/PY	δ of H^{d} PY	Δδ
1	0.5	2.367	0.045	0.5	2.322	0.000
2	1.0	2.380	0.058	1.0	2.322	0.000
3	5.0	2.374	0.052	10.0	2.325	0.003

Table 3.1.19 ^{1}H chemical shift of observed product peak in comparison to H^{b}(PA) in the presence of matching concentrations of Hg^{2+}. Standard H^{b} = 4.048ppm.

Exp No.	Ratio of Hg^{2+}/D	δ of H^{b} product	Δδ from Standard H^{b}(PA)	Ratio of Hg^{2+}/PA	δ of H^{b} PA	Δδ
1	0.5	4.198	0.150	0.5	4.181	0.133
2	1.0	4.207	0.159	1.0	4.211	0.163
3	5.0	4.171	0.123	10.0	4.211	0.163

The metal's influence on the chemical shift of the nuclei of diazinon can in addition be examined over preliminary ratios were diazinon peaks are still present in the spectra. This assists in giving valuable information about the location of binding and the effect Hg^{2+} has on the nuclei of diazinon itself. Surprisingly the effect on the phosphorus nuclei of diazinon due to Hg^{2+} is much reduced from that observed in the presence of Ag^{2+} (Column 4, Table 3.1.20, compared to Column 4, Table 3.1.11).

Table 3.1.20 ^{31}P chemical shift data for diazinon in the ground state in the presence of Hg^{2+} ions.

Exp no.	Ratio of Hg^{2+}/D	(δ) ^{31}P diazinon	Δδ from standard diazinon	(δ) ^{31}P Product
1	0.5	61.150	0.381	36.66
2	1.0	60.852	0.679	35.71
3	5.0	Complete hydrolysis	n/a	35.91

Equally scrutiny of ^{1}H signals shows a reduced chemical shift change in comparison to diazinon in the presence of Ag^{+}. Of most significance is the minimal effect on CH_2[b] (highlighted in bold), indicating weak and limited binding of Hg^{2+} to diazinon in the reactant state. In contrast the protons associated with the ring still show downfield shifts (column 4, Tables 3.1.21-3.1.22). The low affinity of $Hg^{2+}$for nitrogen as observed in the PY NMR study in the presence of Hg^{2+} would suggest that the observed shifts are a result of protonation rather than Hg^{2+} interaction.

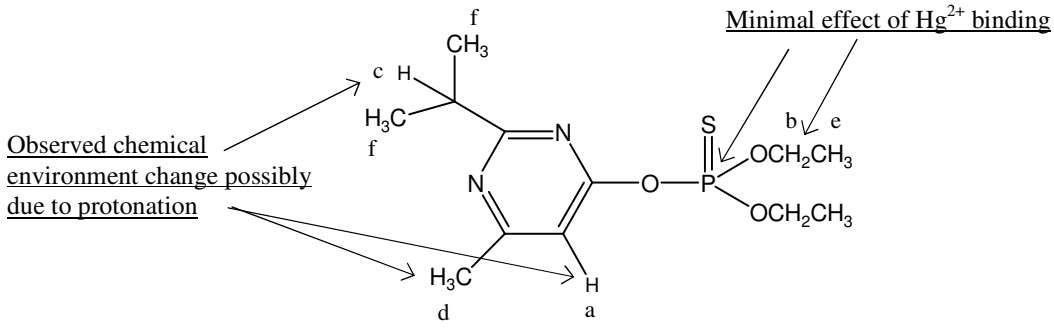

Table 3.1.21 ^{1}H chemical shift data for diazinon in the presence of Hg^{2+} ions. Ratio Hg^{2+}/D = 0.5

^{1}H	(δ) of diazinon	(δ) of diazinon in the presence of Hg^{2+} (ratio 0.5)	Δδ from standard diazinon
H^{a}	6.891	6.942	0.051
H^{b}	**4.371**	**4.374**	**0.003**
H^{c}	3.129	3.163	0.034
H^{d}	2.538	2.566	0.028

Table 3.1.22 ^{1}H chemical shift data for diazinon in the presence of Hg^{2+} ions. Ratio Hg^{2+}/D = 1.0

^{1}H	(δ) of diazinon	(δ) of diazinon in the presence of Hg^{2+} (ratio 1.0)	Δδ from standard diazinon
H^{a}	6.891	6.977	0.086
H^{b}	**4.371**	**4.378**	**0.007**
H^{c}	3.129	3.178	0.049
H^{d}	2.538	2.580	0.042

3.1.4.2.3 Kinetic profile: The pseudo first order rate constant was estimated for a 1:1 ratio of Hg^{2+}/D. Table 3.1.23 shows the obtained integrals with Figure 3.1.35 depicting the plot of ln(Integral diazinon $_{initial}$ – Integral product$_{time}$) versus time.

Table 3.1.23 NMR Kinetic data obtained for the hydrolysis of diazinon in the presence of Hg^{2+}, ratio 1.0 Hg^{2+}/D.

Time	Integral of diazinon ^{31}P signal	Integral of product(PA) ^{31}P signal	ln(Integral diazinon$_{initial}$ – Integral product$_{time}$)
Immediate	0.0238	0.00224	-3.83
1hr	0.0169	0.0043	-3.92
2hr	0.0149	0.00787	-4.12
3hr	0.0122	0.0095	-4.23
4hr	0.0114	0.0131	-4.37

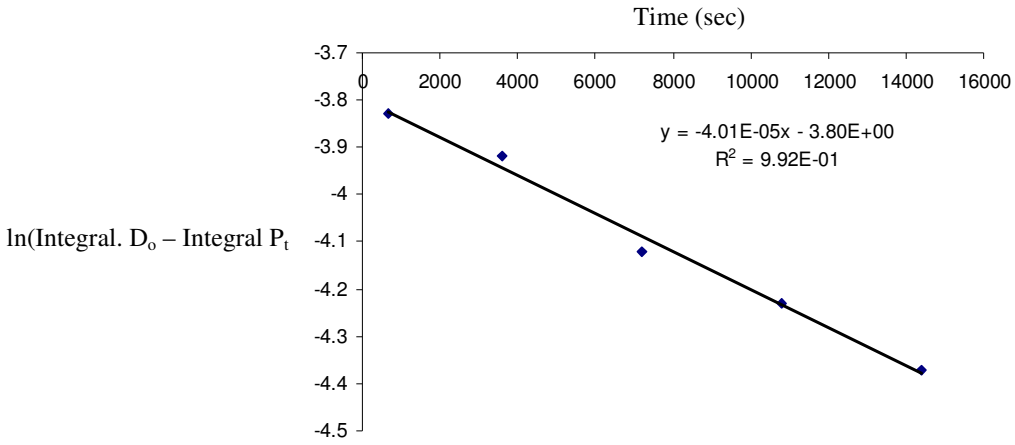

Figure 3.1.35 Plot of ln(Integral diazinon$_{initial}$ – Integral product$_{time}$) versus time for Hg^{2+}/diazinon (ratio 1).

3.1.4.4 Diazinon hydrolysis in the presence of cadmium nitrate (Cd^{2+})

The effect Cd^{2+} has on the hydrolysis of diazinon was investigated at a ratio of Cd^{2+}/D 25:1. This higher ratio was chosen due to slow rate increases observed in preliminary UV kinetic studies at lower ratios. The observed slow rate increase is almost certainly in relation to the reduced chemical environment change of the phosphorus nuclei of PA in the presence of Cd^{2+} ions (see Figure 3.1.14). The spectra obtained over 8 days are shown in Figure 3.1.36 and clearly show the reduced effect Cd^{2+} has on the hydrolysis of diazinon.

3.1.4.4.1 Product profile: Similar to Hg^{2+} and Ag^{+}, diazinon hydrolysis in the presence of cadmium shows the appearance of one phosphorus product peak. Comparison of the ^{31}P product chemical shift to authentic PA in the presence of an equivalent ratio of Cd^{2+} gives excellent agreement; supporting attack at phosphorus as the pathway for hydrolysis (compare columns 3 and 6, Table 3.1.24).

Table 3.1.24 ^{31}P chemical shift of observed product peak in comparison to PA in the presence of matching concentrations of Cd^{2+}. Standard PA = 60.165ppm.

Exp No.	Ratio of Cd^{2+}/D	(δ) ^{31}P Product	Δδ from standard PA	Ratio of PA/Cd^{2+}	(δ) ^{31}P	Δδ
1	25.0	49.59	10.757	25.0	49.051	11.114

3.1.4.4.2 Chemical shift profile: The chemical environment of the phosphorus nuclei of diazinon also changes on addition of Cd^{2+} showing binding in the reactant state.

Table 3.1.25 ^{31}P chemical shift data for diazinon in the presence of Cd^{2+} ions.

Exp no.	Ratio of Cd^{2+}/D	(δ) ^{31}P diazinon	Δδ from standard diazinon	(δ) ^{31}P Product
1	25.0	60.087	1.44	49.59

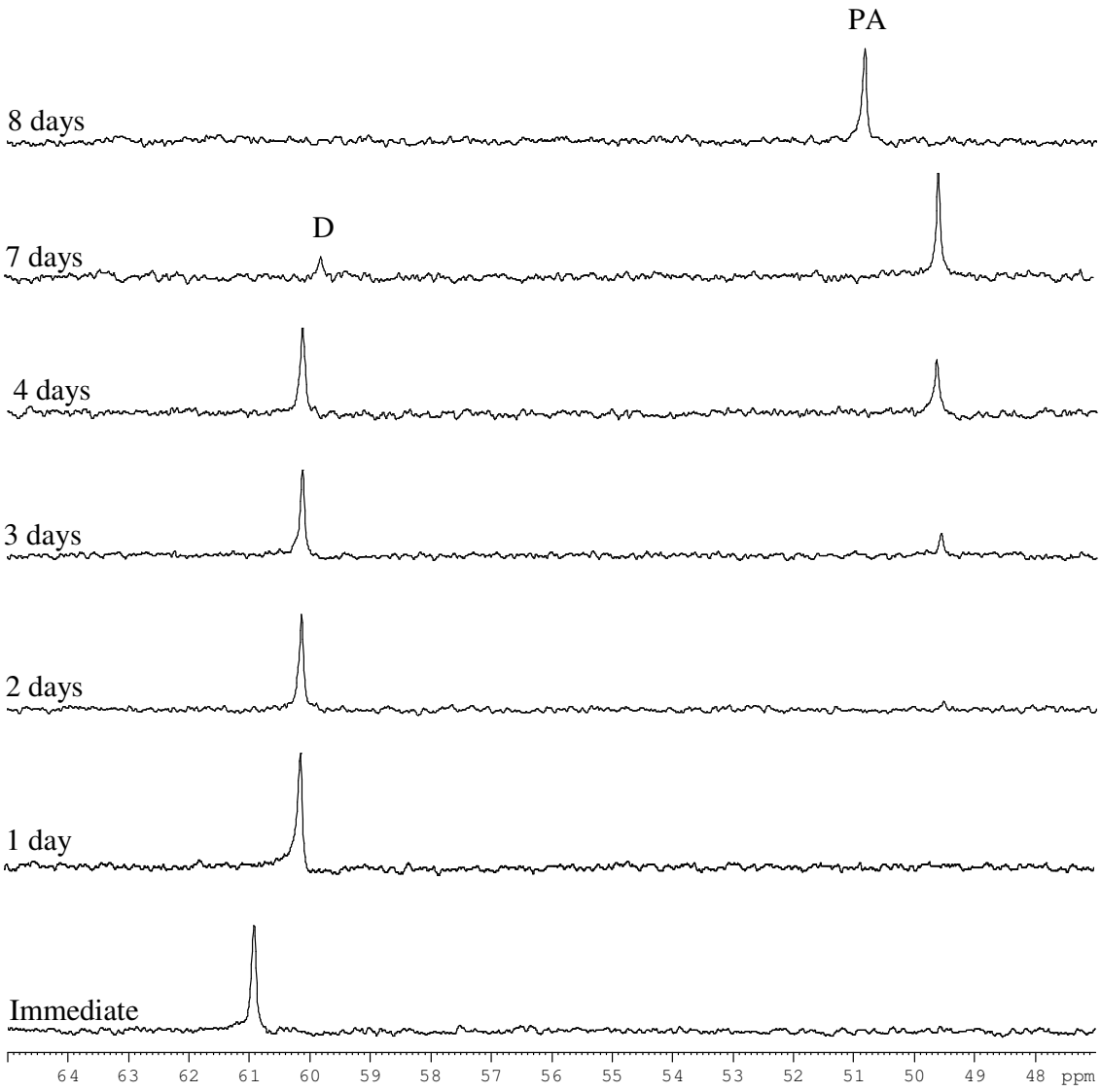

Figure 3.1.36 ^{31}P spectra of the hydrolysis of diazinon in the presence of Cd^{2+}. Ratio of 25.0 Cd^{2+}/D.

3.1.4.5 Diazinon hydrolysis in the presence of copper nitrate (Cu^{2+})

Diazinon hydrolysis in the presence of Cu^{2+} was studied over 3 ratios including 0.5, 1 and 5 times Cu^{2+}/D. Due to the paramagnetic nature of Cu^{2+} only ^{31}P was employed, with the overlaid spectra for the separate ratios shown in Figures 3.1.37-3.1.39.

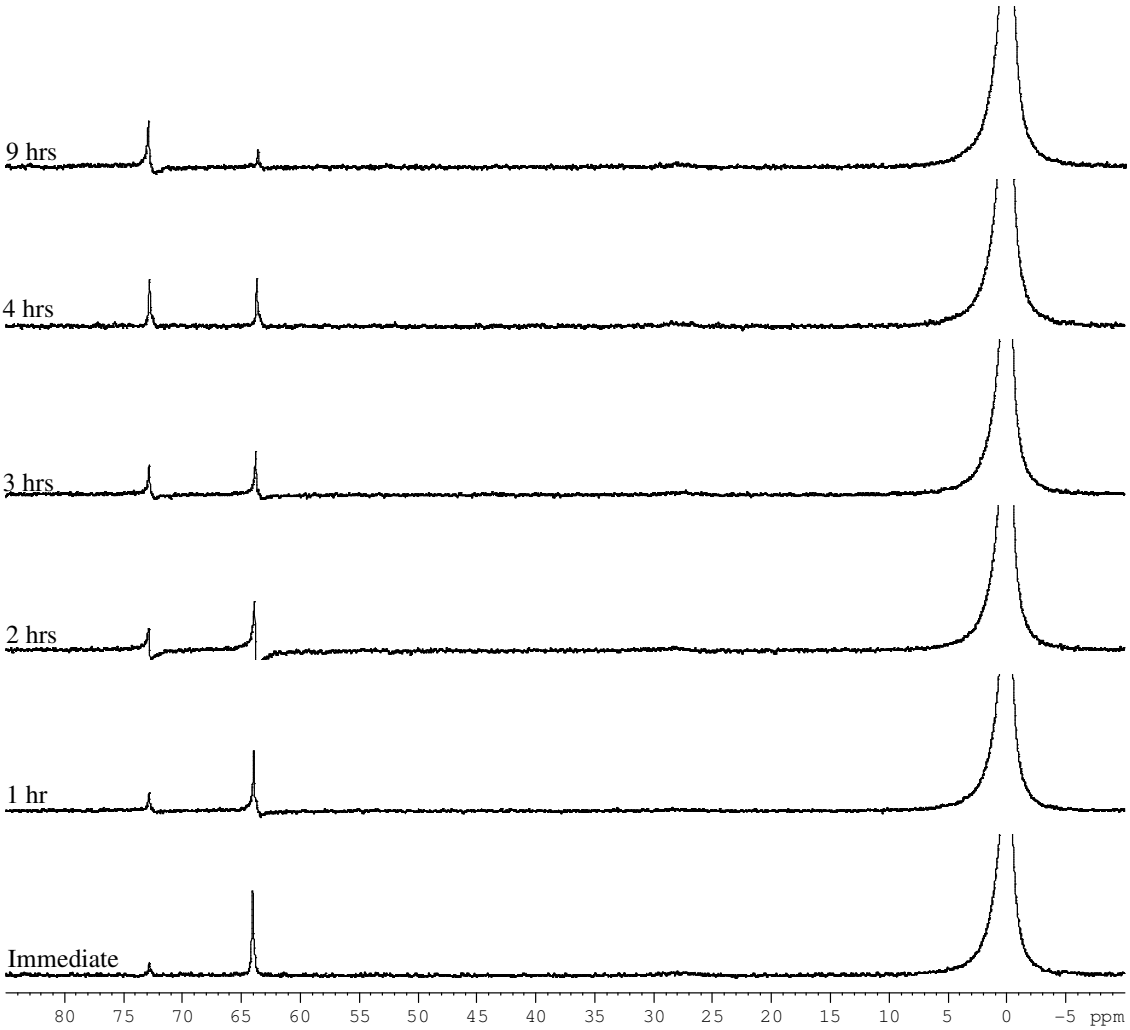

Figure 3.1.37 ^{31}P spectra of the hydrolysis of diazinon in the presence of Cu^{2+}. Ratio of 5.0 Cu^{2+}/D.

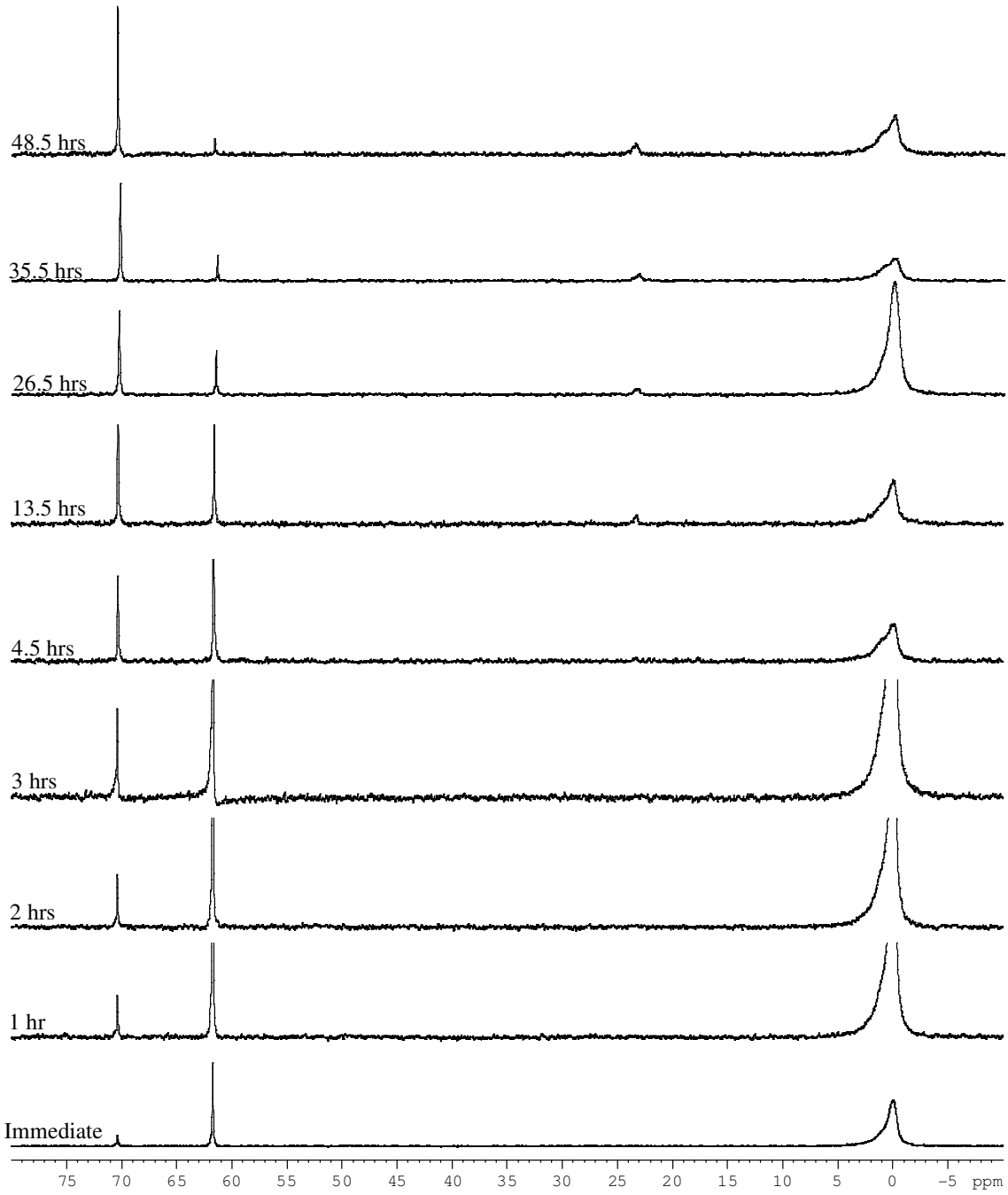

Figure 3.1.38 ^{31}P spectra of the hydrolysis of diazinon in the presence of Cu^{2+}. Ratio of 1.0 Cu^{2+}/D.

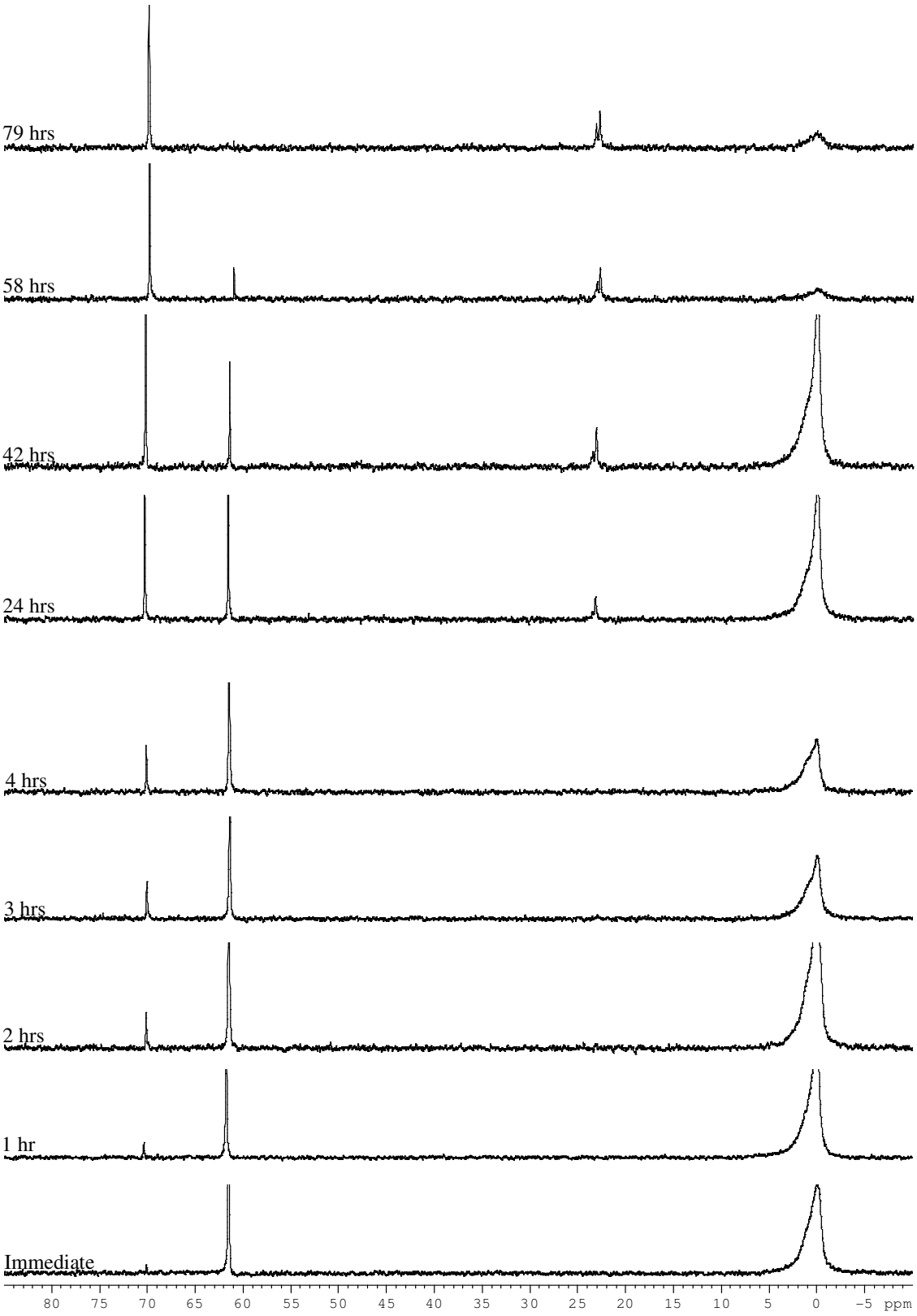

Figure 3.1.39 ^{31}P spectra of the hydrolysis of diazinon in the presence of Cu^{2+}. Ratio of 0.5 Cu^{2+}/D.

The obtained spectra show the capability of Cu^{2+} to accelerate the rate of hydrolysis of diazinon, although at a slower rate than in the presence of $Ag^{+}$and Hg^{2+} under the stated NMR conditions.

3.1.4.5.1 Product profile: Contrasting hydrolysis in the presence of Ag^{+} and Hg^{2+}, Cu^{2+} shows the appearance of two ^{31}P product peaks in the obtained spectra. At the outset there is the appearance of a product peak at 70-73 ppm later followed by the appearance of a peak at ≈23 ppm. The peak at 23 ppm gives excellent agreement with the observed ^{31}P chemical shift of PA in the presence of Cu^{2+}. It is therefore suggested that the peak at 70-73 ppm points to the formation of PA followed by a successive interaction with Cu^{2+} ions to form a product at ≈23ppm as observed in the PA study. Corroborative evidence of S_N2 attack at P is found in the UV kinetic studies.

3.1.4.5.2 Chemical shift profile: Evidence of copper complexation with diazinon was obtained with an unexpected downfield shift observed in the phosphorus nuclei as the concentration of Cu^{2+} was increased. This is contrary to the up-field shifts observed for the phosphorus nuclei of both PA and diazinon in the presence of the other metal cations. Similarly the product PA shows a significant downfield shift from its standard value of 60.165 ppm. These downfield shifts increase with Cu^{2+} concentration and imply binding of Cu^{2+} in both diazinon and in the product PA. The reactant-state effect is greater than that observed with Hg^{2+} but smaller than for Ag^{+} (column 4, Table 3.1.26).

Table 3.1.26 ^{31}P chemical shift data for diazinon in and product peak in the presence of Cu^{2+} ions.

Exp no.	Ratio of Cu^{2+}/D	(δ) ^{31}P diazinon	Δδ from standard diazinon	(δ) ^{31}P Product
1	0.5	61.520	+0.011	70.06
2	1.0	61.622	-0.091	70.33
3	5.0	63.824	-2.293	72.84

3.1.5 Metal binding study to diazinon in CD_3OD.

The accelerated hydrolysis of diazinon under NMR conditions in a co-solvent of 70%CD_3OD/30%H_2O made it difficult to ascertain the strength of metal binding to the substrate, especially at elevated ratios. A second set of experiments were carried out in neat CD_3OD to eliminate the effect of hydrolysis and enable one to determine the strength of interaction between the metal ions and substrate over a series of M^{n+}/D. Prior to this, the effect of using CD_3OD in place of the co-solvent was examined over a series of Hg^{2+}/PA ratios, with comparison then made to those shifts obtained in the co-solvent. Figure 3.1.40 shows the obtained spectra in CD_3OD.

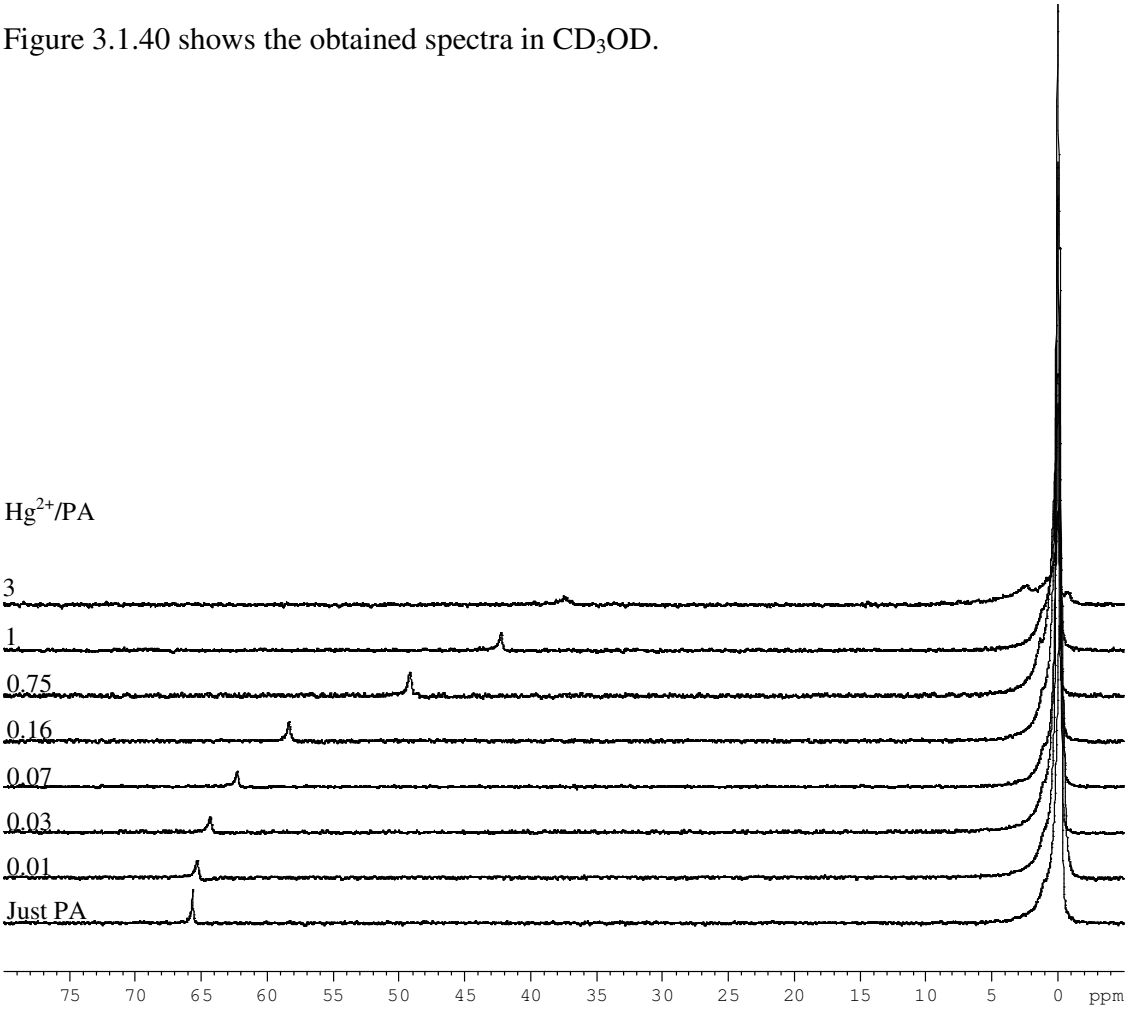

Figure 3.1.40 ^{31}P NMR spectra depicting the chemical shift change of PA phosphorus peak in the presence of increasing Ag^+ concentrations in CD_3OD.

It is now possible to compare the shift data obtained in CD_3OD versus co-solvent by plotting the observed chemical shift change (ppm) against Hg^{2+}/PA ratio (Figure 3.1.41).

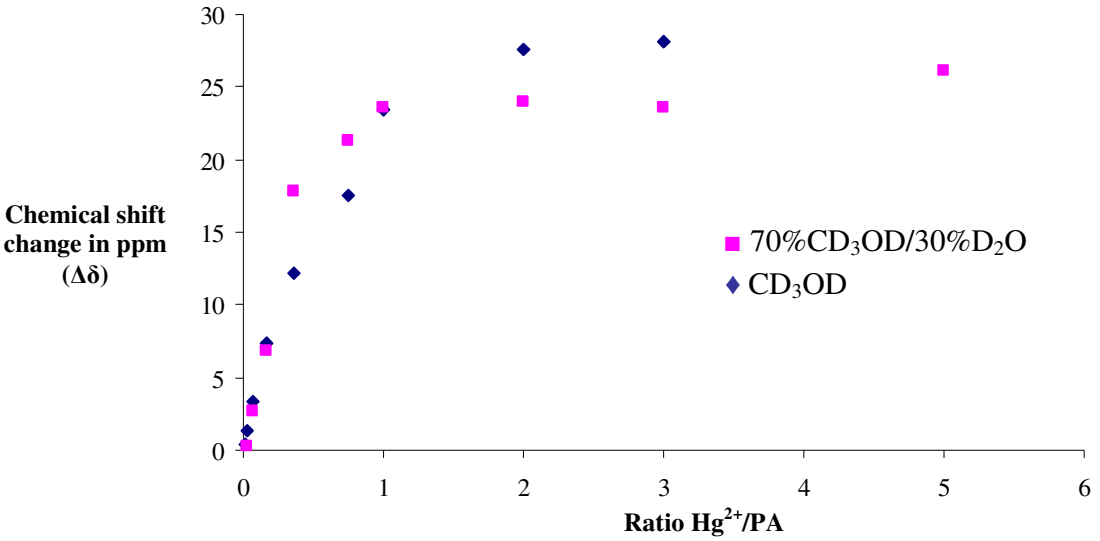

Figure 3.1.41 Effect on the chemical shift of the phosphorus nuclei of PA upon the addition of increasing concentrations of Hg^2, ♦; CD_3OD, ■; 70%CD_3OD/30%D_2O.

The overlaid plots show a correspondence between the observed chemical shift changes in the phosphorus signal of PA in both solvent systems, suggesting that the speciation is of a similar nature. It is therefore reasonable to examine the different metal cation effects on the phosphorus nuclei of diazinon in CD_3OD and derive information about the strength of these interactions. The ^{31}P spectrum of diazinon in the absence of metal ions was obtained in CD_3OD, giving a chemical shift of 61.876ppm.

3.1.5.1 Ag^+ binding to diazinon in CD_3OD

Ag^+ binding with diazinon was examined over a series of ratios to try and reveal the extent of interaction between the metal ion and diazinon. Table 3.1.27 and Figure 3.1.42 depict the chemical shift change observed in the phosphorus nuclei of diazinon upon addition of increasing Ag^+ concentrations.

Table 3.1.27 ^{31}P chemical shift of D in the presence of increasing concentrations of Ag^+ in CD_3OD. [PA] = 1.67 x 10^{-2} Mol L^{-1}.

Ratio of Ag^+/D	Observed chemical shift (ppm)	Chemical shift change (ppm)
0	61.876	N/A
0.2	61.246	0.63
0.5	60.111	1.765
1	59.047	2.829
2	58.812	3.064
4	58.724	3.152

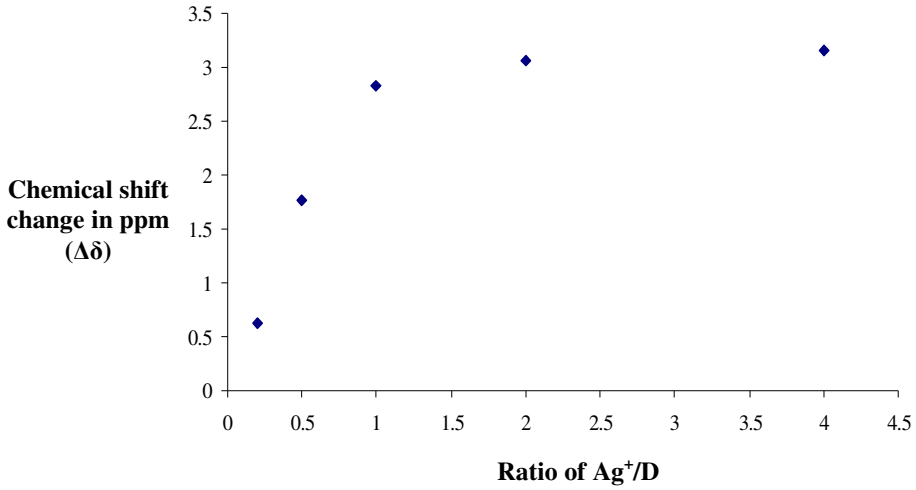

Figure 3.1.42 Effect on the chemical shift of phosphorus nuclei of diazinon upon addition of increasing concentrations of Hg^{2+} in CD_3OD.

Figure 3.1.42 shows clear evidence of a strong interaction between Ag^+ and diazinon. This supports previously obtained shifts in the phosphorus nuclei in the presence of Ag^+ (see Table 3.1.11).

3.1.5.2 Hg^{2+} to diazinon in CD_3OD.

Analogous to Ag^+ a series of experiments were carried out to examine the interaction of Hg^{2+} with diazinon, with Table 3.1.28 showing the obtained chemical shift changes observed with various concentrations of Hg^{2+}. Due to the smaller changes observed each ratio was run in duplicate and some cases quadruplicate (Table 3.1.28 shows the average values). The most significant point is the small chemical shift changes observed in the phosphorus nuclei, especially when compared against the changes obtained in the presence of Ag^+ ions. This suggests a weak association of Hg^{2+} with the sulfur of diazinon, with the observed accelerations caused by Hg^{2+} possibly due to a greater interaction in the transition-state than the unaltered substrate.

Table 3.1.28 ^{31}P chemical shift of D in the presence of increasing concentrations of Hg^{2+} in CD_3OD. [PA] = 1.67 x 10^{-2} Mol L^{-1}.

Ratio of Hg^{2+}/D	Observed chemical shift (ppm)	Chemical shift change (ppm)
0	61.88	N/A
0.07	61.83	0.05
0.36	61.90	-0.02
1	61.83	0.05
2	61.82	0.06
3	61.83	0.05
4	61.75	0.13
5	61.88	0

The result supports previous data obtained using the co-solvent, additionally indicating a reduced interaction of Hg^{2+} with Diazinon. These smaller changes in the chemical shift of proton and phosphorus nuclei close to the sulfur ligand can be seen in Table 3.1.20 and Table 3.1.21 ($\mathbf{H^b}$). An important observation to bring forth is the comparable effect both Hg^{2+} and Ag^{+} binding to the sulfur ligand of PA had on the chemical shift environment of phosphorus nuclei (Figure 3.1.6 and Figure 3.1.10). This similarity however does not transfer to binding with Diazinon, where the interaction seems to be significantly stronger with Ag^{+}. Previously obtained rate data on similar organophosphorus pesticides and kinetics performed in the present study indicate Hg^{2+} facilitates the rate of hydrolysis to a greater extent than Ag^{+}; certainly at neutral and acidic conditions. These accelerations together with the lack of substantiation of Hg^{2+} co-ordination to Diazinon, may indicate that the facilitation of hydrolysis in the presence of Hg^{2+} is due to a stronger interaction with the negatively charged transition state, with resultant stabilisation.

3.1.5.3 Cd^{2+} binding to diazinon in CD_3OD.

Cd^{2+} interaction with diazinon was also assessed over a series of Cd^{2+}/D ratios. Table 3.1.29 and Figure 3.1.43 depict the chemical shift changes observed upon addition of Cd^{2+} (ratio 1.0 omitted from plot). The plot clearly depicts an interaction between Cd^{2+} and diazinon, however not as strong as that observed with Ag^{+}. This corresponds to the results obtained in the PA study in the presence of Ag^{+} and Cd^{2+}. This implies cadmium's minimal effect on the rate of hydrolysis of diazinon in comparison to the other metals studies is due to its reduced effect on the phosphorus nuclei of diazinon.

Table 3.1.29 ^{31}P chemical shift of D in the presence of increasing concentrations of Cd^{2+} in CD_3OD. [PA] = 1.67 x 10-2 Mol L-1.

Ratio of Cd^{2+}/D	Observed chemical shift (ppm)	Chemical shift change (ppm)
0	61.876	N/A
0.5	61.823	0.053
1.0	61.864	0.012
2.5	61.802	0.074
5	61.782	0.094
10	61.712	0.164
25	61.610	0.266

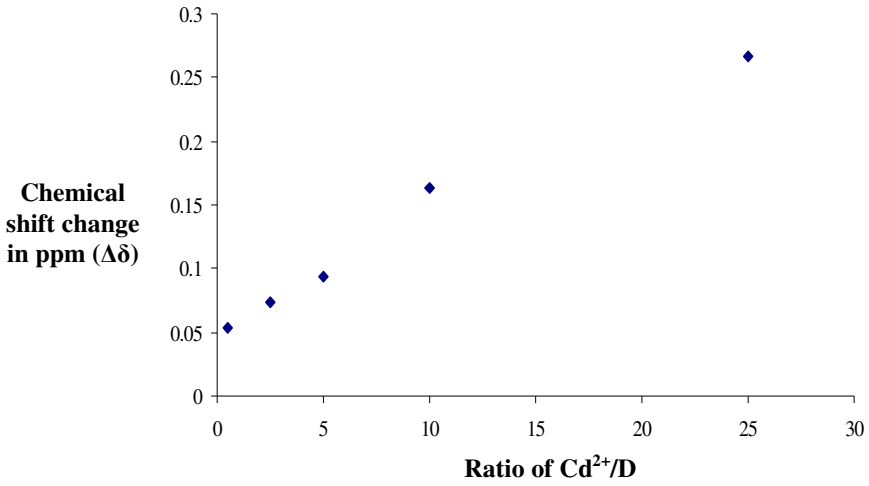

Figure 3.1.43 Effect on the chemical shift of phosphorus nuclei of diazinon upon addition of increasing concentrations of Cd^{2+} in CD_3OD.

3.2 Electrospray mass Spectrometry

3.2.1 General overview

Electrospray Mass Spectrometry was used as a technique to probe and pinpoint the location of metal complexation to diazinon. ^{1}H and ^{31}P NMR have revealed to a large extent the probable interactions of the metal cations with the ligand sites of both diazinon and its hydrolysis products PA and PY. These proposed metal-to-substrate interactions identified in the NMR study were further elaborated upon using Electrospray mass spectrometry in conjunction with tandem MS/MS. The ionisation technique of Electrospray was primarily chosen to benefit from its soft ionisation process. Electrospray, in comparison to harsher ionisation techniques such as Electron Impact, causes significantly reduced fragmentation; therefore increasing the chances of observing the desired metal-diazinon complex without the appearance of complicated fragmentation patterns.

Low energy collision-induced dissociation MS/MS analysis of the parent complex obtained in conventional MS spectra can be subsequently performed. This will aid in giving substantial information about the site or sites of complexation of the metal cations with diazinon itself. This is effected by observing specific fragmentations (daughter ions) containing the ligand(s) with metal bound, confirmed by the presence of the isotopic pattern relative to that metal. These metal-to-substrate interactions may further be substantiated by running a parallel set of experiments where ESI-MS is performed on the hydrolysis products PA and PY in the presence of metal cations.

3.2.2 ESI-MS in the absence of metal ions

Initial ESI mass spectra were obtained of an unbuffered solution of diazinon in the absence of metal ions using positive ion mode. This was done adjusting the pH to 4.0 using 0.1M HCl and 0.1M NaOH, resulting in protonation at the site with highest proton affinity in diazinon. The resultant ESI-MS spectrum of diazinon and its fragmentation pattern is shown in Figure 3.2.1, with interpretation of the different m/z ratios shown in Table 3.2.1. The important structures are shown overlaid on the spectrum.

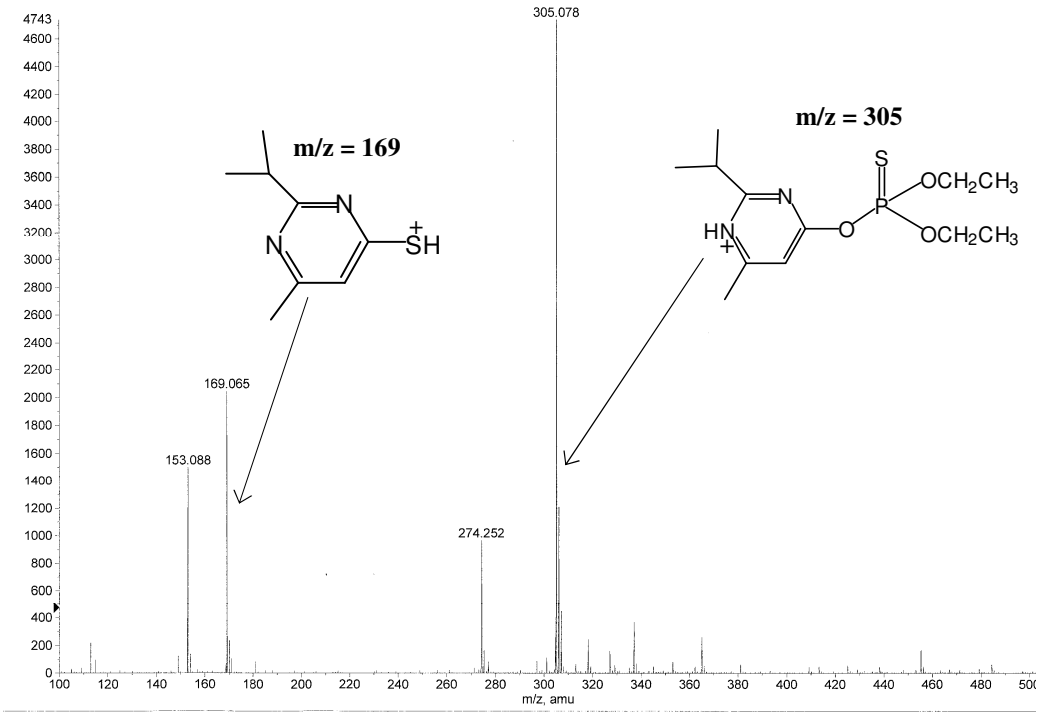

Figure 3.2.1 Positive ion ESI spectrum of an unbuffered methanol solution of diazinon (10.28µM).

Table 3.2.1 Interpretation of ESI-MS data for the unbuffered solution of diazinon.

Concentration of D	Ions at *m/z*	Identification of ions
1.028×10^{-5}M	153	$[PY + H]^+$
	169	Rearrangement (Thiono-thiolo)
	305	$[D + H]^+$

Isolation and fragmentation of protonated diazinon produced 3 significant ions with m/z ratios of 153, 169 and 305. The softness of the ionisation technique is confirmed by the presence of a strong signal at m/z ratio of 305, with signifies protonated diazinon. Its appropriateness as a soft ionisation process ideally suited to observe the complexed diazinon is further established by the absence of m/z ratios at 277 and 249. These are formed by the sequential loss of ethene from the ethoxy groups. The observed peak at 169 is due to a thiono-thiolo rearrangement of protonated diazinon with subsequent fragmentation. This has been reported before in work by Barr et al.[23], who studied the fragmentations and reactions of diazinon by Electrospray ionisation ion trap mass spectrometry. The author noted the same peak at m/z of 169 and attributed it to a novel intramolecular thiono-thiolo rearrangement. The peak at m/z 153 is attributed to protonated pyrimidinol.

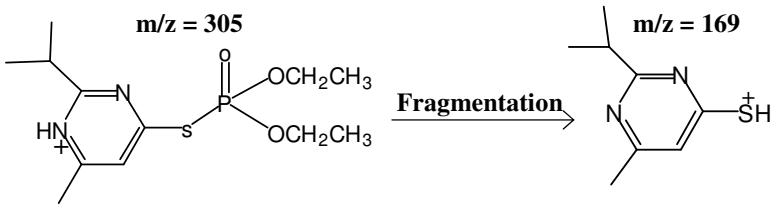

Scheme 3.2.1 Thiono-thiolo rearrangement with subsequent fragmentation observed at 169 m/z.

The placement of the proton shown in Figure 3.2.1 is assigned based on experimental proton affinities obtained from literature sources. These are shown in Table 3.2.2.

Table 3.2.2 Proton affinities of the different basic groups of diazinon.

Group	Proton affinity (kJ mol^{-1})
P=S	880
P=O [a]	890
P-OR	780
2-Isopropyl-4-methyl-6-pyrimidinol[1].	945 (N-1) 956 (N-3) enol form 957 (N-3) keto form

a = Obtained from Barr. J. D. et al.[25]

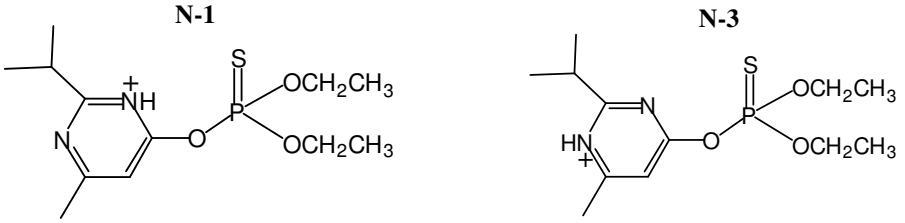

Figure 3.2.2 Different protomers of diazinon with proton affinities given in Table 3.2.2.

The proton affinities listed in Table 3.3.2 show that N-3 is considered the most likely point of protonation of the hereoatoms in diazinon. This is further confirmed by the presence of a m/z of 153 in the ESI-MS spectrum representing protonated PY. The above structures may also exist in their oxonium forms.

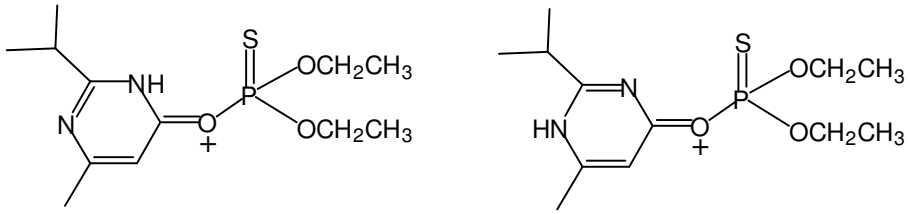

Figure 3.2.3 Oxonium forms of protonated diazinon.

3.2.3 ESI-MS of diazinon in the presence of Ag^+

The ESI-MS spectrum of diazinon was studied in the presence of 1 x 10^{-3}M Ag^+. This was effected by initially spraying diazinon solution (1.028 x 10^{-5}M) into the ionisation source and obtaining a spectrum with m/z ratio 305 present. The low micromolar Ag^+ solution was then injected through a separate loop into the ionisation source to give the optimum chance of obtaining the desired complexed ion of $[D + Ag]^+$. Ag^+ containing ions can be readily interpreted based on their isotopic pattern of ^{107}Ag and ^{109}Ag, with natural abundance ratio 52:48 % respectively[26]. Figure 3.2.4 shows the spectrum prior to Ag^+ injection, with Figure 3.2.5 depicting the change after introduction of the metal ion into the ionisation source.

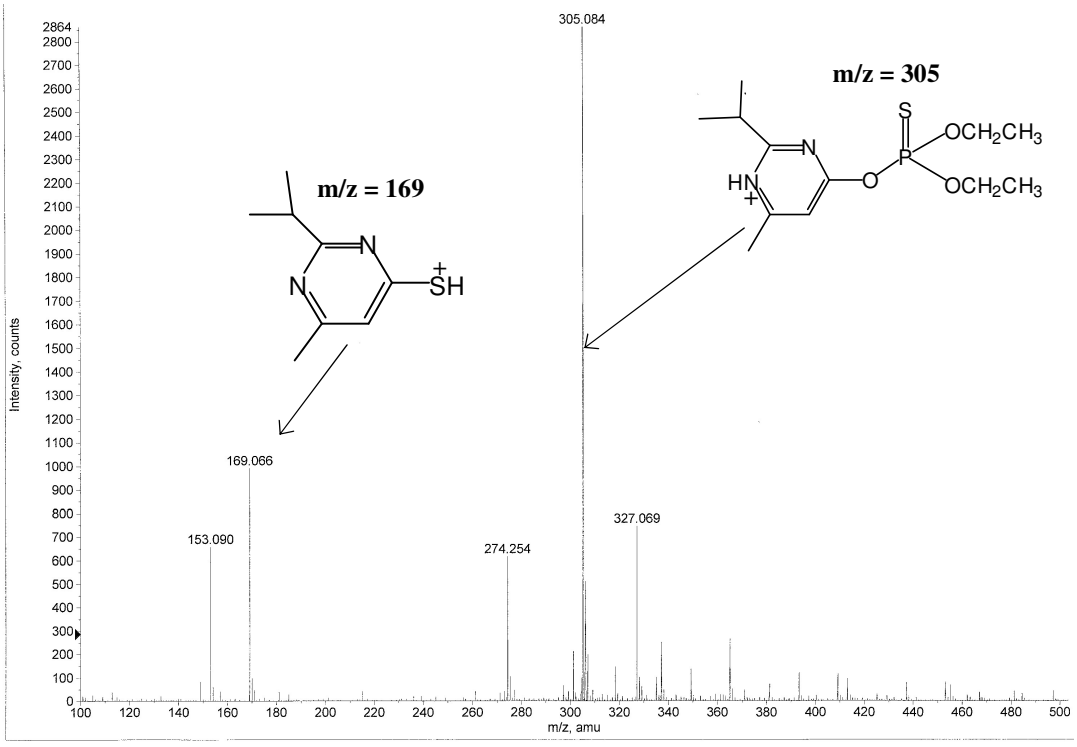

Figure 3.2.4 Positive ion mode spectrum of diazinon prior to Ag^+ injection.

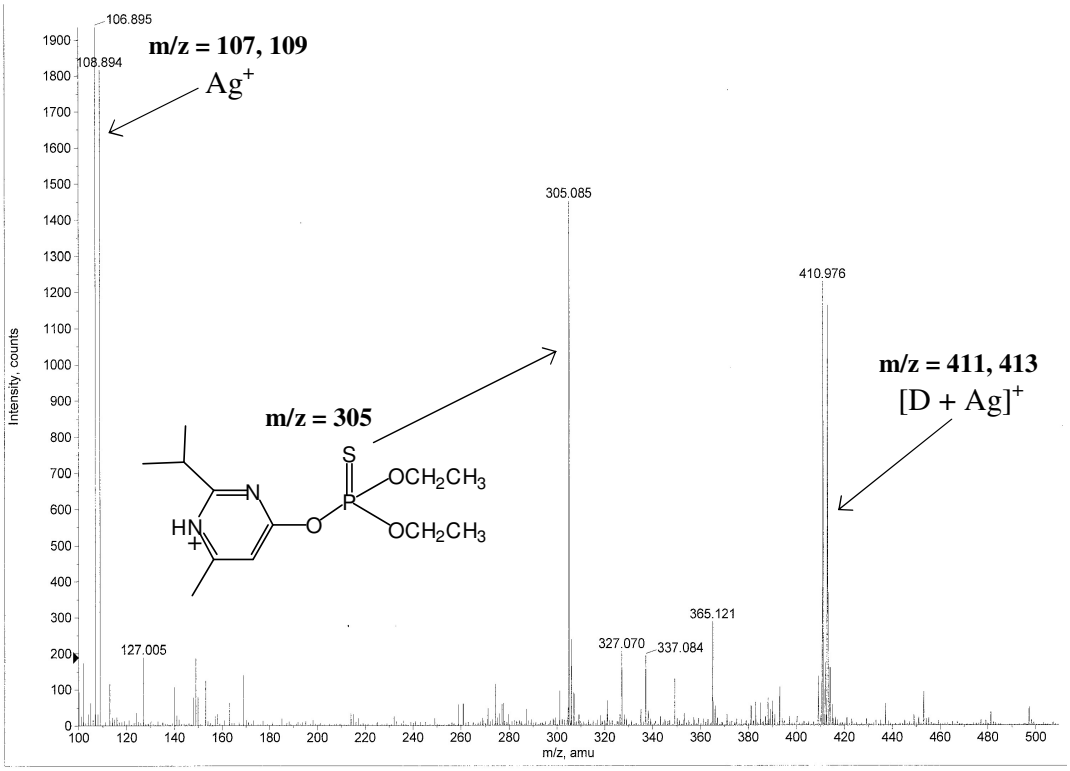

Figure 3.2.5 Positive ion mode spectrum of diazinon in the presence of Ag^+.

As before the ESI-MS spectrum of diazinon shows the protonated form at 305 m/z, the thiono-thiolo rearrangement at 169 m/z and protonated PY at 153 m/z. The spectrum obtained upon addition of Ag^+ ions (Figure 3.2.5) shows some significant changes. The major peaks in the spectrum are those of Ag^+ itself at 107 and 109 m/z with its characteristic isotopic ratio of 52:48 %, in addition to the protonated form of diazinon at 305 m/z. The most important observation however is the appearance of peaks at 411 and 413 m/z exhibiting the isotopic ratio of Ag^+. This indicates diazinon (304 amu) complexed with Ag^+ (107, 109 amu) and is clear evidence of the ability of the cation to complex the substrate. On a separate run a further complexation of Ag^+ with 2 molecules of diazinon was noted at 715, 717 m/z.

Verification of Ag^+ complexation to diazinon was made by performing low energy CID experiments on the proposed complexed ion (411, 413 m/z) and interpreting its fragmentation pattern. These CID or MS/MS experiments may also allow one to give definitive structural information of the location of Ag^+ binding to diazinon. It is important to point out that CID experiments are performed by isolating one m/z ratio at a time; therefore separate CID experiments were performed on each isotopic ratio, namely 411 and 413 m/z. Figure 3.2.6 shows the obtained CID spectrum of the peak at m/z 411.

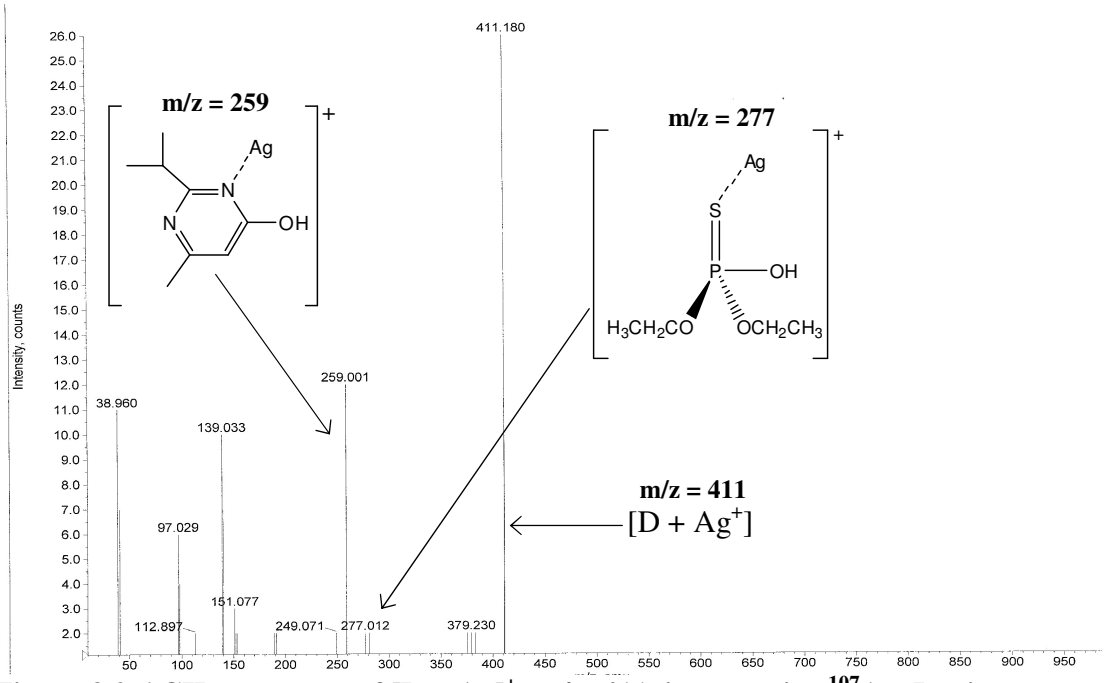

Figure 3.2.6 CID spectrum of $[D + Ag]^+$; m/z=411, i.e. contains ^{107}Ag. Depicts various fragmented ions.

The daughter ions at m/z 259 and 277 are fragments pertaining to Ag^+-bound PY and PA originating from the parent peak of m/z 411. The m/z at 259 is PY (152 amu) + Ag^+ (107 amu) whilst the m/z at 277 is PA (170 amu) + Ag^+ (107 amu). This shows that the parent peak was in fact Ag^+-bound diazinon. Significantly the fragmentation of the parent peak caused by the collision gas shows Ag^+ bound at both nitrogen and sulfur ligand sites. It

was noted at this point that the parent peak (411 m/z) still had a significant intensity and the peak corresponding to Ag^+-bound PA (277 amu) was correspondingly small. It was therefore decided to increase the energy of the collision gas in an attempt to fragment a greater percent of the parent ion. Figure 3.2.7 shows the fragmentation with increased collision energy. The spectrum shows a significant decrease in the intensity of the parent ion and a more intense peak at 277 for Ag^+-bound-PA.

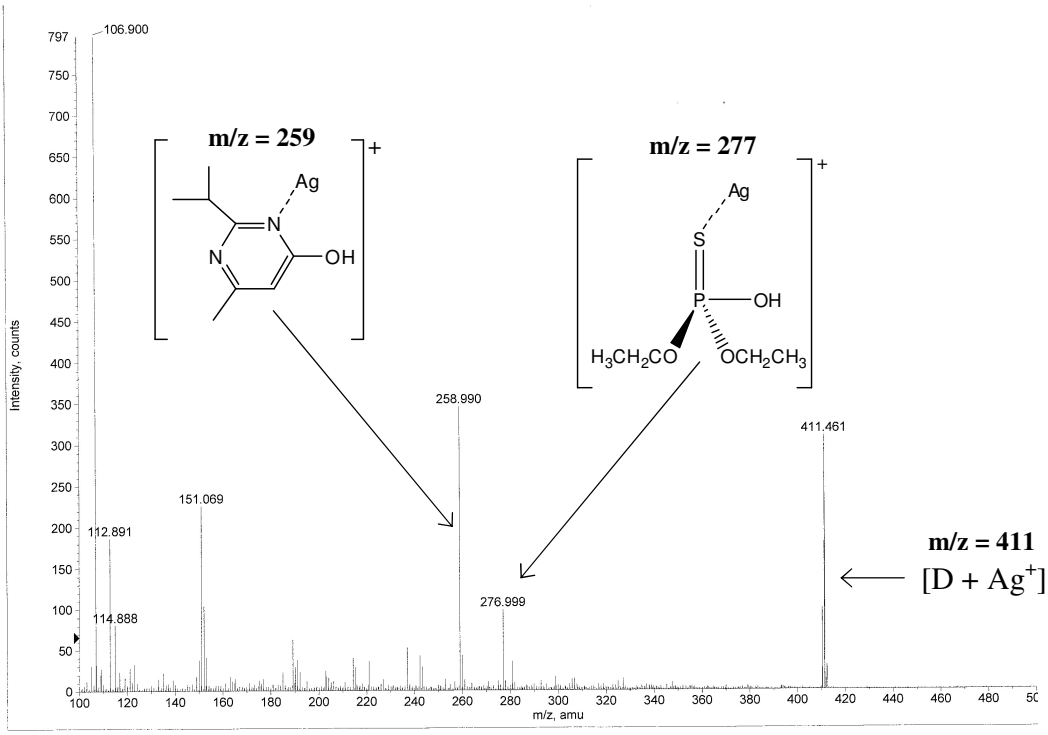

Figure 3.2.7 CID spectrum of $[D + Ag]^+$ with increased collision energy (m/z=411, i.e. contains ^{107}Ag). Depicts a decrease in intensity of the parent ion (411 m/z) due to greater fragmentation.

An identical CID experiment was run on the 413 m/z isotopic peak with Figure 3.2.8 showing the obtained spectrum. Analogous to the 411 m/z peak, this parent peak produced fragments of m/z 261 and 279 corresponding to PY (152 amu) + Ag^+ (109 amu) and PA (170 amu) + Ag^+ (109 amu). The difference of 2 amu between the fragments obtained from the separate isotope ratios is evident.

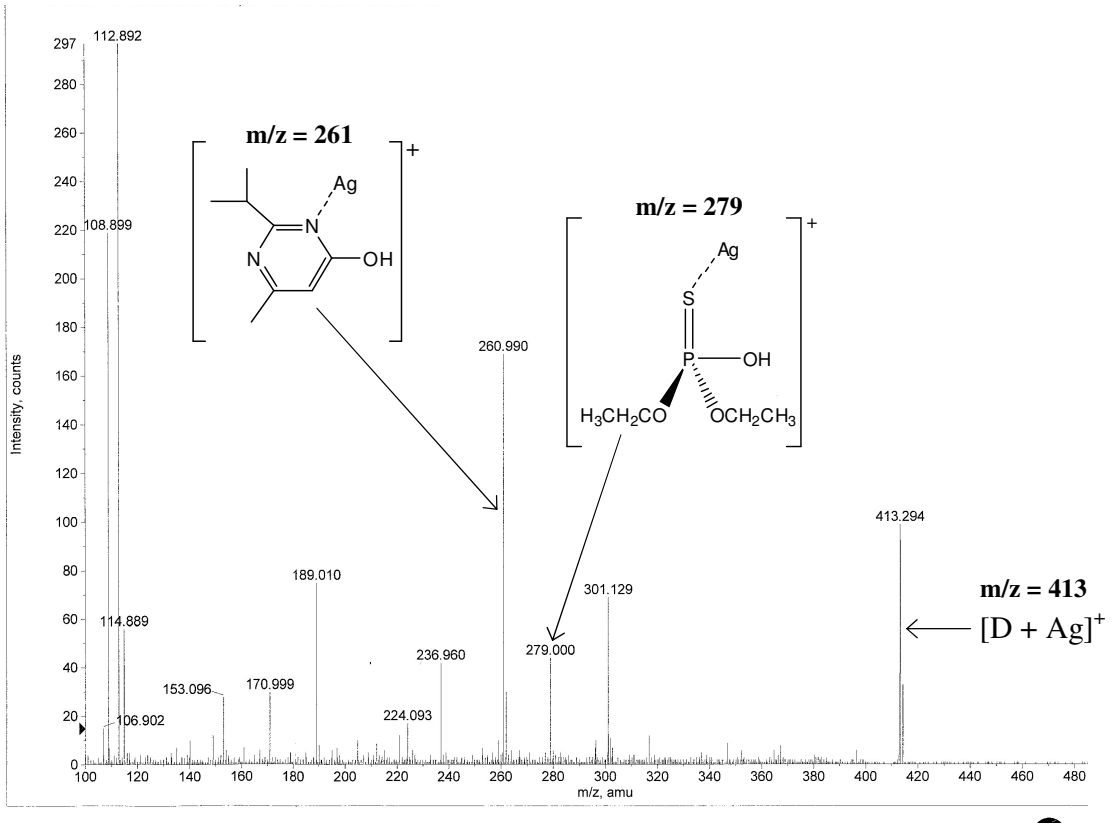

Figure 3.2.8 CID spectrum of $[D + Ag]^+$; m/z=413, i.e. contains ^{109}Ag. Depicts various fragmented ions.

Table 3.2.3 outlines the different m/z ratios observed in both the initial ESI-MS spectra and subsequent CID experiments on selected peaks.

Table 3.2.3 Interpreted ESI-MS data for the interaction of Ag^+ with diazinon. Includes initial ESI-MS spectral ions and resultant CID fragmentation on selected ions. diazinon (D) = 1.028 x 10^{-5}M, Ag^+ = 1 x 10^{-3}M.

Experiment	Ions (m/z)	Identification of ions
Initial ESI-MS of D	305	$[D + H]^+$
	169	Thiol-thiono rearrangement
	153	$[PY + H]^+$
ESI-MS of D in the presence of Ag^+	305	$[D + H]^+$
	411-413	$[D + {}^{107}Ag]^+$ and $[D + {}^{109}Ag]^+$

Continued...Table 3.2.3

Experiment	Ions (m/z)	Identification of ions
ESI-MS of D in the presence of Ag^+, cont…	107-109	Ag^+
CID experiment on m/z 411	411	$[D + {}^{107}Ag]^+$
	259	$[PY + {}^{107}Ag]^+$
	277	$[PA + {}^{107}Ag]^+$
CID experiment on m/z 413	413	$[D + {}^{109}Ag]^+$
	261	$[PY + {}^{109}Ag]^+$
	279	$[PA + {}^{109}Ag]^+$

3.2.3.1 Ag^+ binding to hydrolysis products PA and PY

The Ag^+-diazinon interactions observed in the above experiments were further investigated by analysing Ag^+ binding to both diazinon hydrolysis products, PA and PY. Figure 3.2.9 shows PY in the presence of Ag^+ and analogous to the CID experiments, confirms Ag binding to PY at m/z 259, 261 (i.e. PY (152 amu) + Ag^+ (107, 109 amu)). This further establishes Ag^+ affinity for the nitrogen ligand. The other peaks observed include $[PY + H]^+$ at 153 m/z and Ag^+ itself at 107, 109 m/z.

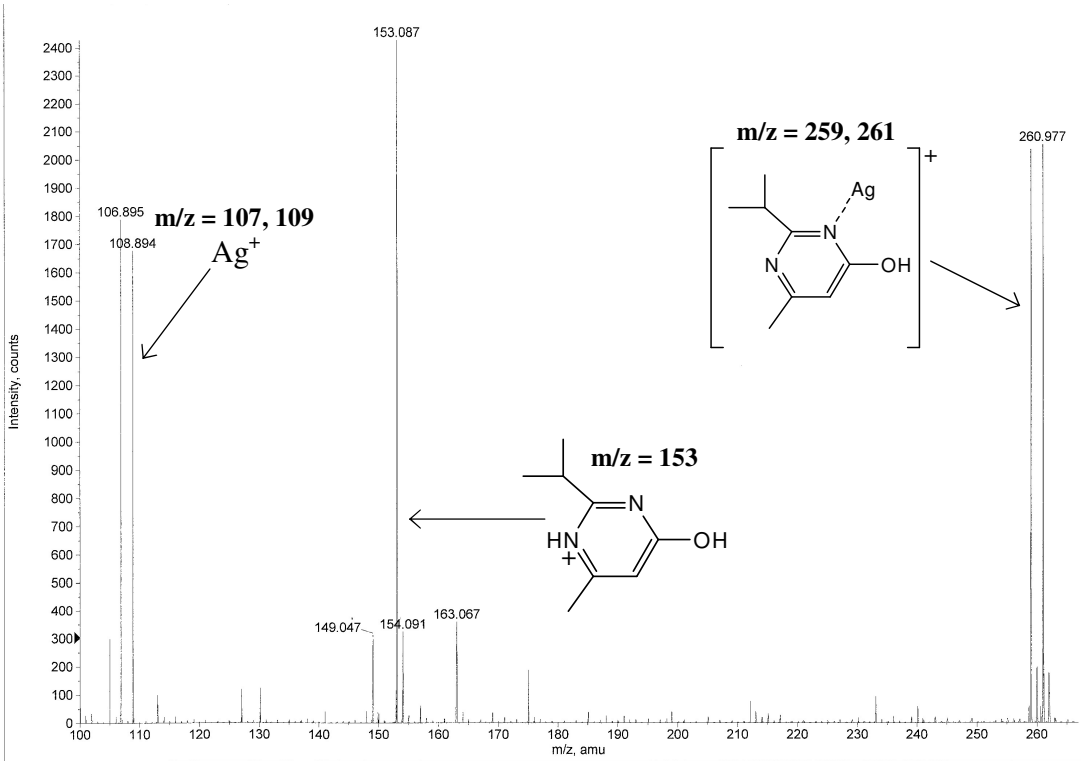

Figure 3.2.9 Positive ion mode ESI mass spectrum of 10.0 µM of pyrimidinol with 1000 µM Ag^+.

Initial positive ion mode analysis of PA in the presence of Ag^+ did not yield any complexation between the substrate and metal ion. However, once negative ion mode was employed complexation between Ag^+ and PA was observed. Figure 3.2.10 and 3.2.11 shows the negative ion spectrum of PA in the absence and presence of Ag^+ ions. The initial spectrum shows the unbound PA at 169 m/z. Addition of Ag^+ results in the appearance of peaks at 445 and 447 m/z with the isotopic pattern of Ag. These peaks signify Ag complexed with two PA molecules as shown in Figure 3.2.11 (2PA (338 amu) + Ag (107, 109 amu). The ESI-MS data clearly show Ag^+ coordination at both sulfur and nitrogen ligands in conformity with observed NMR data. The CID experiments also gave invaluable insight into binding of diazinon itself and suggest chelation as a possible mode of action for the Ag^+ ions. This will be discussed in more detail in later sections.

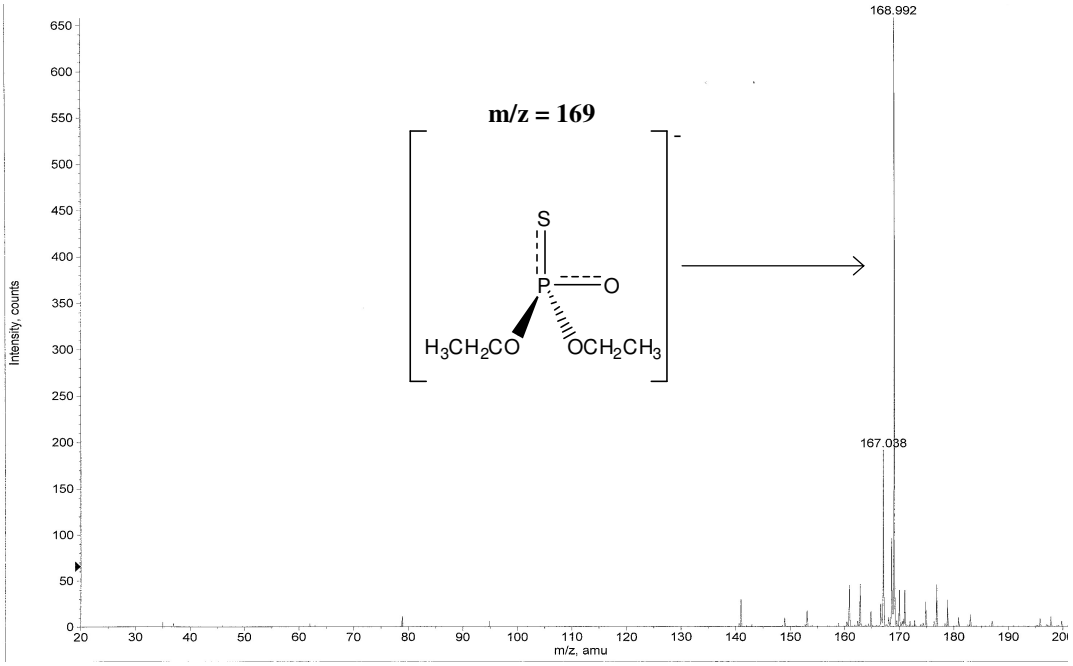

Figure 3.2.10 Negative ion mode ESI mass spectrum of 10.8µM PA in the absence of Ag^+ ions.

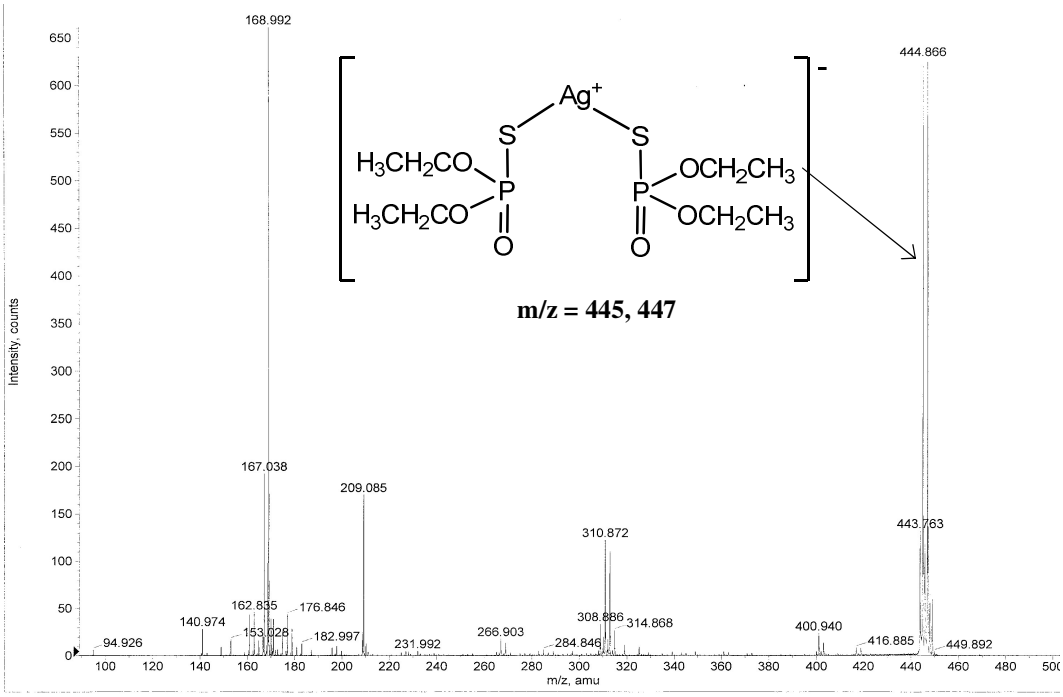

Figure 3.2.11 Negative ion mode ESI mass spectrum of 10.8µM PA in the presence of 1000µM of Ag^+.

3.2.4 ESI-MS of diazinon in the presence of Cu^{2+}

As in the case of Ag^{+}, the complexation of Cu^{2+} with diazinon was studied using ESI-MS by analysing the different m/z ratios observed with 1.028 x 10^{-5}M diazinon in the presence of 1 x 10^{-3} M Cu^{2+}. Any Cu^{2+}-containing species are readily identifiable by its isotopic pattern ^{63}Cu and ^{65}Cu, with natural abundance 69% and 31 % respectively[3]. Analogous to Ag^{+}, diazinon was sprayed into the ionisation chamber and an initial ESI-MS spectrum was recorded in the absence of Cu^{2+} ions. Subsequently, Cu^{2+} ions were sprayed into the ionisation source through a separate loop. The resultant ESI-MS spectrum is shown in Figure 3.2.12.

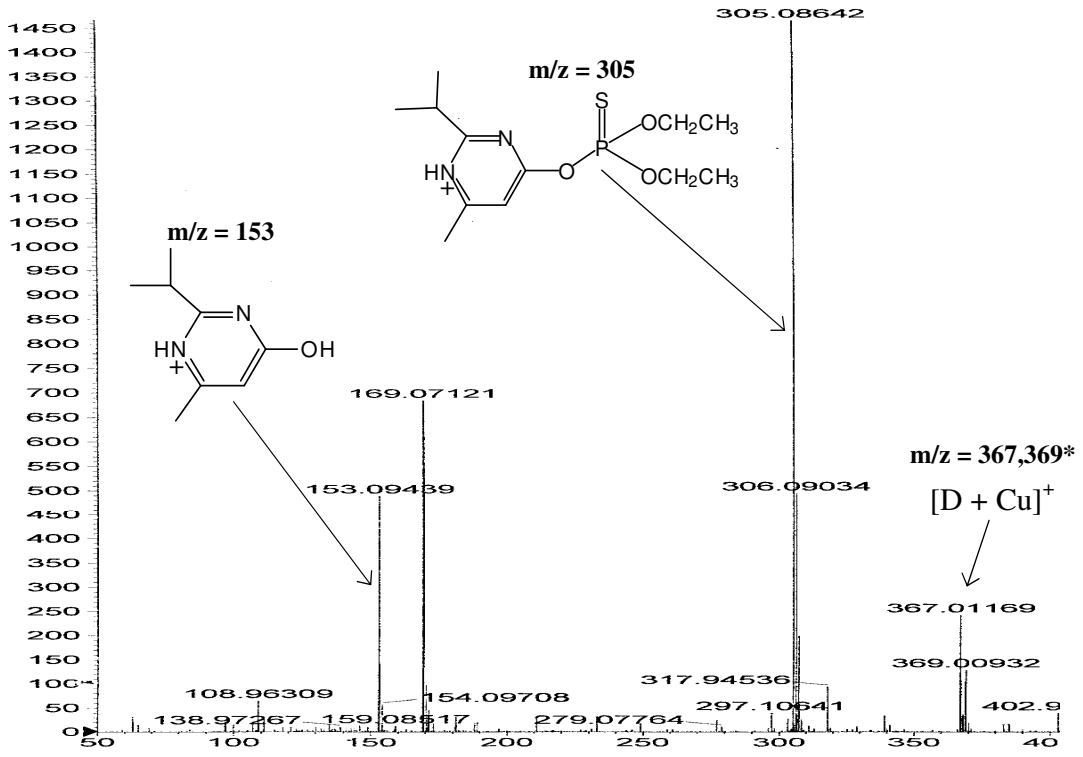

Figure 3.2.12 Positive ion mode spectrum of diazinon in the presence of Cu^{2+}.

In common with the Ag^+ experiments, the ESI-MS spectrum of diazinon shows the appearance of a peak at 305 m/z which is consistent with protonated diazinon. There are in addition peaks at 169 and 153 m/z, corresponding to thiono-thiolo rearrangement and protonated PY respectively. Of greater importance is the isotopic pattern of Cu^{2+} observed at 367 and 369 m/z, which is consistent with Cu-bound diazinon (D (304 amu) + Cu^+ (63, 65 amu)). This gives clear evidence of the ability of Cu to complex diazinon. Figure 3.2.13 depicts an expanded view of the proposed complex.

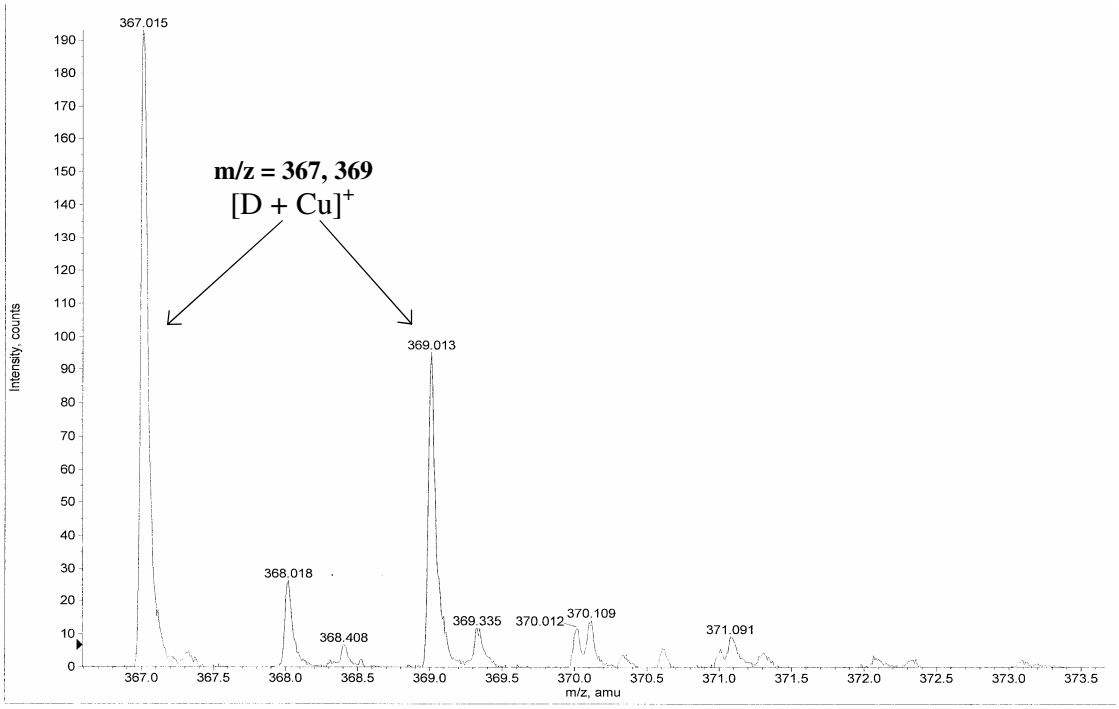

Figure 3.2.13 Expanded view of proposed [D + Cu] with m/z of 367, 369 and isotopic ratio of 69:31%.

The complex is further confirmed by the appearance of a Cu isotopic pattern at 339/341 m/z, which indicates the loss of ethene (28 amu) from the complexed ion. There is also a Cu isotopic pattern at 671, 673 m/z which would indicate two diazinon molecules coordinated with Cu. An important point to note is that the complex ions at 367, 369 m/z

and 671, 673 m/z suggest Cu binding to diazinon in the +1 oxidation state. If binding occurred in the +2 oxidation state one would expect to see half the amu observed. Although this is a gas phase study the suggested binding of Cu in the +1 oxidation state is in agreement with observations made in the NMR studies. Cu^{+} is a 'softer' metal than its +2 oxidation state and would be expected to have a greater affinity for sulphur than the +2 state.

Verification of Cu complexation to diazinon was made by performing low energy CID experiments on the proposed complexed ion (411, 413 m/z) and interpreting its fragmentation pattern. The CID or MS/MS experiments will also allow one to pinpoint the site or sites of Cu co-ordination to diazinon. The CID experiment was carried out on the observed parent peak at 367 m/z (i.e. [D + ^{63}Cu]). The obtained spectrum is shown in Figure 3.2.14.

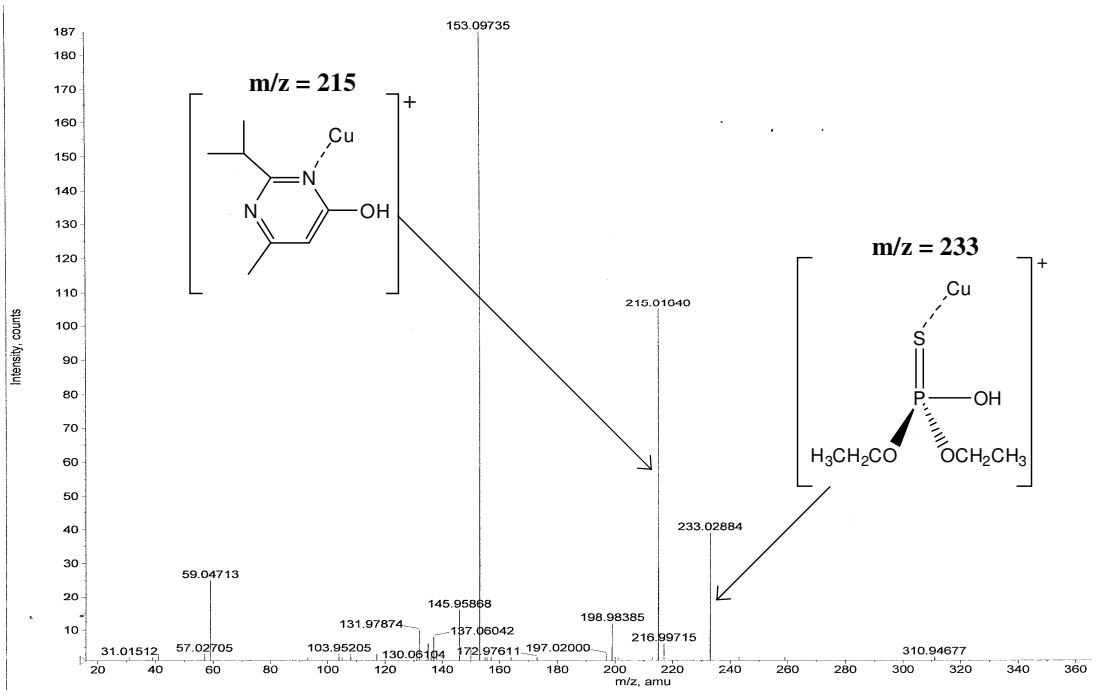

Figure 3.2.14 CID spectrum of [D + Cu]$^{+}$; m/z=367, i.e. contains ^{63}Cu. Depicts various fragmented ions

The daughter ions at m/z 215 and 233 are fragments pertaining to Cu-bound PA and PY originating from the parent peak of m/z 367. They signify PY (152 amu) + Cu^+ (63 amu) and PA (170 amu) + Cu^+ (63amu). This shows that the parent peak was in fact Cu-bound diazinon. The fragmentation of the parent complex caused by the collision gas resulted in fragments with Cu bound at both nitrogen and sulfur ligand sites and is corresponding result as that obtained with Ag ions. Similarly to Ag this suggests the formation of a chelate could be an important influence on the role Cu ions play in the hydrolysis of Diazinon. Table 3.2.4 outlines the different m/z ratios observed in both the initial ESI-MS spectra and subsequent CID experiments on selected peaks.

Table 3.2.4 Interpreted ESI-MS data for the interaction of Cu^{2+} with diazinon. Includes initial ESI-MS spectral ions and resultant CID fragmentation on selected ions. diazinon (D) = 1.028 x 10^{-5}M, Cu^{2+} = 1 x 10^{-3}M.

Experiment	Ions (m/z)	Identification of ions
Initial ESI-MS of D	305	$[D + H]^+$
	169	Thiol-thiono rearrangement
	153	$[PY + H]^+$
ESI-MS of D in the presence of Cu^{2+}	305	$[D + H]^+$
	367-369	$[D + {}^{63}Cu]^+$ and $[D + {}^{65}Cu]^+$
	671-673	$[2D + {}^{63}Cu]^+$ and $[2D + {}^{65}Cu]^+$
CID experiment on m/z 367	215	$[PY + {}^{63}Cu]^+$
	233	$[PA + {}^{63}Cu]^+$

3.2.4.1 Cu binding to hydrolysis products PA and PY

The Cu interactions with diazinon proposed from the initial ESI-MS and CID experiments were further explored by analysing Cu binding to both diazinon hydrolysis products PA and PY. Figure 3.2.15 shows PY in the presence of Cu^{+}. The peaks exhibiting the isotopic ratios of Cu at 215, 217 m/z confirms Cu coordination with PY. This is consistent with the m/z results obtained with the CID experiments on the complex ion (Figure 3.2.14). This further establishes Cu affinity for the nitrogen ligands. The other peaks observed include $[PY + H]^{+}$ at 153 m/z.

As with Ag^{+} a negative ion mode experiment was carried out with Cu in the presence of PA, with Figure 3.2.16 depicting the obtained spectra. The peaks at 401, 403 m/z contain the isotopic pattern of Cu which indicates 2PA (338 amu) molecules bound by Cu (63, 65 amu). This further corroborates Cu interaction with the sulphur ligand. The obtained mass to charge ratios observed for the complexes between Cu and the hydrolysis products indicate Cu binding in the +1 oxidation state.

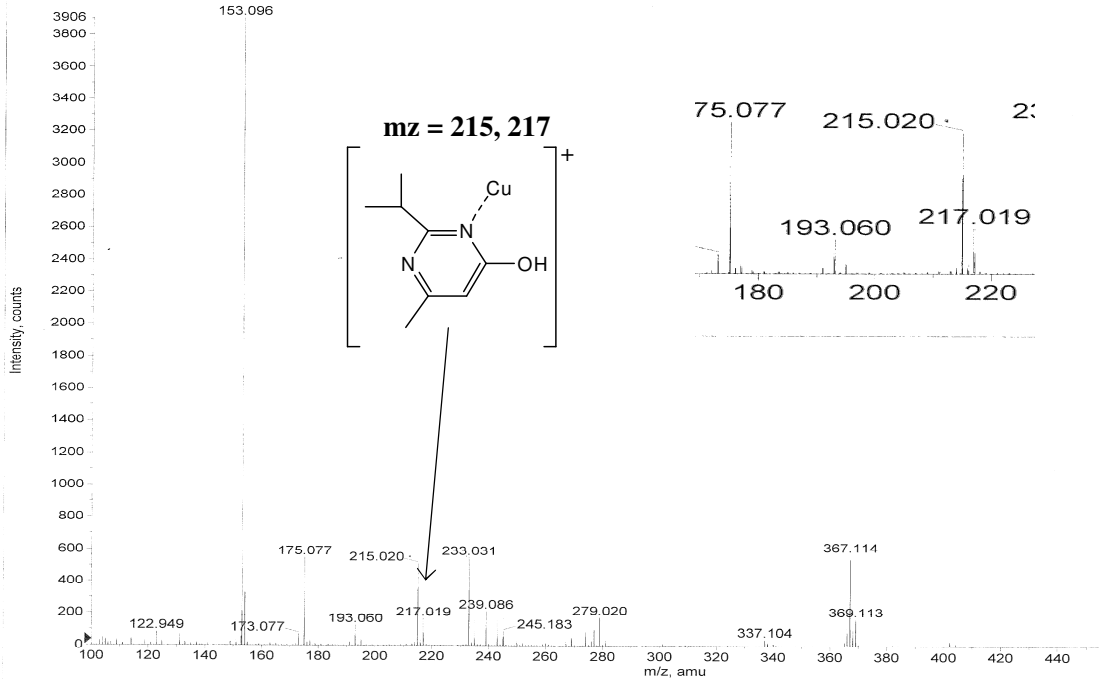

Figure 3.2.15 Positive ion mode ESI mass spectrum of 10.0 µM of pyrimidinol with 1000 µM Cu^{2+}. Inset; Expanded view of complexed PY.

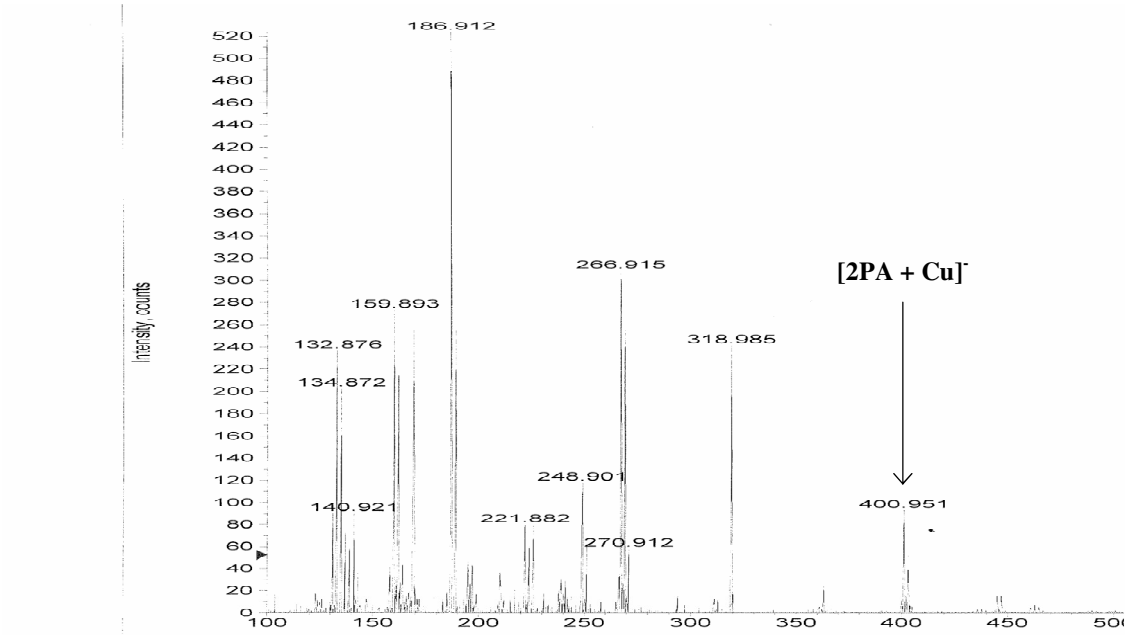

Figure 3.2.16 Negative ion mode ESI mass spectrum of 10.8µM PA in the presence of 1000µM of Cu^{2+}.

3.2.5 ESI-MS of diazinon in the presence of Hg^{2+}

Analogous to the Ag^{+} and Cu^{2+} ESI-MS studies, the complexation between Hg^{2+} and diazinon was examined to try pinpoint the locality of the interaction between the metal and substrate. Any species complexed with mercury are readily identified by its characteristic isotopic pattern consisting of ^{196}Hg, ^{198}Hg, ^{199}Hg, ^{200}Hg, ^{210}Hg, ^{202}Hg and ^{204}Hg. The natural abundance of each isotope is as follows, 0.14, 10.02, 16.84, 23.13, 13.22, 29.80 and 6.85 respectively [3]. If for example Hg^{2+} was to bind with diazinon one would expect to see a peak of 304 amu + the isotopic pattern of Hg^{2+}. Prior to the introduction of metal into the ionisation source a spectrum of diazinon was obtained which is shown in Figure 3.2.17.

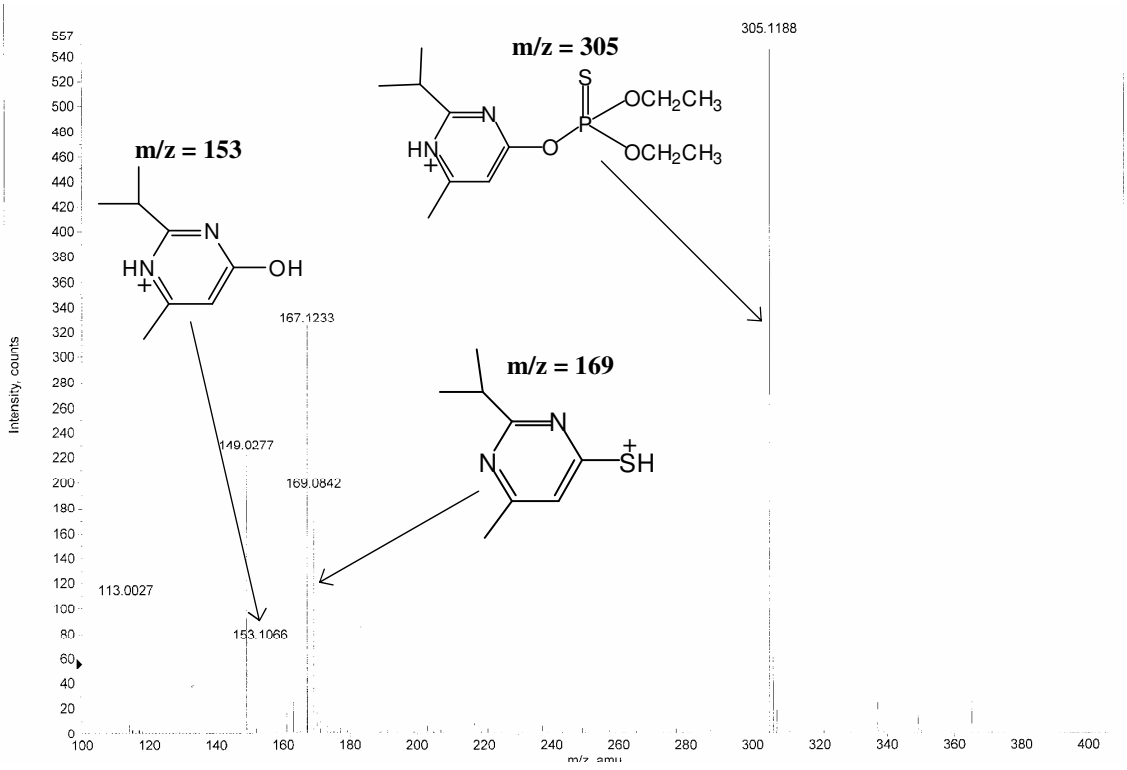

Figure 3.2.17 Positive ion mode spectrum of diazinon prior to Hg^{2+} injection.

In contrast to the metals studied previously, the addition of Hg^{2+} into the ionisation source did not result in the observation of the complexed ion D-Hg^{2+}. Figure 3.2.18 shows the spectrum obtained after 1.5 min. A striking observation however is the disappearance of the parent compound diazinon at m/z 305. This disappearance suggests an extremely fast rate of decomposition of diazinon in the presence of Hg^{2+}, as confirmed later by rate data determined by UV-spectroscopy.

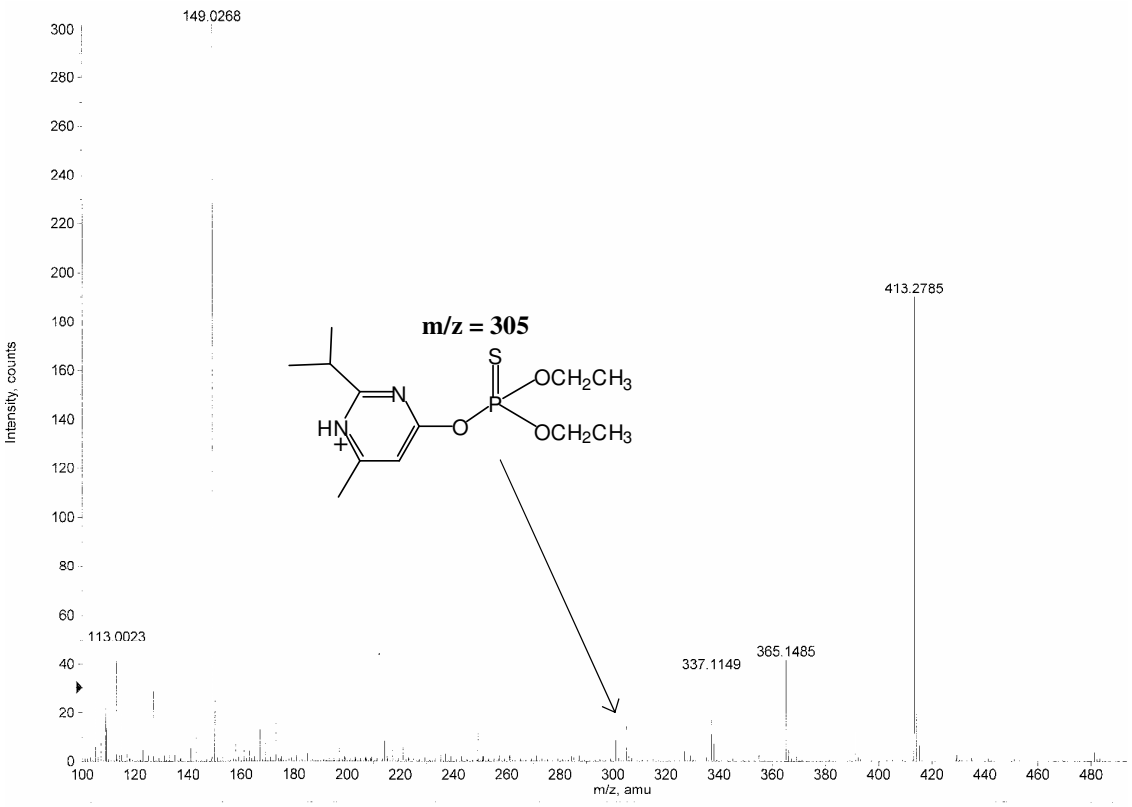

Figure 3.2.18 Rapid disappearance of diazinon peak upon addition of Hg^{2+}.

Further evidence of the fast disappearance of diazinon upon addition of Hg^{2+} is depicted in Figure 3.2.19, showing the total ion count for protonated diazinon (m/z = 305) over time. The injection of Hg^{2+} into the ionisation source occurred at approximately 1.0 - 1.3min. Directly preceding its introduction one can clearly see the rapid drop in the

intensity of the diazinon signal until it bottoms out. Once all the Hg^{2+} is used up there is then a pick up in the intensity of the diazinon signal, as can be seen after 5 min.

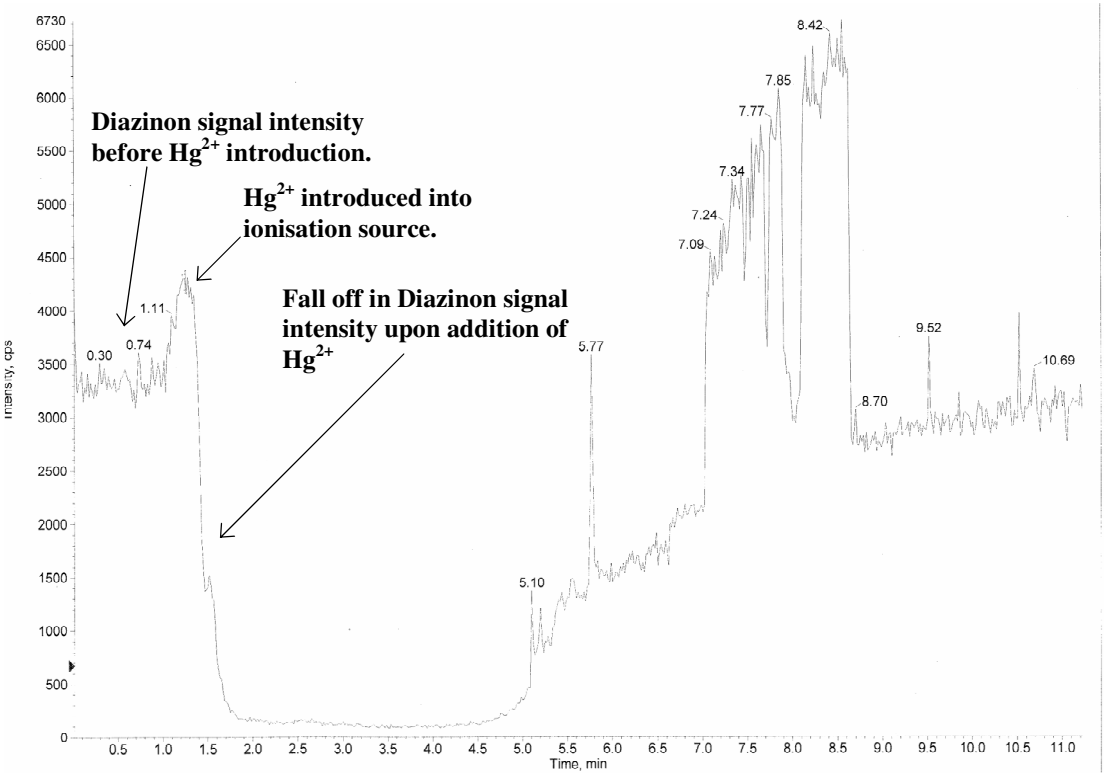

Figure 3.2.19 Intensity count for diazinon before and after addition of Hg^{2+}.

This rapid hydrolysis as viewed in Figure 3.2.19 may preclude one from being able to view any complexation between Hg^{2+} and the substrate. It is also plausible that complexation between Hg^{2+} and diazinon is not significant in the ground state, therefore explaining the absence of any complexed ion in the initial MS experiment. This may suggest that metal binding with the negatively charged transition state is of more significance for Hg^{2+}. The resultant electrostatic stabilization of the transition state structure may result in the large rate enhancement observed in the kinetic studies. It was shown previously that presence of Hg^{2+} induced very small changes in the phosphorus

chemical shift of diazinon in comparison to the other metals investigated. This NMR evidence in tandem with a lack of a complexed ion in the MS study may point to transition-state binding in preference to ground-state binding for Hg^{2+}.

3.2.5.1 Hg^{2+} binding to hydrolysis products PA and PY

Complexation between diazinon and Hg^{2+} was not observed in the initial MS experiments; however Hg^{2+} affinity for sulphur and nitrogen ligands was further examined by looking at possible binding to diazinon's hydrolysis product, PA and PY. Figure 3.2.20 shows the obtained positive ion spectrum of PA in the presence of Hg^{2+}. Significantly, binding with PA is observed at m/z 541, which corresponds to 2PA-Hg^{2+}. This set of peaks exhibits the characteristic isotopic pattern of Hg^{2+} as shown in an expanded view in Figure 3.2.21. This clearly shows Hg^{2+} affinity for sulphur ligands.

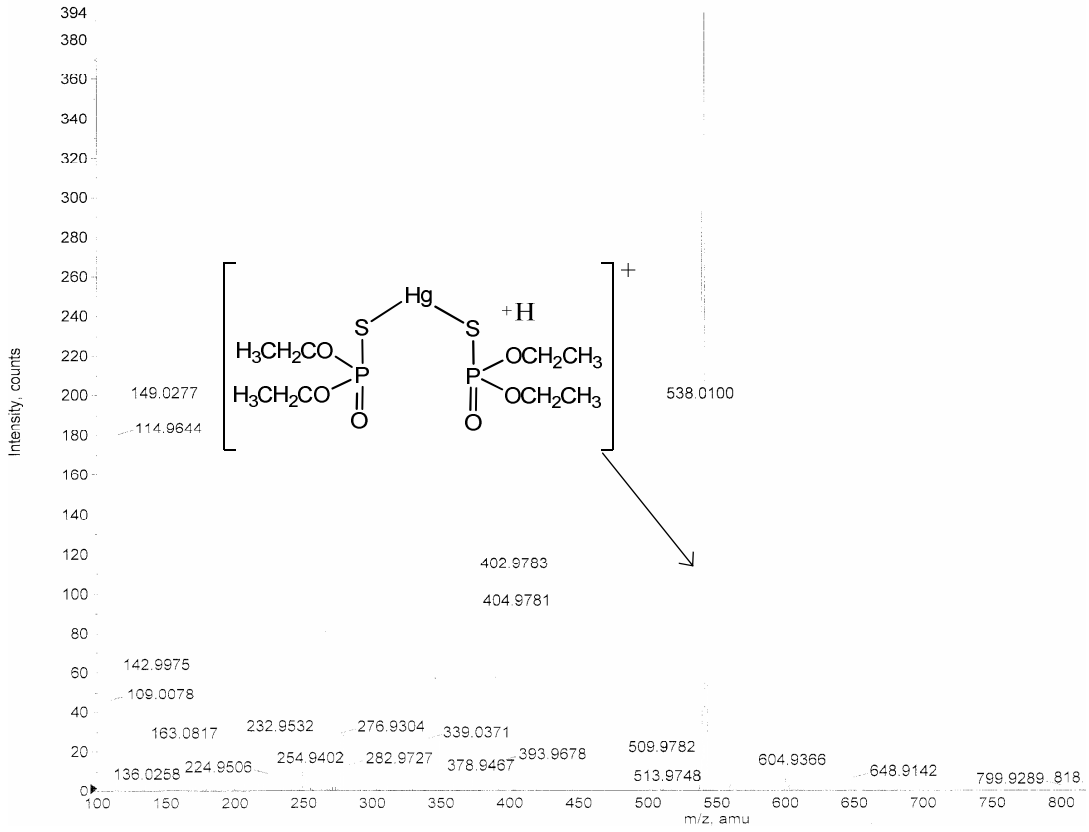

Figure 3.2.20 Positive ion mode spectrum of PA in the presence of Hg^{2+}.

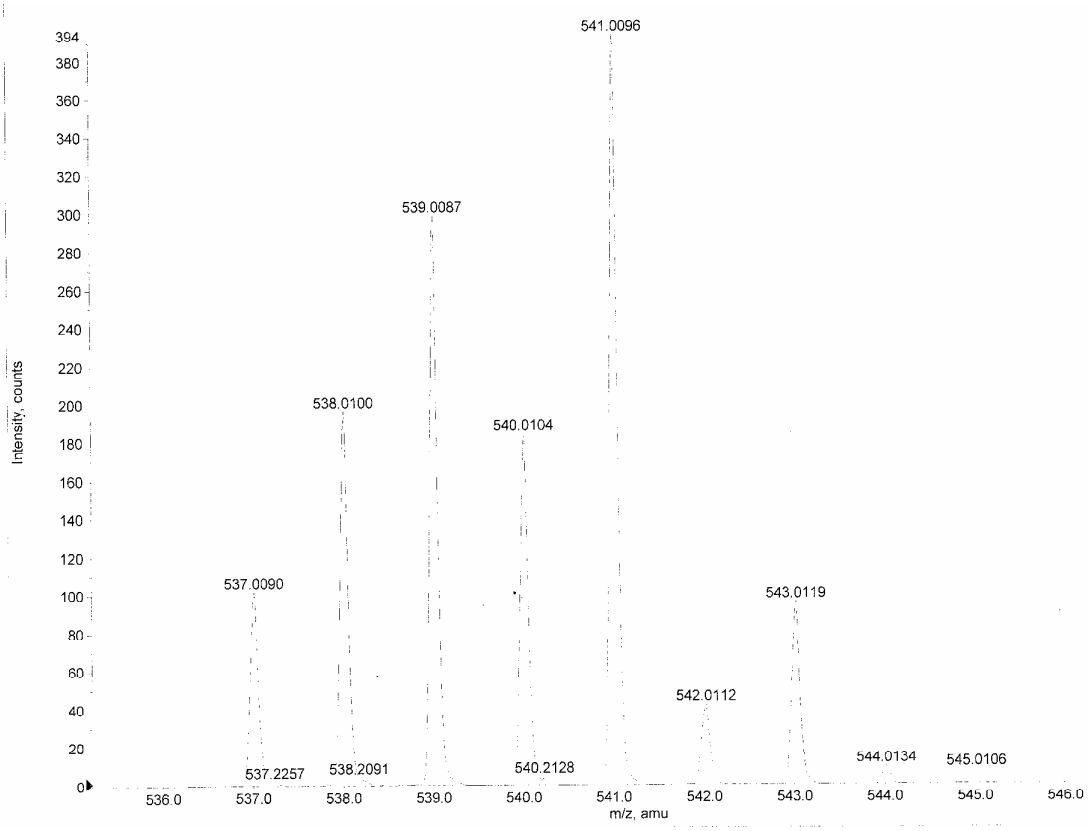

Figure 3.2.21 Shows the characteristic Hg^{2+} isotopic pattern for peak at m/z=541. This represents to PA molecules bond to Hg^{2+}.

No observable complex was seen between PY and Hg^{2+} which corroborates NMR data where little interaction between the nitrogens of PY and Hg^{2+} was evident. This suggests along with the NMR data, that Hg^{2+} role in the acceleration of the rate of hydrolysis is initiated through binding with the sulphur atom of diazinon.

3.3 Kinetic studies of the hydrolysis of Diazinon using UV/VIS spectrometry

Diazinon, pyrimidinol and O,O diethyl phosphorothioic acid were investigated by UV/VIS spectrometry to determine their molar absorbtivities under alkaline conditions. The spectra obtained for the Beer Lambert plots allowed the assessment of substrate and product spectral ovelap and the identification of a suitable peak to follow kinetically during the hydrolysis of diazinon in alkaline conditions. This was determined to be 266nm, an absorption attributed to PY. The plots in addition were used to calculate the theoretical absorbance at infinite time (A_∞) at 266nm. The spectra obtained in alkaline conditions for substrate and PY along with their Beer Lambert plots and molar absorptivities are shown in Figures 3.3.1-3.3.2. Spectral overlap of diazinon and PY is depicted in Figure 3.3.3. Comparison of both spectra shows good spectral separation between diazinon and PY peaks at 266nm. The ε_{266} of PY was found to be 4.72 x 10^3 cm^{-1} M^{-1}.

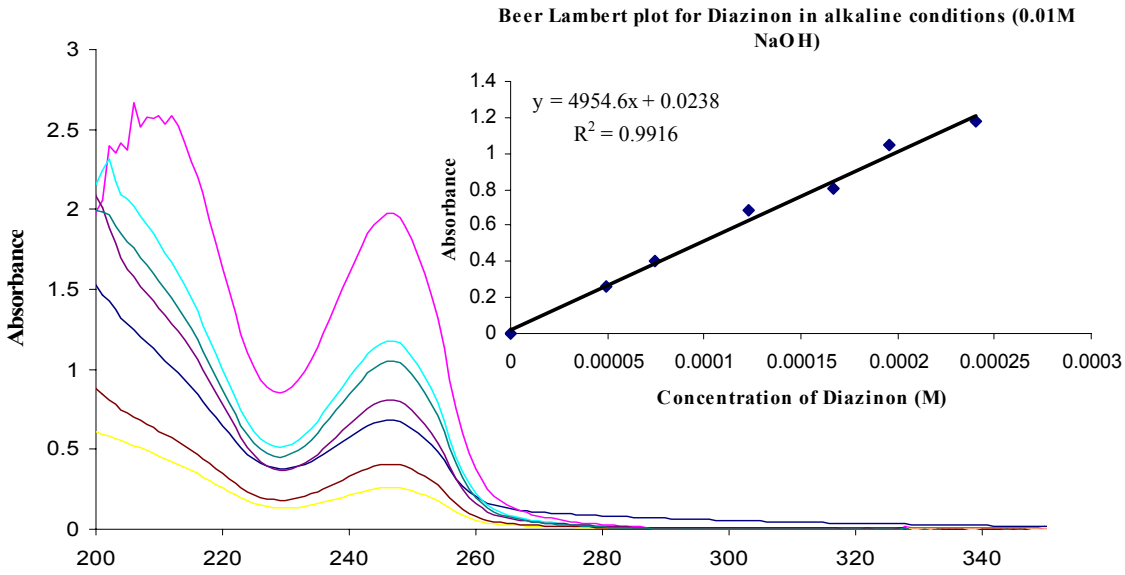

Figure 3.3.1 Beer Lambert spectra of diazinon in alkaline media (70%MeOH/30%H2O). Inset: Beer Lambert plot at 246nm.

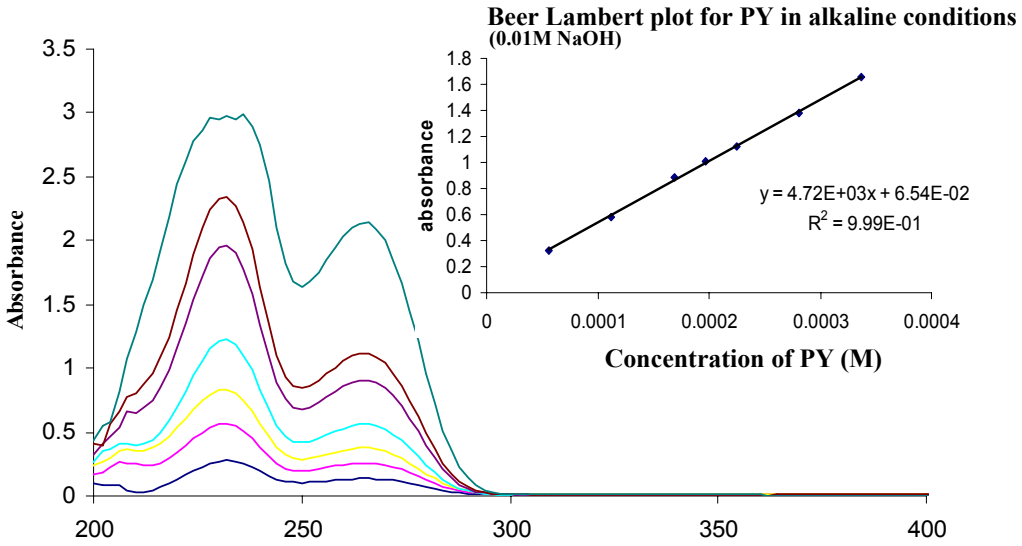

Figure 3.3.2 Beer Lambert spectra of PY in alkaline media (70%MeOH/30%H2O). Inset: Beer Lambert plot at 266nm.

Table 3.3.1 List of λ max's and extinction coefficients obtained for diazinon and Pyrimidinol.

Substrate	λ max (nm)	ε (cm^{-1} M^{-1})
Diazinon	246	4,950
Pyrimidinol	266	4,720

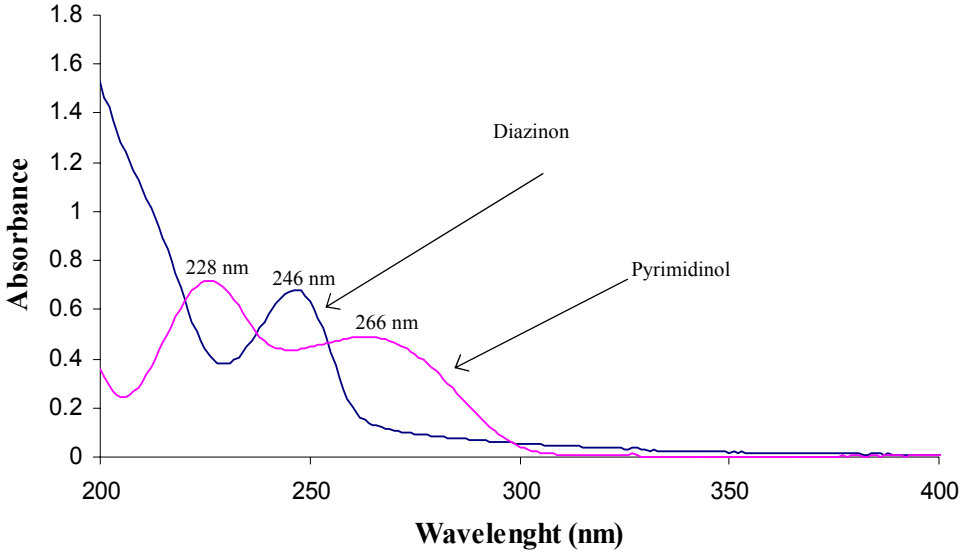

Figure 3.3.3 Comparison of spectral overlap between diazinon and PY.

3.3.1 Base catalysed hydrolysis of diazinon using Pseudo first order conditions

The base catalysed hydrolysis of diazinon was studied spectrophotometrically by following the formation of PY at 266 nm. The hydrolysis reactions in the presence of NaOH were carried out at 22°C under pseudo first order conditions with the concentration of base in at least a 100 fold excess of diazinon (8.25×10^{-5}M). The reaction was typically followed for 10 half-lives (99.9% completion of reaction) with the pseudo first order rate constants determined over three half-lives. All reactions were carried out in triplicate. A typical base run (0.285M NaOH) with overlaid spectra is shown in Figure 3.3.4, with growth plot (266 nm) and subsequent manipulation of data to obtain k_{obs} is depicted in Figure 3.3.5-3.3.6.

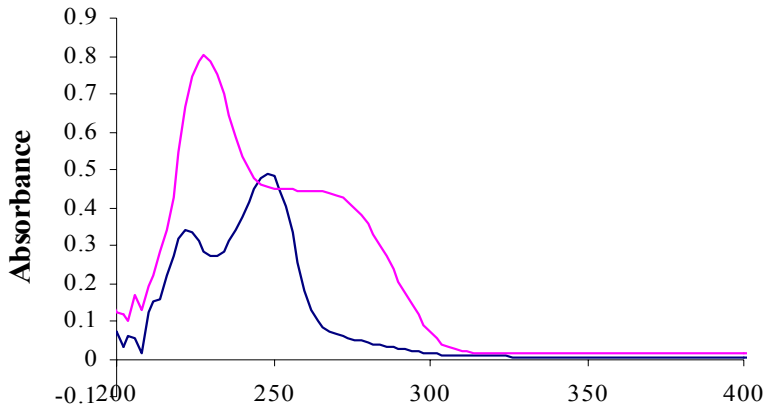

Figure 3.3.4 Typical base run (0.285 M NaOH)

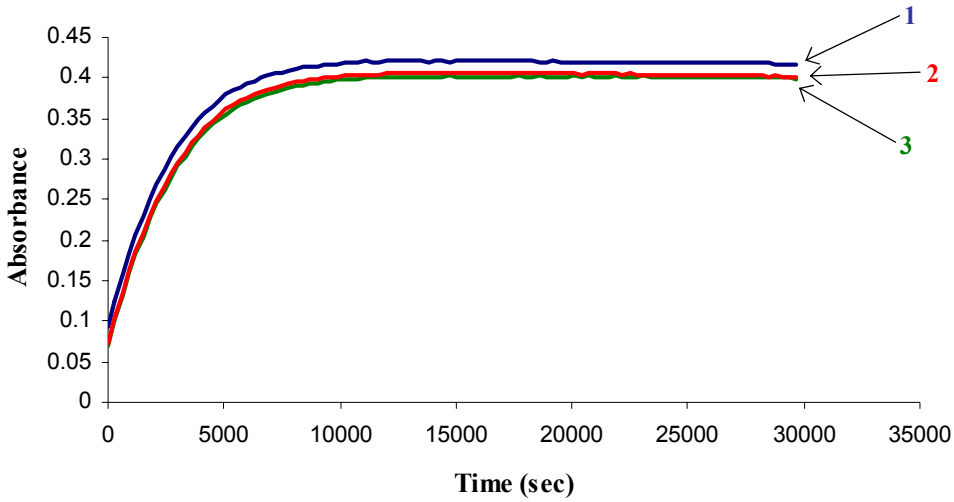

Figure 3.3.5 Representative kinetic run in triplicate, depicting the change in absorbance at 266nm over time for the reaction of diazinon (8.25×10^{-5}M) with 0.285M NaOH at 22°C.

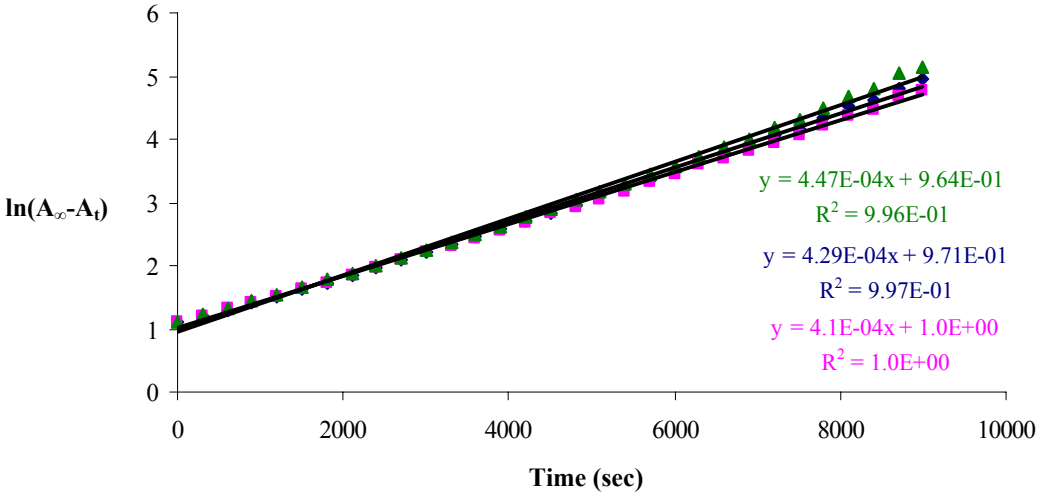

Figure 3.3.6 Plot of $\ln(A_\infty - A_t)$ versus Time to determine k_{obs} for the hydrolysis of diazinon in 0.285M NaOH.

The slope of the plot shown in Figure 3.3.6 is equal to $k_{obs.}$ Identical plots were prepared for separate runs with varying [NaOH], with Table 3.3.2 showing the obtained pseudo first order rate constants (See Appendix 4 for individual runs). A subsequent plot of k_{obs} versus [NaOH] yields a straight line whose slope is equal to the second order rate

constant k_2 (M^{-1} s^{-1}). Figure 3.3.7 shows the clear linear relationship between [NaOH] concentration and k_{obs}. The obtained value for 0.475M NaOH was omitted from the plot as it exhibits a significant deviation from this straight line, presumably as a result of its high viscosity. The obtained second order rate constant is 1.51 ± 0.016 x 10^{-3} M^{-1} s^{-1}. This is in fair agreement with the reported second order rate constant by Pedia[10] of 3.06 x 10^{-3} $M^{-1}s^{-1}$ in H_2O at 25°C, noting the different solvent and temperature.

Table 3.3.2 Pseudo-first order rate constants (k_{obs}) for the hydrolysis of diazinon (8.25 x 10^{-5} M) in the presence of varying [NaOH] at 22°C.

Experiment no.	$[NaOH]_o$ (M)	Calculated pH	k_{obs} (x 10^{-4} s^{-1})
1	0.00095	10.98	0.031 (single run)
2	0.00949	11.98	0.148 ± 0.013
3	0.0189	12.28	0.252 ± 0.017
4	0.0949	12.98	1.53 ± 0.029
5	0.285	13.46	4.29 ± 0.123
6	0.475	13.68	5.60 ± 0.047

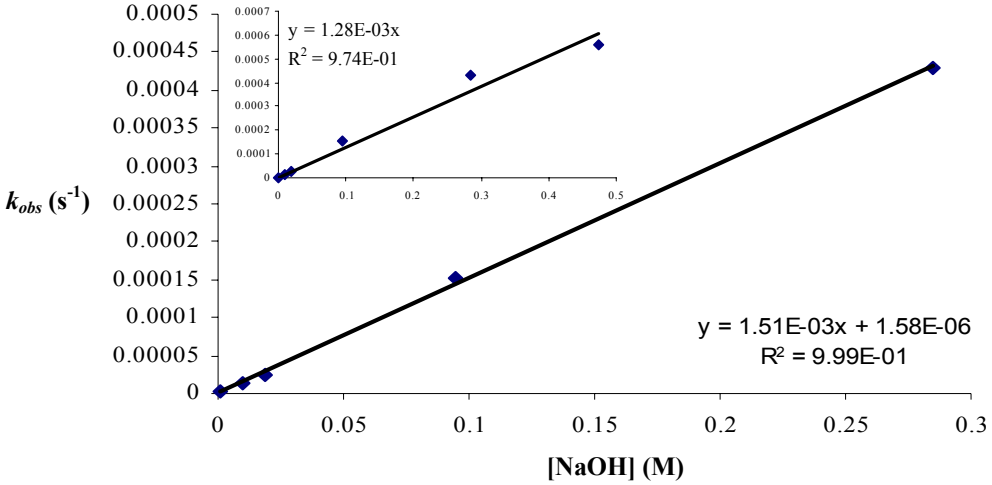

Figure 3.3 7 A plot of k_{obs} versus $[NaOH]_o$ for the base catalysed hydrolysis of diazinon in 70%MeOH/30%H_2O. Inset: Loss of linearity with 0.475M NaOH.

3.3.2 Base catalysed hydrolysis of diazinon in the presence of metal ions under pseudo first order kinetics

Preliminary experiments in the presence of metal ions were carried out at pH 11 to maintain pseudo first order conditions i.e. [NaOH] at least 28 times greater than [diazinon]. Prior to hydrolysis experiments it was necessary to analyse the absorption spectrum of PY in the presence of metal ions to check if any shift in the λmax had occurred due to metal-PY interaction. This was observed for PY in the presence of Cu^{2+} (10:1 ratio Cu^{2+}/D), where a shift from 266nm to 270nm was noted. This new wavelength was monitored during the base hydrolysis of diazinon in the presence of Cu^{2+}, in addition to placing an equivalent amount of Cu^{2+} in the blank. Figure 3.3.8 shows the start and end spectra obtained for the hydrolysis of diazinon in the presence of Cu^{2+} (ratio 10:1 Cu^{2+}/D), with the product growth plot at 270 nm shown inset.

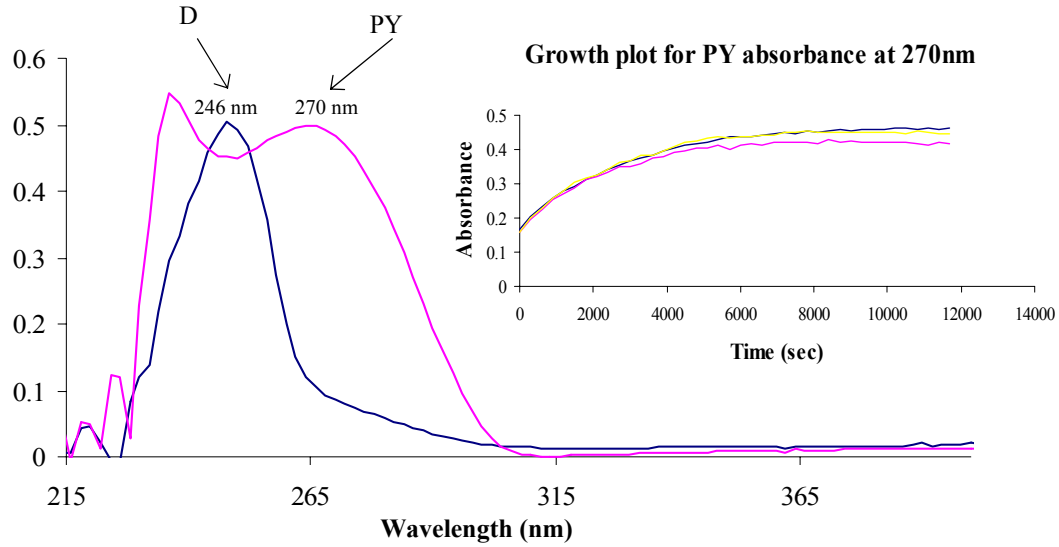

Figure 3.3.8 Start and end spectra for the hydrolysis of diazinon in the presence of Cu^{2+} (ratio 10:1 Cu^{2+}/D). -, start spectrum; -, End spectrum. Inset, Growth plot for PY absorbance at 270nm.

A plot of $\ln(A_\infty - A_t)$ against time (Figure 3.3.9) results in a slope equal to the pseudo rate constant k_{obs}. The calculated k_{obs} of 3.93 x 10^{-4} s^{-1} (mean) shows a significant rate increase from that observed in the absence of Cu^{2+} ions (3.1 x 10^{-6} s^{-1}, Table 3.3.2).

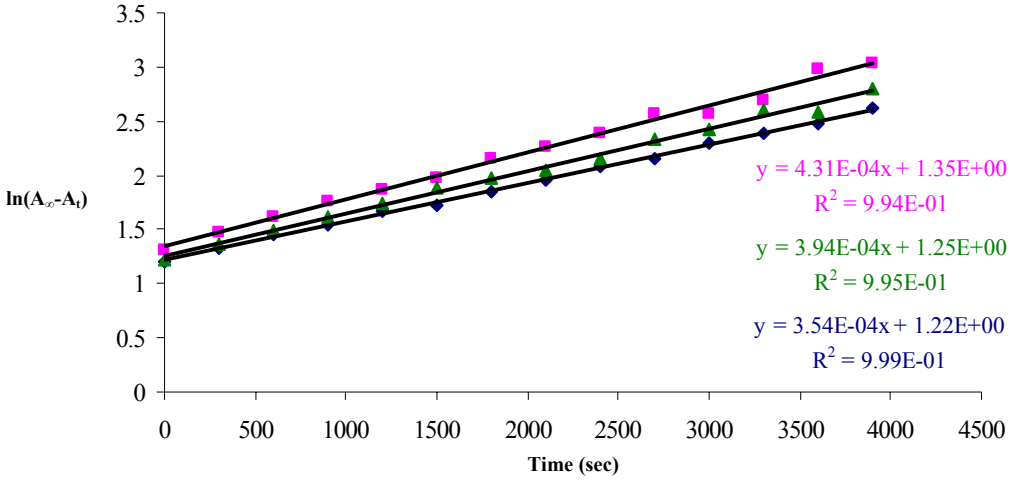

Figure 3.3.9 Plot of $\ln(A_\infty - A_t)$ versus Time to determine k_{obs} for the base hydrolysis of diazinon in the presence of Cu^{2+} (ratio 10:1 Cu^{2+}/D). Shown in triplicate.

Subsequent difficulties arose in assessing the effect of different metals on the rate of hydrolysis at pH 11 due to the insolubility of some metals at this pH. This solubility problem is attributed to metal speciation, specifically the formation of insoluble hydroxo species. This is clearly evident in Figure 3.3.10 where the absorption spectrum of Ag^+ at several pH's in the pertinent co-solvent is shown. One can clearly see the rise in the absorption spectrum at elevated pH due to the insolubility of species such as $Ag(H_2O)_3(OH)$, however no such rise in the spectrum is observed at pH 10. The solubility of each metal was examined in an analogous manner; with the result that pH 10 was found to be a suitable pH to show the effect of different metals on the rate of hydrolysis.

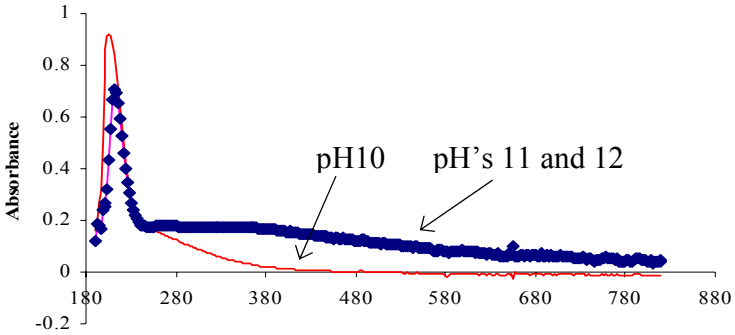

Figure 3.3.10 Formation of hydroxy species at different pH's with resultant effect on the UV spectrum of Ag^{+}.

The need to investigate the catalytic effects of the metal ions at pH 10 meant that pseudo first order conditions no longer prevailed. It was therefore necessary to re-examine the effect of NaOH concentration on the rate of hydrolysis of diazinon using the method of initial rates.

3.3.3 Base catalysed hydrolysis of diazinon using the method of initial rates

This method requires one to measure the initial rate r for several concentrations, varying the initial concentration of one of the reactants at a time. To achieve this, a series of experiments were performed where the concentration of one reagent was varied i.e. NaOH, whilst keeping the other constant. The initial rate of the reaction was then measured for each concentration, upon which it was possible to determine the order of the reaction in respect of that reagent. The order of the reaction is determined from the slope of a plot of log r versus $\log[OH]_o$ according to Equation 1; α and β are the order of the reaction with respect to diazinon and OH^-. The intercept is equal to $\log k + \alpha\log[D]_o$, where D=diazinon.

$$\log r = \log k + \alpha\log[D]_o + \beta\log[OH^-]_o \qquad (1)$$

A parallel set of experiments was carried out where diazinon concentration was varied whilst maintaining NaOH concentration, with its order determined from a plot of log r versus $\log[D]_o$. Knowing the order of reaction in respect of both reactants enables one to determine the second order rate constant k_2 from Equation 2 using any set of concentrations and rate obtained.

$$\text{Rate} = k_2 [D]^{\alpha}_o [OH^-]^{\beta}_o \qquad (2)$$

Comparison of the second order rate constant obtained using the method of initial rates against that obtained using pseudo first order conditions can be made. Figure 3.3.11 shows a typical initial rate plot for the reaction of 0.285M NaOH with 8.25 X 10^{-5}M diazinon (in triplicate). The acquired absorbance values obtained at 266nm were converted to concentration using the equation A = εcl, were ε_{266} was 4.720 x 10^3 cm^{-1} M^{-1} and pathlength was 1cm.

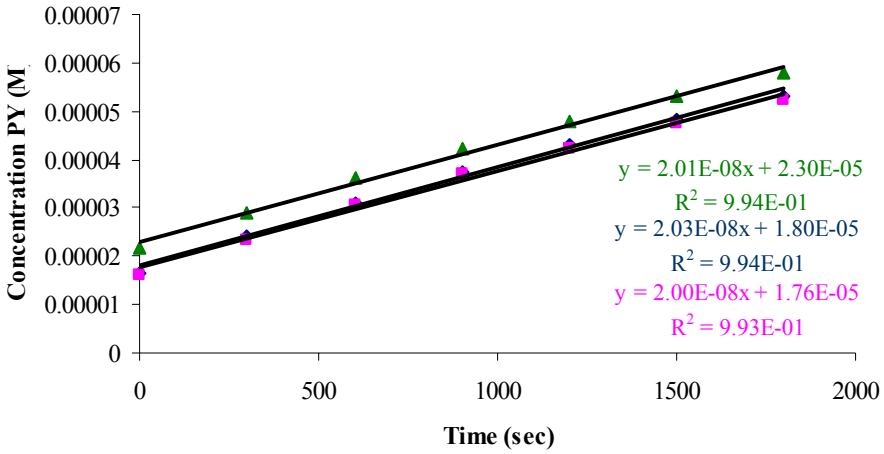

Figure 3.3.11 A representative initial rate plot (triplicate) showing the reaction of diazinon (8.25 x 10^{-5}M) with 0.285M NaOH in 70%MeOH/H_2O

Table 3.3.3 shows the obtained rates with varying NaOH concentration with subsequent plot of log r versus $[NaOH]_o$ showing the order of the reaction with respect to base to be 1.0. A second plot of rate ($M\ s^{-1}$) versus [NaOH] shows excellent linearity with $r^2 = 0.993$. This plot maybe used to determine the rate of reaction at any [NaOH]. A third plot is shown of k_{obs} versus [NaOH] from which the second order rate constant k_2 can be obtained from the slope. k_{obs} values are calculated using equation 4. The slope of the plot is $8.37 \pm 0.068 \times 10^{-4}\ M^{-1}\ s^{-1}$ which shows reasonable agreement with the second order rate constant obtained under pseudo first order conditions of $1.51 \pm 0.016 \times 10^{-3}\ M^{-1}\ s^{-1}$.

$$\text{Rate} = k\,[D]^1\,[NaOH]^1 \qquad (3).$$

If $[NaOH]_o >> [D]_o$

Then; $$\text{Rate} = k_{obs}\,[D]_o \qquad (4).$$

Table 3.3.3 Rate values and k_{obs} obtained for the hydrolysis of diazinon (8.25×10^{-5}M) with varying concentration of NaOH using the method of initial rates. Carried out in 70%MeOH/30%H_2O).

Experiment no.	[NaOH] (M)	Calculated pH	Rate ($\times 10^{-9}$ M s^{-1})	K_{obs} ($\times 10^{-5}\ s^{-1}$)
1	0.0095	11.98	1.00 (single run)	1.21 (single run)
2	0.0189	12.28	1.52 ± 0.087	1.84 ± 0.087
3	0.0949	12.98	8.06 ± 0.050	9.77 ± 0.050
4	0.189	13.28	13.4 ± 0.267	16.2 ± 0267
5	0.285	13.46	20.1 ± 0.102	24.4 ± 0.102

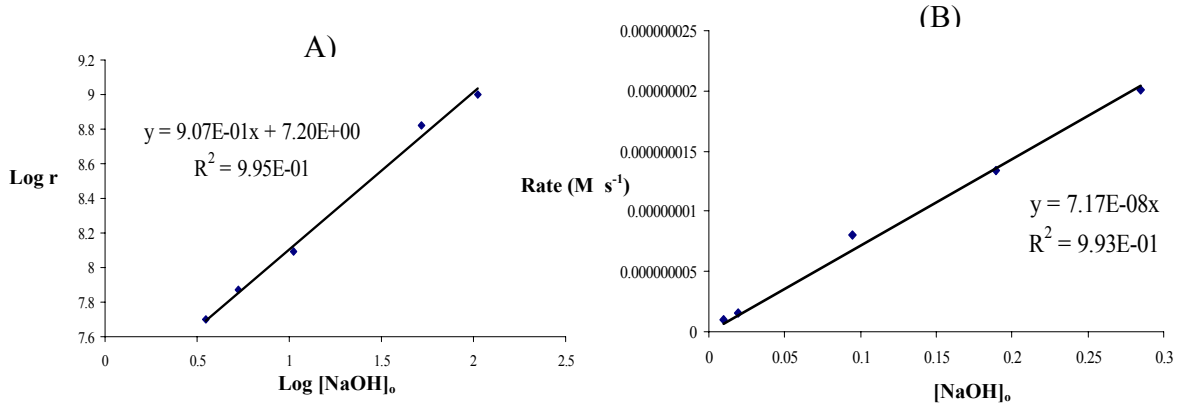

Figure 3.3.12 Plot (A) depicts log r versus log $[NaOH]_0$ from which the order of the reaction in respect of NaOH is determined (β=1). Plot (B) is rate (M s^{-1}) versus $[NaOH]_0$. The equation of this line maybe used to estimate the rate of reaction at any [NaOH].

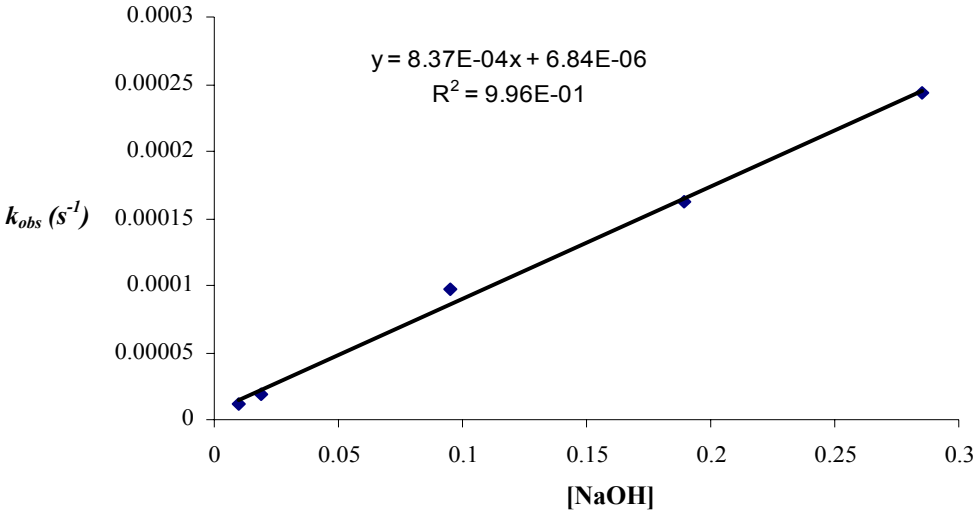

Figure 3.3.13 Plot of k_{obs} versus [NaOH] to determine the k_2, the second order rate constant for the base hydrolysis of diazinon in 70%MeOH/30%/30%H_2O at 22°C.

A comparable set of experiments was performed where diazinon concentration was varied whilst maintaining constant [NaOH]. Table 3.3.4 shows the obtained rates with varying diazinon concentration with subsequent plot of log r versus log $[D]_o$ to determine the order of the reaction depicted in Figure 3.3.14.

Table 3.3.4 Rate values obtained for the hydrolysis of diazinon (varying) with NaOH (0.0095M) using the method of initial rates in 70%MeOH/30%H_2O) at 22°C.

Experiment no.	[Diazinon] (M)	Rate (M s^{-1})
1	5.50 x 10^{-5}	6.63 x 10^{-10}
2	8.25 x 10^{-5}	1.00 x 10^{-9}
3	1.375 x 10^{-4}	1.68 x 10^{-9}
4	2.20 x 10^{-4}	2.66 x 10^{-9}

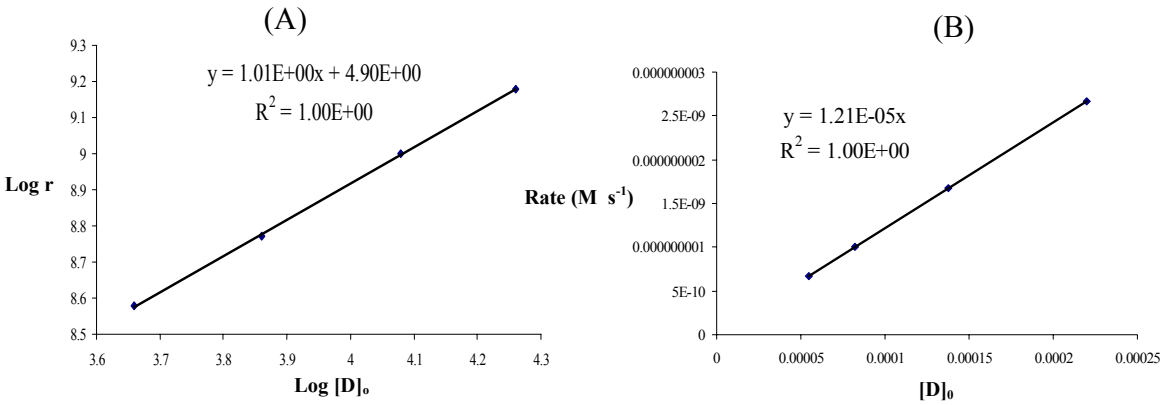

Figure 3.3.14 Plot A depicts log r versus log $[D]_0$ from which the order of the reaction in respect of diazinon is determined (α=1). Plot (B) is rate (M s^{-1}) versus $[D]_0$. The equation of this line maybe used to estimate the rate of reaction at any [D] with 0.0095M NaOH.

As the order for both reactants was determined to be 1.0 the rate equation can therefore be written as;

$$\text{Rate} = k\,[D]^1[OH]^1 \qquad (5)$$

It is also possible to calculate the second order rate constant k_2 using Equation 5, with Table 3.3.5 showing calculated k_2 values for initial rate experiments. This enables a further comparison of second order rate constant determined using the method of initial rates versus that obtained under pseudo first order conditions.

Example for 0.0949M NaOH: $8.06 \text{ X } 10^{-6} \text{ M s}^{-1} = k\,[8.25 \text{ x } 10^{-5}\text{M}]^1[0.0949\text{M}]^1$

$$k = \frac{8.06 \text{ x} 10^{-6} \text{ M s}^{-1}}{7.89 \text{ x } 10^{-6} \text{ M}^2} \quad k = 1.03 \text{ x } 10^{-3} \text{ M}^{-1} \text{ s}^{-1}$$

Table 3.3.5 Calculated second order rate constant k_2 for the hydrolysis of diazinon in the presence of NaOH obtained using the method of initial rates in 70%MeOH/30%H_2O) at 22°C.

Experiment no.	[NaOH] (M)	[D] x 10^{-5} (M)	Calculated k_2 x (10^{-3} M^{-1} s^{-1})
1	0.0095	8.25	1.28[b]
2	0.0189	"	0.97 ± 0.087
3	0.0949	"	1.03 ± 0.050
4	0.189	"	0.86 ± 0.267
5	0.285	"	0.86 ± 0.102

The mean k_2 obtained from varying OH experiments is 1.00 x 10^{-3} ± 0.142 M^{-1} s^{-1} which compares reasonably with the second order rate constant obtained under pseudo first order conditions of 1.51 ±0.016 x 10^{-3} M^{-1} s^{-1}. This shows that the method of initial rates compares favorably with the pseudo first order method and may be used as an accurate method to asses metal ion effects on the rate of hydrolysis of diazinon.

3.3.4 Base catalysed hydrolysis of diazinon in the presence of metal ions using the method of initial rates.

The metal ions effect on the rate of hydrolysis of diazinon in base medium was examined using the method of initial rates in unbuffered co-solvent at 22°C. The method of initial rates was shown to be a suitable method to determine the metal ion effect on the hydrolysis of diazinon (Section 3.3.3). The ratio of M^{n+}/D was 10:1 and 25:1 M^{n+}/D. In a typical kinetic run a UV cell was prepared by adding 15 μL of Diazinon (0.011M) using a gas tight syringe. The requisite volume of co-solvent was then added to ensure a final volume of 2 ml. Following the addition of co-solvent, 20 μl of 0.01M NaOH was added to give a pH of 10.0. The appropriate metal solution was then added. All metal solutions were prepared in co-solvent to a concentration of 0.011M, therefore requiring either 150 μL or 375 μL to obtain the desired M^{n+}/D ratio. NaOH solutions were also prepared in the pertinent co-solvent consequently maintaining the same solvent properties as employed in NMR and MS studies. The blank UV cells contained an equivalent concentration of M^{n+}.

Figures 3.3.15-3.3.18 shows typical start and end spectra obtained for the hydrolysis of diazinon in the presence of Hg^{2+} and Cu^{2+} (10:1 and 25:1 M^{n+}/D) in addition to initial rate plots (triplicate). All other spectra and initial rate plots can be seen in Appendix A4.

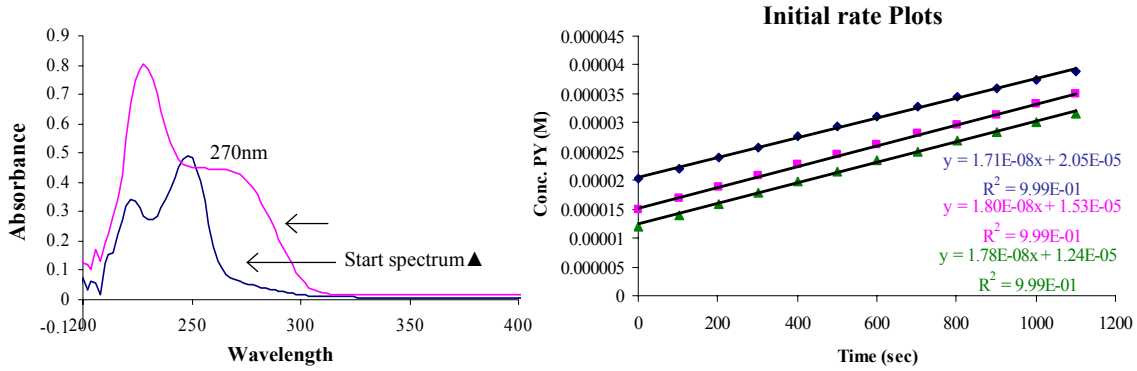

Figure 3.3.15 Initial rate experiments for the base hydrolysis of diazinon in the presence of Hg^{2+} (ratio 10:1 Hg^{2+}/D). -; start spectrum, -; End spectrum. Plots shows the obtained initial rate plots for PY absorbance at 270nm in the presence of Hg^{2+}.

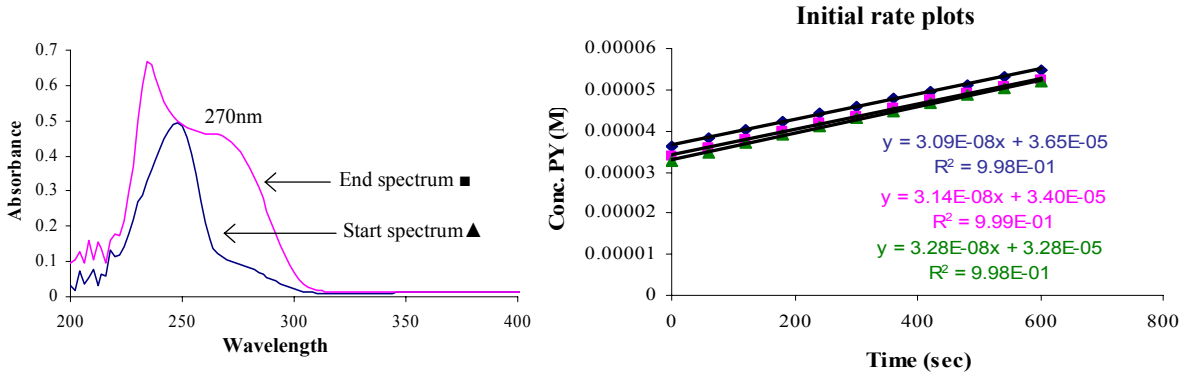

Figure 3.3.16 Initial rate experiments for the base hydrolysis of diazinon in the presence of Hg^{2+} (ratio 25:1 Hg^{2+}/D). -; start spectrum, -; End spectrum. Plots show the obtained initial rate plots for PY absorbance at 270nm in the presence of Hg^{2+}.

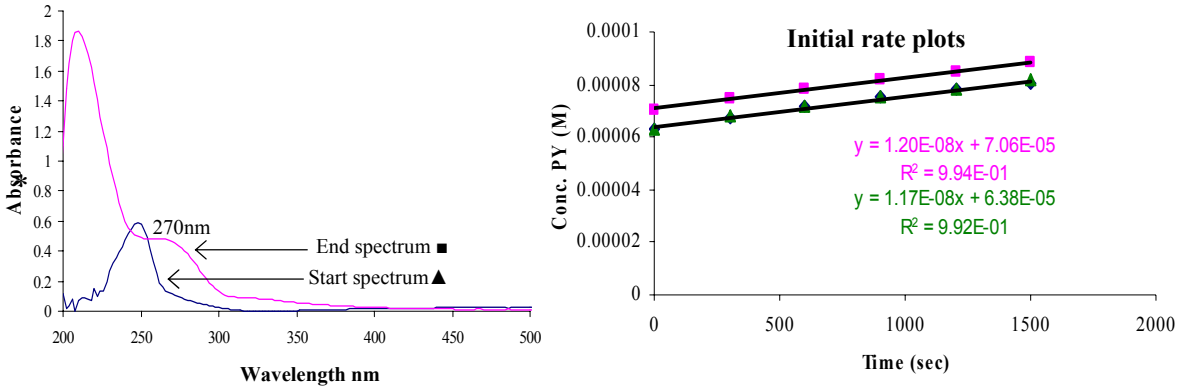

Figure 3.3.17 Initial rate experiments for the base hydrolysis of diazinon in the presence of Cu^{2+} (ratio 10:1 Cu^{2+}/D). -: start spectrum -: End spectrum. Plot shows the obtained initial rate plots for PY absorbance at 270nm in the presence of Cu^{2+}.

Final spectrum taken after 1 day.

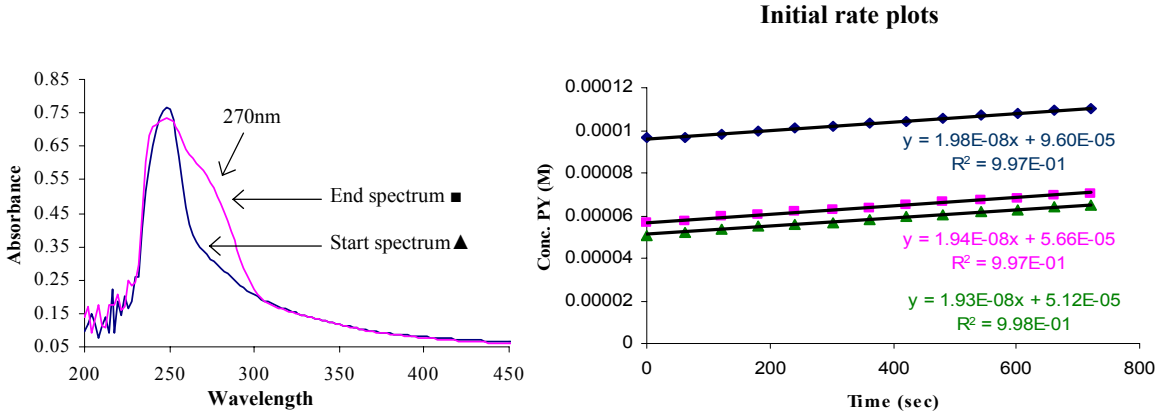

Figure 3.3.18 Initial rate experiments for the base hydrolysis of diazinon in the presence of Cu^{2+} (ratio 25:1 Cu^{2+}/D). -; start spectrum, -; End spectrum. Plot shows the obtained initial rate plots for PY absorbance at 270nm in the presence of Cu^{2+}.

Table 3.3.6 shows the obtained rates (M s^{-1}) for each metal at ratios 10 and 25:1 M^{n+}/D. An estimate of the k_{obs} in the presence of metal ions can be made by using the assumption that Rate = k_{obs} [diazinon], where diazinon concentration is 8.25 x 10^{-5} M. The observed acceleration in k_{obs} due to metal ions is explored further in the pH profile section (Section 3.3.7).

Table 3.3.6 Rate values obtained for the hydrolysis of diazinon in the presence of metal ions at pH 10 using the method of initial rates in 70%MeOH/30%H_2O at 22°C.

M^{n+}	$[M^{n+}]$ x 10^{-4} (M)	[D] x 10^{-5} (M)	Ratio $[M^{n+}]/[D]$	Rate x 10^{-8} (M s^{-1})	k_{metal} x 10^{-4} (s^{-1})
Hg^{2+}	8.25	8.25	10	1.77 ± 0.033	2.1 ± 0.033
Hg^{2+}	20.6	8.25	25	3.17 ± 0.065	3.8 ± 0.065
Cu^{2+}	8.25	8.25	10	1.16 ± 0.012	1.4 ± 0.012
Cu^{2+}	20.6	8.25	25	1.95 ± 0.018	2.4 ± 0.018
Ag^{+}	8.25	8.25	10	0.349 ± 0.003	0.42 ± 0.003
Ag^{+}	20.6	8.25	25	0.446 ± 0.020	0.54 ± 0.020
Cd^{2+}	20.6	8.25	25	0.024 ± 0.007	0.029 ± 0.007

3.3.5 Acid catalysed hydrolysis of diazinon in the absence of metal ions using the method of initial rates

The acid catalysed hydrolysis of diazinon in 70%MeOH/30%H_2O was studied specrophotometrically by following the appearance of PY peaks at 228nm or 264nm depending an acid concentration. A Beer Lambert plot of PY was carried out in acidic conditions to determine its molar absorptivity. Figure 3.3.19 shows the obtained spectra, with Beer Lambert plots at 228nm and 264nm shown inset. The ε_{228}nm and ε_{264}nm were determined to be 6420 and 4720 cm^{-1} M^{-1} respectively. At higher acid concentrations the

peak at 228 was followed spectrophotometrically due to difficulties in observing the peak at 264 nm.

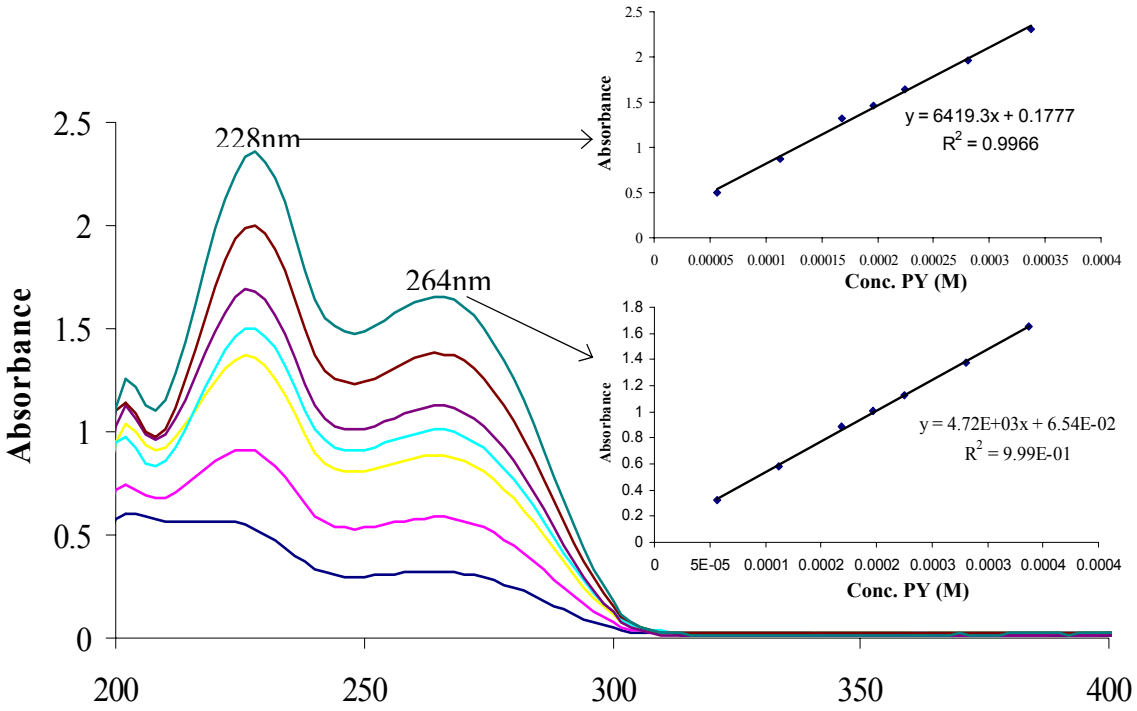

Figure 3.3.19 Beer Lambert spectra for PY in acid conditions. Inset: Beer Lambert plots at 264nm and 228nm.

A typical start and end spectra for an acid run is shown in Figure 3.3.20 with initial rate plots for 230 nm shown alongside.

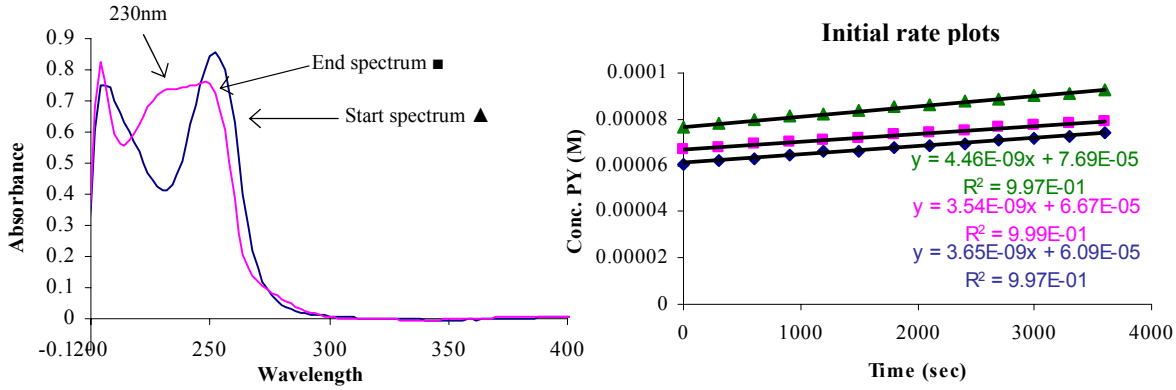

Figure 3.3.20 Start and end spectra for the acid (0.1M) hydrolysis of diazinon using the method of initial rates in 70% MeOH/30%H_2O at 22°C. -; start spectrum, -; End spectrum. Plots show the obtained initial rate plots for PY absorbance at 230nm.

Table 3.3.7 shows the obtained rates at various $[H^+]$. k_{obs} maybe calculated from the expressions;

$$\text{Rate} = k\,[D]^1\,[H^+]^1 \qquad \text{Equation 5.}$$

If $[H^+]_o >> [D]_o$

Then; $\text{Rate} = k_{obs}\,[D]_o \qquad \text{Equation 6.}$

Table 3.3.7 Rate values obtained for the hydrolysis of diazinon (8.25×10^{-5}M) with varying concentration of HCl using the method of initial rates in 70%MeOH/30%H_20 at 22°C.

Experiment no.	$[H^+]$ (M)	Calculated pH	Rate ($\times 10^{-9}$ M s^{-1})	k_{obs} ($\times 10^{-5}$ s^{-1})
1	0.01	2.0	1.21 ± 0.037	1.47 ± 0.037
2	0.1	1.0	3.60 ± 0.335	4.36 ± 0.335
3	1.0	0.0	12.9 ± 0.379	15.6 ± 0.379

There is clear decrease in the observed rate as the $[H^+]$ is decreased.

3.3.6 Acid hydrolysis of diazinon in the presence of metal ions using the method of initial rates

Analogous to base conditions the catalytic effects of metal ions on the rate of hydrolysis of diazinon in acid was examined over two ratios at pH 4. Figure 3.3.21-3.3.23 shows typical start and end spectra obtained for the acid hydrolysis of diazinon in the presence of Hg^{2+}, Cu^{2+} and Ag^+ (10:1 M^{n+}/D), in addition to initial rate plots (triplicate). The rate of reactions in the presence of M^{n+} was monitored at 264nm.

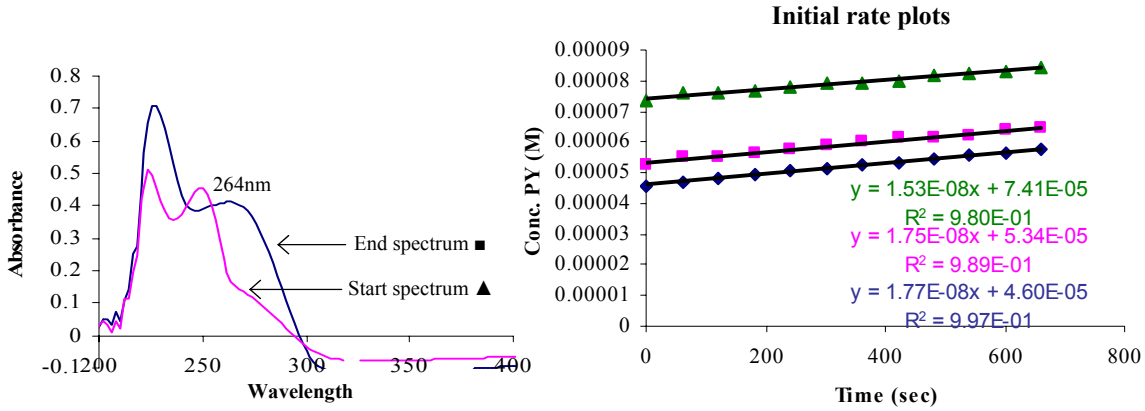

Figure 3.3.21 Initial rate experiments for the acid hydrolysis of diazinon in the presence of Hg^{2+} (ratio 10:1 Hg^{2+}/D). -; start spectrum, -; End spectrum. Plots show the obtained initial rate plots for PY absorbance at 264nm in the presence of Hg^{2+}.

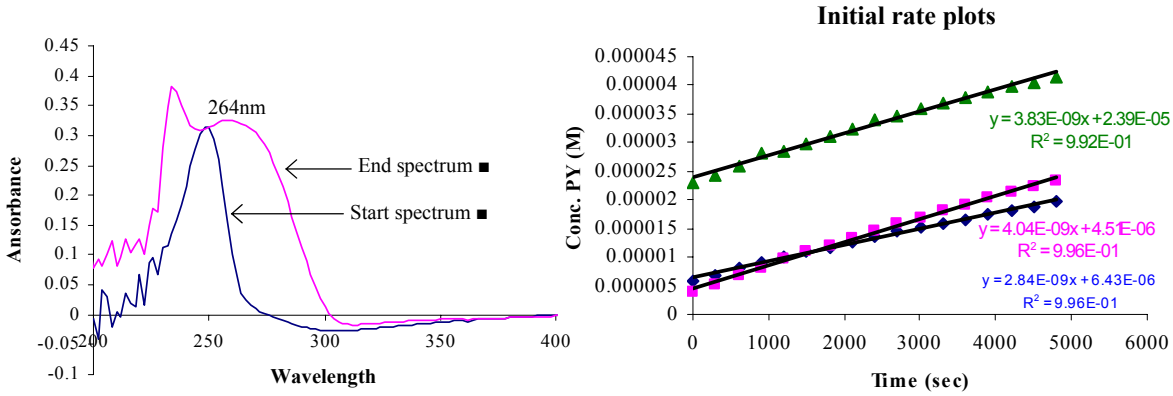

Figure 3.3.22 Initial rate experiments for the acid hydrolysis of diazinon in the presence of Cu^{2+} (ratio 10:1 Cu^{2+}/D). -; start spectrum, -; End spectrum. Plots show the obtained initial rate plots for PY absorbance at 264nm in the presence of Cu^{2+}.

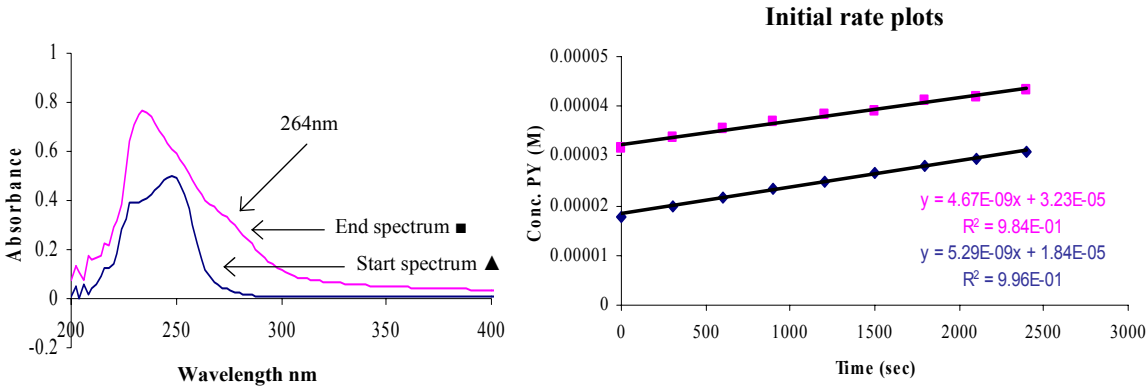

Figure 3.3.23 Initial rate experiments for the acid hydrolysis of diazinon in the presence of Ag^+ (ratio 10:1 Ag^+/D). -: start spectrum -: End spectrum. Plots shows the obtained initial rate plots for PY absorbance at 264nm in the presence of Ag^+.

Table 3.3.8 depicts the obtained rate values for the hydrolysis of diazinon in the presence of various metal ions. Analogous to the base runs the k_{obs} is estimated from the assumption that the Rate = k_{obs} [diazinon], where diazinon concentration is 8.25 x 10^{-5} M.

Table 3.3.8 Initial rate experimental rate values obtained for the hydrolysis of diazinon in the presence of metal ions at pH 4. Carried out in 70%MeOH/30%H_2O at 22°C.

M^{n+}	$[M^{n+}]$ x 10^{-4} (M)	[D] x 10^{-5} (M)	Ratio $[M^{n+}]$/[D]	Rate x 10^{-8} (M s^{-1})	k_{metal} x 10^{-4} (s^{-1})
Hg^{2+}	8.25	8.25	10	1.68 ± 0.089	2.03 ± 0.089
Hg^{2+}	20.6	8.25	25	2.03 ± 0.065	2.46 ± 0.065
Cu^{2+}	8.25	8.25	10	0.357 ± 0.043	0.43 ± 0.043
Cu^{2+}	20.6	8.25	25	0.818 ± 0.016	0.99 ± 0.016
Ag^+	8.25	8.25	10	0.498 ± 0.029	0.60 ± 0.029
Ag^+	20.6	8.25	25	0.805 ± 0.019	0.98 ± 0.019

3.3.7 pH-rate profile for the hydrolysis of diazinon

The results of this work in acidic and basic conditions in combination with data from the literature and previous studies within the Buncel-vanLoon laboratory can be used to produce a pH rate profile for the hydrolysis of diazinon. The Hammett acidity function H_o was used in the strong acid region of the pH profile, as this is a better indication of the acidity of the solution compared to the pH scale[27]. Table 3.3.9 shows the obtained k_{obs} and half-life's; with Figure 3.3.24 depicts the rate profile.

Table 3.3.9 Kinetic data for the hydrolysis of diazinon from this research and literature other sources [28,10].

pH or (H_o)	k_{obs} (s^{-1})	$t_{1/2}$
13.68	*5.60×10^{-4}*	*20.6 min*
13.46	*4.29×10^{-4}*	*27.0 min*
12.98	*1.53×10^{-4}*	*75.5 min*
12.28	*0.252×10^{-4}*	*7.64 hrs*
11.98	*0.148×10^{-4}*	*13.0 hrs*
10.98	*0.031×10^{-4}*	*62.1 hrs*
8.0	1.49×10^{-7}	54 days
7.0	1.15×10^{-7}	70 days
6.0	1.47×10^{-7}	55 days
5.0	5.73×10^{-7}	14 days
4.5	25.5×10^{-7}	3.2 days
2.59	6.07×10^{-5}	190 min
0.084	4.36×10^{-4}	26.5 min
0.0543	7.55×10^{-4}	15.3 min
-0.2617	1.56×10^{-4}	74.0 min

pH or (H_o)	k_{obs} (s^{-1})	$t_{1/2}$
-0.282	4.85 x 10^{-4}	23.8 min
-1.02	2.09 x 10^{-4}	55.3 min
-2.23	1.06 x 10^{-4}	109 min
-3.24	2.88 x 10^{-4}	40.1 min

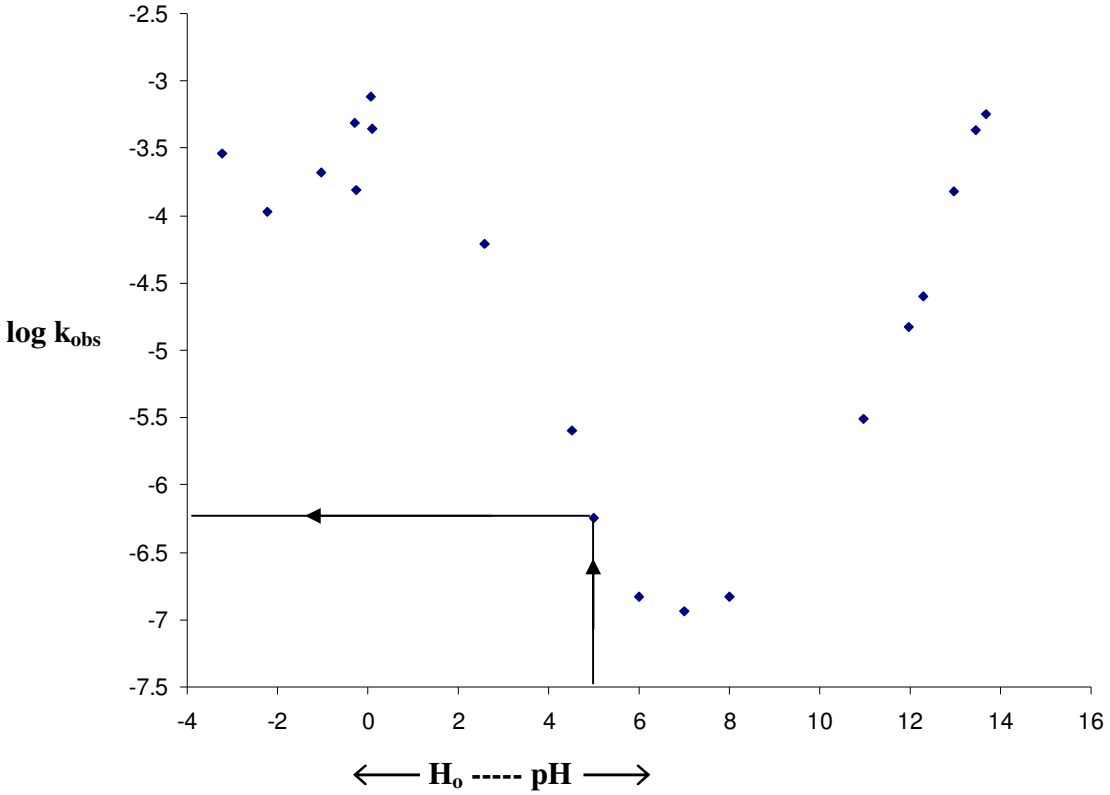

Figure 3.3.24 pH rate profile for the hydrolysis of diazinon [1, 2].

This pH profile can be used to estimate the expected rate of hydrolysis in the absence of metal ions under the reaction conditions ($k_{control}$). The unbuffered nature of the reaction solutions made it necessary to measure the pH of the solution upon addition of the different metal cations. Metal ions once solvated, are known to speciate with the resultant formation of hydroxy species. This in turn has the effect of changing the acidity of the

solution as shown in Equation 7. The extent of speciation for the different metal cations is examined in detail in the Discussion section (4.1.3).

$$[M(OH_2)_x]^{n+} \rightleftharpoons [M(OH_2)_{x-1}(OH)^{(N-1)}]^{+} + H^{+} \qquad (7)$$

On examining the pH of the base reaction mixtures it was shown to change significantly for all the metal cations examined, with the base solutions containing metal ions found to display pH values between 5.0 and 7.5. The pH for Ag^{+} solutions (25 and 10:1 M^{n+}/D) ranged from 7.15-7.4; for Hg^{2+} solutions from 6.5 to 6.8; for Cu^{2+} from 5.0 to 5.25 and for Cd^{2+} (25:1 M^{n+}/D) 6.7. Table 3.3.10 shows the obtained k_{metal} and half lifes in presence of metal ions, with Table 3.3.11 showing this relative to a $k_{control}$ value estimated from the pH profile. The $k_{control}$ values are obtained from the pH profile using the measured pH of each metal solution. The $k_{control}$ calculated for Cu^{2+} (25:1 M^{n+}/D, pH 5.0) is depicted in Figure 3.3.23 (-log k_{obs}= -6.3, k_{obs} = 5.0 x 10^{-7} s^{-1}, half life 16 days).

Table 3.3.10 k_{metal} obtained for the hydrolysis of diazinon in the presence of metal ions using the method of initial rates in 70%MeOH/30%H_2O at 22°C.

M^{n+}	$[M^{n+}]$ x 10^{-4} (M)	[D] x 10^{-5} (M)	Ratio $[M^{n+}]/[D]$	Rate x 10^{-8} (M s^{-1})	k_{metal} x 10^{-4} (s^{-1})	$t_{1/2}$
Hg^{2+}	8.25	8.25	10	1.77 ± 0.033	2.1 ± 0.033	55.0 min
Hg^{2+}	20.6	8.25	25	3.17 ± 0.065	3.8 ± 0.065	30.4 min
Cu^{2+}	8.25	8.25	10	1.16 ± 0.012	1.4 ± 0.012	82.5 min
Cu^{2+}	20.6	8.25	25	1.95 ± 0.018	2.4 ± 0.018	48.1 min
Ag^{+}	8.25	8.25	10	0.349 ± 0.003	0.42 ± 0.003	4.6 hrs
Ag^{+}	20.6	8.25	25	0.446 ± 0.020	0.54 ± 0.020	3.6 hrs
Cd^{2+}	20.6	8.25	25	0.024 ± 0.007	0.029 ± 0.007	2.8 days

Table 3.3.11 Comparison of k_{obs} in the presence and absence of metal ions.

M^{n+}	Ratio $[M^{n+}]/[D]$	pH of solution	$k_{metal} \times 10^{-4}$ (s^{-1}) (a)	$k_{control}$ (s^{-1}) (b) (pH profile)	$k_{metal}/k_{control}$	$t_{1/2}$
Hg^{2+}	10	6.8	2.1 ± 0.033	1.25×10^{-7}	1680	55.0 min
Hg^{2+}	25	6.5	3.8 ± 0.065	1.58×10^{-7}	2405	30.4 min
Cu^{2+}	10	5.25	1.4 ± 0.012	2.0×10^{-7}	700	82.5 min
Cu^{2+}	25	5.0	2.4 ± 0.018	2.5×10^{-7}	960	48.1 min
Ag^{+}	10	7.4	0.42 ± 0.003	1.25×10^{-7}	336	4.6 hrs
Ag^{+}	25	7.15	0.54 ± 0.020	1.00×10^{-7}	540	3.6 hrs
Cd^{2+}	25	6.7	0.029 ± 0.007	1.25×10^{-7}	23	2.8 days

(a); k_{metal} is the rate obtained in the presence of metal ions.
(b); $k_{control}$ is obtained from the pH profile using the measured pH of the metal solution and is the rate in the absence of metal ions.

Table 3.3.11 clearly shows the ability of the metal cations to accelerate the rate of hydrolysis of diazinon. This will be explored in more detail in the discussion section.

Table 3.3.12 similarly shows the obtained k_{metal} and half lifes in the presence of metal ions in acidic conditions. Analogous to base solutions the pH of each acid solution in the presence of metal ions was measured. The pH was not found to vary significantly on addition of metal ions at pH 4; therefore the $k_{control}$ was estimated at this pH. Table 3.3.13 shows the acceleration in rate in the presence of metal ions relative to $k_{control.}$ The results obtained both in acid and neutral conditions will be explored further in terms of rate enhancement, pH and speciation in the discussion section.

Table 3.3.12 Rate values obtained for the hydrolysis of diazinon in the presence of metal ions at pH 4.0 using the method of initial rates in 70%MeOH/30%H_2O at 22°C.

M^{n+}	$[M^{n+}] \times 10^{-4}$ (M)	$[D] \times 10^{-5}$ (M)	Ratio $[M^{n+}]/[D]$	Rate $\times 10^{-8}$ (M s^{-1})	$k_{obs} \times 10^{-4}$ (s^{-1})	$t_{1/2}$
Hg^{2+}	8.25	8.25	10	1.68 ± 0.089	2.0 ± 0.089	57.8 min
Hg^{2+}	20.6	8.25	25	2.03 ± 0.065	2.5 ± 0.065	46.0 min
Cu^{2+}	8.25	8.25	10	0.357 ± 0.043	0.43 ± 0.043	4.5 hrs
Cu^{2+}	20.6	8.25	25	0.818 ± 0.016	1.0 ± 0.016	1.9 hrs
Ag^{+}	8.25	8.25	10	0.498 ± 0.029	0.60 ± 0.029	3.2 hrs
Ag^{+}	20.6	8.25	25	0.805 ± 0.019	0.98 ± 0.019	1.9 hrs

Table 3.3.13 Comparison of k_{obs} in the presence and absence of metal ions in acid conditions.

M^{n+}	Ratio $[M^{n+}]/[D]$	pH of solution	$k_{metal} \times 10^{-4}$ (s^{-1}) [(a)]	$k_{control}$ (s^{-1}) [(b)] (pH profile)	$k_{metal}/k_{control}$	$t_{1/2}$
Hg^{2+}	10	4.0	2.0 ± 0.089	5.0×10^{-6}	40.0	57.8 min
Hg^{2+}	25	"	2.5 ± 0.065	"	50.0	46.0 min
Cu^{2+}	10	"	0.43 ± 0.043	"	8.6	4.5 hrs
Cu^{2+}	25	"	1.0 ± 0.016	"	20.0	1.9 hrs
Ag^{+}	10	"	0.60 ± 0.029	"	12.0	3.2 hrs
Ag^{+}	25	"	0.98 ± 0.019	"	19.6	1.9 hrs

CHAPTER 4 Discussion

4.1 Factors to be considered in the hydrolysis of diazinon in the presence of metal ions.

Hydrolysis is known to be a major degradation pathway for organophosphorus pesticides and is a thoroughly studied process. The hydrolysis itself can occur by either homogenous mechanism, where H_2O and ^-OH act as nucleophiles commonly in an S_N2 mechanism. Alternatively dissolved matter such as metal ions may influence the rate of hydrolysis, this being a less studied and understood phenomenon. A principal aim of this research is the development of a greater understanding of the role these metal ions play in the enhancement of the rate of hydrolysis of organophosphorus pesticides such as diazinon.

Dissolved metal ions are known to play a wide and varied role in affecting the rates and transformations of hydrolysis reactions, typically through complexation of one form or another. Various postulates have been put forward as to the exact mechanism of their action, of which some will be examined in the following passages. Smolen et al. suggested up to six distinct mechanisms of metal catalysed nucleophilic substitution of which the most recurrent will be examined in this thesis [29]. Hendry also discussed the various modes of action of metal ions in catalyzing reactions of phosphate derivatives[30]. Several other factors play important functions in influencing the mechanistic role of metal ions in catalysing the rate of hydrolysis of diazinon. The properties of both the metal ions and ligands encompassing compatibility, size, charge etc. can be hugely

influential on the reaction in terms of the mechanistic routes available. These factors will also be examined.

4.1.1 Metal binding to ligands of OP's

One common and generally accepted reason for the observed acceleration is the ability of metals to bind to certain ligands frequently found in organophosphorus pesticides. This affinity for such ligands can influence the rate of hydrolysis in several ways;

1) The metal ion acts as a Lewis acid and co-ordinates the thionate sulfur. This has the effect of enhancing the electrophilicity of the phosphorus electrophilic centre making it more prone to attack by ^{-}OH or H_2O as depicted in Scheme 4.1.

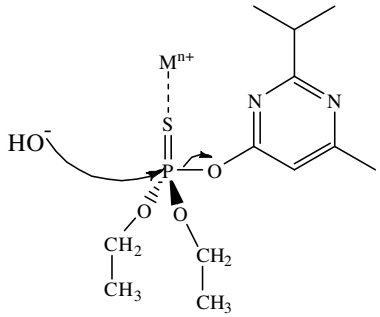

Scheme 4.1 Metal binding to thionate sulfur, with resultant increase in the electrophilicity of phosphorus

2) Metal ion co-ordinates the leaving group as shown in Scheme 4.2, with resultant facilitation of its departure by weakening the O-P bond. The lower the pKa of the conjugate acid of the leaving group the better the leaving group. One must consider therefore the pKa values for the two possible leaving groups with S_N2 attack at P, namely phenolate and the alcholate leaving groups.

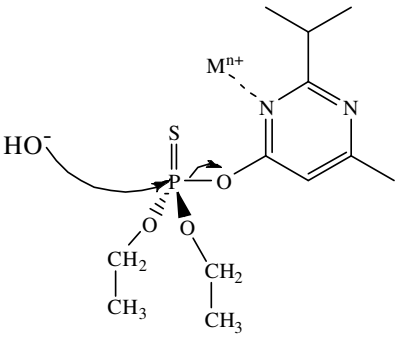

Scheme 4.2 Metal binding to leaving group facilitating its departure

3) When two ligands are present the interplay of both mechanism (1) and (2) are possible. Furthermore either sulfur or nitrogen may be considered an auxiliary donor ligand in diazinon. This proximity of a secondary ligand may result in chelation through co-ordination of the metal at both nitrogen and the thionate sulfur. It is important to note here that the chelate may not be symmetrical in nature and depends on the strength of interaction between the ligand and metal ion.

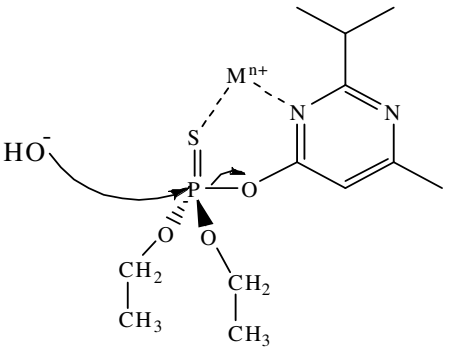

Scheme 4.3 Metal chelation

The three mechanisms shown above suggest metal binding to the ligand sites of organophosphorus pesticides with resultant electronic effects as the driving force for the observed acceleration of hydrolysis of certain organophosphorus pesticides. Assessment of these mechanisms must include evaluation of metal and ligand compatibility in regards of their properties.

4.1.2 Metal and ligand complementarity

Many factors control metal ion complementarity to ligands with much written about the understanding of different metals affinity for certain ligands. Complementarity can be viewed as the degree of structural correspondence between the ligands and the metal[31]. One of the earliest and simplest concepts is the Hard Soft Acid Base (HSAB) principle developed by Pearson in the 1960's to explain certain metals affinity for selective ligands and is still widely applicable today[32]. Metals were classified according to which type of

ligand they prefer. “Hard” Lewis acids or Type A metals prefer ligands such as oxygen whilst type B metals or “soft acids” tend to have affinity for donors such as sulfur. The hardness and softness terms used were related to the polarisibilty of the metal i.e. the ability of the electron cloud of the metal ion to become deformed during bond formation. Some of the properties of hard acids include;

- Small ionic radius
- High positive charge
- Species that do not contain electron pairs in their valence shells
- Low electron affinity

Whilst for soft acids;

- Large ionic radius
- Low positive charge
- Electron pairs in the valence shell
- Easily polarizable

Another commonly considered concept in describing ligands is the idea of general and selective complexing agents as described by Schwarzenbach[33]. This concept describes oxygen as a general complexing agent with the ability to combine with any metal with a charge more than one. The strength of the bonds is found to increase significantly with the charge on the metal ion and decrease with its radius, a concept familiar to HSAB. This behavior is termed electrovalent. Contrasting this is non-electrovalent behavior exhibited by ligands such as sulfur and to a lesser extent nitrogen. These ligands do not favor binding with type A metal ions i.e. those having a noble gas electronic structure, instead favoring transition metal cations or class B cations. However charge and radius

are not considered the dominant factors for bond strength but rather the electronegativities of the atoms to be combined. It suggests that the bond strength generally increases with increasing electronegativity of the metal ions and decreasing electronegativity of the ligand. An example of this is Ag^{+} which exhibits almost pure electrovalent behavior. The above concepts may be used to explain observations in the NMR and MS studies of metal affinities for certain ligands. The metal ions studied possess well characterised chemical properties which may be used to shed light on the mechanistic pathways of hydrolysis.

4.1.3 Formation of hydroxy species (speciation)

The mechanisms outlined above of metal catalysis have proposed metal binding to the ligand sites of the organophosphorus pesticide itself. A fourth possible mechanism suggests metal co-ordination to the nucleophile. This involves formation of metal hydroxy species that may play a catalytic role especially in neutral or acidic conditions, where $M^{n+}OH$ can act as a nucleophile due to the low concentration of ^{-}OH (shown in Scheme 4.4).

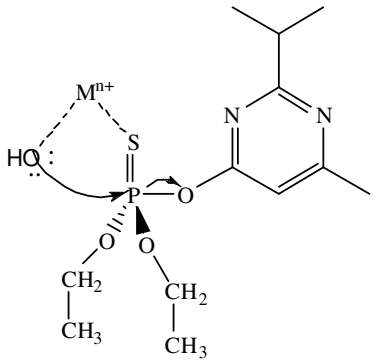

Scheme 4.4 Intramolecular nucleophilic attack

These hydroxy species may take part in intramolecular nucleophilic attack, such a mechanism involving metal binding followed by ^{-}OH attack. Such pull-push mechanisms

are often used to explain metal catalysis of hydrolysis of OP pesticides. Another important factor of the formation of metal-hydroxide species is the reduction of "free" metal ions to influence mechanisms 1-3.

This formation of such hydroxy species occurs when the metal ions become solvated by water (or methanol) molecules. The metal ions once solvated act much like they do in binding to the thionate sulfur. The metal draws electron density away from the O-H bond in water increasing the bonds polarity. This has the effect of making the hydrogen of the H_2O molecule more acidic, which is then readily removed by a second water molecule forming the first hydroxy species as shown in Scheme 4.5 and Equation 1.

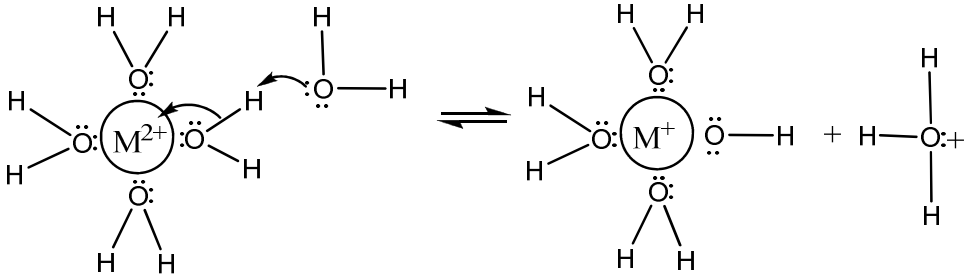

Scheme 4.5 Formation of first hydroxy species.

This is also known as the monohydroxoaqua complex. An important side effect is to make the solution more acidic, a factor discussed later in terms of rate data.

$$[M(OH_2)_x]^{n+} \rightleftharpoons [M(OH_2)_{x-1}(OH)]^{(n-1)+} + H^+ \qquad (1)$$

The ability of a metal ion to act as a Lewis acid is dependent upon several factors including ionic radius, charge on the metal, pH and total metal ion concentration. The

counter-ion is also a factor as will be examined in the rate increases observed with two different mercury salts, $HgCl_2$ and $Hg(NO_3)_2$.

Literature data is readily available in regards to metal hydrolysis and the concentration of hydroxy species for different metal cations as a function of pH. The work by Baes and Mesmer, once they made corrections for size and charge of the metal ion, showed that hard metals belonging to groups 1 and 2 are generally more resistant to hydrolysis whereas a soft transition cation such as Hg^{2+} undergoes hydrolysis to other species much more readily[34,35]. These authors in-addition designated a group of "hard" cations that are slightly less resistant to speciation than those found in groups 1 and 2. These included Ag^{+}, Cu^{2+} and Cd^{2+}, metals of interest in the present study. Their work determined equilibrium constants for the first hydrolysis step as outlined in Table 4.1 (the larger the value of the pKa, the less acidic the cation).

Table 4.1 Hydrolysis constants for metal cations[34].

Metal cation	pKa value	
K^{+}	14.5	Hard cations; resistant to hydroxide formation.
Na^{+}	14.2	
Ag^{+}	12.0	Moderately resistant to hydroxide formation.
Cd^{2+}	10.1	
$*Cu^{2+}$	*7.93	
Hg^{2+}	3.4	Soft cation; Little resistance to hydroxide formation.

* Cu^{2+} data from Paulson[36].

The value for Cu^{2+} was obtained from the work of Paulson et al. who investigated the first and second hydrolysis constants for Cu^{2+} using the ion-selective-electrode pontentiometric method[36]. The most striking point is the equilibrium constant for Hg^{2+} at 9 log units higher than the "hard" cations and up to three log units higher than metals such as Ag^{+}, Cu^{2+} and Cd^{2+}. It is useful to remember that the metals resistance to hydrolysis is explained in terms of softness and hardness ($K^{+}>Na^{+}>Ag^{+}>Cd^{2+}>Cu^{2+}>Hg^{2+}$); a concept also widely used to explain metal cation affinity for certain ligands of the organophosphorus compounds.

A second convenient way to observe the different species present at various pH's is to use speciation profiles. Such profiles were obtained from the work of Esbata[37] who evaluated metal speciation according to Equation 2, with the pKa values taken from Bjerrum[38].

$$\alpha = 1/(1 + 10^{pH-pKa}) \qquad (2).$$

The speciation profile for Ag^{+} shows that at pH 10.0 and 4.0 the predominant species is $Ag(H_2O)_4^{+}$, and it is not until higher basic conditions prevail that the first hydroxy species exists.

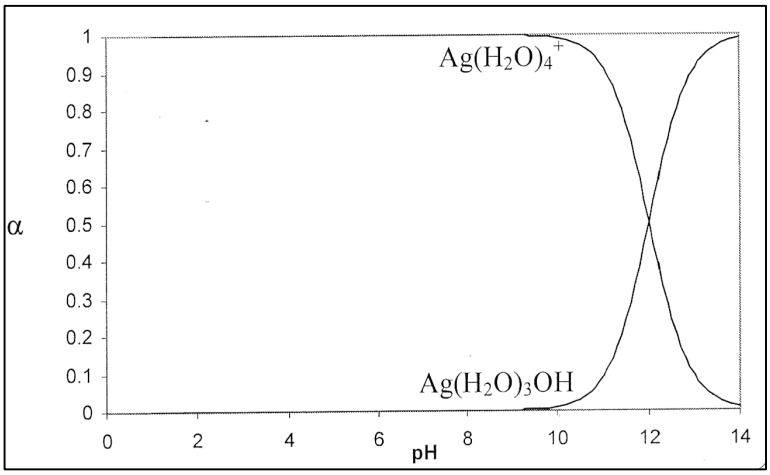

Figure 4.1 Species distribution for 0.1mmol L^{-1} Ag^{+} as a function of pH[22].

The speciation profile for Cu^{2+} as a function of pH is shown in Figure 4.2. At pH 4.0 Cu^{2+} is in the from $Cu(H_2O)_4^{2+}$, whilst at pH 10.0 the first hydroxy species $Cu^{+}(OH)(H_2O)_3$ prevails.

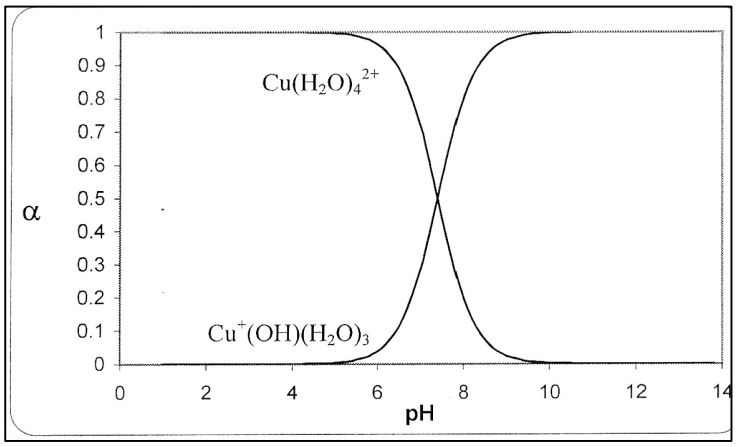

Figure 4.2 Species distribution for 0.1 mmol L^{-1} of Cu^{2+} as a function of pH[9].

The speciation profile for Hg^{2+} as a function of pH is shown in Figure 4.3. The distribution diagram shows the extent to which Hg^{2+} undergoes hydrolysis. At pH 4.0 11% is in the form $Hg(H_2O)_4^{2+}$, 39% in the form $Hg^{+}(OH)(H_2O)_3$ and 50% in the form $Hg(OH)_2(H_2O)_2$. At pH10.0 only $Hg(OH)_2(H_2O)_2$ exists. The speciation profiles correlate well with the pKa values determined by Baes and Mesmer [34].

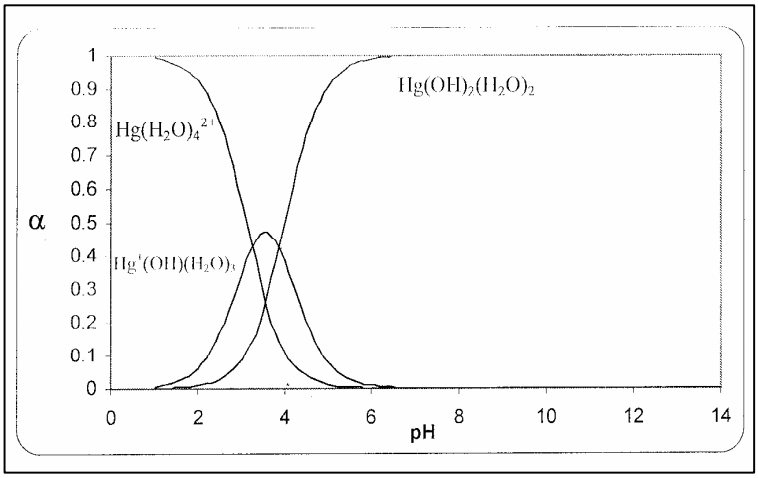

Figure 4.3 Species distribution graph as a function of pH for 0.01 mmol L^{-1} Hg^{2+} at 25° C

4.1.4 Metal ion catalysis; Transition state versus ground state binding

The mechanistic picture that covers the above effects of metal ions on the hydrolysis of organophosphorus pesticides relates to a strong interaction of the cations with the reactant -state, followed by nucleophilic attack. This may be viewed as nucleophilic activation. There is also a possibility that the catalytic ability of the metal ions is due to strong transition-state interaction rather than reactant-state; that is to say that the metal ions may bind the transition state more strongly than the reactant state. This stabilisation of the transition-state occurs due to a lowering of the free energy of activation for the formation of the negatively charged transition state. This is a result of strong metal binding to the altered substrate which stabilises the developing negative charge, sometimes referred to as electrostatic stabilization, as shown in Figure 4.4.

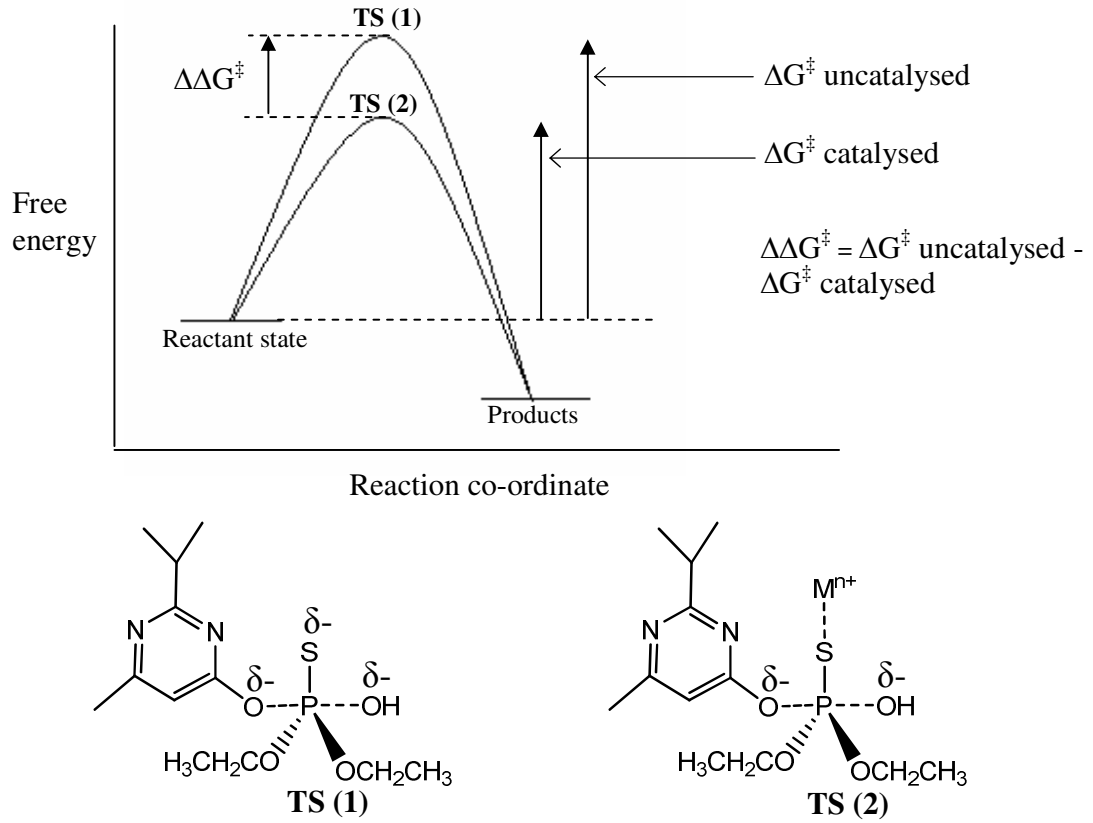

Figure 4.4 Reaction coordinate diagram for catalysed versus uncatalysed reaction, where the catalyst lowers the energy of the transition state.

Figure 4.4 depicts the reaction co-ordinate diagram for a metal catalysing the reaction through strong binding in the transition state with resultant lowering of the $\Delta G^{\ddagger}$ of reaction. Figure 4.4 contrasts Figure 4.5 in which there is a change in mechanism as a result of complex formation between substrate (D) in the reactant state and the metal ion.

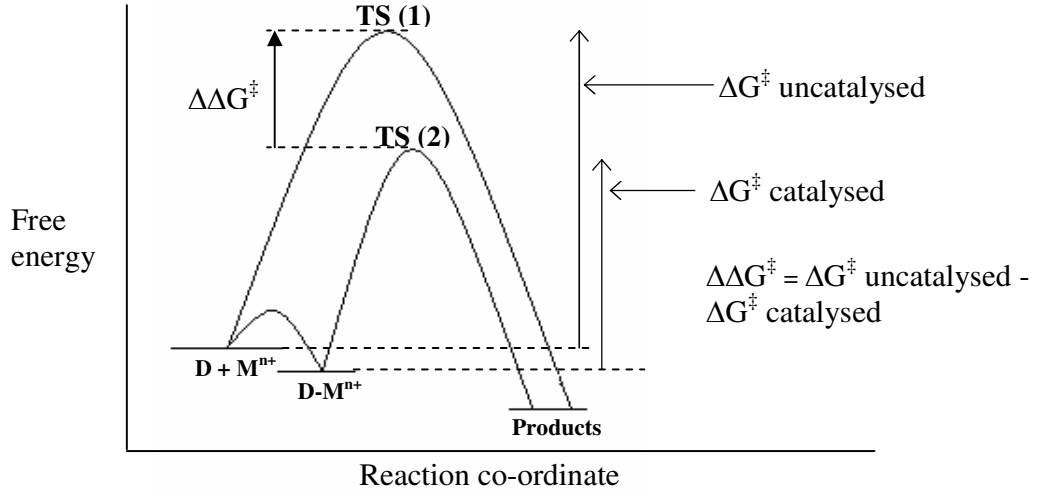

Figure 4.5 Reaction coordinate diagram for catalysed versus uncatalysed reaction, where the catalyst binds the reactant state strongly.

The approach of strong metal interaction in the transition state currently plays a very significant part in the interpretation of enzyme catalysis of many important phosphoryl transfer reactions. Hydrolysis of phosphate esters is of crucial importance in biological systems, being involved in energy transduction, biosynthesis, control of secondary messengers and regulation of protein function. It has been proposed that enzymes lower the activation barrier by lowering the energy of the transition-state. It is now widely thought that the active sites of enzymes are structurally similar and bind tighter to the transition-state than the reactant-state. Several examples of this interpretation of enzyme catalysis can be found in the literature[39, 40]. In fact a recent study by Efremenko et al.[41] investigated the catalytic degradation of phosphorus containing pesticides using the enzyme organophosphate hydrolase.

4.2 Identification of hydrolysis products in the presence and absence of metal ions by NMR

In order to determine the hydrolysis products of diazinon a set of NMR experiments were carried out. The hydrolysis of diazinon in the absence of metal ions was studied over several days by recording ^{31}P spectra at regular time intervals and comparing the phosphorus peak(s) resulting from hydrolysis against authentic PA spectra and relevant literature sources. The authentic ^{31}P NMR spectrum of PA (60.165 ppm) is shown in Figure 3.1.1, with the hydrolysis spectra for diazinon depicted in Figure 3.1.25. The spectra shows the appearance of one phosphorus-containing product at an equivalent ppm shift as that obtained in the authentic PA spectrum. This points to attack at phosphorus (S_N2 P) as the preferred hydrolysis route for diazinon as shown in Scheme 4.1. Although S_NAr attack would result in the same products, it is not considered a plausible hydrolysis route due to the insufficient electron withdrawal by ring substituents. Thus S_N2 (P) is the proposed route of hydrolysis for diazinon as reported in previous studies.

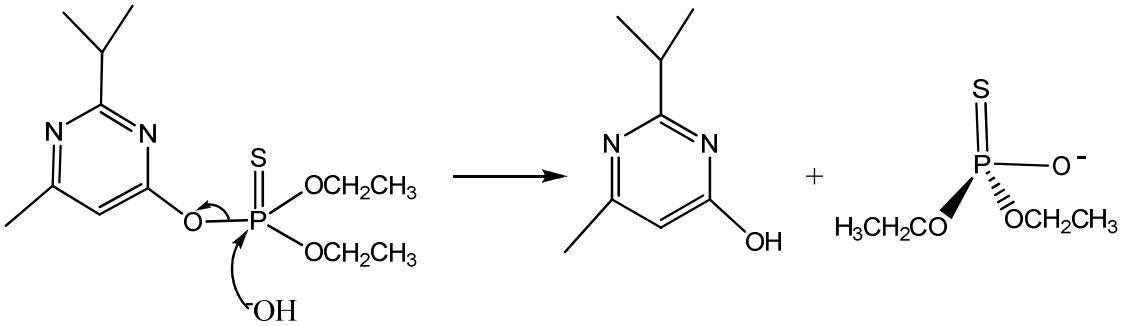

Scheme 4.6 Proposed S_N2 attack at phosphorus centre for the hydrolysis pathway of diazinon.

A similar set of hydrolysis experiments was carried out in the presence of metal ions in order to investigate pathways in metal ion catalysis. Identification of products was aided by comparison of the chemical shifts obtained in authentic PA and PY studies in

the presence of various metal cations with the ^{31}P and ^{1}H chemical shifts obtained on hydrolysis. The results are outlined in Section 3 under product profiles for the separate metal cations. The appearance of only one phosphorus-containing compound in the presence of Ag^{+}, Hg^{2+} and Cd^{2+} indicates that diazinon undergoes hydrolysis by a single pathway. The comparison of ^{31}P product chemical shifts with authentic PA in the presence of matching concentrations of metal gave excellent agreement, signifying S_N2 (P) attack. The large up-field ^{31}P shifts in the presence of metal ions is noticeable in both the authentic PA study and the products obtained from hydrolysis.

Further substantiation of S_N2 (P) attack as the preferred hydrolysis route is found in the proton NMR. Comparison of ppm shifts of ^{1}H products peaks with authentic ^{1}H shifts for PY and PA in the presence of equivalent metal concentrations gives good agreement, further confirming S_N2 (P) attack as being the favored route of hydrolysis.

It is noteworthy that the ^{31}P chemical shifts observed in the present work show contrasting behavior to the normally observed ^{1}H NMR shifts with respect to electronic effects of substituents. An example of this contrasting behavior is given below, with Figure 3.1.7 depicting the downfield shifts in the proton nuclei of PA in the presence of Ag^{+}. Contrasting this is Figure 3.1.6 which depicts the large upfield shifts experienced by the phosphorus nucleus of PA in the presence of similar concentrations of Ag^{+}.

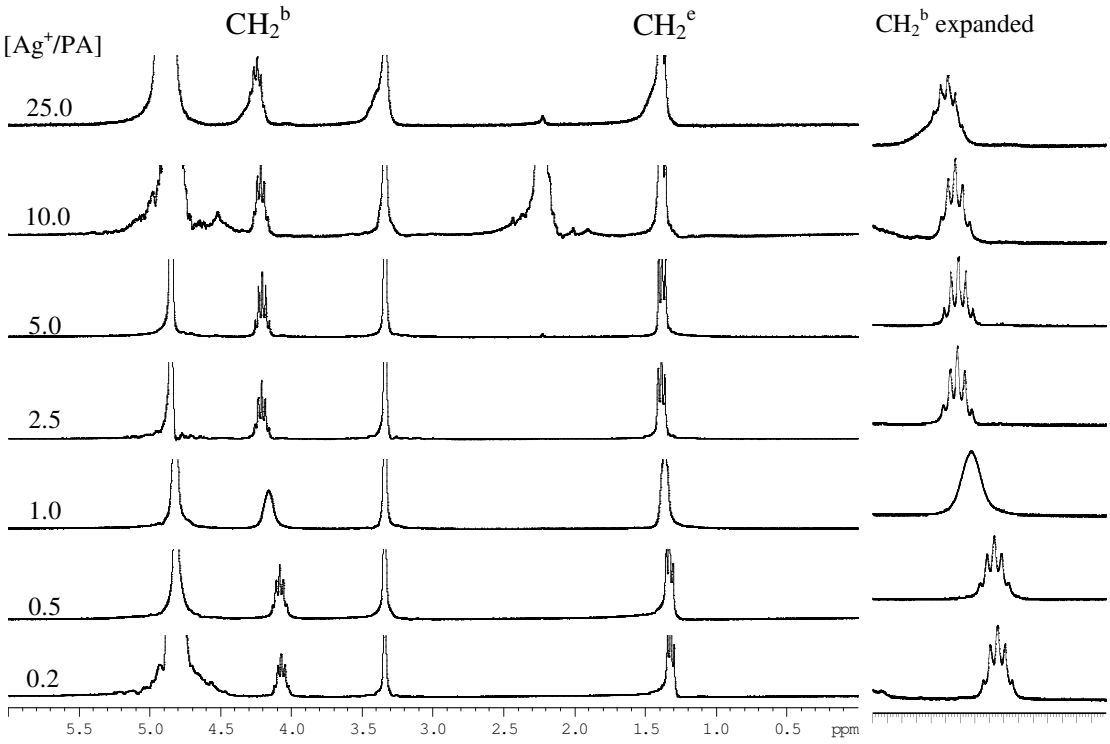

Figure 3.1.7 ^{1}H spectra depicting the chemical shift change of PA proton peaks with increasing Ag^{2+} concentrations (with expanded CH_2^b peaks).

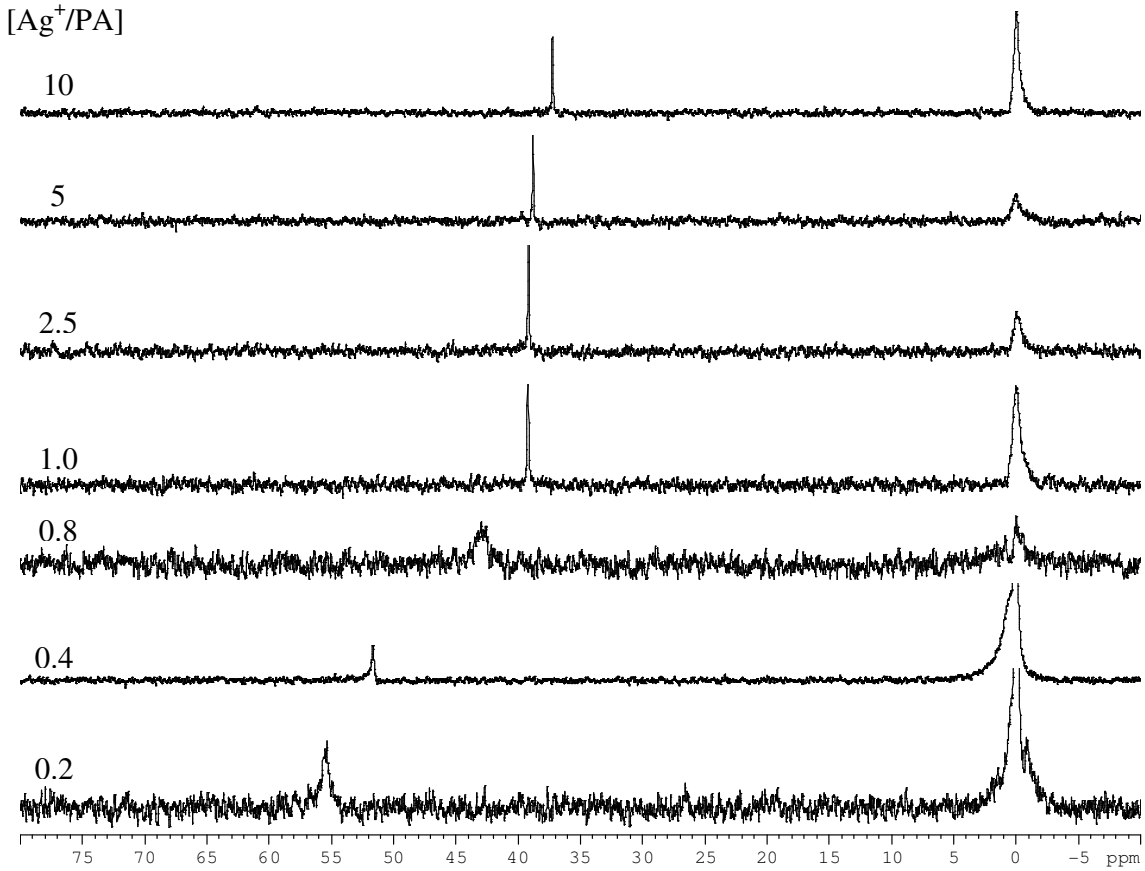

Figure 3.1.6 ^{31}P NMR spectra depicting the chemical shift change of PA phosphorus peak in the presence of increasing Ag^+ concentrations (70%CD_3OD-30%D_2O v/v).

This type of contrasting behavior was observed previously in work emanating from our laboratory[37] and is currently receiving theoretical examination (unpublished work by Dr. Insun Koo). A full description will follow in due course.

4.3 Metal binding characterisation

The mechanisms outlined in Section 4.1, whilst differing in approach, are all contingent on strong metal binding to specific ligand sites in diazinon. In view of this, an extensive metal binding characterisation study was undertaken by NMR and ESI-MS to help reveal the site or sites of metal binding to diazinon. Such elucidation of the individual metals co-ordination with specific ligands enables one to draw conclusions of how the metal ions accelerate the rate of hydrolysis of diazinon. Certainly the comparison of results from both techniques will facilitate a greater understanding of the location and strength of binding.

In respect of this potential binding, the role of the sulfur bound to phosphorus and the nitrogens of pryrimidinol as potential ligand sites must be kept in mind. A third potential site of co-ordination exists in diazinon, that of oxygen. Oxygen however is considered to be a very 'hard' base, whilst the metals being studied are generally considered soft to intermediate in nature. According to Hard-Soft-Acid-Base theory or Schwarzenbach's electrovalent or non-electrovalent behavior, these are not considered to be an ideal Lewis acid-ligand arrangement. The location and strength of binding observed for the metal ions studied will be outlined individually in short sections for clarity, with NMR and ESI-MS data dealt with collectively. The NMR and ESI-MS evaluation of the various cations binding affinity and strength with the ligands of diazinon and its hydrolysis products is extremely useful in accurately establishing the role that these metal ions play in the hydrolysis process. Further appraisal is made in terms of any relevant literature sources where possible and previous studies in the Buncel-vanLoon Laboratory.

4.3.1 Ag^+ binding interpretation

A set of ^1H NMR, ^{31}P NMR and ESI-MS experiments entailing binding and hydrolysis experiments in the presence of Ag^+ were carried out as outlined in Section 3. The observed acceleration of the rate of hydrolysis in the presence of Ag^+ (10 minutes for complete hydrolysis against 16 days in the absence of Ag^+, see Figure 3.1.28) conclusively shows Ag^+ facilitation of hydrolysis. This observed acceleration of the rate was first assessed in terms of Ag^+ co-ordination to both hydrolysis products, giving an insight into Ag^+ affinity for both Lewis sites, nitrogen and sulfur. The NMR and ESI-MS data of PY and PA in the presence of Ag^+ is considered collectively below.

Appreciable changes in the ^{31}P and ^1H chemical shits of both PA and PY were observed on addition of Ag^+ ions (Figure 3.1.6 and 3.1.7 for PA and Figure 3.1.18 for PY). These changes are calculated relative to standard ppm values obtained in the absence of metal ions. The maximum ^{31}P chemical shift change of PA was 25 ppm, observed with a ratio 25:1 Ag^+/PA. Significant shifts where also noted in the CH_2^b protons belonging to PA, demonstrating that the changes in the chemical shift due to Ag^+ co-ordination at sulfur are felt further along the chain. These substantial changes in the chemical environment of nuclei surrounding sulfur comparative to standard values, alludes to the metals influence on the rate of hydrolysis. Such a scenario is outlined in mechanism 1, where co-ordination to the thionate sulfur has the affect of increasing the electrophilicity of the phosphorus atom, making it more prone to nucleophilic attack. A plot of chemical shift change (ppm) versus ratio of Ag^+/PA shown in Figure 3.1.8 indicates a binding ratio of 1:1. This understanding is drawn from the sharp rise in the chemical shift change up to a Ag^+/D ratio of 1:1, with subsequent leveling in the chemical shift change at higher ratios.

Changes in the chemical shifts of PY protons were also observed in the presence of Ag^+, the most affected proton being H^c. This is strongly suggestive of Ag^+ co-ordination to one of the nitrogens of PY, a second potential mechanism of hydrolysis acceleration by means of leaving group facilitation. Plots of change in the chemical shift versus Ag^+ concentration for all protons (Figure 3.1.19) describe a dynamic equilibrium between bound and unbound Ag^+. The NMR study of Ag^+ interaction with the ligand sites of PA and PY show the ability of Ag^+ to complex both N and S, with resultant appreciable effects on the surrounding chemical environment.

The ESI-MS analysis of Ag^+ interaction with PA and PY supports the NMR findings that the cation co-ordinates both N and S Lewis sites. The cation's affinity for nitrogen of PY was revealed by the appearance of a set of peaks at 259, 261 corresponding to PY (152 amu) + Ag^+ (107/109 amu). Similarly, Ag interaction with sulfur was established in negative ion mode by the appearance of a set of peaks at mz 445 and 447. This corresponds to two PA molecules (338 amu) co-ordinated to one Ag^+ (107/109 amu) as shown in Figure 4.6. In addition both sets of peaks exhibited the isotopic ratio of Ag^+ of 52, 48%.

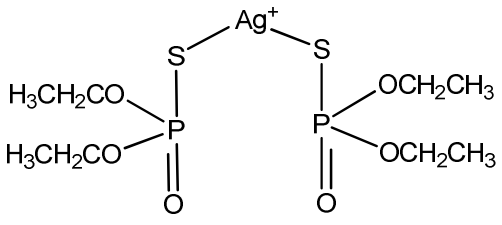

Figure 4.6 Ag^+ bound PA

The assessment of Ag^+ interaction with PY and PA clearly point to its capacity to bind both N and S ligand sites.

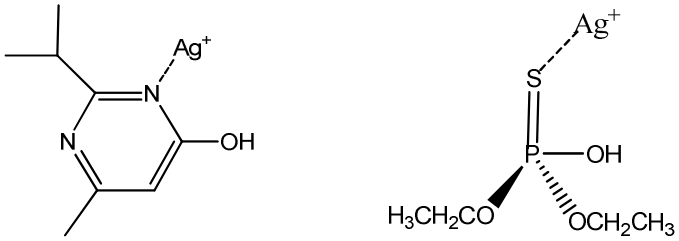

Figure 4.7 Proposed co-ordination of Ag^+ to hydrolysis products PA and PY, ensuing from interpretation of NMR and ESI-MS results.

Whilst particularly useful in identifying the probable sites of binding for catalysis, it was desirable to carry out a comparable set of experiments with diazinon in the presence of Ag^+. The ^{31}P chemical shift of diazinon furthermore shows a change in chemical environment in the presence of Ag^+ ions when compared to chemical shifts in the absence of Ag^+ ions (see Table 3.1.11). This strongly suggests Ag^+ co-ordination of the sulfur ligand as an important contributor to its ability to accelerate the rate of hydrolysis. Due to the rapid hydrolysis of diazinon in the presence of Ag^+ it was only possible to observe the ^{31}P chemical shift of the substrate at higher ratios of Ag^+/D. For this reason a set of experiments was carried out in CD_3OD to eliminate hydrolysis, thus enabling an improved assessment of Ag^+ co-ordination to diazinon. In support of previous data, a concomitant up-field shift in the ^{31}P signal was observed with increasing Ag^+ concentration (Figure 3.1.41), further confirming co-ordination to sulfur.

Appraisal of H^1NMR is an even better probe of the interactions of Ag^+ with diazinon, as this allows assessment of the chemical environment of protons in the vicinity of both ligand sites, N and S. Interestingly both heterocyclic (near nitrogen) and aliphatic (near sulfur) protons show appreciable changes in their chemical environment relative to

standard ppm shifts obtained in the absence of metal ions (See Tables 3.1.12 and 3.1.13). The shift change was also seen to increase with increasing Ag^+ concentration. The simultaneous change in the chemical shift of nuclei (phosphorus and proton) close to both ligand sites points to co-ordination at both locations. Although individual co-ordination of both ligands is plausible, a more feasible suggestion is chelation, with the resultant formation of a six membered ring. Markedly the analysis of the proton and phosphorus chemical shifts of the product peaks i.e. post hydrolysis, also indicate Ag^+ co-ordination of sulfur and nitrogen (Tables 3.1.7-3.1.10). The obtained chemical shifts for product peaks from the hydrolysis study gave good agreement with those obtained in the independent analysis of PA and PY in the presence of Ag^+. This further substantiates Ag^+ binding at both N and S Lewis sites. The NMR data of diazinon in the presence of Ag^+ points strongly to complexation through bidentate chelation as Shown in Figure 4.8.

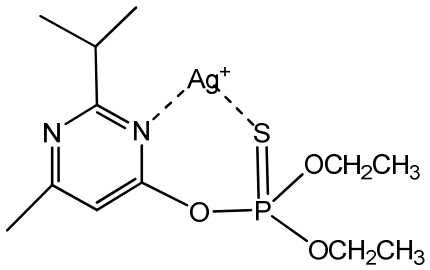

Figure 4.8 Proposed complexation of Ag^+ with diazinon

Further evidence for such a projection was established in the ESI-MS study of diazinon in the presence of Ag^+ by the appearance of a set of peaks at 411,413 mz. These peaks correspond to diazinon (304 amu) + Ag (107, 109 amu). Added confirmation that the peaks signify Ag^+-bound diazinon was obtained by performing CID (MSMS) experiments on the separate m/z ratios, and observing the relevant daughter ions produced in the fragmentation process. Significantly the fragmentation of the individual

m/z isotopes i.e. 411 and 413 mz, leads to daughter ions that indicate Ag^+ bound at both PY and PA (see Figures 3.2.7 and 3.2.8). The fragmentation of 411m/z (D (304 amu) + Ag^+ (107 amu)) results in daughter ions with m/z 259 and 277, corresponding to PY (152 amu) + Ag^+ (107 amu) and PA (170 amu) + Ag^+ (107 amu) respectively. Equally fragmentation of the 413 m/z (D + Ag^+ (109 amu) results in daughter ions at mz 261 and 279 m/z, representing Ag^+ (109 amu) bound PY (152 amu) and PA (170 amu).

The aforementioned MS experiments give definitive confirmation of Ag^+ complexation with diazinon, with MS/MS experiments showing once more the metal bound at N and S ligand sites. Analogous to the NMR outcome it is proposed that rather than individual co-ordination at N and S sites, the ESI-MS results equally support chelation as the mode of action of Ag^+. As outlined previously ESI-MS analysis of Ag^+ complexation with PA and PY gave matching results. The overall understanding of Ag^+ binding with diazinon and its hydrolysis products is summarized in Table 4.2, with the final proposed complexation structure arrived at from interpretation of ESI-MS and NMR data shown on the following page.

Table 4.2 Interpretation of Ag^+ co-ordination with diazinon and its hydrolysis products using NMR and ESI-MS.

Substrate	Ligand	NMR		MS	
		Yes	No	Yes	No
PA	S	√		√	
PY	N	√		√	
D	S	√		√	
	N	√		√	

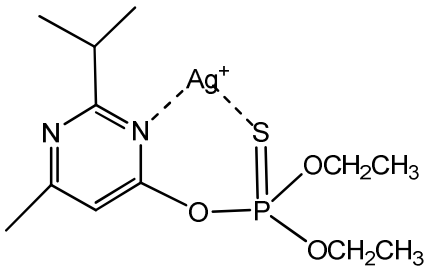

Proposed complexation of Ag^+ with diazinon

Previous investigations of metal ion promoted hydrolysis of organophosphorus pesticides performed in the Buncel-vanLoon laboratory supports the proposed bidentate chelation between diazinon and Ag^+ ions. Esbata[37] et al. reported similar co-ordination results whilst studying Ag^+ interactions with Quinalphos and its hydrolysis products, HQ (hydroxyquinaoxaline) and PA (see Figure 4.9 for structures). The author reported observing interactions in the ESI-MS study between Ag^+ and both hydrolysis products containing N and S Lewis sites. Markedly Esbata also observed the complexed ion between Quinalphos and Ag^+, indicated by the presence of a set of peaks at m/z 405 and 407 (Q (298 amu) + Ag^+ (107, 109amu)). Subsequent CID experiments on the parent complex using both 405 and 407 m/z peaks, revealed co-ordination at both nitrogen and sulfur ligand sites by the appearance of various fragments relating to Ag^+ bound HQ and PA. This is analogous to the results reported in the study of diazinon in the presence of Ag^+.

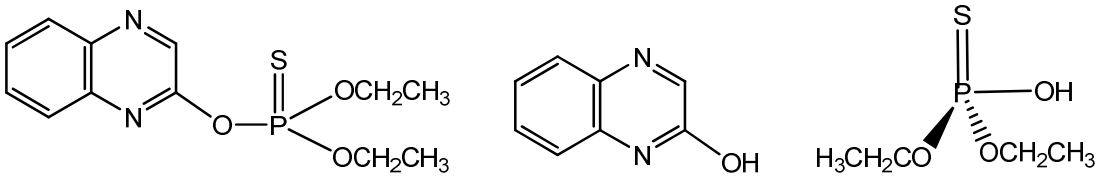

Figure 4.9 Quinalphos and its hydrolysis products HQ and PA.

Esbata additionally substantiated the proposed interactions interpreted from ESI-MS data by running a parallel set of NMR experiments on Q and its hydrolysis products. The NMR analysis similarly revealed strong interactions between Ag^+ and the Lewis base sites N and S, through observed chemical shift changes in various nuclei including proton and phosphorus. From the obtained ESI-MS and NMR data the author concluded that Ag^+ complexation with Q was through chelation with N and S, with the consequent formation of a six membered ring as depicted in Figure 4.10. This is comparable to the proposed complexation between diazinon and Ag^+ in the present study.

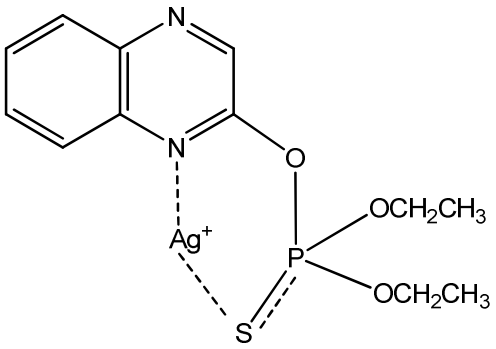

Figure 4.10 Esbata's proposed complexation between Q and Ag^+.

Recent work by Koo[42] et al. carried out in the Buncel-vanLoon laboratory also revealed Ag^+ affinity for sulfur ligands in organophosphorus pesticides. The work investigated the catalytic effect of Ag^+ and Hg^{2+} on the hydrolysis of Fenitrothion (FN) using ESI-MS and NMR techniques. Equivalent to the aforementioned studies the ^{31}P chemical shift of phosphorus nuclei of both FN and its hydrolysis product PA (PA, $-OCH_3$) were seen to shift on addition of Ag^+ ions, latter attributed to metal co-ordination at the sulfur ligand.

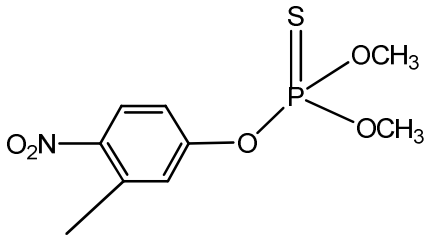

Figure 4.11 Fenitrothion

The ESI-MS results also indicated Ag^+ complexation with FN by the appearance of a set of peaks at 338 and 340 m/z, assigned to FN (231 amu) + Ag^+ (107,109 amu). Ensuing CID experiments on the parent complex revealed Ag^+ co-ordinated PA at m/z 249 (PA (142 amu) + Ag^+ (107 amu)). An interesting observation with FN is the lack of a secondary or auxiliary nitrogen ligand for co-ordination or facilitation of formation of a chelate. Keller et al.[43] also investigated the potential complexation between diazinon and Ag^+ ions by ESI-MS; where they found a similar interaction between the metal ion and the nitrogens of the heterocycle. However no interaction was reported between Ag^+ and the sulfur Lewis site in contrast to the present study.

ESI-MS and ^{31}P NMR studies of Ag complexation have been reported elsewhere. Sekabunga[44] et al. investigated Ag^+ complexation with nitrogen-bridged ligands such as $(C_6H_5)_2PN(H)P(C_6H_5)_2$ (dppa) and $(C_6H_5)_2PN(CH_3)P(C_6H_5)_2$ (dppma). Several complexed species were observed by both ESI-MS and ^{31}P NMR including $Ag_2(\mu\text{-dppa})^{2+}$, $Ag_2(\mu\text{-dppa})_2{}^{2+}$, $Ag_2(\mu\text{-dppa})_3{}^{2+}$, $Ag_2(\mu\text{-dppma})^{2+}$, $Ag_2(\mu\text{-dppma})_2{}^{2+}$, and $Ag(\eta^2\text{-dppma})_2{}^+$. The work showed the ability of Ag^+ ions to chelate, albeit with two nitrogen ligands.

4.3.2 Hg^{2+} binding interpretation

Analogous to Ag^{+}, a set of ^{1}H NMR, ^{31}P NMR and ESI-MS experiments entailing binding and hydrolysis experiments in the presence of Hg^{2+} were carried out as outlined in Section 3. The acceleration of the rate of hydrolysis in the presence of Hg^{2+} is clearly evident in Figure 3.1.34, where complete hydrolysis of the pesticide occurs within 10 minutes against 16 days in the absence of metal ions. This observed acceleration of the rate is evaluated initially in terms of co-ordination to both hydrolysis products, followed by interpretation of complexation with the substrate itself. Both ESI-MS and NMR data are dealt with collectively for clarity.

Similar to Ag^{+}, significant changes in the ^{31}P and ^{1}H chemical environments of PA were observed on the addition of Hg^{2+}, relative to standard ppm shifts (Figure 3.1.10 and 3.1.11). The maximum chemical shift change of 26 ppm observed for a ratio of 5:1 Hg^{2+}/PA was slightly higher than that attained by Ag^{+} co-ordination to PA (25 ppm). The change in chemical environment due to Hg^{2+} interaction was also apparent further along the chain with observed downfield shifts for the $CH_2{}^{b}$ protons of PA. Hg^{2+} ability to co-ordinate PA through the sulfur Lewis site may point to its role in accelerating the rate of hydrolysis owing to its capacity to reduce electron density on the phosphorus atom. Hg^{2+} ability to co-ordinate S is unsurprising due to the "soft" nature of both Lewis site and acid. A plot of chemical shift change (ppm) versus Hg^{2+}/PA ratio shown in Figure 3.1.12 indicates a binding ratio of 1:2, in contrast to a 1:1 binding ratio for Ag^{+}/PA. This conclusion is arrived at from the sharp rise in the chemical shift change up to a ratio of 0.5:1 Hg^{2+}/PA, with subsequent leveling in the chemical shift change at elevated ratios. An important observation is the fact that Hg^{2+} has the same or slightly greater effect on

the phosphorus nuclei of 2 PA as compared to Ag^+ bound to one PA molecule. This may explain the increased rate of hydrolysis of Diazinon in the presence of Hg^{2+} when compared to Ag^+.

A second dissimilarity to Ag^+ in conjunction with binding ratio is the lack of changes in the chemical shifts of PY protons in the presence of Hg^{2+} as shown in Figure 3.1.20. There are no measurable changes in the chemical environment of protons up to a ratio of 1:1 Hg^{2+}/PY, with only small changes at higher ratios particularly when compared to Ag^+ interaction with PY (Figure 3.1.19). This suggests Hg^{2+} co-ordination with nitrogen is weak at best and will not play a role in its catalytic effect. The ESI-MS analysis of Hg^{2+} interaction with PA and PY supports the NMR findings that the cation co-ordinates to the S ligand only. Hg^{2+} affinity for S was shown by the detection of a series of peaks in positive ion mode around m/z ratio 541, exhibiting the isotopic pattern of Hg^{2+}. These set of peaks correspond to 2PA + H (341) + Hg^{2+} (Figure 3.2.20). The assessment of the chemical shifts of PY in the presence of Hg^{2+} shows no observable interaction between the cation and substrate.

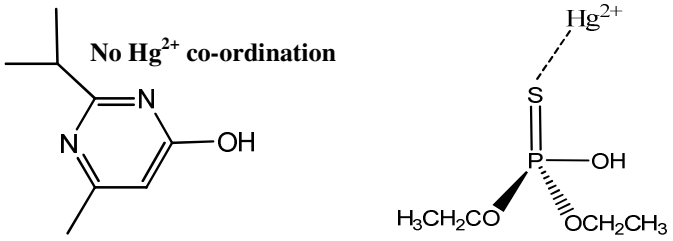

Figure 4.12 Proposed co-ordination of Hg^{2+} to hydrolysis products PA and PY, ensuing from interpretation of NMR and ESI-MS data.

The evaluation of Hg^{2+} interaction with PA and PY point to Hg^{2+} capacity to bind to sulfur. Further evidence for this inference was obtained by carrying out a similar set of

experiments on diazinon in the presence of Hg^{2+}. Surprisingly, only small chemical shift changes were observed in the phosphorus nucleus of diazinon in the presence of Hg^{2+} (see Table 3.1.20), even more apparent when compared to those shifts obtained in the presence of Ag^{+} (Table 3.1.11). Due to the rapid hydrolysis of diazinon in the presence of Hg^{2+} it was difficult to ascertain whether this remarkably reduced effect on the phosphorus nucleus was additionally apparent at higher ratios of Hg^{2+}/D. To remove this obstacle, Hg^{2+} ability to complex diazinon was examined in CD_3OD, with Table 3.1.28 showing the obtained chemical shifts. In support of previous results, little effect was noted on the chemical environment of the phosphorus nucleus in the presence of Hg^{2+}, particularly when compared to the equivalent study for Ag^{+} (Table 3.1.27). Further substantiation of Hg^{2+} reduced interaction with diazinon is the negligible shift in the chemical environment of $CH_2{}^{b}$ protons of diazinon as indicated in Tables 3.1.21 and 3.1.22 (highlighted in bold). Both the $CH_2{}^{b}$ protons and phosphorus are in the vicinity of the sulphur ligand and the small shift changes observed suggest weak interaction of Hg^{2+} with the sulfur ligand of diazinon. This is in contrast to Hg^{2+} capacity to co-ordinate the sulfur of PA with resultant effects on the environment of phosphorus as outlined previously.

Contrasting the minimal observed changes in the environment surrounding sulfur is the chemical shift change of the protons in the vicinity of the nitrogen ligands (see Tables 3.1.21 and 3.1.22). The low affinity of Hg^{2+} for nitrogen as observed in the PY study would suggest that the observed shifts are not a result of Hg^{2+} co-ordination of N, but rather protonation of one of the nitrogens (N3).

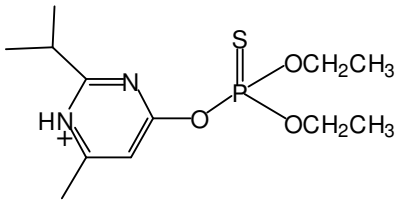

Figure 4.13 Protonated Diazinon

The small shift changes observed at CH_2^b and phosphorus preclude Hg^{2+} binding at S from causing these chemical environment changes at the more distant heterocyclic protons, and bidentate chelation between N and S would have resulted in significant changes in the environment of P and CH_2^b, as observed with Ag^+.

The known affinity of Hg^{2+} for soft Lewis sites such as S is difficult to overcome; however the lack significant chemical environment changes in the vicinity of sulfur certainly indicates weak interaction of Hg^{2+} with sulfur in the unaltered reactant state. The fact remains that the rate of hydrolysis is undoubtedly accelerated in the presence of Hg^{2+} ions. It may therefore be possible that strong binding in the altered transition-state is the basis for the Hg^{2+} ion promoted hydrolysis of diazinon. Evidence for such a suggestion is found in the chemical shifts of the product peaks which clearly show Hg^{2+} bound to PA post hydrolysis (see Table 3.1.16 and Table 3.1.19). The obtained chemical shift of both the phosphorus and CH_2^b protons give excellent agreement with values obtained in the independent analysis of PA in the presence of Hg^{2+}, therefore showing Hg^{2+}-bound PA post hydrolysis.

The NMR data of diazinon in the presence of Hg^{2+} suggests the possibility of a stronger interaction between Hg^{2+} and the transition-state. The negative charge transferred from the incoming nucleophile to the thionate sulfur may be responsible for much stronger

binding of the metal electrophile to the altered transition-state than in the unaltered reactant-state. The ensuing rate increases result from a stabilization of the negatively charge TS, or electrostatic stabilization. Tellingly no complexed ion between Hg^{2+} and diazinon was observed in the ESI-MS study, in contrast to both Ag^{+} and Cu^{2+} ions. The complexed ions observed in ESI-MS between diazinon and the previous metal ions reveal strong binding in the reactant-state; however its absence in the case of Hg^{2+} may further point to preferential transition-state binding over reactant-state. It is important to note nevertheless that Hg^{2+}, particularly in slightly acidic conditions, shows the largest rate acceleration. The fact that the ESI-MS experiments were performed at pH 4 may preclude one from observing such a complex, solely due to the rate of disappearance of such a complex. Such a scenario is evident in Figure 3.2.19 where the diazinon signal at m/z 305 is seen to disappear within 1 min of Hg^{2+} introduction into the ionisation source. Put simply the reactions conditions in the ESI-MS studies may not have permitted one to view the complexed ion.

Although the absence of the complexed ion D-Hg^{2+} in the ESI-MS study can be disputed in terms of reaction conditions, its absence in combination with the small changes in chemical shift observed in the vicinity of the sulfur ligand for both proton and phosphorus nuclei strongly point to a weak interaction of Hg^{2+} with the reactant-state. This points to strong TS binding as a possibility. In either circumstance binding is expected to be through the sulfur ligand, with protonation of heterocyclic nitrogen a further effect in acidic conditions. The overall understanding of Hg^{2+} binding with diazinon and its hydrolysis products is summarized in Table 4.3, with the final proposed

complexation structure arrived at from interpretation of ESI-MS and NMR data shown beneath.

Table 4.3 Interpretation of Hg^{2+} co-ordination with diazinon and its hydrolysis products using NMR and ESI-MS.

Substrate	Ligand	NMR			MS	
		Yes	Weak	No	Yes	No
PA	S	√			√	
PY	N			√		√
D	S		√			√
	N	Protonation				√

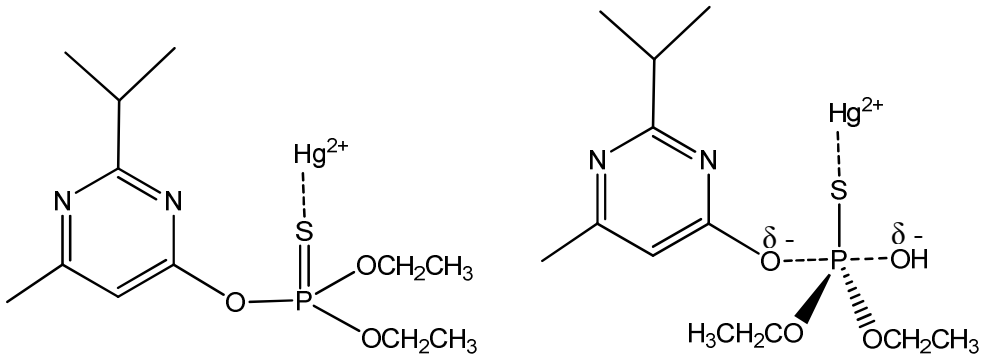

Figure 4.14 Proposed complexation of Hg^{2+} with diazinon. Shows binding both with sulfur in the reactant state and binding in the transition state.

Previous investigations of Hg^{2+} catalysis of organophosphorus pesticides in the Buncel-vanLoon laboratory reported similar observations to diazinon results. Esbata's ESI-MS study of Hg^{2+} complexation with Quinalphos (Figure 4.6) failed to yield the desired complexed ion, however equivalent to results reported here, Hg^{2+} was found to complex with PA at m/z 563 (2PA (340 amu) + Na (22 amu) + Hg (200 amu). Additionally the author did not report any complexation between Hg^{2+} and HQ. No interaction of Hg^{2+} with the nitrogens of HQ was evident lower ratios (up to 0.81 Hg^{2+}/HQ), with small

downfield shifts in the ^{1}H shifts at more elevated ratios of Hg^{2+}/Q. More importantly however are the small changes observed in the ^{31}P chemical shift of Q in the presence of Hg^{2+}. This complements the view in the present study that Hg^{2+} co-ordination with diazinon in the reactant-state is relatively weak, especially when compared against Ag^{+}. Esbata found a similar strong interaction between PA and Hg^{2+} in the NMR investigation reporting a 31.15 ppm shift from the standard ppm at the highest ratio of Hg^{2+}/PA.

Additionally Koo et al.[11] observed large up-field shifts in the ^{31}P signal of PA (O-CH_3) in the presence of increasing concentrations of Hg^{2+}, confirming its ability to complex the sulfur Lewis site and effect its chemical environment. A study by Pehkonen et al. investigated the Hg^{2+} promoted hydrolysis of the organophosphorus pesticide Demeton-S as shown in Figure 4.15.

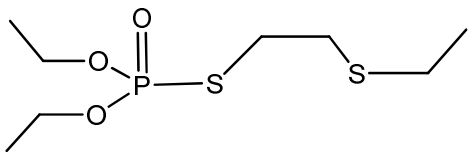

Figure 4.15 Demeton-S

The authors used both ^{1}H and ^{31}P NMR to pinpoint the location of complexation between the metal cation and pesticide. They concluded that Hg^{2+} binds to two sulfur atoms of the side chain of Demeton-S simultaneously, rather than the central P=O. This had the effect of stabilizing the Demeton-S molecule a phenomenon not previously reported for any metal ion-OP system studied (Figure 4.16). The aforementioned studies all point to strong Hg^{2+} interaction with sulfur Lewis site and support the conclusion that the location of co-ordination between the metal cation and diazinon is sulfur.

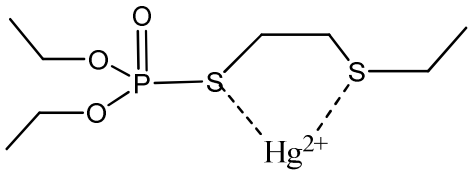

Figure 4.16 Demeton S-Hg complex

4.3.3 Cu^{2+} binding interpretation

A set of ^{1}H NMR, ^{31}P NMR and ESI-MS experiments were carried out on both hydrolysis products and substrate in the presence of Cu^{2+}. The observed acceleration shown in Figure 3.1.37 due to Cu^{2+} complexation was first assessed in terms of co-ordination with hydrolysis products PA and PY. In contrast to previous metals studied copper did not show a continuing up-field shift in the ^{31}P NMR signal of PA with increasing Cu^{2+} concentrations. Instead there is the recurrent appearance of a peak at 23 ppm in combination with a colour change in the NMR solution upon addition of Copper nitrate solution. It is suggested that the colour change indicates a reduction of Cu^{2+} to Cu^{+} either by reaction of the metal cation with PA or with the solvent system in an oxidation reduction process. The appearance of a peak at 23 ppm was also important in terms of identifying hydrolysis products in the presence of Cu^{2+} as reported earlier in the mechanism outline. Significant changes in the chemical shifts of PY protons were observed with the addition of Cu^{2+} ions. Broadening in the ^{1}H signals of PY were noted due to the paramagnetic effect of Cu^{2+}.

NMR analysis of Cu^{2+} interaction with PA and PY is supported by the appearance of certain m/z peaks in the attained ESI-MS spectra. The cations affinity for nitrogen of PY was confirmed by the appearance of a set of peaks at m/z 215, 217 corresponding to PY

(152 amu) + Cu (63/65 amu). Similarly Cu^{2+} interaction with PA was revealed in negative ion mode by the appearance of peaks at m/z 401, 403. These peaks signify 2PA (338 amu) + Cu (63, 65 amu). The above complexed peaks for PY and PA both exhibited the characteristic isotopic ratio of Cu^{2+}, 69:31%. The m/z peaks assigned to complexation of PY and PA by Cu suggests that the metal cation is binding in the +1 oxidation state rather than +2. If PY was complexed with Cu in the +2 state one would expect to see half the m/z observed in the spectrum, as Cu-bound PY would be carrying a +2 charge overall. Correspondingly the negative ion mode analysis of Cu interaction with PA reveals a +1 oxidation state for Cu in the gas phase. One must consider that the two PA's are carrying a negative charge each whilst copper carries +1 oxidation state, leaving the complexed molecule with -1 charge overall. Although Cu^{2+} is known as an 'intermediate' Lewis acid with favorable complexation with nitrogen, the appearance of a +1 oxidation state will certainly facilitate its co-ordination with sulfur as indicated by its complexation with PA. Cu^{+} is a 'softer' cation than its +2 oxidation state. Reduction of Cu^{2+} to Cu^{+} in ESI-MS studies has been reported in several other studies[45, 46, 47, 48].

The assessment of Cu interaction with PA and PY points to its ability to co-ordinate both N and S ligand sites. Confirmation of the proposed ability to co-ordinate both ligand sites was accomplished by running a set of ESI-MS spectra of Cu^{2+} in the presence of diazinon. The appearance of a set of peaks at m/z 367, 369 signifies diazinon (304 amu) + Cu (63/65 amu). Subsequent CID experiments on m/z 367 showed Cu bound at both PY and PA. The m/z at 215 is PY (152 amu) + Cu (63 amu) whilst the m/z at 233 is PA (170 amu) + Cu (63 amu). The m/z values once more indicate Cu bound in the +1 oxidation state. These results are in accord with those obtained in the study of diazinon in the

presence of Ag^{+} and suggest bidentate chelation is the mode of action for copper (Figure 4.17).

Further support for this is found in the ^{31}P NMR, where significant shifts in the phosphorus signal of diazinon are observed in the presence of Cu^{2+} (Table 3.1.26). These ^{31}P shifts are downfield in contrast to the up-field shifts of Ag^{+}-bound diazinon. These shifts however are more significant than those changes observed in the presence of Hg^{2+}.

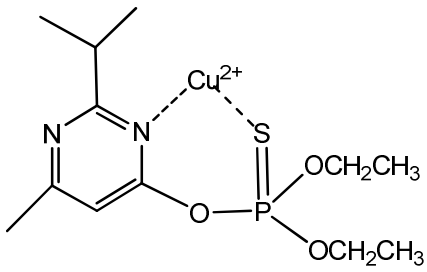

Figure 4.17 Proposed complexation of Cu with diazinon

The overall understanding of Cu^{2+} co-ordination with diazinon and its hydrolysis products is summarized in Table 4.4, with the final proposed complexation structure arrived at from interpretation of ESI-MS and NMR data shown in Figure 4.17.

Table 4.4 Interpretation of Cu^{2+} co-ordination with diazinon and its hydrolysis products using NMR and ESI-MS.

Substrate	Ligand	NMR			MS	
		Yes	Weak	No	Yes	No
PA	S	Reaction			√	
PY	N	√			√	
D	S	√			√	
	N	√			√	

Esbata[37] similarly proposed Cu co-ordination to Quinalphos was through bidentate chelation as shown in Figure 4.18. The author observed the proposed complex between Cu and Q in the ESI-MS study at m/z 361, 363 (Q (298 amu) + Cu (63, 65 amu). The study supports the conclusion that Cu binds in the +1 oxidation state in the gas phase. Subsequent CID experiments on the complex ion revealed Cu^{+} bound to HQ moiety only. Although the ESI-MS study did not show Cu co-ordination with PA, the ^{1}H and ^{31}P NMR analysis of Q and its hydrolysis products in the presence of Cu indicated a weak Cu affinity for S. The author therefore proposed an unsymmetrical bidentate chelate with stronger interaction at N site over S as shown in Figure 4.18.

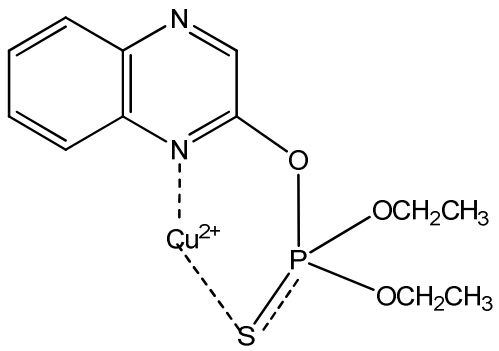

Figure 4.18 Esbata's proposed complexation between Q and Cu^{2+}.

Mortland et al.[49] studied the catalytic hydrolysis of several organic phosphate pesticides by Cu^{2+}, including Diazinon and Dursban. The author suggested that the Cu^{2+} ion promoted hydrolysis of Diazinon and Dursban to be bidentate chelation through nitrogen in the ring structure and sulfur on the phosphate side chain, identical to that proposed in the present study. This has the effect of forming a closed cyclic resonance structure (Figure 4.19), with electron shifts in the proposed ring structure weakening the bonding of the side chain to pyrimidinol, promoting hydrolysis.

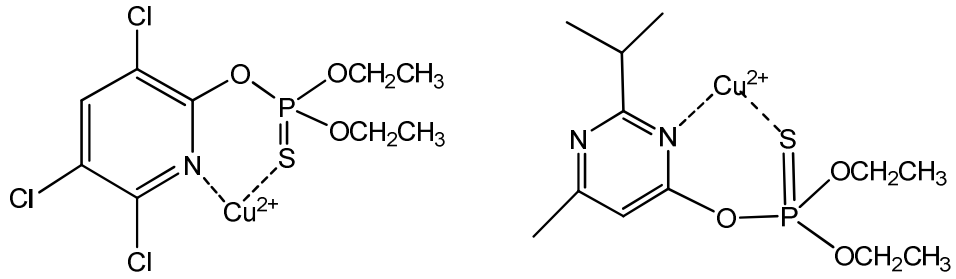

Figure 4.19 Mortland et al.[18] proposed complexation between $Cu^{2+}$and the organophosphorus pesticides Dursban and Diazinon.

Mortland also investigated the pesticides Ronnel and Zytron (Figure 4.20), consisting of chlorinated benzene rings. The hydrolysis of these pesticides was also catalysed by the presence of Cu^{2+} ions but to a much slower extent than observed for Diazinon and Dursban. The slowness in the hydrolysis when compared to Diazinon and Dursban was attributed to different interaction between the pesticides and Cu^{2+}. In the case of Zytron the nitrogen is located for out on the side chain, therefore co-ordination with sulfur and nitrogen will not result in the formation of a six membered ring but rather a four membered. It maybe that catalysis occurs through the four ring bidentate or unidentate co-ordination at nitrogen. Interestingly Ronnel was seen to hydrolyse quicker than Dursban in the presence of Cu^{2+}. Ronnel does not have a nitrogen Lewis site and would indicate that Cu^{2+} can catalyses the hydrolysis through interaction with sulfur alone.

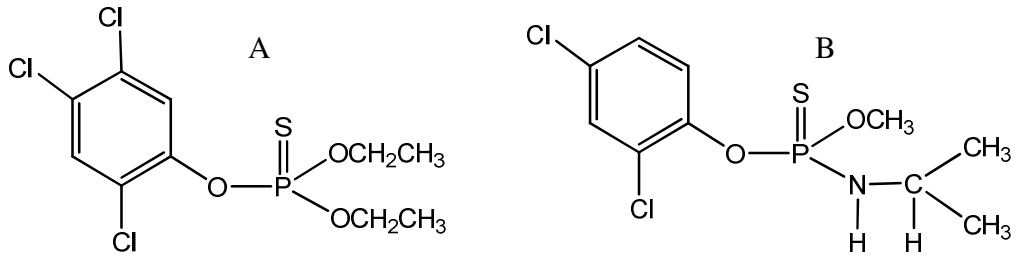

Figure 4.20 Ronnel (A) and Zytron (B).

Martell et al.[50] similarly showed that Cu^{2+} was especially active in such reactions where the possibility of a chelate was present. The author investigated the hydrolysis of Chlorpyrifos in the presence of Cu^{2+} and observed a catalytic effect on the rate of hydrolysis. This was similarly attributed to metal chelation between S and N Lewis sites, with resultant formation of a six membered ring.

A separate study of the Cu^{2+} promoted hydrolysis of Alicarb by Bank et al[51] interestingly proposed complexation through chelation of oxygen and nitrogen, with the resultant formation of β-thioiminiun ion as shown in Figure 4.21. The study suggested that fragmentation rather than hydrolysis is the important decomposition pathway for Alicarb.

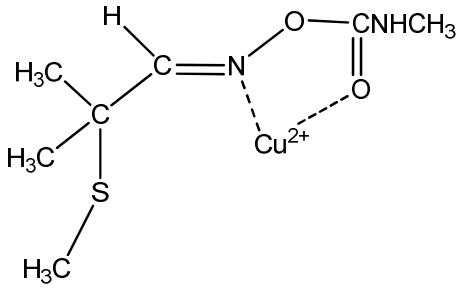

Figure 4.21 Cu^{2+} complexation of Alicarb.

Of more importance however, is the proposed formation of a 5-membered ring between oxygen and nitrogen to promote this decomposition. It must therefore be considered that nitrogen may chelate through oxygen on the side chain rather than the sulfur Lewis site in diazinon (Figure 4.19). Of all the metals investigated in the present study Cu^{2+} is generally considered to be 'harder' than the other metals, as a result making it more likely to interact with oxygen Lewis sites.

4.3.4 Cadmium binding interpretation

Dissimilar to the previous metals studied Cd^{2+} did not significantly accelerate the rate of hydrolysis of diazinon even at very high ratios of Cd^{2+}/D (Figure 3.1.36). Cadmium's ability to bind N and S ligand sites was first assessed in terms of the hydrolysis products PA and PY.

Changes in the ^{31}P and ^{1}H chemical shifts of PA where observed on addition of Cd^{2+} ions (Figure 3.1.14 and 3.1.15), with the changes calculated relative to standard ppm values obtained in the absence of metal ions. The maximum ^{31}P chemical shift change of PA was 11 ppm, observed with a ratio 25:1 Cd^{2+}/PA. These ^{31}P shifts are significantly reduced from those observed in the presence of Ag^{+} and Hg^{2+} and may be a reason for Cd^{2+} reduced catalytic ability. Small shifts where also noted in the $CH_2{}^{b}$ protons belonging to PA, demonstrating that the changes in the chemical shift due to Cd^{2+} co-ordination at sulfur is not significantly felt further along the chain, contrasting Hg^{2+} and Ag^{+}. A plot of chemical shift change (ppm) versus ratio of Cd^{+}/PA shown in Figure 3.1.16 indicates a binding isotherm, suggestive of an equilibrium between bound and unbound Cd^{2+}.

Cd^{2+} affinity for the nitrogens of PY was also investigated with shifts observed for all protons in the presence of Cd^{2+} shown in Figure 3.1.23. These shifts were greater than those obtained in the presence of Hg^{2+} but significantly reduced from that observed with either Cu^{2+} or Ag^{+}. Interestingly the proton most affected by cadmium co-ordination was that of H^{d}, in contrast to H^{c} in the presence of Ag^{+} and Cu^{2+}. This may suggest Cd^{2+} interacting with the ring system rather than either of the nitrogens of the ring. The plot of

chemical shift change (ppm) versus ratio of Cd^{2+}/PY once more depicts a binding isotherm.

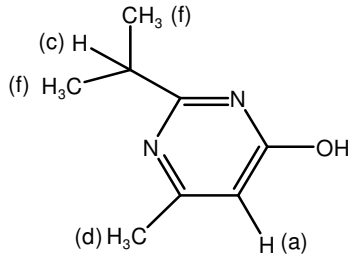

Pyrimidinol (PY)

The minimal effect of Cd^{2+} complexation on rate of hydrolysis of diazinon in attributed to its reduced influence on the chemical environment of neighboring nuclei upon complexation in comparison to the other metals studied. This is evident in the assessment of Cd^{2+} complexation with diazinon in CD_3OD as shown in Figure 3.1.43. Although phosphorus chemical shift changes are observed indicating Cd^{2+} complexation with diazinon, the shifts are small relative to those induced by Ag^{+} or Cu^{2+}. Interestingly they are greater than those induced in the presence of Hg^{2+}, once more indicating stronger co-ordination of Hg^{2+} in the transition-state.

4.4 Rate enhancement due to metal co-ordination

^{31}P, ^{1}H NMR and ESI-MS results provided a valuable insight into the site(s) of co-ordination between metal ions and organophosphorus pesticide diazinon. Such co-ordination data maybe used to explain rate enhancements observed spectrophotometrically in the hydrolysis of diazinon in the presence of metal ions. The rate of hydrolysis of diazinon was studied by following the appearance of PY. The kinetic results show a set of metal ions, Hg^{2+}, Ag^{+}, Cu^{2+} catalyse the hydrolysis of diazinon in the pH range 5.25-7.4, with Cd^{2+} showing a much reduced effect. The metal ions were also found to accelerate the rate in acidic conditions but to a lesser extent. Tables 3.3.10 - 3.3.13 show the obtained k_{metal} and half lifes in the presence Hg^{2+}, Cu^{2+}, Ag^{+} and Cd^{2+} in comparison to a $k_{control}$ values obtained from the pH profile.

Hg^{2+} is found to accelerate the rate of hydrolysis to the greatest extent and most appreciably in the pH range 6.5-6.8. This is in agreement with several other studies where Hg^{2+} was shown to significantly accelerate the rate of hydrolysis of organophosphorus pesticides. Wan et al.[52] reported the accelerated hydrolysis of several organophosphorus pesticides in the presence of $HgCl_2$ (20 mg/l) at pH 5.5. The study found the hydrolysis was typically accelerated by two to three orders of magnitude for pesticides Malathion, Fenitrothion, Fenthion and Parathion methyl (shown in Figure 4.22). The present study found the hydrolysis of diazinon was accelerated by three orders of magnitude in the presence of $HgCl_2$ at pH 6.5-6.8.

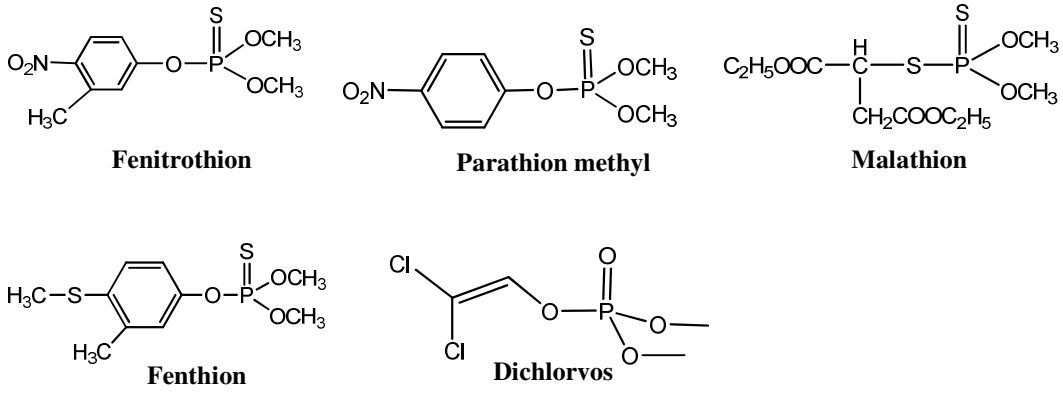

Figure 4.22 Organophosphorus pesticides investigated by Wan et al.[24] in the presence of $HgCl_2$.

Interestingly the author did not observe any acceleration in the rate of hydrolysis of Dichlorvos in the presence of $HgCl_2$. Its structure (Figure 4.22), in contrast to the other pesticides studied, does not contain any sulfur Lewis base sites for interaction with the Hg^{2+}, but rather a 'harder' oxygen Lewis site. The lack of complimentary ligands in Dichlorvos for Hg^{2+} co-ordination, together with the accelerations observed in pesticides containing sulfur, substantiates Hg^{2+} facilitation of the hydrolysis is through S co-ordination. A study by Pehkonen et al.[53] investigated the Hg^{2+} promoted hydrolysis of Demeton-S at pH 5.1-5.4, a pesticide which contains both oxygen and sulfur Lewis sites. Two salts were used in the study namely $HgCl_2$ and $Hg(NO_3)_2$, with the observed rates found to be radically different and largely dependent upon the speciation profile of the metal salts. The authors proposed that $Hg(NO_3)_2$ salt forms a stable complex with the sulfur ligands of Demeton-S consequently slowing the rate of hydrolysis, contrasting the rapid hydrolysis observed in the presence of $HgCl_2$ (pseudo first order rate constant of 0.01 min^{-1}). This study highlights the importance of salts used and their different speciation profiles.

A small pilot NMR study of the mercury promoted hydrolysis of diazinon in the presence of $Hg(NO_3)_2$ was carried out in the present dissertation. The hydrolysis was seen to accelerate even at low ratios of D/Hg^{2+} (0.16) and was attributed to the greater percentage of free Hg^{2+} when compared to the $HgCl_2$ salt. Of even greater significance were the larger ^{31}P chemical shifts observed for the PA product, suggesting Hg^{2+} has a greater influence on the phosphorus nuclei than $Hg(OH)_2$ (dominant species for $HgCl_2$ at pH 6.5-6.8). The general trend for electrophilicity would be;

$$\mathbf{Mn^{n+} \quad Me(OH)^{+} \quad Me(OH)_2}$$

$$\longleftarrow$$

Electrophilicity

The speciation profile of $HgCl_2$ obtained from a study by Zeinali et al.[54], indicates that $Hg(OH)_2$ is the dominant species at pH 6.5-6.8 (Figure 4.23). Other species are present in lesser amounts in the following order; $HgCl_2$> Hg(OH) >HgCl. The rate enhancements observed in the present study at pH 6.5-6.8 suggests that hydroxy species, specifically $Hg(OH)_2$, may play a dominant role in the mercury promoted hydrolysis of diazinon at this pH.

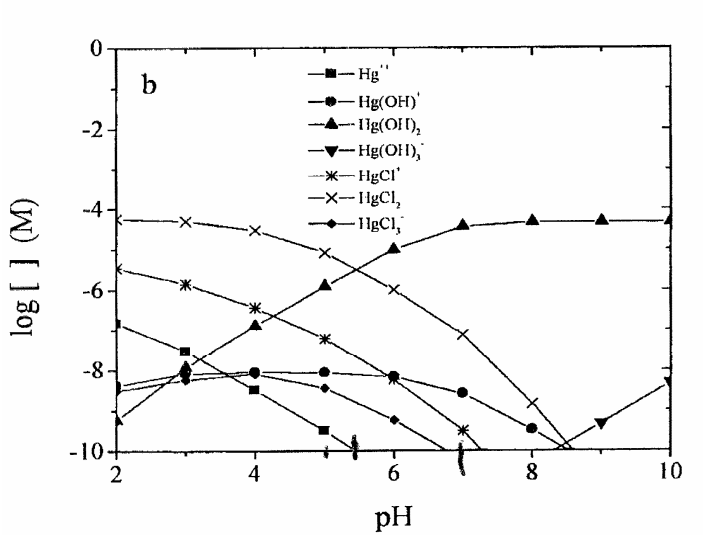

Figure 4.23 Mercury speciation in 10mM $NaNO_3$ of $HgCl_2$

Although rate experiments in the presence of Hg^{2+} in acid showed rate enhancements of ≈ 50 times in comparison to the absence of metal ions, they were not as significant as those observed at pH's 6.5-6.8. This differs from previous results obtained in the vanLoon-Buncel laboratory where Esbata et al. observed significant rate increases in the hydrolysis of Quinalphos in the presence of Hg^{2+} at pH 4. It is noteworthy that the Quinalphos study used $Hg(NO_3)_2$ salt in contrast to $HgCl_2$ employed in the present dissertation. $Hg(NO_3)_2$ is a more labile salt resulting in a greater percent of free Hg^{2+} and $Hg(OH)_2$ ions at pH 4.0, whilst $HgCl_2$ species dominate for the mercuric chloride salt at Ph 4.0. Furthermore a the study by Zeinali et al.[26] investigated the mercury promoted hydrolysis of parathion methyl (Figure 4.22) at pH 3.5-5.5, with reported trends similar to those obtained in the present study. At pH 3.5 the second order rate constant ($k_{(obs)}$) decreased with increasing $HgCl_2$, while at pH 5.5 the rate was seen to increase with increasing $HgCl_2$. The authors attributed this to $HgCl_2$ species been dominant at pH 3.5 and having an inhibitory effect on the mercury promoted hydrolysis of Parathion-methyl. This may be considered a plausible explanation for the reduced enhancement of rate in the presence of $HgCl_2$ at pH 4 in comparison to pH 6.5-6.8 in the present thesis. Protonation of one of the nitrogens (N-3, pKa 2.6[55]) of the ring must also be considered in terms of the rate enhancement observed at pH 4.0. The protonation itself will accelerate the rate of hydrolysis and may be viewed as a competing reaction to mercury promoted hydrolysis (see equations 3 and 4), therefore limiting the effect of metal co-ordination when compared to pH 6.5-6.8.

$$D \underset{}{\overset{H^+}{\rightleftharpoons}} DH^+ \xrightarrow{H_2O} PY + PA \qquad \textbf{(3)}$$

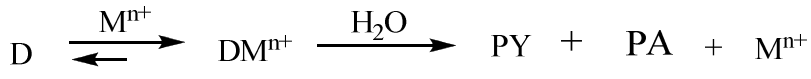

(4)

As previously described in the appraisal of NMR and ESI-MS data, Hg^{2+} co-ordination is proposed to be solely through the sulfur Lewis base site. The data with Hg^{2+} in contrast to Cu^{2+}, Cd^{2+} and Ag^{+} does not suggest binding in the reactant state, but rather strong binding in the transition state with resultant electrostatic stabilization (Figure 4.4). Supporting evidence for such co-ordination is the dominant Lewis acids at pH 6.5 are $Hg(OH)_2$ and $Hg^{+}(OH)$ (see Figure 4.23). Although $HgCl_2$ is the most prevalent species at pH 4.0, it would not be expected to participate as an electrophile in the reaction as indicated by Zeinali et al.[26]. As shown below hydroxy species are weaker electrophiles than Hg^{2+} and may require the developing negative charge on the sulfur ligand in the altered transition state to facilitate much stronger binding of the metal electrophile. A second possibility is $Hg(OH)_2$ coordination in the reactant state followed by intramolecular attack as depicted in Scheme 4.4.

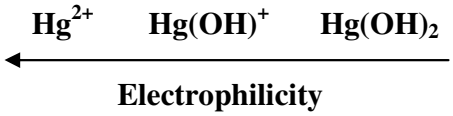

Cu^{2+} was shown to accelerate the hydrolysis of diazinon especially at pH 5.0-5.25, where a 960 fold increase in the k_{obs} was observed at 25:1 Cu^{2+}/D. Several authors have previously reported Cu^{2+} promoted hydrolysis of organophosphorus pesticides under similar pH conditions. Esbata et al. found Cu^{2+} accelerated the rate of hydrolysis of Quinalphos by a factor of 140 at pH 7.0. Smolen et al.[56] also investigated the metal ion catalyzed hydrolysis of several phosphorothionate ester pesticides including Chloropyrifos methyl, Zinolphos, parathion methyl, Ronnel and Diazinon. The author

investigated the catalytic ability of several divalent transition metal cations including Cu^{2+}, with 1.0 mM Cu^{2+} yielding significant rate increase in the hydrolysis of all five thionate pesticides. Interestingly the maximum increase in k_{obs} was observed at slightly acidic pH values, analogous to pH conditions for Cu^{2+} promoted hydrolysis of diazinon in the present study. Mortland et al.[57] also studied the Cu^{2+} promoted hydrolysis of diazinon in the pH range 5-6 using $CuCl_2$ as salt, observing a significant rate enhancement with an estimated half life of 4 hrs. The half life is less than that determined in the present study of 82.5 min; however this may be attributed to the authors use of $Cu(Cl)_2$ versus $Cu(NO_3)_2$ used in the present study , further highlighting the significance of the salt and its speciation profile. Mortland concluded that Cu^{2+} catalyses the rate through formation of a chelate as shown in Figure 4.24, suggesting $Cu(OH)_2$ to be the coordinating electrophile.

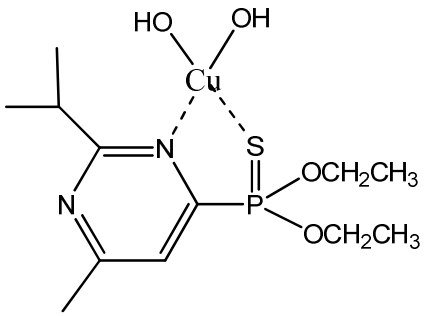

Figure 4.24 Proposed chelate for the Cu^{2+} promoted hydrolysis of diazinon by Mortland et al

An analogous chelate is proposed for Cu^{2+} co-ordination to diazinon in the present study; however the Lewis acid is likely free Cu^{2+} over the hydroxy form. This conclusion is arrived at from the speciation profile of $Cu(NO_3)_2$ (Figure 4.3), which indicates that copper will be in the Cu^{2+} form at the pH's under consideration (pH 4-5.25).

Cu^{2+} was also seen to accelerate the rate at pH 4 but to a much lesser extent than that observed at pH 5.0-5.25. Analogous to Hg^{2+} results, the slowing in the rate of acceleration maybe be explained by a competing reaction of protonation at one of the nitrogens of the ring (acid catalysis). Protonation of diazinon would be expected to occur at the N-3 position, as this nitrogen has the higher pKa (2.6)[27]. The positive charge on the nitrogen will pull electron density towards it, making the phosphorus more prone to nucleophilic attack. The two competing reactions are outlined in equations 3 and 4 (page 43).

$pK_a = 2.6$[27]

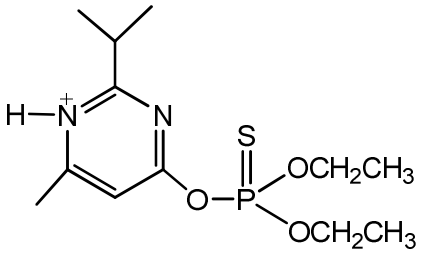

Of even more importance is that protonation at the N-3 position with resultant electron withdrawing effects may substantially lower the basicity of the N-1 nitrogen making it an unlikely participant in chelate ring formation. This lack of an auxiliary ligand upon protonation of the N-3 nitrogen may hinder the catalytic ability of Cu^{2+}, whose metal promoted hydrolysis of diazinon is proposed through the formation of a 6 membered ring. This is also strong evidence that the accelerated rate at pH 5.0-5.25 is due to chelate ring formation.

The ESI-MS and NMR data as described in Section 4.3.3 support the conclusion that Cu^{2+} promoted hydrolysis of diazinon is through the formation of a six membered ring as shown in Figure 4.17. Martell et al.[58] has shown that Cu^{2+} is especially active in reactions where a chelate was present and several papers have shown that chelate formation with

divalent metal ions is particularly favorable when the chelating atoms are four atoms apart[59, 60, 61]. This is the case with the proposed co-ordination between Cu^{2+} and diazinon. Scheme 4.7 shows the hydrolysis of diazinon in the presence of Cu^{2+}, including strong binding in the reactant state followed by nucleophilic attack of H_2O (the expected nucleophile under the stated pH conditions). Also shown is the energy co-ordinate diagram for such a reaction.

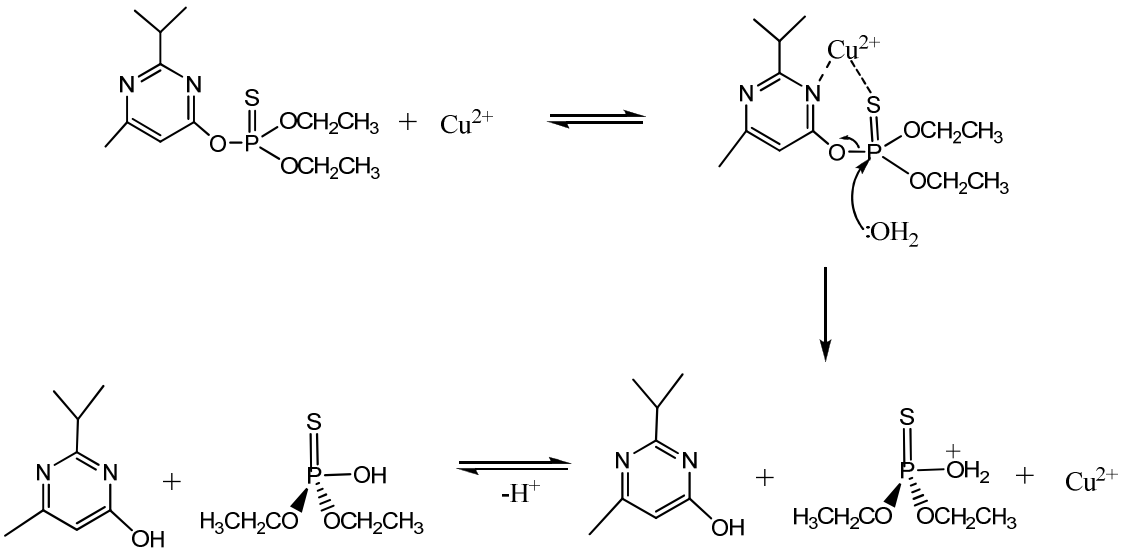

Scheme 4.7 Hydrolysis of diazinon in the presence of Cu^{2+}

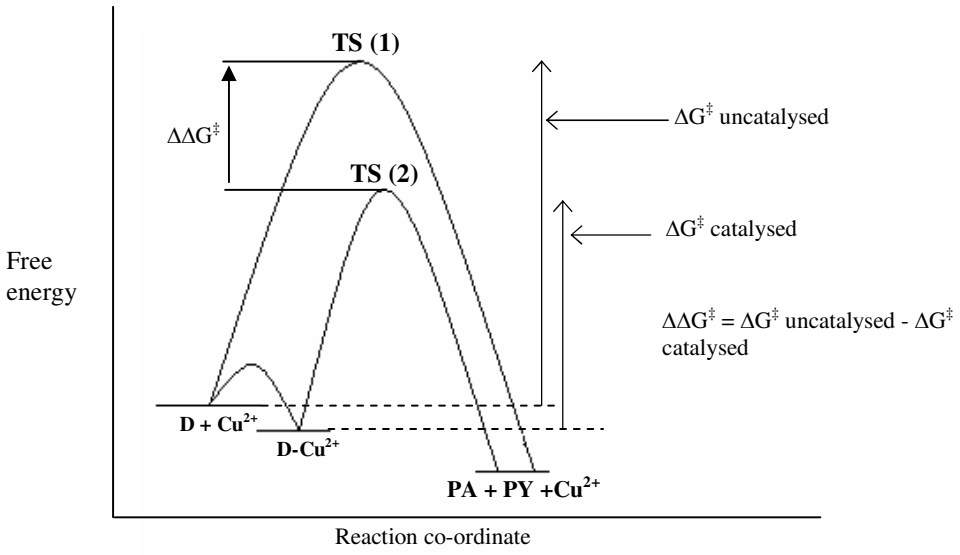

Figure 4.25 Reaction coordinate diagram for catalysed versus uncatalysed hydrolysis of diazinon in the presence of Cu^{2+}

A competing reaction may also occur at pH 4.0 involving protonation at N-3. The mechanism for such a reaction is shown in Scheme 4.8.

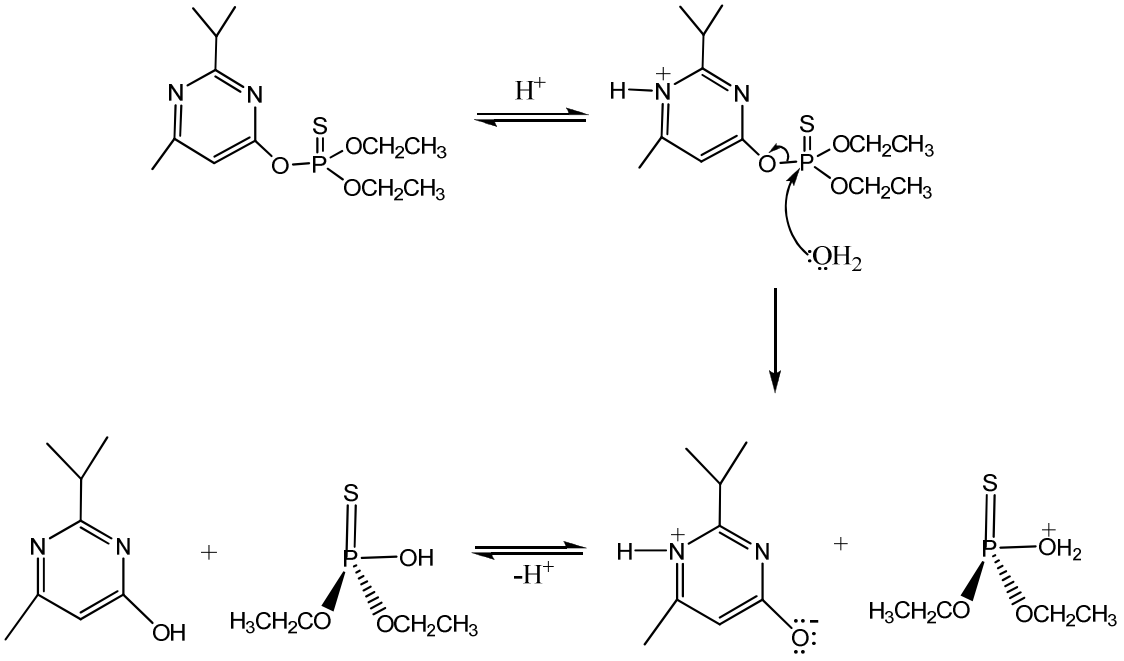

Scheme 4.8 Acid catalysed hydrolysis of diazinon with attack at phosphorus (S_N2 (P))

Analogous to Cu^{2+}, Ag^{+} was seen to significantly promote the rate of hydrolysis of diazinon. This was most apparent at pH 7.15-7.4, where a 540 fold increase in the rate of hydrolysis of diazinon was observed in the presence of Ag^{+}. Esbata et al[9]. found a comparable effect with Quinalphos, observing a 420 fold increase in the rate of hydrolysis in the presence of Ag^{+}. The Ag^{+} ion promoted hydrolysis like Cu^{2+}, is attributed to the formation of a six-membered ring. This conclusion is arrived at from interpretation of both ESI-MS and NMR data of diazinon and its hydrolysis products in the presence of Ag^{+} as described earlier in Section 4.3.1. The speciation profile for Ag^{+}

(Figure 4.1) would indicate that free Ag^+ ions are coordinating the diazinon molecule at the pH's under consideration. Scheme 4.9 shows the hydrolysis of diazinon in the presence of Ag^+ ions with the energy co-ordinate diagram shown beneath.

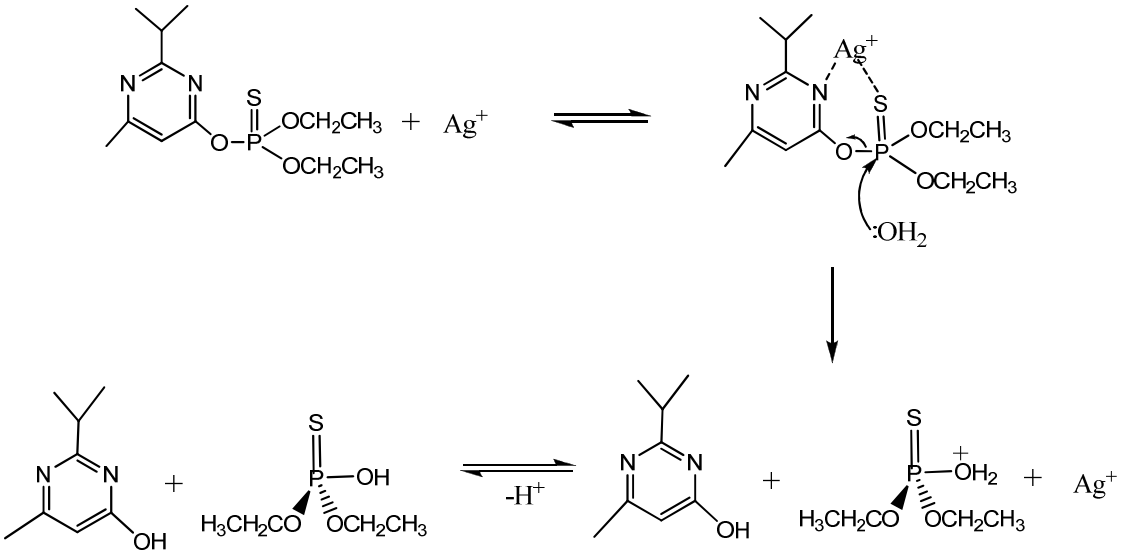

Scheme 4.9 Hydrolysis of diazinon in the presence of Cu^{2+}

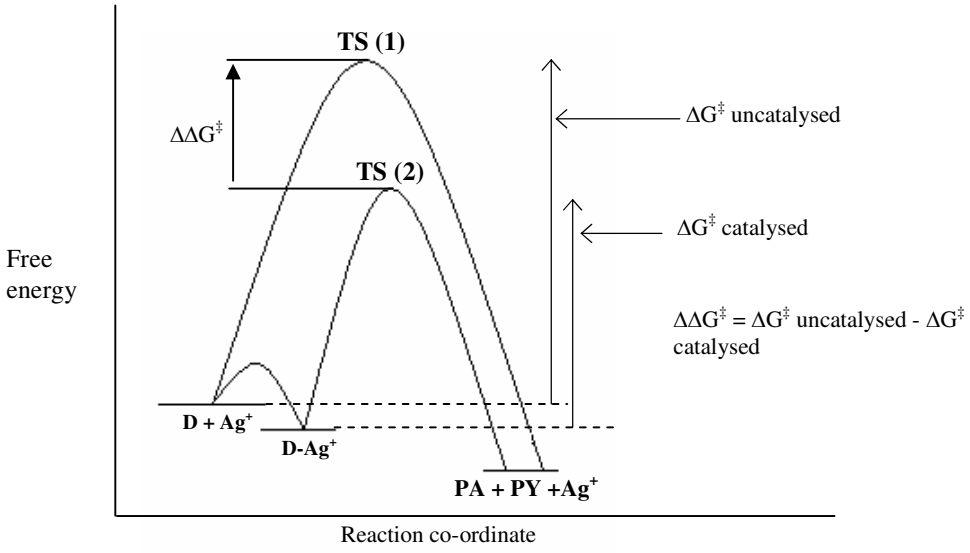

Figure 4.26 Reaction coordinate diagram for catalysed versus uncatalysed hydrolysis of diazinon in the presence of Ag^+

Although Ag^{+} is seen to accelerate the rate of hydrolysis of diazinon at pH 4.0, the acceleration is less than that observed at pH 7.15-7.4. This, as in the case of Cu^{2+}, is attributed to a competing reaction involving protonation at the N-3 nitrogen (Scheme 4.8). This competing reaction as described previously decreases the basicity of the N-1 nitrogen, with the result of possibly hindering the formation of a six-membered ring between diazinon and Ag^{+}.

CHAPTER 5 Conclusion

The rate of hydrolysis of diazinon has been studied under various conditions; specifically focusing on the effect dissolved metal ions on the rate of hydrolysis both in acid and basic media. Several postulates have been put forward as to the mechanism of metal-ion promoted hydrolysis, most involving coordination of metal cation to the organophosphorus pesticides through Lewis base sites. Two broad methods were employed to probe the different interactions between metal ions and diazinon including ^{1}H and ^{31}P NMR and ESI-MS. The effect of such coordination on the rate of hydrolysis of diazinon was followed spectrophotometrically by monitoring the appearance of PY (Shown in Scheme 5.1). The following sections will present the important findings in each area.

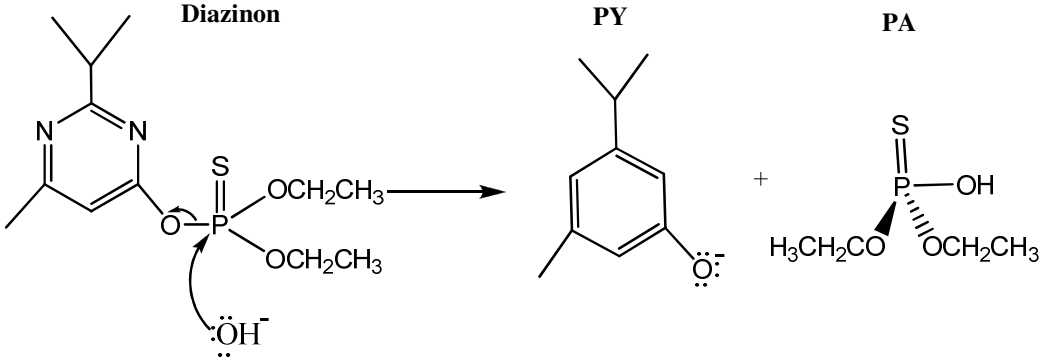

Scheme 5.1 Hydrolysis of diazinon (S_N2 (P))

5.1 NMR studies

In order to try and pinpoint the different interactions between the various metal ions and the substrate, particularly in coordinating to Lewis sites, solution phase NMR was employed. ^{1}H and ^{31}P NMR spectra of diazinon, PA and ^{1}H NMR of PY, were obtained

in the presence of increasing concentrations of metal cations including Hg^{2+}, Cu^{2+}, Cd^{2+} and Ag^{+}. This gave vital information about the ability of the metal ions to complex to N, S, or possibly both Lewis base sites, by observing any changes in the chemical shift (ppm) of proton and phosphorus nuclei in the vicinity of the Lewis base sites, relative to the chemical shifts in the absence of metal ions. Any changes in the ^{1}H or ^{31}P chemical shift (ppm) may provide evidence of metal binding at specific ligands, with resultant effect on the chemical environment of surrounding nuclei. In the case of PA significant shifts were observed both in the ^{31}P and ^{1}H signals ($CH_2{}^{b}$) with increasing Hg^{2+}, Cd^{2+} and Ag^{+} concentrations. The observed change in chemical shifts relative to standard values was in the order $Hg^{2+} > Ag^{+} > Cd^{2+}$. Contrasting this was PA in presence of Cu^{2+} which showed the appearance of a peak at 23 ppm in combination with a solution colour change. Its is suggested that the colour change indicates a reduction of Cu^{2+} to Cu^{+} in an oxidation-reduction type process.

Analogous experiments were performed on PY in the presence of metal ions, to examine the different metal's affinity for nitrogen. Downfield changes in the chemical shift of PY protons were observed in the presence of Cu^{2+}, Ag^{+} and Cd^{2+}, suggestive of their ability to coordinate nitrogen Lewis sites. The observed changes relative to standard chemical shifts was in the order $Cu^{2+} > Ag^{+} > Cd^{2+}$. Contrasting this was PY in the presence of Hg^{2+}, where little effect on the ^{1}H chemical shifts was observed, indicating Hg^{2+} has weak affinity for nitrogen Lewis sites.

The proposed binding with PA and PY was further assessed in terms of coordination to diazinon by performing a set of experiments at different M^{n+}/D ratios (hydrolysis

experiments). Considerable changes in the chemical shifts of nuclei of diazinon in the vicinity of nitrogen and sulfur Lewis sites were observed in the presence of both Ag^{2+} and Cu^{2+}, and to a lesser extent Cd^{2+}. In the presence of Hg^{2+} surprisingly, no significant change in the chemical shift of the phosphorus nucleus was observed. This contrasts with the large upfield shifts noted in the position of the phosphorus nucleus of PA in the presence of Hg^{2+}. Downfield shifts where observed, however, in the position of protons in the vicinity of nitrogen, attributed to protonation at one of the nitrogens rather than Hg^{2+} complexation.

The prominent lack of NMR evidence of Hg^{2+} coordination to diazinon at the sulfur Lewis site is considered in terms of;

1) Preferential binding of mercury to the altered transition state. This can be explained by the prevalence of the weaker Lewis acid $Hg(OH)_2$ at pH 6.5-6.8, which may favorably coordinate the partially negative sulfur of the transition state.

2) Equally, the dominance of $Hg(OH)_2$ may have a reduced effect on the phosphorus nuclei upon sulfur complexation in comparison to free metal ions such as Hg^{2+}, Ag^{+} and Cu^{2+}. The rate is presumably accelerated due to facilitation of intramolecular OH attack, a push-pull mechanism often used to explain such rate enhancements.

Evidence contradicting such a proposal is the large shifts experience by the phosphorus nuclei of PA upon coordination of mercury, presumably in the $Hg(OH)_2$ form. Finally the NMR hydrolysis experiments also showed metal-ion promoted hydrolysis of diazinon in the cases of Hg^{2+}, Cu^{2+} and Ag^{+}, with a reduced effect with Cd^{2+}.

5.2 ESI-MS studies

To further substantiate the proposed binding emanating from NMR studies, Electrospray Ionisation-mass spectrometry experiments were performed on diazinon and its hydrolysis products (PY and PA) in the presence of Hg^{2+}, Cu^{2+} and Ag^{+}. In the case of both Cu^{2+} and Ag^{+}, complexation between D and the metal ions was observed at specific m/z ratios. These peaks are readily identifiable by the appearance of isotopic patterns pertaining to the metal ions. Isolation and further fragmentation of the complexed ions using MS/MS, showed Cu^{2+} and Ag^{+} binding to nitrogen and sulfur Lewis base sites (i.e. PA and PY). The fact that these m/z ratios originate from the complexed ion ($D\text{-}M^{n+}$) gives definitive structural information on the sites of metal complexation in diazinon. Furthermore it is strong evidence that Cu^{2+} and Ag^{+} form a chelate with diazinon through co-ordination at N and S, with the formation of a 6-membered ring. Further substantiation of Cu^{2+} and Ag^{+} facility to bind both N and S was established by observing the formation of complexes between the metal ions and hydrolysis products PA and PY. Contrasting behavior was seen with Hg^{2+}, where no complexation between diazinon and Hg^{2+} was observed. This lack of binding, as in the NMR study, is possibly due to stronger binding of Hg^{2+} to the altered transition state than the reactant state. The observed rapid hydrolysis of diazinon may also have precluded one from viewing such a complex. The analysis of PA in the presence of Hg^{2+} did, however, show the formation of a PA-Hg^{2+} complex, indicating that Hg^{2+} ion promoted hydrolysis of Diazinon through co-ordination at the sulfur Lewis site.

5.3 Hydrolysis of diazinon in the presence of metal ions

Using UV-vis spectrophotometry, hydrolysis of diazinon was studied in the presence of metal ions to determine the effects the aforementioned co-ordination has on the rate of hydrolysis. Addition of each metal ion was seen to significantly promote the rate of hydrolysis of diazinon, in addition to varying the pH of the solution presumably due to metal speciation. The metal ion promoted hydrolysis was seen to be most significant in neutral to slightly acidic conditions, when compared to a $k_{control}$ values obtained from the pH rate profile for diazinon. The observed increases were most significant with Hg^{2+} (2400 fold) followed by Cu^{2+} (960 fold) then Ag^{+} (540 fold). Rate enhancements where also observed in acidic conditions but to a much lesser extent. This was attributed to a number of factors including; (1) A competing acid hydrolysis reaction involving protonation at the N-3, (2) In the case of mercury the dominant nature of the $HgCl_2$ species at this pH.

5.4 Summary

Overall, the objectives of the study as outlined in Section 1.7 were met successfully. The co-ordination of several metal ions to diazinon was examined using ^{1}H, ^{31}P NMR and ESI-MS. The proposed binding of Cu^{2+} and Ag^{+} to diazinon is through chelation, with simultaneous coordination at both nitrogen and sulfur Lewis base sites. In contrast to Cu^{2+} and Ag^{+}, the Hg^{2+} ion promoted hydrolysis of diazinon is proposed to occur through coordination at sulfur alone. The accelerated hydrolysis with Hg^{2+} may result from speciation, with preferential coordination of specific Hg species to the altered transition state, with resultant electrostatic stabilization. The rate may equally be accelerated via

facilitation of OH intramolecular attack due to the prevalence of $Hg(OH)^+$ and $Hg(OH)_2$. The effect of coordination of the selected metals to diazinon was then examined kinetically. A significantly increases in the rate of hydrolysis of diazinon was observed especially in neutral to slightly acidic conditions.

REFERENCES

[1] Pehkonen, S. O.; Zhang, Qi. The degradation of Organophosphorus pesticides in natural waters: A critical review. Critical Reviews in Environmental Science and Technology. 32(1), 17-72, 2002.

[2] Lewis, Regenstein. America the Poisoned (Washington, DC: Acropolis Books, 1982), 103.

[3] Plimmer, J. r. Kreiger R. Handbook of pesticide toxicology. Academic Press, London. Vol.2, 2nd edition, 2001.

[4] Chambers, H. W.; Boone, S. J.; Carr, R. L.; Chambers, J. E. Kreiger R. Handbook of pesticide toxicology. Academic Press, London, Vol.2, 2nd edition, 2001.

[5] Dong, R. A.; Chang, W. H. Photoassisted titanium dioxide mediated degradation of organophosphorus pesticides with hydrogen peroxide. *J. Photochem. Photobiol*, *A-Chem*, **107**, 239-244, 1997.

[6] Hasegawa, K.; Kanbara, T.; Kagaya, S. Photocatalysed degradation of agrochemicals in TiO_2 aqueous suspensions. *Denki Kagaku*, **66**, 625-634, 1998.

[7] Mak, M. K.; Hung, S. T. Degradation of neat and commercial samples of organophosphorus pesticides in illuminated TiO_2 suspensions. Toxicol. Environ. Chem, **36**, 155-168, 1992.

[8] Dong, R. A.; Chang, W. H. Photoassisted iron compound catalytic degradation of organophosphorus pesticides with hydrogen peroxide. *Chemosphere,* **37,** 2563-2572, 1998.

[9] Schwarzenbach, R. P.; Gschwend, P. M.; Imboden, D. M. Environmental Organic Chemistry, John Wiley and Sons, New York, 2003.

[10] Pedia, D. C.; M.Sc. Thesis. Queen's University, Kingston, Ont., 2001.

[11] Churchill, D.; Dust, J. M.; Buncel, E. Concerted rate limiting proton transfer to sulfur with nucleophilic attack at the phosphorus-A new proposed mechanism for hydrolytic decomposition of the P=S pesticide, Diazinon, in moderately sulfuric acid media. Can. J. Chem. 85, 421-431 , 2007.

[12] Noblet, J. A.; Smith, L. A.; Suffet, I. H. Influence of natural dissolved organic matter, temperature, and mixing on the abiotic hydrolysis of Triazine and organophosphorus pesticides.

[13] Michel, F. C.; Reddy, C. A.; Forney, L. J. Fate of carbon-14 Diazinon during the composting of yard trimmings. *J. Environ. Qual*, **26**, 200-205, 1997.

[14] Pudovik, A. N. Chemistry of phosphorus compounds. MIR publishers, Moscow, 1989.

[15] Kirby, A. J.; Warren, S. G. The organic chemistry of phosphorus. Elsevier, Amsterdam, 1967.

[16] Thatcher, G. R. J.; Kluger, R. Advances in physical organic chemistry. D. Bethel, ed., Academic press, London, Vol. 25, 1989.

[17] Balakrishnan, V. K. M.Sc. Thesis. Queen's University, Kingston, Ont., 1996.

[18] Miyata, Y.; Talakahashi, Y; Ando, H. Analysis of organophosphorus pesticides using FT-NMR. Kagaku Keisatsu Kenkyusho Hokoku, Hokagaku-hen. 1988, 41, 159; Chem. Abstr. 1989, 111, 92231n.

[19] Ross, R. T.; Biros, F. J. Correlations between ^{31}P NMR Chemical Shifts and structures of some Organophosphorus Pesticides. *Anal. Chim. Acta,* 1970, 52, 139.

[20] Babad H. *Anal. Chim. Acta*, 1968, 41, 259-268.

[21] Keith, Lawrence H.; Garrison, Arthur W.; Alford, Ann L. Journal - Association of Official Analytical Chemists (1968), 51(5), 1063-94.

[22] Esbata, Abdelhamid Abdalla. Homogeneous and heterogeneous catalysis of the hydrolysis of the organophosphorothioate compound, quinalphos. (2005), 267 pp. CAN 143:401121 AN 2005:1184223 CAPLUS

[23] Barr, J. D.; Bell, A. J.; Bird, J. L.; Murrell, J.; Timperley, C. M.; Watts, P. Fragmentations and Reactions of the Organophosphate Insecticide Diazinon and its oxygen Analog Diazoxon Studied by Electrospray Ionisation Ion Trap Mass Spectrometry. J Am Soc Mass Spectrom, 16, 515-523, 2005.

[24] Keller et al.; Proceedings of the 52nd ASMS Conference on Mass Spectrometry and Allied Topics, Nashville, Tennessee, May 23-27, 2004. Low energy CID MS/MS of transition metal-organophosphorus pesticide complexes.

[25] Barr. J. D. Fragmentations and reactions of some istotopically labeled dimethyl methylphosphono and trimethyl phosphoro thiolates and thionates studied by Electrospray ionisation ion trap mass spectrometry, unpublished.

[26] Weast. R. C. Handbook of Chemistry and Physics. 50th Edition, The Chemical Rubber Co., Cleveland, Ohio, 1969.

[27] Rochester. C. H. Acidity functions. Academic Press, New York, 1970.

[28] Chapman. R. A. Cole. C. M. J. Environ. Sci. Technol. B17, 487, 1982.

[29] Smolen, J. M.; Stone, A. T. Divalent metal ion-catalyzed hydrolysis of phosphorothioate ester pesticides and their corresponding oxonates. Environ. Sci. Technol, 1997, 31, 1664-1673.

[30] Hendry, P.: Sargeson, A. M. Metal ion promoted reactions of phosphate derivitives. In progress in Inorganic Chemistry: Bioinorganic Chemistry; Lippard, S. J., Ed.; Wiley Interscience: New York, 1990; Vol 38, pp 201-258.

[31] Cram, D. J.; Lehn, J. M. J. Am. Chem. Soc, 1985, 107, 3657.

[32] Pearson, R. G. Chem. Br. 1967, 3, 103.

[33] Scwarzenbach, G. Relationships between metal complex stability and the structure of complexing agents. Helv. Chim. Acta. 1952, 35, 2344.

[34] Baes, B. F.; Mesmer, R. E. The hydrolysis of cations. Wiley-Interscience, New York, 1976.

[35] Burgess, J. Metal ions in solution. Wiley, New York, 1978, 264-266.

[36] Paulson, A. J.; Kester, D. R. Copper (11) Ion Hydrolysis in aqueous solution. Journal of Solution Chemistry, 1980, 9(4), 269-77.

[37] Esbata, A. A.; M.Sc. Thesis. Queen's University, Kingston, Ont., 2004.

[38] Bjerrum, J.; Schwarzenbach, G.; Sillen, L. G. Stability constants of metal ion-complexes, with solubility products of inorganic substances, IUPAC, London, 1958.

[39] Bruice, T. C.; Benkovic, S. J. Biochemistry, 39, 6267, 2000.

[40] Wolfenden, R.; Acc. Chem. Res. Vol. 5, 10, 1972.

[41] Erfremenko, E. N.; Sergeeva, V. S. Organophosphate hydrolase- an enzyme catlyzing degradation of phosphorus-containing toxins and pesticides. Russian Chemical Bulletin, vol. 50, 1826-1832, 2001.

[42] Koo, I.; Unpublished work. Queen's University, Kingston, Ont., 2007.

[43] Keller et al.; Proceedings of the 52nd ASMS Conference on Mass Spectrometry and Allied Topics, Nashville, Tennessee, May 23-27, 2004. Low energy CID MS/MS of transition metal-organophosphorus pesticide complexes.

[44] Sekabunga, E. J.; Smith, Michele L.; Webb, T. R.; Hill, W. E. Coordination Chemistry of Silver(I) with the Nitrogen-Bridged Ligands (C6H5)2PN(H)P(C6H5)2 and (C6H5)2PN(CH3)P(C6H5)2: The Effect of Alkylating the Nitrogen Bridge on Ligand Bridging versus Chelating Behavior. Inorganic Chemistry (2002), 41(5), 1205-1214.

[45] Gianelli L.; Amendola V.; Fabbrizzi L.; Pallavicini.; Mellerio G.G. Rapid Commun. Mass Spectrom. 15, 2347 2001.

[46] Seto, C.; Stone, J. A. J. Mass Spectrom. Ion processes. 175, 263, 1998.

[47] Gatlin, C. L.; Turecek, F.; Vaiser, T. J. Anal. Chem. 6, 3950, 1994.

[48] Gatlin, C, L.; Turecek, F.; Vaisar, T. J. Mas. Spectrom. 30, 1617, 1995.

[49] Mortland, M. M.; Raman, K. V.; Catalytic Hydrolysis of Some Organic Phosphate Pesticides by Copper(11). J. Agr. Food Chem. Vol 15, No. 1, Jan-Feb, 1967.

[50] Martell, A, E.; Chaberek, S.; Courtney, R, C.; Westerback, S.; Hyytiainen, H. Ibid, 79, 3036, 1957.

[51] Bank, S.; Tyrell, J, r. Cu^{2+}-Promoted Aqueous Decomposition of Alicarb. J. Org. Chem. 50, 4938-4943, 1985.

[52] Wan, H. B.; Wong, M. K.; Mok, C. Y. Pesticide Science. 42, 93, 1994.

[53] Pehkonene, S. O.; Zaher, M.; Judah, A. Mechanism of Interactions between Hg^{2+} and Demeton S: an NMR Study. *Environ. Sci. Technol*. 39, 2586-2591, 2005.

[54] Zeinali, M.; Torrents, A. Mercury-Promoted Hydrolysis of Parathion-methyl: Effect of Chloride and Hydrated Species. *Environ. Sci. Technol*. *32*, 2338-2342, 1998.

[55] Zweig, G. Analytical Methods for Pesticides, Plant Growth Regulators and Food Additives. Academic Press, Vol. 2, New York, 1964.

[56] Smolen, M. J.; Stone, A. T. Divalent Metal Ion-Catalyzed Hydrolysis of Phosphorothionate Ester Pesticides and Their Corresponding Oxonates. *Environ. Sci. Techno*. *31*, 1664-1673, 1997.

[57] Mortland, M. M.; Raman, K. V. Catalytic Hydrolysis of Some Organic Phosphate Pesticides by $Copper^{2+}$. J. Agr. FOOD. CHEM. Vol. 15, NO 1, JAN.-FEB., 1967.

[58] Martell, A. E.; Chaberek, S.; Courtney, R. C.; Westerback, S.; Hyytiainen, H. *Ibid*. **79**, 3036, 1957.

[59] Fife, T. H.; Squillacote, V. L. *J. Am. Chem. Soc*. *100*, 4787, 1978.

[60] Fife, T. H.; Przystas, T. V.; Squillacote, V. L. *J. Am. Chem. Soc*. *101*, 3017, 1979.

[61] Suh, J.; Lee. E.; Jang, E. S. Inorg. Chem. 20, 1981.

Appendix 1

Identification and characterisation of Diazinon and O,O diethyl phosphorothioic acid.

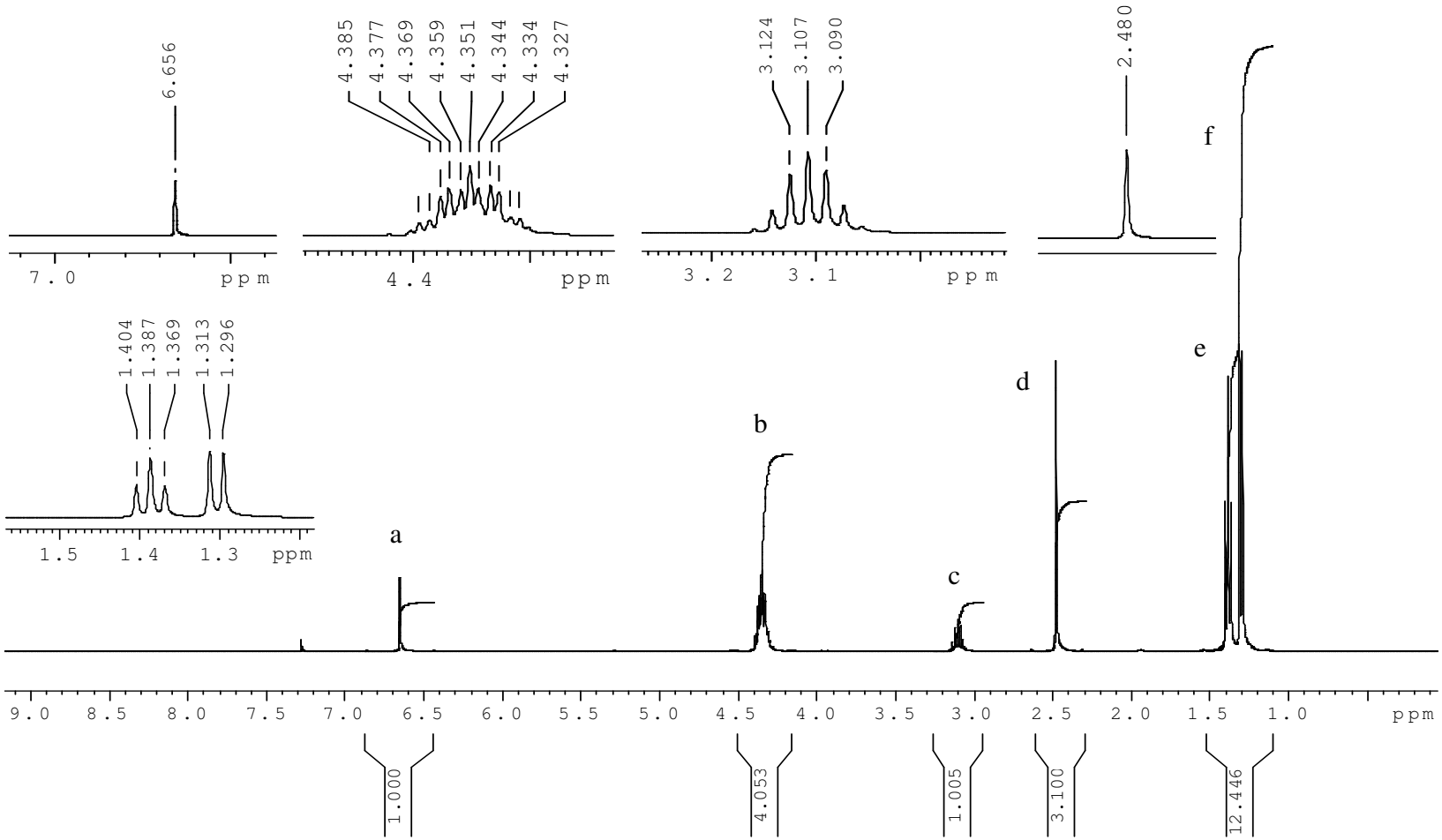

Figure A1.1 ^{1}H NMR of Diazinon in $CDCl_3$ (400 MHz)

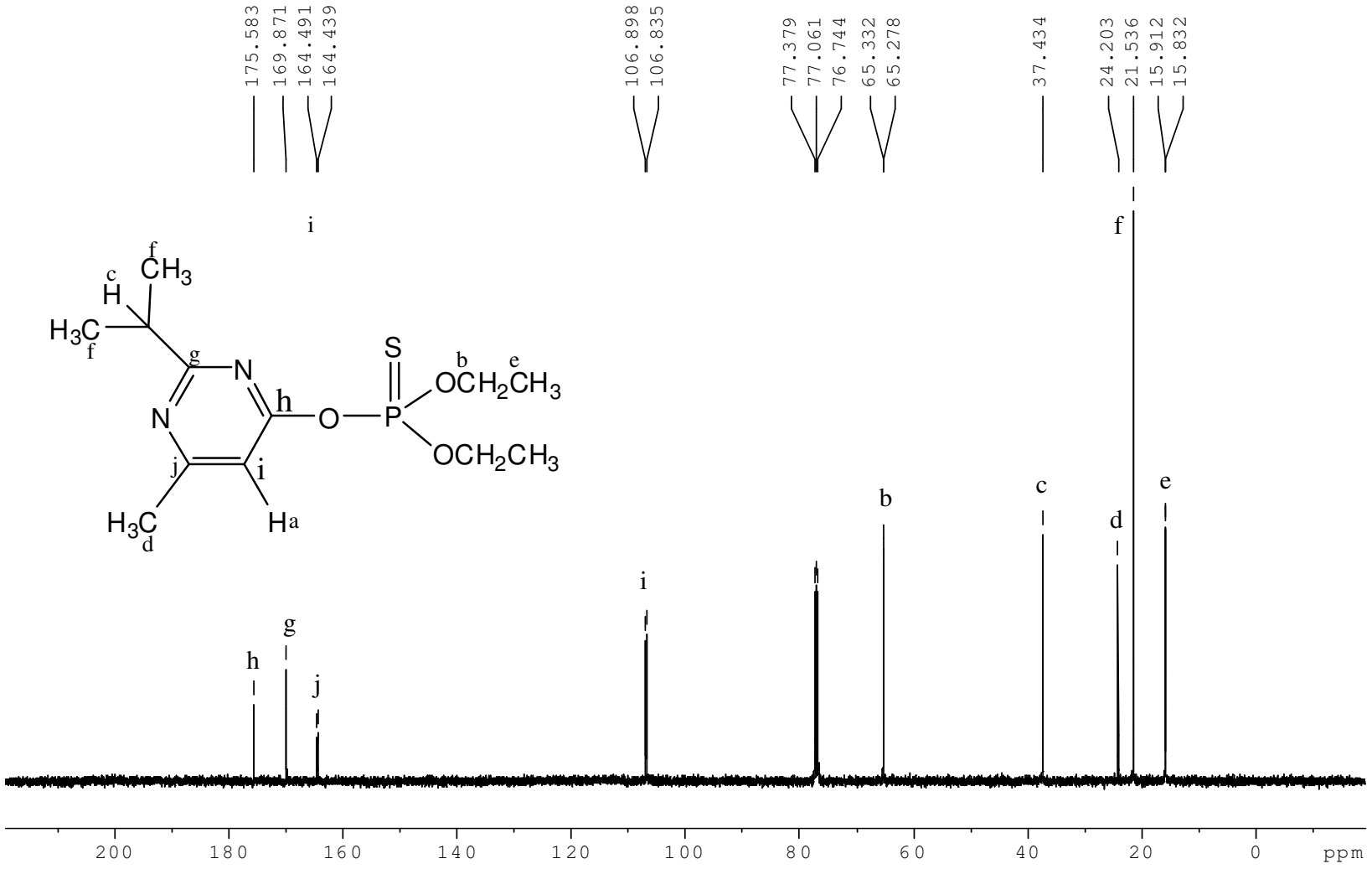

Figure A1-2. ^{13}C NMR of Diazinon in $CDCl_3$ (400 MHz)

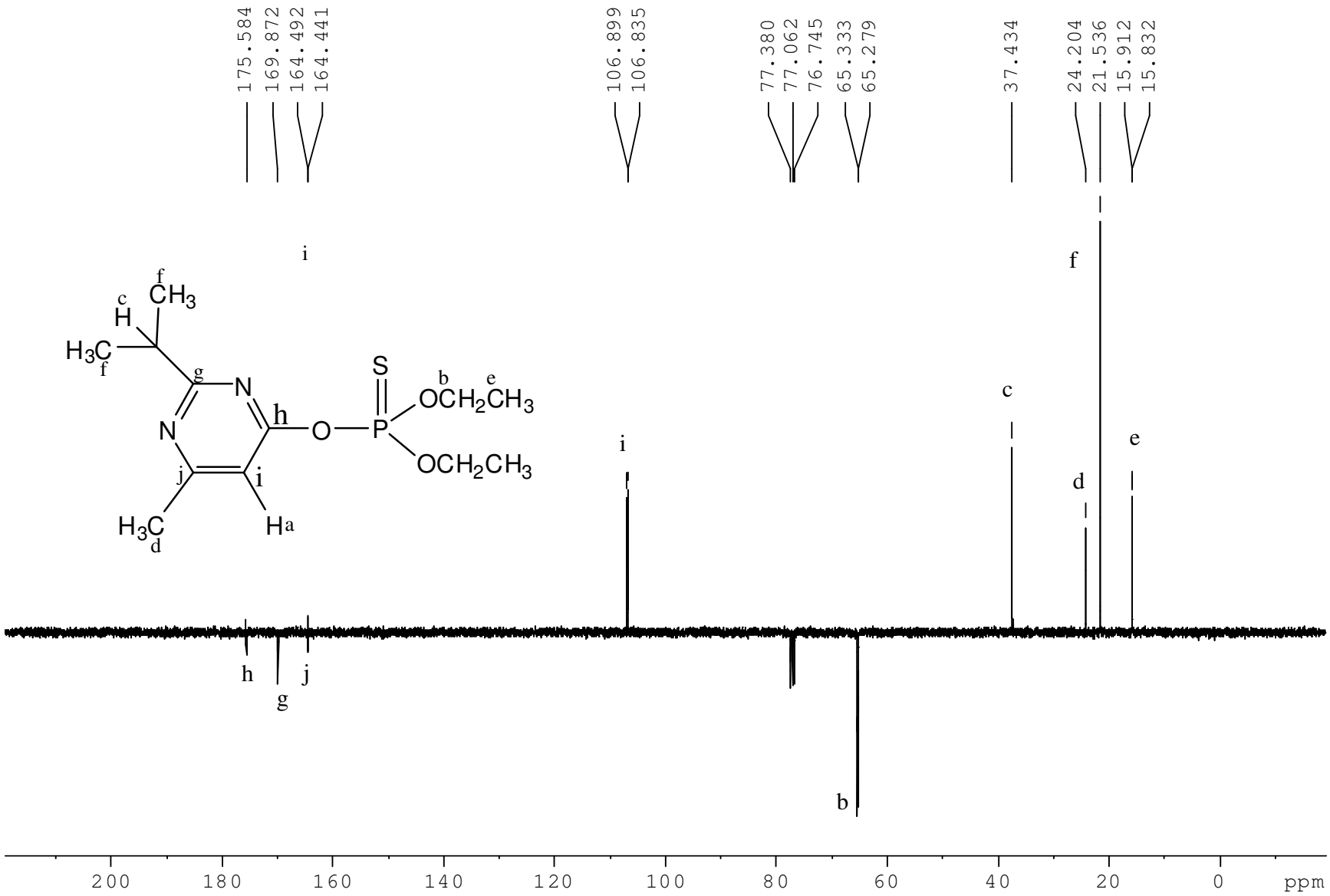

Figure A1.3. ^{13}C (J-modulated) NMR spectrum of Diazinon in $CDCl_3$ (400 MHz)

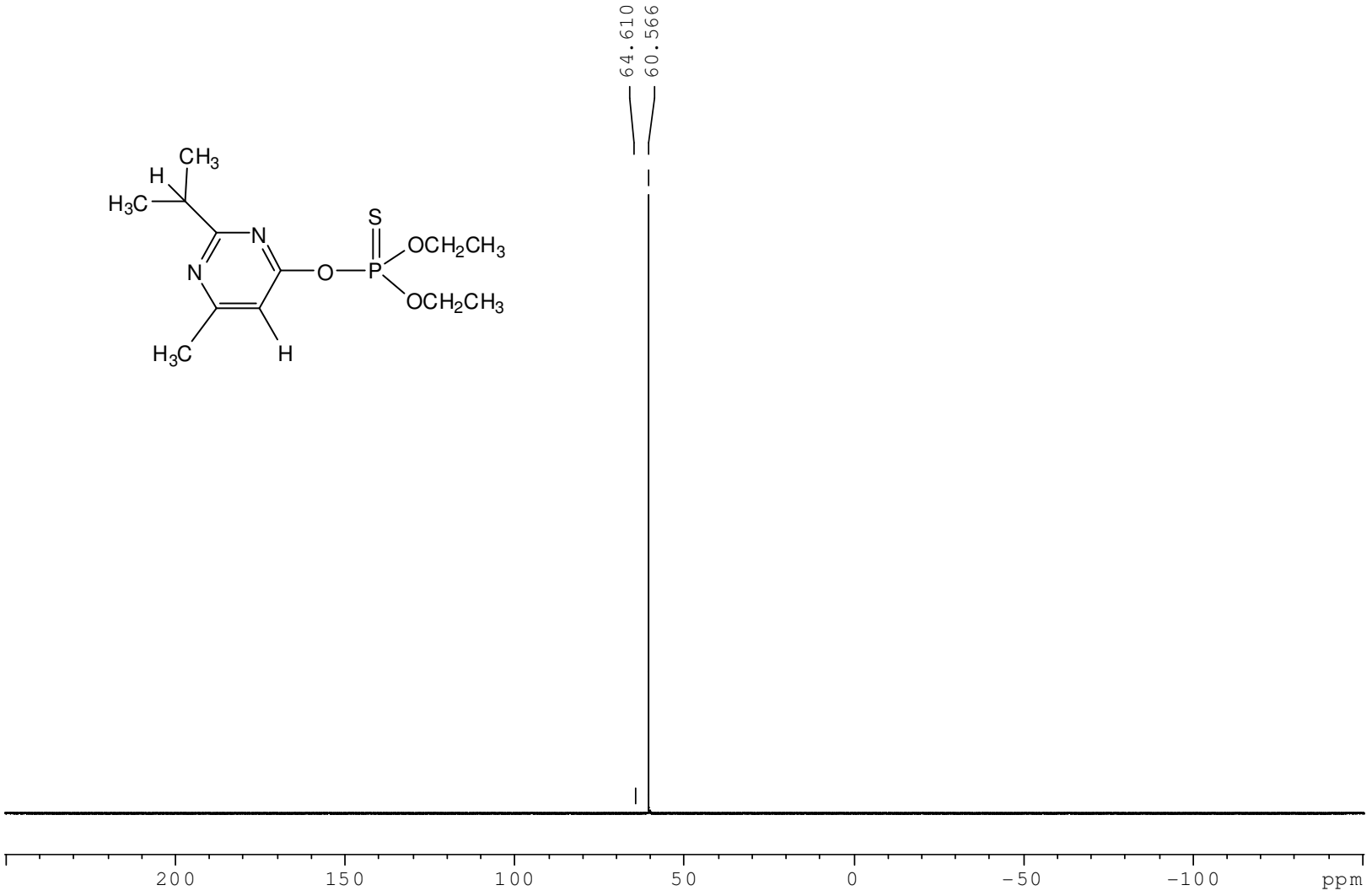

Figure A1.4 ^{31}P NMR spectrum of Diazinon in $CDCl_3$ (400 MHz)

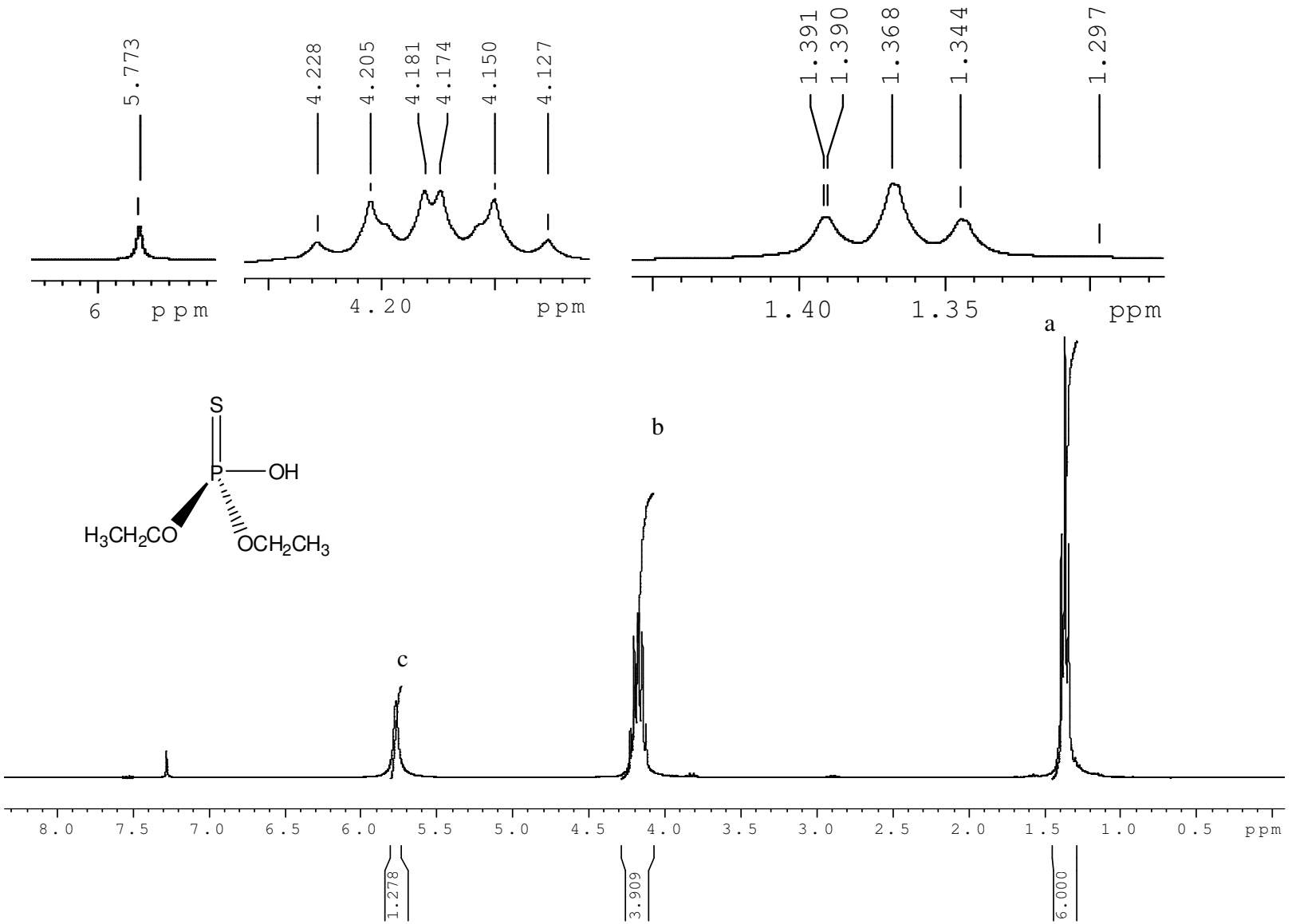

Figure A1.5 ^{1}H NMR spectrum of PA in $CDCl_3$ (400 MHz)

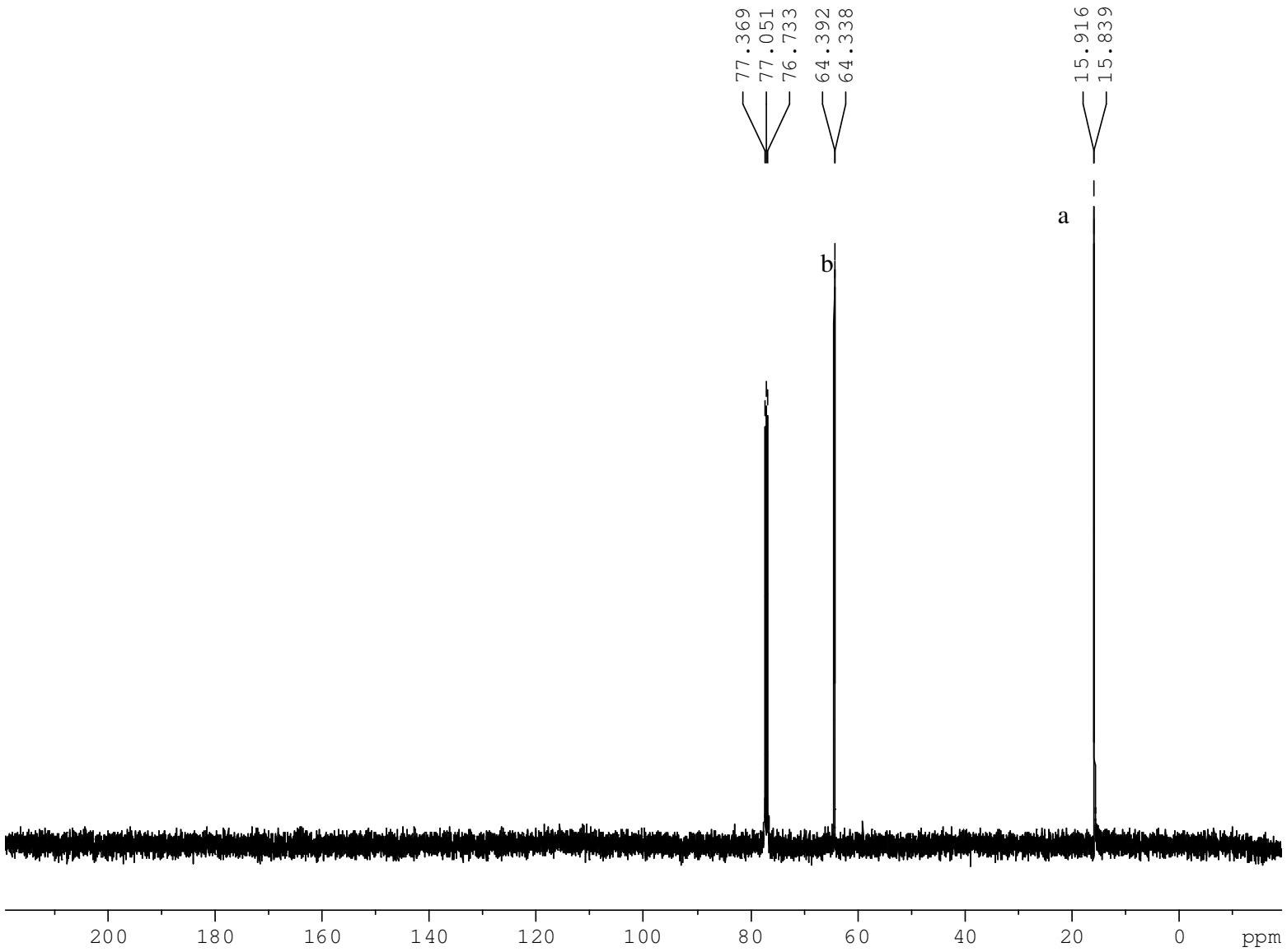

Figure A1.6 ^{13}C NMR spectrum of PA in $CDCl_3$ (400 MHz)

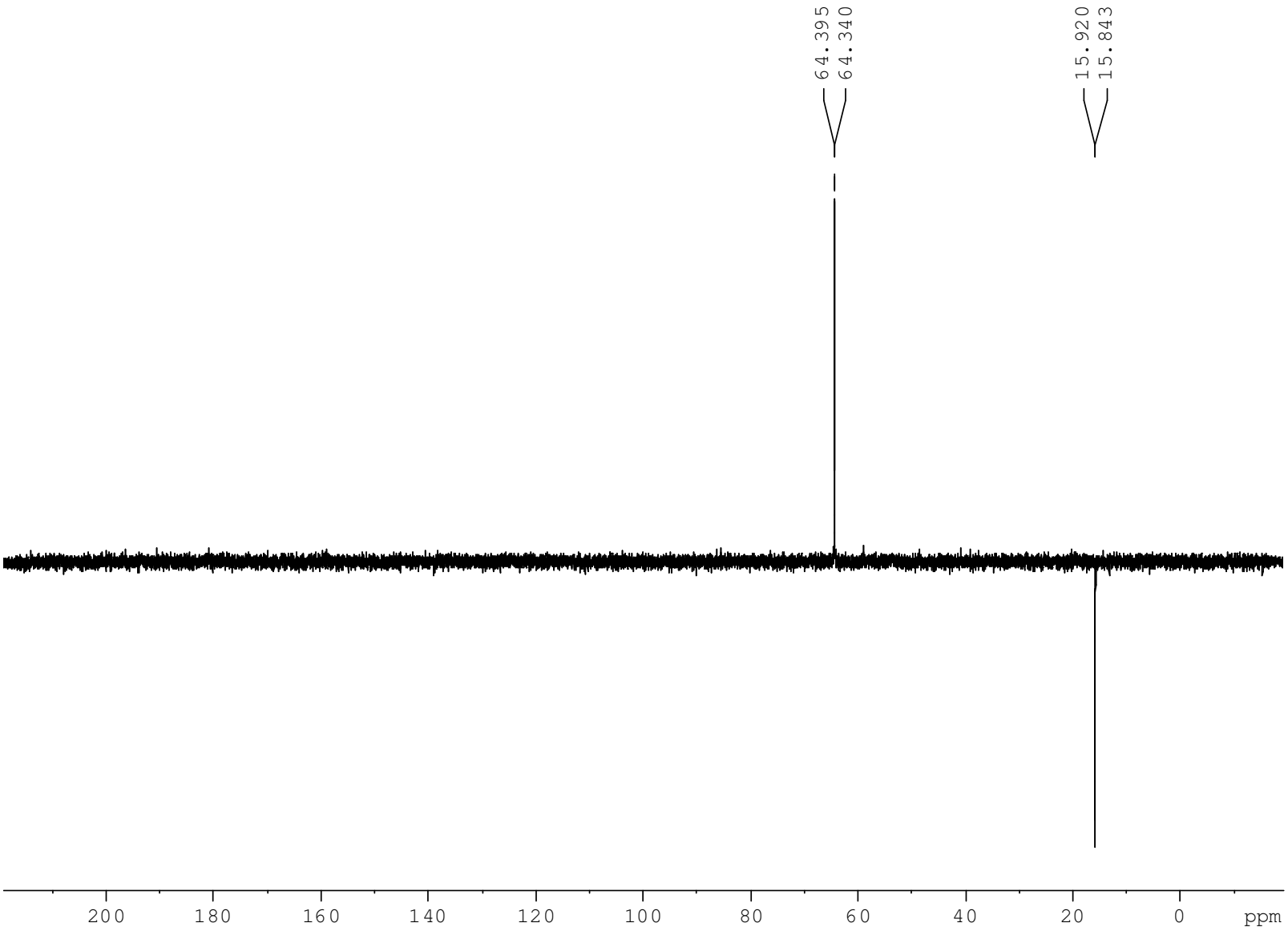

Figure A1.7. ^{13}C NMR (J-modulated) spectrum of PA in $CDCl_3$ (400 MHz)

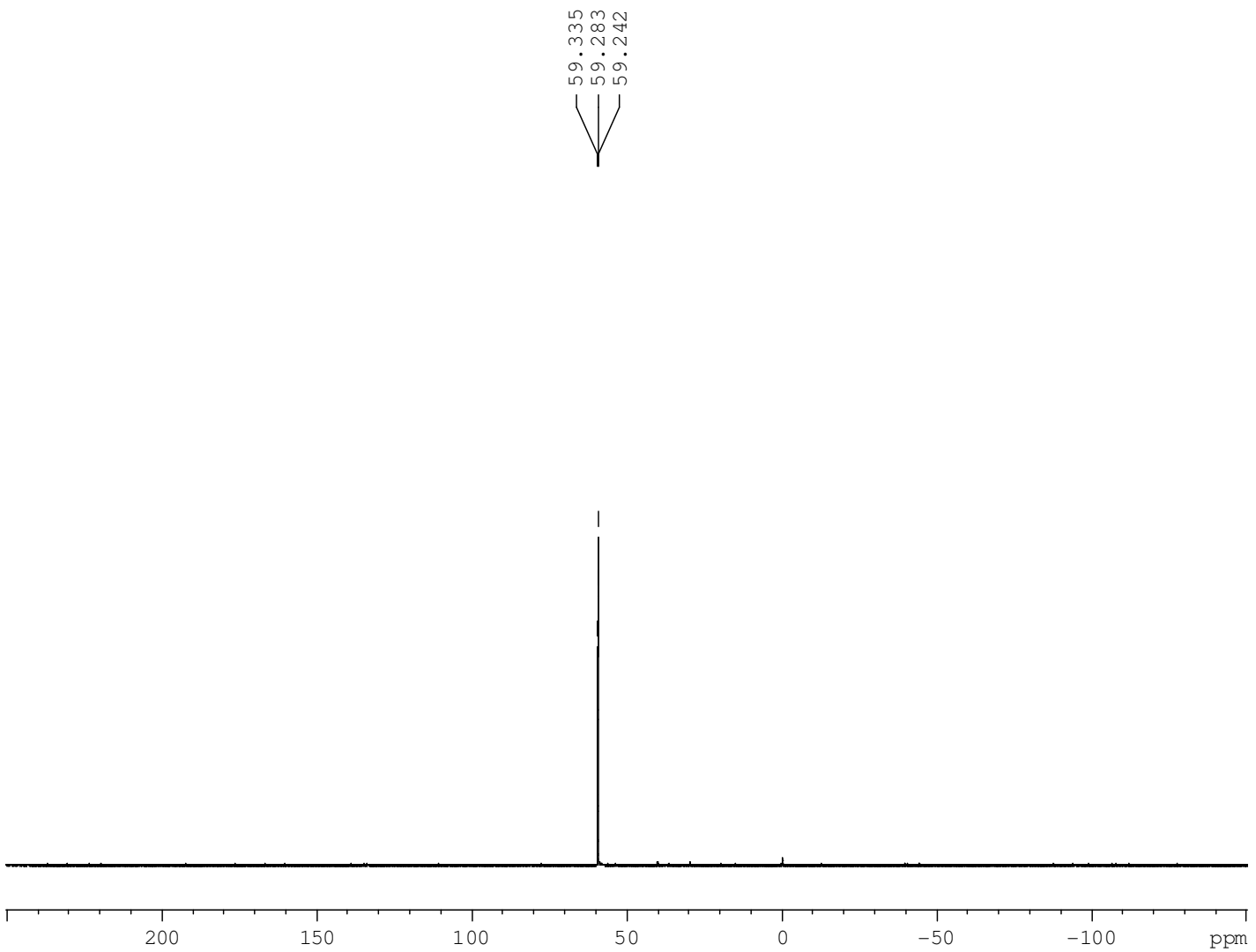

Figure A1.8. ^{31}P NMR spectrum of PA in $CDCl_3$ (400 MHz)

Appendix 2

Tabulated data for NMR solutions used in metal ion binding studies to PA and PY and hydrolysis experiments.

Incorporates concentrations of substrate and metal.

Cu^{2+} solutions

Changes in the chemical shift of PA and PY nuclei were examined over several ratios of Cu^{2+}/Substrate as indicated in Table A2.1.

Table A2.1 ^{1}H and ^{31}P NMR chemical shift changes in the presence of Cu^{2+}. Concentrations of O, O diethyl phosphorothioic acid, pyrimidinol and Cu^{2+} in each NMR tube.

NMR tube Number	$[Cu^{2+}] \times 10^{-2}$ Mol L^{-1}	[PA] x 10^{-2} Mol L^{-1}	Ratio Cu^{2+}/PA	NMR tube Number	$[Cu^{2+}] \times 10^{-2}$ Mol L^{-1}	[Py] x 10^{-2} Mol L^{-1}	Ratio Cu^{2+}/Py
1	0.83	1.67	0.5	1	0.83	1.67	0.5
2	1.67	1.67	1.0	2	1.67	1.67	1.0
3	4.17	1.67	2.5	3	4.17	1.67	2.5
4	8.33	1.67	5	4	8.33	1.67	5.0
5	16.7	1.67	10.0	5	16.7	1.67	10
6	41.7	1.67	25	6	41.7	1.67	25

The aqueous hydrolysis of Diazinon in the presence of Cu^{2+} was studied using ^{31}P NMR over three ratios of Cu^{2+}/Diazinon.

Table A2. 2 ^{1}H and ^{31}P NMR study of the aqueous hydrolysis of Diazinon in the presence of Cu^{2+}. Concentrations of Diazinon and Ag^{+} in each NMR tube.

NMR tube Number	$[Cu^{2+}] \times 10^{-2}$ Mol L^{-1}	[D] x 10^{-2} Mol L^{-1}	Ratio Cu^{2+}/D
1	4.17	8.33	0.5
2	8.33	8.33	1.0
3	41.6	8.33	5

Table A2.3 ^{1}H and ^{31}P NMR chemical shift changes in the presence of Cd^{2+}. Concentrations of O, O diethyl phosphorothioic acid, pyrimidinol and Cd^{2+} in each NMR tube.

NMR tube Number	$[Cd^{2+}] \times 10^{-2}$ Mol L^{-1}	$[PA] \times 10^{-2}$ Mol L^{-1}	Ratio Cd^{2+}/PA	NMR tube Number	$[Cd^{2+}] \times 10^{-2}$ Mol L^{-1}	$[Py] \times 10^{-2}$ Mol L^{-1}	Ratio Cd^{2+}/Py
1	0.83	1.67	0.5	1	0.83	1.67	0.5
2	1.67	1.67	1.0	2	1.67	1.67	1.0
3	4.17	1.67	2.5	3	4.17	1.67	2.5
4	8.33	1.67	5	4	8.33	1.67	5.0
5	16.7	1.67	10.0	5	16.7	1.67	10
6	41.7	1.67	25	6	41.7	1.67	25

Table A2. 4 ^{1}H and ^{31}P NMR study of the aqueous hydrolysis of Diazinon in the presence of Cd^{2+}. Concentrations of Diazinon and Cd^{2+} in each NMR tube.

NMR tube Number	$[Cd^{2+}] \times 10^{-2}$ Mol L^{-1}	$[D] \times 10^{-2}$ Mol L^{-1}	Ratio Cd^{2+}/D
1	41.7	1.67	25

Table A2.5 ^{31}P chemical shift of Diazinon in the presence of Cd^{2+} in CD_3OD. Concentrations of Diazinon and Cd^{2+} in each NMR tube.

NMR tube Number	$[Cd^{2+}] \times 10^{-2}$ Mol L^{-1}	$[D] \times 10^{-2}$ Mol L^{-1}	Ratio Cd^{2+}/D
1	0.83	1.67	0.5
2	1.67	1.67	1.0
3	4.17	1.67	2.5
4	8.33	1.67	5
5	16.7	1.67	10
6	41.7	1.67	25

Hg^{2+} solutions

Table A2.6 Study of ^{1}H and ^{31}P NMR chemical shift changes in the presence of Hg^{2+}.Concentrations of O, O diethyl phosphorothioic acid, pyrimidinol and Hg^{2+} in each NMR tube.

NMR tube Number	$[Hg^{2+}] \times 10^{-2}$ Mol L^{-1}	$[PA] \times 10^{-2}$ Mol L^{-1}	Ratio Hg^{2+}/PA	NMR tube Number	$[Hg^{2+}] \times 10^{-2}$ Mol L^{-1}	$[Py] \times 10^{-2}$ Mol L^{-1}	Ratio Hg^{2+}/Py
1	0.0167	1.67	0.01	1	0.0167	1.67	0.01
2	0.05	1.67	0.03	2	0.05	1.67	0.03
3	0.117	1.67	0.07	3	0.117	1.67	0.07
4	0.267	1.67	0.16	4	0.267	1.67	0.16
5	0.60	1.67	0.36	5	0.60	1.67	0.36
6	0.833	1.67	0.50	6	0.833	1.67	0.50
7	1.67	1.67	1.0	7	1.67	1.67	1.0
8	3.33	1.67	2.0	8	3.33	1.67	2.0
9	5.0	1.67	3.0	9	5.0	1.67	3.0
10	8.33	1.67	5.0	10	8.33	1.67	5.0

Table A2.7 ^{1}H and ^{31}P NMR study of the hydrolysis of Diazinon in the presence of Hg^{2+}. Concentrations of Diazinon and Hg^{2+} in each NMR tube.

NMR tube Number	$[Ag^{+}] \times 10^{-2}$ Mol L^{-1}	$[D] \times 10^{-2}$ Mol L^{-1}	Ratio Ag^{+}/PA
1	0.83	1.67	0.5
2	1.67	1.67	1.0
3	8.33	1.67	5

Table A2. 8 Study of the ^{31}P chemical shift of Diazinon in the presence of Hg^{2+} in CD_3OD. Concentrations of Diazinon and Hg^{2+} in each NMR tube.

NMR tube Number	$[Hg^{2+}] \times 10^{-2}$ Mol L^{-1}	$[D] \times 10^{-2}$ Mol L^{-1}	Ratio Hg^{2+}/D
1	0.83	1.67	0.5
2	1.67	1.67	1.0
3	4.17	1.67	2.5
4	8.33	1.67	5
5	16.7	1.67	10
6	41.7	1.67	25

Appendix 3

Tabulated data for O,O diethyl phosphorothioic acid (PA) metal ion NMR binding study.

Incorporates concentrations, ratio of PA to metal, observed chemical shift data (ppm) and the induced change in the chemical shift ($\Delta\delta$, ppm) due to metal binding.

Table A3.9 ^{31}P chemical shift of PA in the presence of increasing concentrations of Ag^{+}. [PA] = 1.67 x 10^{-2} Mol L^{-1}.

Experimental Number	[Ag^{+}] x 10^{-2} Mol L^{-1}	Ratio Ag^{+}/PA	(δ) of ^{31}P	Δδ
0	*0.00*	*N/A*	*60.165*	*N/A*
1	0.33	0.2	55.355	4.81
2	0.67	0.4	51.658	8.507
3	1.33	0.8	42.976	17.189
4	1.67	1.0	39.569	20.596
5	4.17	2.5	39.173	20.992
6	8.33	5.0	38.809	21.356
7	16.7	10.0	37.239	22.836
8	41.7	25.0	35.124	25.041

Table A3.10 ^{1}H chemical shifts of PA (CH_2^b) in the presence of increasing Ag^{+} concentrations. [PA]= 1.67 x 10^{-2} Mol L^{-1}.

Experimental Number	[Ag^{+}] x 10^{-2} Mol L^{-1}	Ratio Ag^{+}/PA	(δ) of CH_2	Δδ
0	*0.00*	*N/A*	*4.048*	*N/A*
1	0.33	0.2	4.078	0.03
2	-	0.5	4.085	0.037
3	1.67	1.0	4.213	0.165
4	4.17	2.5	4.210	0.162
5	8.33	5.0	4.209	0.161
6	16.7	10.0	4.218	0.170
7	41.7	25.0	4.245	0.197

Table A3.11 ^{31}P chemical shift of PA in the presence of increasing concentrations of Hg^{2+}. [PA] = 1.67 x 10^{-2} Mol L^{-1}.

Experimental Number	$[Hg^{2+}]$ x 10^{-2} Mol L^{-1}	Ratio Hg^{2+}/PA	(δ) of ^{31}P	Δδ
0	*0.00*	*N/A*	*60.165*	*N/A*
1	0.0167	0.01	60.165	0.0
2	0.05	0.03	59.910	0.255
3	0.117	0.07	57.525	2.64
4	0.267	0.16	53.306	6.859
5	0.60	0.36	42.309	17.856
6	0.833	0.50	39.785	20.38
7	1.67	1.0	36.571	23.594
8	3.33	2.0	36.219	23.946
9	5.0	3.0	36.533	23.632
10	8.33	5.0	33.990	26.175

Table A3.12 ^{1}H chemical shifts of PA (CH_2^b) in the presence of increasing Hg^{2+} concentrations. [PA] = 1.67 X 10 Mol L^{-1}.

Experimental Number	$[Hg^{2+}]$ x 10^{-2} Mol L^{-1}	Ratio Hg^{2+}/PA	(δ) of CH_2^b	Δδ
0	*0.00*	*N/A*	*4.048*	*N/A*
1	0.0167	0.01	4.053	0.005
2	0.05	0.03	4.063	0.015
3	0.117	0.07	4.076	0.028
4	0.267	0.16	4.101	0.053
5	0.60	0.36	4.176	0.119
6	0.833	0.50	4.181	0.133
7	1.67	1.0	4.211	0.163
8	3.33	2.0	4.207	0.159
9	5.0	3.0	4.208	0.160
10	8.33	5.0	4.211	0.163

Table A3.13 ^{31}P chemical shift of PA in the presence of increasing concentrations of Cd^{2+}. [PA] = 1.67 x 10^{-2} Mol L^{-1}.

Experimental Number	$[Cd^{2+}]$ x 10^{-2} Mol L^{-1}	Ratio Cd^{2+}/PA	(δ) of ^{31}P	Δδ
0	*0.00*	*N/A*	*60.165*	*N/A*
1	0.83	0.5	54.541	5.624
2	1.67	1.0	52.407	7.758
3	4.17	2.5	50.741	9.424
4	8.33	5.0	49.994	10.171
5	16.7	10.0	49.539	10.626
6	41.7	25.0	49.051	11.114

Table A3.14 ^{1}H chemical shifts of PA (CH_2^b) in the presence of increasing Cd^{2+} concentrations. [PA] = 1.67 X 10 Mol L^{-1}.

Experimental Number	$[Cd^{2+}]$ x 10^{-2} Mol L^{-1}	Ratio Cd^{2+}/PA	(δ) of CH_2^b	Δδ
0	*0.00*	*N/A*	*4.048*	*N/A*
1	0.83	0.5	4.071	0.023
2	1.67	1.0	4.073	0.025
3	4.17	2.5	4.074	0.026
4	8.33	5.0	4.072	0.024
5	16.7	10.0	4.071	0.023
6	41.7	25.0	4.052	0.004

Appendix 4

Tabulated data for Pyrimidinol (PY) metal ion binding study.

Incorporates concentrations, ratio of PY to metal, observed chemical shift data (ppm) and the induced change in the chemical shift ($\Delta\delta$, ppm) due to metal binding.

Table A4.1 ^{1}H chemical shifts of PY (H^{a}, H^{c}) in the presence of increasing concentrations of Ag^{+}. [PY] = 1.67 X 10^{-2} Mol L^{-1}.

Experimental Number	$[Ag^{+}]$ x 10^{-2} Mol L^{-1}	Ratio Ag^{+}/PY	δ of H^{a}	Δδ	δ of H^{c}	Δδ
0	**0.00**	**N/A**	**6.208**	**N/A**	**2.936**	**N/A**
1	0.167	0.1	6.219	0.011	2.966	0.03
2	0.833	0.5	6.241	0.033	3.036	0.100
3	1.67	1	6.253	0.045	3.065	0.129
4	4.17	2.5	6.261	0.053	3.083	0.147
5	8.33	5	6.261	0.053	3.086	0.150
6	16.7	10	6.266	0.058	3.088	0.152
7	41.7	25	6.277	0.069	3.092	0.156

Table A4.2 ^{1}H chemical shifts of PY (H^{d}, H^{f}) in the presence of increasing concentrations of Ag^{+}. [PY] = 1.67 x 10^{-2} Mol L^{-1}.

Experimental Number	$[Ag^{+}]$ x 10^{-2} Mol L^{-1}	Ratio Ag^{+}/PY	δ of H^{d}	Δδ	δ of H^{f}	Δδ
0	**0.00**	**N/A**	**2.322**	**N/A**	**1.329**	**N/A**
1	0.167	0.1	2.334	0.012	1.353	0.024
2	0.833	0.5	2.362	0.04	1.411	0.082
3	1.67	1	2.376	0.054	1.434	0.105
4	4.17	2.5	2.386	0.064	1.450	0.121
5	8.33	5	2.388	0.066	1.452	0.123
6	16.7	10	2.391	0.069	1.451	0.122
7	41.7	25	2.393	0.071	1.447	0.118

Table A4.3 ^{1}H chemical shifts of PY (H^{a}, H^{c}) in the presence of increasing concentrations of Hg^{2+}. [PY] = 1.67 X 10^{-2} Mol L^{-1}.

Experimental Number	$[Hg^{2+}]$ x 10^{-2} Mol L^{-1}	Ratio Hg^{2+}/PY	δ of H^{a}	Δδ	δ of H^{c}	Δδ
0	**0.00**	**N/A**	**6.208**	**N/A**	**2.936**	**N/A**
1	0.167	0.01	6.213	0.005	2.935	-0.001
2	0.05	0.03	6.205	-0.003	2.935	-0.001
3	0.117	0.07	6.202	-0.006	2.934	-0.002
4	0.267	0.16	6.203	-0.005	2.934	-0.002
5	0.60	0.36	6.203	-0.005	2.934	-0.002
6	0.833	0.50	6.201	-0.007	2.933	-0.003
7	1.67	1.0	6.203	-0.005	2.935	-0.001
8	3.33	2.0	6.202	-0.006	2.935	-0.001
9	5.0	3.0	6.204	-0.004	2.938	0.002
10	8.33	5.0	6.208	0.000	2.942	0.006

Table A4.4 ^{1}H chemical shifts of PY (H^{d}, H^{f}) in the presence of increasing concentrations of Hg^{2+}. [PY] = 1.67 x 10^{-2} Mol L^{-1}.

Experimental Number	$[Hg^{2+}]$ x 10^{-2} Mol L^{-1}	Ratio Hg^{2+}/PY	δ of H^{d}	Δδ	δ of H^{f}	Δδ
0	**0.00**	**N/A**	**2.322**	**N/A**	**1.329**	**N/A**
1	0.167	0.01	2.322	0.000	1.330	0.001
2	0.05	0.03	2.323	0.001	1.331	0.002
3	0.117	0.07	2.320	-0.002	1.330	0.001
4	0.267	0.16	2.322	0.000	1.330	0.001
5	0.60	0.36	2.322	0.000	1.331	0.002
6	0.833	0.50	2.322	0.000	1.331	0.002
7	1.67	1.0	2.322	0.000	1.331	0.002
8	3.33	2.0	2.321	-0.001	1.332	0.003
9	5.0	3.0	2.323	0.001	1.333	0.004
10	8.33	5.0	2.325	0.003	1.334	0.005

Table A4.5 ^{1}H chemical shifts of PY (H^{a}, H^{c}) in the presence of increasing concentrations of Cd^{2+}. [PY] = 1.67 X 10^{-2} Mol L^{-1}.

Experimental Number	$[Cd^{2+}]$ x 10^{-2} Mol L^{-1}	Ratio Cd^{2+}/PY	δ of H^{a}	Δδ	δ of H^{c}	Δδ
0	**0.00**	**N/A**	**6.208**	**N/A**	**2.936**	**N/A**
1	0.833	0.5	6.203	-0.005	2.936	0.000
2	1.67	1	6.201	-0.007	2.935	-0.001
3	4.17	2.5	6.212	0.004	2.945	0.009
4	8.33	5	6.228	0.020	2.959	0.023
5	16.7	10	6.247	0.039	2.975	0.039
6	41.7	25	6.294	0.086	3.008	0.072

Table A4.6 ^{1}H chemical shifts of PY (H^{d}, H^{f}) in the presence of increasing concentrations of Cd^{2+}. [PY] = 1.67 X 10^{-2} Mol L^{-1}.

Experimental Number	$[Cd^{2+}]$ x 10^{-2} Mol L^{-1}	Ratio Cd^{2+}/PY	δ of H^{d}	Δδ	δ of H^{f}	Δδ
0	**0.00**	**N/A**	2.322	**N/A**	**1.329**	**N/A**
1	0.833	0.5	2.322	0.000	1.331	0.002
2	1.67	1	2.322	0.000	1.329	0.000
3	4.17	2.5	2.329	0.007	1.333	0.004
4	8.33	5	2.339	0.017	1.335	0.006
5	16.7	10	2.350	0.028	1.338	0.009
6	41.7	25	2.373	0.051	1.341	0.012